

BEDROCK DEFORMATION IN THE COOLING WATER TUNNELS

**Perry Nuclear Power Plant
Units 1 & 2**

VOLUME I

POOR ORIGINAL

**THE CLEVELAND ELECTRIC
ILLUMINATING COMPANY**

1241 001



Gilbert/Commonwealth
ENGINEERS/CONSULTANTS Reading, PA / Jackson, NJ

7910300269

GAI REPORT NO. 2063
Prepared for Cleveland Electric Illuminating Co.

BEDROCK DEFORMATION IN THE
COOLING WATER TUNNELS
PERRY NUCLEAR POWER PLANT
NORTH PERRY, OHIO

OCTOBER 1979

Compiled by

L. D. Schultz
Project Geologist
Perry Nuclear Power Plant
Gilbert Associates, Inc.

Reviewed by

W. J. Santamour
Geotechnical Section Supervisor
Gilbert Associates, Inc.

Approved for Release by

P. B. Gudikunst
Project Manager
Perry Nuclear Power Plant
Gilbert Associates, Inc.

1241 002

78-267

THE CLEVELAND ELECTRIC ILLUMINATING COMPANY
PERRY NUCLEAR POWER PLANT

BEDROCK DEFORMATION IN THE
COOLING WATER TUNNELS
PERRY NUCLEAR POWER PLANT
NORTH PERRY, OHIO

OCTOBER 1979

Compiled by:

Lane D. Schultz

L. D. Schultz
Project Geologist
Gilbert Associates

Reviewed by:

W. J. Santamour

W. J. Santamour
Geotechnical Section Supervisor
Gilbert Associates, Inc.

Approved by:

Paul B. Gudikunst

P. B. Gudikunst
Project Manager
Gilbert Associates, Inc.

1241 003

TABLE OF CONTENTS

		<u>Page</u>
1.0	<u>SUMMARY</u>	1
2.0	<u>INTRODUCTION</u>	3
2.1	<u>STATEMENT OF PROBLEM</u>	3
2.2	<u>INVESTIGATIVE CHRONOLOGY</u>	5
2.3	<u>GEOLOGIC SETTING</u>	9
3.0	<u>METHODS OF INVESTIGATION</u>	13
3.1	<u>GEOLOGIC</u>	14
3.1.1	LITERATURE REVIEW AND PERSONAL COMMUNICATIONS	14
3.1.2	EXPLORATORY BORINGS	15
3.1.3	SHORELINE RECONNAISSANCE	17
3.1.4	VIDEO EXAMINATION OF LAKE BOTTOM FEATURES	17
3.1.5	DETAILED GEOLOGIC MAPPING IN THE INTAKE AND DISCHARGE TUNNELS	18
3.1.6	MICROCRACK ANALYSIS	19
3.1.7	WATER ANALYSIS	19
3.2	<u>GEOPHYSICAL STUDIES</u>	20
3.2.1	EVALUATION OF PUBLISHED AND UNPUBLISHED DATA	20
3.2.2	MAGNETIC SURVEYS	20
3.2.2.1	<u>Offshore</u>	20
3.2.2.2	<u>Onshore</u>	20
3.2.3	BOREHOLE LOGS	21
3.2.4	IN-SITU VELOCITY MEASUREMENTS	22
3.3	<u>EVALUATION OF LOCAL SEISMICITY ACTIVITY AROUND THE PERRY NUCLEAR POWER PLANT SITE</u>	23
3.4	<u>IN-SITU STRESS MEASUREMENTS</u>	23

1241 004

TABLE OF CONTENTS (Continued)

		<u>Page</u>
4.0	<u>RESULTS</u>	24
4.1	<u>GEOLOGIC</u>	24
4.1.1	LITERATURE REVIEW AND PERSONAL COMMUNICATIONS	24
4.1.2	EXPLORATORY BORINGS	25
4.1.3	SHORELINE RECONNAISSANCE	27
4.1.4	VIDEO EXAMINATION OF LAKE BOTTOM FEATURES	28
4.1.5	DETAILED GEOLOGIC MAPPING IN THE INTAKE AND DISCHARGE TUNNELS	28
4.1.5.1	<u>Stratigraphy</u>	28
4.1.5.2	<u>Tunnel Structural Geology</u>	31
4.1.5.2.1	Intake Tunnel Structure	31
4.1.5.2.2	Discharge Tunnel Structure	32
4.1.6	MICROCRACK ANALYSIS	34
4.1.7	WATER ANALYSIS	36
4.2	<u>GEOPHYSICAL STUDIES</u>	37
4.2.1	EVALUATION OF PUBLISHED AND UNPUBLISHED GEOPHYSICAL DATA	37
4.2.2	MAGNETIC SURVEYS	38
4.2.3	BOREHOLE LOGS	38
4.2.4	IN-SITU VELOCITY MEASUREMENTS	39
4.3	<u>CALCULATION OF LOCAL SEISMICITY ACTIVITY AROUND THE PERRY NUCLEAR POWER PLANT SITE</u>	39
4.4	<u>IN-SITU STRESS MEASUREMENTS</u>	40
5.0	<u>CONCLUSIONS</u>	41
6.0	<u>REFERENCES</u>	44
TABLE 1	ANALYSES OF TUNNEL FAULTING SEEPAGE	46

1248 005

LIST OF FIGURES

<u>FIGURE NO.</u>	<u>TITLE</u>
1	Location Map, Perry Nuclear Power Plant
2	Geologic Map of Tunnel Excavations (23 sheets)
3	Tunneling Plan
4	Bedrock Geologic Map of Northeastern Ohio
5	Glacial Map of Northeastern Ohio
6	Structural Contour Map - Top of Big Lime
7	Structural Contour Map - Top of Packer Shell
8	Isopach Map of Big Lime and Niagaran Shale
9	Fault and Outcrop Location Map
10	Schematic Northwest-Southeast Cross Section, Perry Nuclear Power Plant
11	TX-Series Boring Plan
12	Map of Shoreline Survey
13	Location Map, Video Survey Lake Erie Bottom
14	Longitudinal Section, Discharge Tunnel
15	Longitudinal Section, Intake Tunnel
16	Location Map, Offshore Magnetic Survey
17	Location Map, Onshore Magnetic Survey
18	Location Map, Seismic Spreads, Intake Tunnel
19	Location Map, Seismic Spreads, Discharge Tunnel
20	Schematic Map, Lake Bottom Fractures
21	Sketch of Facies Relationships among the Huron, Chagrin, & Cleveland Shales
22	Detailed Stratigraphic Section, Intake Tunnel East Wall Station 10+30-10+40
23	Detailed Stratigraphic Section, Discharge Tunnel East Wall Station 11+40-11+46
24	Detailed Stratigraphic Section, Discharge Tunnel East Wall Station 13+22-13+28

1241 006

LIST OF FIGURES (Continued)

<u>FIGURE NO.</u>	<u>TITLE</u>
25	Geologic Structure Map, Intake & Discharge Tunnel Faults
26	Intake Tunnel Wall Maps, Stations 10+25-10+95
27	Discharge Tunnel Wall Maps, Stations 13+00-12+00
28	Discharge Tunnel Wall Maps, Stations 11+40-12+00
29	Geologic Maps, Intake & Discharge Tunnels
30	Detailed Map, Intake Tunnel Fault
31	Photographs, Structural Details, Intake Tunnel
32	Detailed Map, Discharge Tunnel Fault
33	Photographs, Structural Details, Discharge Tunnel
34	Offshore for Shipborne Magnetic Profile 14
35	Offshore for Shipborne Magnetic Profiles 10 and 12
36	Offshore for Shipborne Magnetic Profiles 6 and 8
37	Offshore for Shipborne Magnetic Profiles 2 and 4
38	Offshore for Shipborne Magnetic Profiles 0 and 3
39	Offshore for Shipborne Magnetic Profiles 5A and 7
40	Offshore for Shipborne Magnetic Profiles 9 and 11
41	Offshore for Shipborne Magnetic Profiles 13 and 15
42	Offshore for Shipborne Magnetic Profiles 17 and 19
43	Onshore for Land Magnetic Profile 1S-A
44	Onshore for Land Magnetic Profile 1S
45	Onshore for Land Magnetic Profile 1E
46	Onshore for Land Magnetic Profile 2S
47	Onshore for Land Magnetic Profile 3S
48	Onshore for Land Magnetic Profile 3S-A
49	Borehole Logs - Gamma/Sonic, TX Borings 2,3,4,5,6,7
50	Borehole Logs - Gamma/Sonic, TX Borings 8,9,10

1241 007

LIST OF APPENDICES

- APPENDIX A A Study of the Microcracks Associated with Faulting at the
Perry Nuclear Power Plant Site
- APPENDIX B A Study of the Isotopic Composition of Water from the Fault in
the Intake and Discharge Tunnels at the Perry Nuclear Power
Plant Site
- APPENDIX C Geophysical Methods
- APPENDIX D Independent Reviews of Cooling Water Tunnel Faulting - Perry
Nuclear Power Plant
- APPENDIX E Stress Measurements Hydrofracturing Technique - Perry Nuclear
Power Plant
- APPENDIX F TX-Series Geologic Logs
- APPENDIX G Consolidation Tests on Fault Gouge Samples, Perry Nuclear Power
Plant
- APPENDIX H Evaluation of Local Seismicity Around the Perry Nuclear Power
Plant Site

1241 008

Geological, geophysical, and seismological studies were conducted on and in the vicinity of a fault observed in the intake and discharge tunnels at the Perry Nuclear Power Plant site of The Cleveland Electric Illuminating Company. The Perry site is located on the shore of Lake Erie, approximately 35 miles northeast of Cleveland. The general location of the site is shown on Figure 1.

A comprehensive investigative program evolved as a result of the bedrock deformation exposed during the excavation phase of tunnel construction. Deterministic fault study objectives, extent, origin and age, were realized as a consequence of a series of interrelated geologic and geophysical research and engineering. The nature of fault-plane geometry and its gouge and mineralogical as well as chemical constituents were studied. After site specific data had been assembled, the localized anomalous deformation was interpreted in context of its regional geologic setting.

The extent of faulting was defined on the basis of the following: (1) planned, tunnel mapping program (scale 1:120); (2) detailed mapping of tunnel deformation segments (scale 1:12); (3) exploratory borings; (4) geophysical logging of borings; (5) shoreline reconnaissance; (6) offshore magnetic survey; (7) lake bottom reconnaissance mapping and review of seismic track line data; and (8) comparative isotopic analyses of Lake Erie water and fault seepage.

Fault zone gouge and fractured rock samples were obtained for X-ray diffraction, clay-mineralogical determinations, SEM (scanning electron microscope) microcrack analysis, and miscellaneous engineering property determinations including consolidation pressure analysis. No radioactive isotopes, which could have been dated, were identified in fault zone samples. With respect to the site area and locale studies, the following were performed or prepared: (1) in-situ borehole (TX-11) stress measurements to determine existing site stress field orientation and magnitude; (2) structural contour maps of "Big Lime" upper and basal (-50 ft) horizons and isopachous map of intervening interval for Lake and portions of adjacent Ashtabula, Geauga and

1241 009

Cuyahoga Counties; (3) evaluation of microseismicity in northeastern Ohio; (4) literature and field review of area salt mines and interviews with mine personnel (Mr. Jaroslav Vaverka, resident mining engineer, Cleveland mine, International Salt Company and Mr. B. C. Cummings, resident chief engineer, Painesville mine, Morton Salt Division of Morton Norwick).

Independent opinions based on their field inspection of the tunnel deformation and literature review were obtained from the following geologists recognized for their expertise in the indicated disciplines:

Dr. Robert G. LaFleur
Pleistocene Geology and Sedimentology
Rensselaer Polytechnical Institute

Mr. James Murphy
Areal Geology and Stratigraphy of Northeastern Ohio
Ohio Historical Society

Dr. Barry Voight
Structural Geology
Penn State University

It is concluded on the bases of data and interpretation of the aforementioned studies and other site and regional geological, geophysical, and seismological information that the last movement on the cooling water tunnel bedrock deformation was not tectonic. It occurred during Pleistocene time probably associated with deglaciation-rebound rather than ice advance compression. On the basis of geometry alone it is possible that the initial deformation was a pre-Pleistocene event. The presence of the fault deformation intersecting the tunnels was considered during design review and redesign was not required.

1241 010

2.0 INTRODUCTION

2.1 STATEMENT OF PROBLEM

Tunnel excavations for the plant cooling water system exposed low-angle thrust faulting of minor displacement in the Chagrin shale beneath Lake Erie. The presence of faulting within the intake and discharge tunnels did not greatly hinder tunneling operations. Additional rock bolts and tunnel shields were installed in tunnel fault segments to insure crown stability. Methane and water, which had been stored within fault zone fracture porosity, were discharged upon intersection of the intake tunnel fault segment by a horizontal exploratory boring drilled in advance of the tunnel boring machine. Both conditions were short term, within anticipated limits and controlled by normal pumping and ventilation.

Geologic mapping (scale 1:120) of the tunnels was conducted concurrent with tunneling consistent with PSAR (Preliminary Safety Analysis Report) commitments (see Figure 2, 24 sheets). After faulting had been intersected by the tunnel boring machine and the bedrock mapped, preliminary interpretations and the mapping data were forwarded to the NRC (Nuclear Regulatory Commission) in a timely manner. The extent, age, and origin of faulting were not well understood following its initial encounter within the intake tunnel. More than four months elapsed between faulting exposed in the intake and discharge tunnels, respectively.

The fault plane exposed in the intake tunnel subsequently has been determined to have a strike of approximately N51°E which projects in the vicinity of the discharge tunnel deformation. Based on the similarity of structural style, flexural slip and brittle failure attributable to compression, and assuming minor warping of the fault plane along its strike, it is probable that the fault plane is continuous between both tunnels. This determination could not be concluded prior to completion of all tunnel excavations which was accomplished nearly six months after exposing the first deformation.

The origin of the deformation could not be readily determined on the basis of known regional geology. Results of site and regional studies (field and literature) conducted during the preconstruction phase are reported in the PSAR. On the basis of these studies and the opinions of university professors, bedrock in northeastern Ohio is not known to have undergone significant faulting. Professors contacted are listed as follows:

Prof. Eugene J. Synuk, Kent State University,
Prof. Murray R. McComas, Kent State University,
Prof. Tom Lewis, Cleveland State University, and
Prof. Charles M. Somerson, Ohio State University.

In this area a nearly ubiquitous veneer of glacial and glaciolacustrine deposits obscure bedrock except where incised by stream erosion. Accessible outcrops do not reveal evidence of having experienced tectonism, either late Paleozoic associated with the Alleghenian (Appalachian) Orogeny or any other. Subsurface data, geological and geophysical, do not imply the presence of a regional fault system which could have been interpreted to be genetically related to tunnel faulting. The general lack of information to the contrary suggested that this portion of the Central Lowland Physiographic Province is tectonically stable having undergone little if any tectonic deformation.

Shallow bedrock deformation, consisting of small-scale folding and faulting, had been revealed as a consequence of plant foundation excavation during 1975 and 1976. It has been demonstrated by field relationships that this deformation was caused by the direct action of late Wisconsinan glaciation. Similarity of evidence of glacially induced deformation has been found elsewhere in the same bedrock unit within northeastern Ohio.

Within this context, investigations were undertaken to determine the lateral and vertical extent of the tunnel fault, origin and age of deformation, and effect that this deformation could have had on the tunnel design. Many conventional age dating techniques could not be employed because of mineralogy and stratigraphy. Consequentially, in conducting the tunnel faulting study

1241 012

innovative and conventional investigative techniques were employed in supplementing the existing state of site and regional knowledge available for analysis and interpretation.

2.2 INVESTIGATIVE CHRONOLOGY

A comprehensive investigative program evolved as a result of the bedrock deformation exposed during the excavation phase of tunnel construction. Deterministic fault study objectives previously outlined were realized as a consequence of a series of interrelated geologic and geophysical research and engineering. Concurrent with, and subsequent to, tunnel excavations, the nature of the fault plane geometry, gouge, and country rock mineralogical as well as chemical constituents were revealed. After the necessary site specific data had been assembled, the localized anomalous deformation was interpreted in context of its regional geologic setting.

Tunneling activities began in July 1977 after the main shafts and temporary access shafts had been excavated by conventional "drill and shoot" methods. "Drill and shoot" methods were also employed in providing sufficient room at the base of the temporary access shafts for assembling tunnel excavation machines. A DOSCO Roadheader MK-2A tunneling machine excavated 426 linear feet of bedrock mostly south of the temporary access shafts. The remaining 2600 feet of tunneling was accomplished with a Jarva circular bore tunneling machine. The excavation phase was completed in November 1978. Tunnel advancement was documented during the geologic mapping program and is shown on Figure 2. Tunnel and shaft components of the cooling water system are shown on Figure 3.

Tunnel heading advancement was initiated from the intake tunnel access shaft. First, the segment between this access shaft and service water pumphouse intake riser was completed. Then the connecting tunnel to the emergency service water pumphouse was excavated. Both tunnel segments were excavated with the Roadheader MK-2A machine, which was dismantled and removed upon their completion, and reassembled in the discharge tunnel temporary access shaft. Subsequently, tunnel segments between the discharge tunnel access shaft to the

discharge riser in the discharge tunnel entrance structure and a connecting tunnel from this segment to the emergency service water pump house were excavated. Bedrock conditions in these segments were quite good with minimal crown overbreak. Predictably minor, discontinuous and closed vertical to near vertical joints, minimal groundwater seepage, and short-term gas emissions (predominantly methane) were experienced in these tunnel segments. None of these conditions were beyond an anticipated range.

Advancement of the intake tunnel heading to the north from the temporary access shaft began in September 1977 with the Roadheader. In April 1978 the tunneling advancement rate greatly accelerated with the employment of the Jarva. As a routine procedure for these tunneling operations, horizontal exploration boreholes were drilled in advance of the heading. Probe borings which intersected the first tunnel segment containing bedrock deformation yielded gaseous emissions and groundwater. In addition, the variability of probe hole drilling resistance suggested an atypical condition. During the week of April 17, 1978, the Jarva intersected the tunnel fault segment which could not be observed until April 25, 1978, subsequent to sufficient advancement of the Jarva.

A fault plane, oriented normal to the intake tunnel bearing and dipping approximately 16 degrees to the southeast, was identified by the site resident geologists and confirmed by the Project Geologist and an internal project consultant. The apparent displacement, with a thrust sense of motion, was estimated to be less than two feet and the throw less than one foot. The fault plane width was estimated between 0.5 and 18 inches, although the latter was presumed more indicative of gently flexed and/or abruptly kinked or otherwise simply fractured rock. A gray-clay gouge of tough leathery consistency containing small angular shale fragments was observed within the fault zone. This descriptive information was communicated to the NRC.

Samples of gouge were collected and X-ray mineralogical identification conducted on the two micron and smaller size fraction. Results demonstrated a mineralogical assemblage typical of Chagrin shale as reported in the PSAR. On the basis of

the mineralogical data, proximity and physical resemblance between the intake tunnel fault and onshore deformation, and lack of contradictory evidence, a common origin for deformation exposed in the open-onshore and tunnel excavations was suggested. However, the intake tunnel fault exposure occurs more than 100 feet deeper than the deepest known onshore deformation. For this reason other deformational mechanisms, notably stress relief and tectonics, remained plausible origins.

Advancement of the discharge tunnel heading in a northerly direction from the temporary access shaft began in January 1978 with the Roadheader machine, which was withdrawn in February after sufficient room was provided for assembling the Jarva. The Jarva began excavating in August 1978. In late August a tunnel segment was exposed and observed to have been only mildly deformed by compression. A second discharge tunnel segment, more deformed than the first, was encountered. The two discharge tunnel segments containing deformation are separated by approximately 200 feet.

The zones of warping with very small displacement and thrust faulting, respectively, identified in the discharge tunnel were mapped and reported to the NRC. The discharge tunnel fault lies on strike projection with the intake tunnel fault, suggesting that they are the same structure. The zone of minor compressional features preceding the main discharge tunnel deformation was presumed to be either an echelon or a splay of the northeasterly striking thrust fault. Concurrent with exposure of the discharge tunnel deformation, a lake bottom survey and shoreline reconnaissance were conducted. Neither revealed evidence of surface faulting.

More investigative work followed, including a series of exploratory borings, onshore and offshore geophysics, conventional and isotopic analysis of groundwater seepage discharged from the fault, and SEM (scanning electron microscope) analysis of fault gouge. Results of these studies demonstrated that the fault plane maintained a low-angle inclination beneath the intake tunnel more than 600 feet to the southeast. It is uncertain if a deep onshore boring, located at the crest of the shoreline bluff and offset 100 feet from the intake tunnel, intersected the fault. This boring was drilled sufficiently deep so that it

1241 015

should have intersected the fault unless the fault plane attitude changed or the fault zone thins and becomes conformable with bedding.

Borings located approximately one mile west of the plant area along the shoreline and on projection with the fault trace at the bedrock surface did not intersect faulting. Neither the onshore nor offshore magnetic surveys revealed evidence of faulting. Saline discharges from the tunnel fault were determined by isotopic analysis to be meteoric but not Lake Erie water. Preliminary SEM analysis of fault zone gouge showed that new mineral growth bridges had formed across microcracks interpreted to have formed syngenetic with faulting or at least the last fault movement.

A geophysical signature of the fault was provided by compressional wave low-velocity zones. Undeformed bedrock exhibited a relatively high velocity. No low velocity zones were identified in the onshore borings, geophysically logged. It also appeared that a low level of gamma radiation was correlative with fault zone gouge. Longitudinal velocity measurements in the tunnels across the fault indicated that the bedrock was sound in spite of the discontinuity. The velocity values are within the range of those reported in the PSAR for preconstruction site exploration.

Three geologists independently reviewed the tunnel faulting prior to construction of the concrete liner. They determined that the deformation was brittle rather than soft sediment and was not contemporaneous with deposition. Other origins, including direct and indirect glacial action and tectonic, were considered.

A very deep onshore boring was drilled slightly east of the discharge tunnel. In-situ stress measurements employing the hydrofracture technique were performed within the borehole. Subsequent laboratory testing of core from the boring supplemented the in-situ test data. The field and laboratory testing programs were directed by Dr. Jean-Claude Roegiers (Department of Civil Engineering, University of Toronto). Dr. Roegiers also evaluated the in-situ stress and laboratory data.

1241 016

Other aspects of the investigative program included discussions with local resident salt mine engineers, and geologists with knowledge of regional surface and subsurface geology; laboratory determination of gouge physical properties; continuing literature review; and various geological, geophysical, and engineering analyses. Very detailed mapping combined with photographic, video tape, and sound track reproduction of the tunnel bedrock deformation serve as permanent documentation.

2.3 GEOLOGIC SETTING

The Perry Nuclear Power Plant site is situated on the northwestern flank of the Appalachian geosyncline in the Central Lowlands Physiographic Province adjacent to Lake Erie. Bedrock directly beneath the site is the Chagin shale member of the Ohio Shale formation (Upper Devonian). Regionally, these rocks dip gently to the southeast at a gradient of approximately 20 to 40 feet per mile. The Precambrian crystalline basement occurs at a depth slight / greater than 5000 feet. To the south the Devonian strata are overlain by successively younger Paleozoic sediments (see Figure 4).

Lake Erie, which lies several hundred yards north of the plant area, has a maximum depth of approximately 210 feet and an average depth of 58 feet. The western end of the Lake is extremely shallow and is immediately underlain by resistant carbonate bedrock. From the general vicinity of Sandusky, Ohio, to the east beyond the Pennsylvania boundary, Lake Erie has been eroded into Upper Devonian shales which overlie the relatively more resistant rocks comprising the lake bottom strata of the western portion.

In northeastern Ohio glacial drift and glaciolacustrine sediments overlying bedrock reach a maximum thickness of 250 feet. The site is located on the Lake Plains Section, a physiographic subdivision of the Central Lowlands province formerly submerged during higher Lake Erie levels. Here, bedrock overburden deposits ranging in thickness from 55 to 60 feet consist of dense till and lacustrine sediments, respectively. A steep bluff contiguous to the shoreline exposes 40 to 45 feet of overburden stratigraphy (see Figure 5 for glacial deposits).

Secondary structures demonstrative of bedrock deformation in the site vicinity, as well as throughout northeastern Ohio, are rare. This is attributable to the nearly ubiquitous veneer of glacial deposits obscuring bedrock, the minimal effect of the Alleghenian (Appalachian) Orogeny on Paleozoic strata in this region, and the attenuation of Alleghenian orogenic stresses during their northwestward propagation beyond the Appalachian Structural Front.

Most of the subsurface structural interpretations for these regions are founded on deep well data. It is reported by Stone and Webster, based on personal communication with A. Janssens, formerly employed by the Ohio Geological Survey, that the sedimentary sequence above the Middle Devonian Delaware Formation is affected by folding. Structural contours of the Delaware and Dayton Formations prepared by Stone and Webster show persistent small structures, probably folds, especially in Portage County, Ohio.⁽¹⁾ Structural contour maps of the "Big Lime" top (Delaware) and a definable geophysical base (Packer Shell) approximately 50 feet below the stratigraphic base of the "Big Lime," and an isopachous map of the intervening interval were prepared to determine subsurface structure in Lake, and adjacent Counties (see Figures 6, 7, and 8). "Big Lime" is a shortened drillers' expression for the thick Silurian-Devonian carbonate and evaporate sequence known as "Big Niagaran Lime." The only anomalous structures revealed are located in central Ashtabula County. Apparent thickening of the "Big Lime" in this region, due to faulting or folding, may be attributable to Appalachian orogenic stresses. No shallow deformation in that locale is known.

Salt mining has exposed deformation within the Salina beds. Heimlick describes minor folds, amplitude of six inches, and wave length less than twelve inches, locally overturned, in the production interval of the International Salt Co. mine in Cleveland.⁽²⁾ Structural contours of the salt production interval for the Morton Salt Division of Morton Norwick mine in the Painesville area reveal northeasterly trending synclinal troughs interpreted by Jacoby to be salt flowage preceding faulting in response to Appalachian tectonism.⁽³⁾ However, large scale folding in Lake County of either the salt or overlying shale strata is not present in surface or subsurface exposures, nor interpreted from subsurface geological or geophysical data.

Faulting is nearly as anomalous as fold structures but does affect Paleozoic strata to the south and has been exposed in the International Salt Company mine in Cleveland to the west. More locally, Jacoby reports that a high angle thrust fault intersects the salt production interval of the Morton Salt Division of Morton Norwick mine in Fairport Harbor, approximately eight miles southwest of the Perry site.⁽³⁾ He does not believe that this fault is pervasive vertically through the Oriskany Sandstone of Middle Devonian age.

Rock cores from salt strata exploratory borings in the Painesville area occasionally intersect displacements within the "Big Lime" of a very minor nature, amounting to a few inches at most, which are completely healed. Donald R. Richner, consulting geologist, has examined these discontinuities, which range from very minor to miniscule, consisting mainly of stylolites and minor slips with traces of slickensides but having observable displacements of two inches at most. He has not seen any evidence that these discontinuities were of a tectonic origin. Those observed above and below the Salina salt beds appear to result from penecontemporaneous deformation.⁽⁴⁾

Geologists are in agreement that the faulting and folding exposed in the International Salt Co. and Morton Salt Division of Morton Norwick mines in Cleveland and Painesville, respectively, are attributable to dissolution of the salt during sediment lithification.^(2,3,4) Subsequent failure of the overlying strata resulted in graben structures, slumping, and down-warping dependent upon overlying lithology. Locally, salt flowage into fractures and irregularly shaped cavities is evident.

The only well-documented fault near the site locale is a relatively minor localized overthrust with approximately one foot of displacement in the Bedford shale (Mississippian age), known as the Gabor Fault (Prosser).⁽⁵⁾ The minor thrust fault described by Prosser was observed in the field on the east bank of Bates Creek, also known as Warners Creek. The strike of this fault is northeast. Three faults, not reported in the literature, were found on the west bank of the Paine Creek about one mile north of the Bates (Warners) Creek

1241 019

fault. These faults, two gravity faults, and a small bedding thrust fault, named Hell Hollow 1, 2 and 3, were found to be associated with slumping. These site locale faults are shown on Figure 9.

Field investigations and literature studies were completed to determine the characteristics, origin and age of both the Bates (Warners) Creek and Hell Hollow faults. Those faults were determined to be of surficial nature, limited in extent and unrelated to deep-seated faulting. Their origin is concluded to have been glacially induced at Bates Creek and related to rock slumping at Hell Hollow.

Geologic mapping, inspection, and evaluation of bedrock foundations, including excavation cuts and foundation grade, for the plant area structures were initiated in August 1975. Several localized areas of deformed bedrock were revealed as a consequence of the excavation. The deformation consisted of folds and faults within the Chagrin shale. Vertically, the lower limit of the onshore deformation was established at a horizon defined by the deepest foundation excavations, specifically those for the condensate demineralizer and heater bay buildings. The upper limit of this deformation terminates at the base of a boulder layer, which maintains grade at approximate elevation 570 feet and is pervasive throughout the plant site. The boulder layer defines the base of structureless lower till. Below the boulder layer and above competent shale, a six- to eight-foot thick transitory interval was mapped in which the lower till has been incorporated within contorted, blocky, and weathered shale. The relationship of the onshore deformation to tunnel faulting is shown on Figure 10.

1241 020

The purpose of the studies was three-fold: first, to determine lateral extent of the fault observed in the intake and discharge tunnels at the Perry site; second, to analyze the type and degree of fracturing within and adjacent to the fault; third, to examine in detail the seismicity of the area surrounding the Perry plant; and fourth, to investigate the origin of deformation.

The following techniques were used in determining the extent of the fault on land and on the bottom of Lake Erie:

- o Literature review and personal communications with geologists cognizant of area geology (surface and subsurface)
- o Exploratory borings
- o Shoreline reconnaissance
- o A video survey of the bottom of Lake Erie in the vicinity of the updip projection
- o Detailed geologic tunnel mapping of deformation
- o Microcrack analyses of fault zone samples
- o Analysis of water from the fault and from Lake Erie
- o Evaluation of published and unpublished geophysical data
- o Magnetic (total field) profiling (both onshore and offshore)

1246 021

- o Borehole (in hole) logging of (compressional) wave velocity
- o In-situ seismic velocity measurements
- o An evaluation of the seismicity in the area surrounding the Perry plant was made on a very detailed search on period newspapers and other document
- o In-situ borehole stress measurements to determine stress field orientation, magnitude and gradient (vertical)

The detailed mapping, lake bottom survey, and geophysical and seismological studies were performed by the Weston Geophysical Corporation

3.1 GEOLOGIC

3.1.1 LITERATURE REVIEW AND PERSONAL COMMUNICATIONS

Published and unpublished sources were reviewed in order to learn more about the surface and subsurface bedrock structure in northeastern Ohio. These activities were supplemented by personal communications with resident engineers at two salt mines (Mr. Jaroslav Vaveeka, Cleveland mine, International Salt Company and Mr. B. C. Cummings, Painesville mine, Morton Salt Division of Morton Norwick) and Mr. Robert G. Van Horn, Head Regional Geology Section, Division of Geological Survey, Ohio Department of Natural Resources. Two consultant geologists, Mr. Donald R. Richner and Mr. Charles R. Jacoby, with considerable experience of subsurface geology from exploratory drilling and mining operations in northeastern Ohio, were also contacted. Finally, three independent reviews of the cooling water tunnel faulting were performed by the following recognized for their respective specializations:

1241 022

Dr. Robert LaFleur
Pleistocene Geology and Sedimentology
Rensselaer Polytechnic Institute

Mr. James Murphy
Areal Geology and Stratigraphy of Northeast Ohio
Ohio Historical Society,

Dr. Barry Voight
Structural Geology
Penn State University

Mr. Murphy had been contacted previously to provide independent opinions during Applicant evaluations of bedrock faulting in the site locale and onshore plant area bedrock deformation exposed by excavation. He had also arranged for radiocarbon dating of comminuted plant material obtained from the site lacustrine deposits. Results of this dating ($14,480 \pm 310$ B.P.) established an age somewhat older than previously assumed for the retreat of Hiram ice and a minimum age for the onshore plant excavation deformation.

Data and evaluations of an offshore shoreline parallel survey, especially in the vicinity of the site, conducted by the Coastal Engineering Research Center, were forwarded by Mr. S. Jeffress Williams, marine geologist, Geotechnical Engineering Branch. The survey consisted of high resolution seismic reflection profiling suitable for evaluating abrupt elevation changes in the lake floor or acoustic contrasts of sediments, both potential indicators of faulting.⁽⁶⁾

3.1.2 EXPLORATORY BORINGS

The TX-test boring series was conceived for the purpose of tracing the downdip extent of faulting intersecting the cooling water tunnels at the site (see Figure 11). Drilling operations occurred within the intake tunnel excavation, on the shoreline bluff, and along the beach west of the site. TX-1 through 6 were in-tunnel, the first test holes of the series. Limiting conditions dictated the use of a powered drill, mounted on a steel "A" frame, stabilized by two expanding rods braced against the tunnel crown. This system implemented

1241 023

an NX-size, diamond bit, single-tube core barrel. Both air and water were supplied by existing utility lines used in tunnel construction. An additional air line was used to dissipate natural gas inflows encountered in drilling. Drilling operations on the shoreline bluff (TX-7, 11, and 12) were conducted from truck mounted drill rigs. TX-8, 9, and 10 were drilled on the beach from an ATV (all terrain vehicle) mounted rig.

In-tunnel borings were laid out at progressively greater distances south of where the fault plane intersects the intake tunnel invert. TX-1 was located five feet south of the fault-invert contact, assuring advance through the fault plane would occur at a very shallow depth. In order to establish characteristic indicators of test hole advance through faulted rock, close attention was paid to all aspects of sampling in the initial hole. After each core run a gas detection meter was used to measure concentrations of methane emitted from the drill water. This device was also used for safety purposes. Cognizance of indicators from TX-1's advance aided in interpreting intervals in subsequent holes where faulted rock was projected to greater depths.

Test borings drilled from the shoreline bluff sought to encounter the fault at greater depths than those of the in-tunnel boring group (several hundred feet rather than 2 to 90 feet below tunnel invert elevation).

The group of test borings located on the beach was designed to encounter a shallow southwesterly projection of the fault based on limited strike measurements attained from exposures in both tunnels and previous TX-series borings.

Several types of in-hole testing were performed in TX-series holes. The Weston Geophysical Corporation conducted gamma and sonic velocity logging to confirm fault zone identification. In addition to this, a long steel "feeler" probe (length, 10 feet) was implemented in shallow holes TX-1, 2, and 3. A hydrofracture in-situ stress measurement study was performed in the deepest boring of the TX series (730 feet). This effort was planned and directed by Dr. Jean-Claude Roegiers (Project Consultant). Instrumentation was supplied by Serv-Kor, Inc. and pressurized fluid capability by Halliburton Services.

All rock core samples of the TX-series were logged in detail and photographed. All pertinent and representative core was wrapped in clear plastic.

3.1.3 SHORELINE RECONNAISSANCE

Continuous shoreline reconnaissance southwest and northeast of the site was performed with the objective of identifying evidence of offset or structural disturbance in the lacustrine and till deposits exposed by the shoreline parallel bluff contiguous to Lake Erie. Reconnaissance was conducted a considerable distance beyond the land surface projection of the intake and discharge tunnel faulting (see Figure 12).

3.1.4 VIDEO EXAMINATION OF LAKE BOTTOM FEATURES

An underwater camera survey of the lake floor was conducted to permit close examination of the lake bottom by a diver, and provide visual aid and documentation for other technical personnel. The intent was to examine the bedrock surface for the presence of structural features. The floor of Lake Erie, offshore of the Perry Nuclear Power Plant, essentially consists of a bedrock surface with a very thin covering of silt. Locally, the bedrock surface is covered by concentrations of boulders and cobbles.

The video survey consisted of two parallel east-west traverse lines, labeled Lines A and B, approximately 800 feet in length and 200 feet apart, previously located and horizontally surveyed offshore of the Perry Nuclear Power Plant. The lines were selected to cover the vicinity of the updip projection of the fault noted in the intake tunnel, and to cross the projected continuation of the fault to the east.

Each traverse line consisted of five relatively evenly-spaced stations. The video coverage was circular in fashion around each station to a maximum radius of approximately 75 feet. Figure 13 shows the location of the traverse lines and stations, as well as the area of coverage around each station.

1241 025

The diver, equipped with an underwater compass, described and noted the orientation of bottom features as he moved relative to the lake floor. A two-way communication system with surface monitor permitted the surface operator and other technical personnel to discuss the bottom conditions with the diver at the time of the survey, and to request detailed examination of specific features of interest. In all instances, the original videotapes have been retained in their entirety.

3.1.5 DETAILED GEOLOGIC MAPPING IN THE INTAKE AND DISCHARGE TUNNELS

Four hundred lineal feet of tunnel wall rock exposure were mapped to study and document the nature of bedrock deformation encountered in the intake and discharge tunnels at the Perry Nuclear Power Plant. The field mapping was carried out in the period from February 15 through 27, 1979. One structure was mapped in the intake tunnel at Stations 10+25 to 10+95. Two bedrock structures were mapped in the discharge tunnel at Stations 11+40 to 12+00 and 13+00 to 13+70. Both walls were mapped in each area. Rock bolts, straps, and wire mesh on the crown, and muck and rails on the invert prevented mapping of these surfaces. Approximately 7 vertical feet of wall were mapped on each tunnel wall. Figures 14 and 15 show the location of intervals mapped in the intake and discharge tunnels, respectively.

Mapping was carried out subsequent to placement of stations every 5 feet, as well as three constant elevation lines at 2-foot intervals, along the entire mapped tunnel wall area. Survey control for the stations and elevations lines allowed all mappable features to be located by a standard 6-foot rule and transferred to cross section paper at a scale of 1 foot to 1 inch. The minimum resolution of the beds mapped was 0.5 inches or approximately 1.0 centimeter.

Photomosaics of the entire mapped areas were composed from professionally taken photographs. Closeup photomosaics of the fault zones in both tunnels provide detailed documentation of these structures. The mapped areas of both tunnels were videotaped; approximately 3 1/2 hours of videotape were acquired. In all instances, the original videotapes have been retained in their entirety.

1241 026

3.1.6 MICROCRACK ANALYSIS

A microcrack analysis was performed on samples of gouge obtained from the faults in the intake and discharge tunnels at the Perry site. These investigations were performed by Dr. Gene Simmons whose complete report is included as Appendix A to this report. The following is a summary of the methods of investigation employed by Dr. Simmons.

Microcrack samples were acquired by Dr. Simmons and Weston personnel from the fault zone in both the intake and discharge tunnels.

The samples were acquired in such a way as to minimize production of microcracks during sampling. Upon acquisition, the samples were carefully packed and transported to Dr. Simmons' laboratory for analysis.

Laboratory analysis of the samples involved examination of individual microcracks with a scanning electron microscope (SEM) to determine crack length and extent of filling. An electron dispersive X-ray system (EDX) was used to determine the elemental composition of the material filling the observed cracks.

The details of the sampling procedure and laboratory analysis for the microcrack studies are discussed by Dr. Simmons in his report, Appendix A to this study.

3.1.7 WATER ANALYSIS

Chemical analyses of intake and discharge tunnel faulting seepage samples were performed. Ionic concentrations were obtained for chloride, sulfate, and sodium. In addition, salinity and pH measurements were conducted on each sample. Comparative evaluation of data provided information on trends.

The isotopic ratios of D/H and $^{18}\text{O}/^{16}\text{O}$ were measured with a mass spectrograph for three water samples from the fault in the intake tunnel, one sample from the fault in the discharge tunnel, and two samples from Lake Erie. A sulfur

1249 027

isotope analysis was attempted on samples of water from the intake and discharge tunnels and from Lake Erie. The sulfur analysis did not succeed because of the lack of sufficient sulfur for analysis in any of the tunnel samples.

Appendix B to this report prepared by Dr. Gene Simmons presents the basis of the technique for the hydrogen and oxygen isotope analysis.

3.2 GEOPHYSICAL STUDIES

3.2.1 EVALUATION OF PUBLISHED AND UNPUBLISHED DATA

Published and unpublished geophysical data for the immediate vicinity of the Perry nuclear site were examined for any anomalies which could be related to the fault noted in the intake and discharge tunnels. The examination consisted of a review of published and unpublished geological and geophysical data, as well as federal and state government reports and data files.

3.2.2 MAGNETIC SURVEYS

3.2.2.1 Offshore

Total field magnetometer data were obtained over the projected strike of the fault to determine whether or not an associated magnetic signature was present. A shipborne magnetic survey of Lake Erie consisted of 17 lines, perpendicular to the projected strike, at 200-foot intervals (Figure 16). Coverage was essentially continuous along each profile, and the data were displayed by means of a strip charge recorder at a vertical scale of 200 gammas/inch.

3.2.2.2 Onshore

For onshore coverage, four separate lines were traversed with readings taken every 25 feet (Figure 17). Lines were operated along existing roads, which resulted in profiles oriented at 45° to the projected strike.

1243 028

All data were obtained with a proton-precession magnetometer. For a further discussion of the magnetic survey method refer to Appendix C, Section 2.0.

3.2.3 BOREHOLE LOGS

Gamma radiation and velocity logs were obtained in drill holes located in the intake tunnel and on the shore. Figure 11 is a borehole location map. The objective of these measurements was to locate geologic units to be used as markers in determining the offset of the fault and/or to provide means of locating the fault itself.

The velocity logger measures the difference in the travel time for seismic energy, moving up a drill hole from a common source to reach two geophones separated by a known distance. It provides a rapid, accurate measure of the in-situ seismic velocities ("P" and "S" wave values) in the material between the two geophones. For a further discussion of seismic velocity logging refer to Appendix C, Section 4.0.

Measurements were made at 1/2-foot intervals adjacent to the projection of the fault and at 1-foot intervals for a distance of 10 to 20 feet away from the projection. Selected boreholes (TX-6, TX-4, and TX-7) were logged at a 1-foot interval for their entire length.

The gamma logging was accomplished with a probe which measures the gamma radiation incident on an enclosed scintillation sensor as it moves up the hole. In sedimentary rock sequences, the instrument responds primarily to shale content, because radioactive elements tend to concentrate in shales and clays. At the site, the logs were obtained using two rates of ascent up the hole (20 ft/min and 3 ft/min). The slower rate provides a smaller sampling interval and, thus, greater resolution. For further discussion of gamma radiation logging refer to Appendix C, Section 3.0.

1243 029

3.2.4 IN-SITU VELOCITY MEASUREMENTS

A seismic in-situ velocity survey was conducted to examine the condition of the tunnel wall in both the intake and discharge tunnels in the vicinity of the fault.

Seismic velocity values are diagnostic of rock conditions in tunnels and provide a comparison between rock in and adjacent to the fault and rock located some distance from the fault. For further discussion of in-situ velocity measurements refer to Appendix C, Section 4.0.

In the intake tunnel, a 6-geophone spread (each geophone has 3 components) and a 12-geophone spread (each geophone has one horizontal and one vertical component) were used. Geophones were separated by 10-foot intervals, and each spread was centered on the observed fault (Figure 18). In the discharge tunnel, data were obtained across the fault and across a fracture zone located 100 feet south of the fault (Figure 19). Two spreads were used across the fault, both with 12 (two-component) geophones. The first had 10-foot spacings with the fault located 10 feet south of the center of the spread; the second had 5-foot spacings for higher resolution and was centered on the fault. The velocity measurements across the fracture zone were obtained with a 12-geophone spread with 5-foot spacings centered on the fracture zone.

Three-component geophones, which detect vibration energy along vertical, radial, and transverse alignments, were placed on pedestals drilled into both the intake and discharge tunnel walls. Seismic energy was generated by a hammer blow against the tunnel wall adjacent to a geophone.

3.3 EVALUATION OF LOCAL SEISMICITY AROUND THE PERRY NUCLEAR POWER PLANT SITE

A detailed examination of the local seismicity around the Perry site was performed with the purpose of evaluating the validity of each epicentral location and intensity for all reported events.

1298 030

A parallel compilation of all cataloged entries was made, and subsequently a local newspaper search was initiated to collect additional supporting evidence for each event. The details on the sources of the data base and the texts of all new material acquired are presented in Appendix H. A separate summary evaluation was then prepared for each historical event within the 50-mile radius of the site, taking into account cataloged entries as well as the entire file of supporting evidence.

3.4 IN-SITU STRESS MEASUREMENTS

Hydraulic fracturing was performed in test boring TX-11 in order to determine the magnitude and orientation of the in-situ principal stresses. Eight intervals were fractured between a depth of 394 and 718 feet. TX-11 boring rock cores were subsequently tested in the laboratory in order to provide confirmatory tensile stress data of the field data. The in-situ borehole stress program was planned and directed by Dr. J. C. Rocgiers, Department of Civil Engineering, University of Toronto. The in-situ stress program methods results and conclusions are appended to this report (see Appendix E).

124' 031

4.0 RESULTS

4.1 GEOLOGIC

4.1.1 LITERATURE REVIEW AND PERSONAL COMMUNICATIONS

As reviewed in Section 2.3, Geologic Setting, bedrock throughout northeastern Ohio is not known to have been significantly affected by late Paleozoic orogenic stresses or any other tectonic disturbance. Faulting in the sequence of evaporite and carbonate rocks comprising the Salina Group has been exposed in salt mines within the region. These faults are attributed to dissolution of salt beds followed by failure of the overlying carbonate beds. Structures of this type are generally believed to have been developed shortly after sediment lithification. Alternatively, late Paleozoic orogenic stresses may have been sufficiently high to have caused salt flowage which induced brittle deformation of the interbedded, more competent carbonate beds.

Salina Group strata begin at a depth of approximately 1750 feet beneath the site. Correlations between site borings and regional exploratory drill holes do not suggest the existence of any pervasive fault or fault system. Neither top and bottom structure contour nor isopachous maps of the "Big Lime" support the concept of a regional fault or fault system (see Figures 6 to 8). In the context of regional geology there is no basis for lateral extrapolation or deepening of the tunnel faulting. Shallow bedrock deformation is exposed in outcrop seven to eight miles south of the site and had been exposed in plant area excavations. However, these structures terminate with depth on undeformed strata. The outcrop exposure deformation was the result of glacial shove and loading (Bates Creek) and slump (Hell Hollow). Plant area bedrock deformation was caused by late Wisconsinan glacial shove and loading. A minimum age of $14,480 \pm 310$ B.P. (Hiram ice) for the plant area deformation is inferred from a radiocarbon date of the organic debris interbedded within lacustrine sediments.

1241 032

Independent opinions provided by the three reviewing geologists are in agreement that the tunnel faulting is not penecontemporaneous but is most likely caused by localized stresses created during Pleistocene time by either the advance of the ice sheet(s) and concomitant depression of the crust, or in reaction to removal of weight of the overlying ice (glacial rebound). In addition, Dr. Robert LaFleur was requested to review the data, interpretations, and conclusions of earlier investigations regarding the stated origin of the Bates Creek, Hell Hollow, and plant area deformation. He concurs that the Bates Creek and plant area deformation are the result of glacial shove and loading (active glaciotectionics) and the Hell Hollow vertical faults were the result of post glacial slumping. These opinions had been stated in the earlier investigations by Mr. James Murphy. Dr. LaFleur does not believe the tunnel faulting is demonstrative of either active or passive glaciotectionics. In his opinion the deeper tunnel faulting is a response to the state of stress imposed by glaciation during advance or subsequent to recession (glacial rebound). Dr. Barry Voight considered other modes of Paleozoic deformation in addition to late Paleozoic tectonism including Mesozoic-Tertiary tectonics and miscellaneous Pleistocene - Recent faulting mechanisms. Opinions of the three reviewers are attached to this report in Appendix D.

4.1.2 EXPLORATORY BORINGS

Fault zone indicators, revealed in the advance of X-1, 2 and 3, were as follows: (1) increased vibration in drill rods; (2) a creamy grey influx to a normally light grey drill wash; (3) platy clay particles in drill wash; (4) a release of gas when the core barrel was pulled after the run; (5) a 0 to 80 percent recovery in the cored fault zone (recovery in undisturbed rock was consistently very high); (6) highly broken, rotated rock frags speckled with remnant grey clay for those portions of the fault zone that were recovered; and (7) a change in the dip to normally flat lying laminae, above, and below the fault zone.

1241 033

All indicators did not occur in each boring where a fault zone was suggested. In fact, only the loss of recovery and the character of rock that was recovered from suspect fault zones remained consistent throughout those borings. Using these indicators, a fault zone was detected in all of the in-tunnel borings, TX-1 through 6. The boring locations and depth where faulted rock was identified revealed a constant fault plane dip of 17 degrees SE. Low gamma radiation levels and low P-wave (compressional) velocity values coincided with zones of disturbed rock at elevations where a fault zone was logged from drilling program indicators in TX-2, 3, 4, and 6. TX-1 was too shallow to log geophysically and TX-5 caved at the fault preventing geophysical logging of the suspect zone.

The constant 17 degree fault plane dip derived from TX-1 through 6 aided in the location of TX-7 through 12. TX-7 was initially advanced to a depth of 395 feet from the shoreline bluff. Increased rod vibration, loss of core recovery, remnant clay on broken, rotated shale fragments, and a stuck core barrel (eventually retrieved and coated on the bottom three feet with a thin grey clay) indicated a disturbed zone from 371.3 to 372.4 in TX-7. Geophysical logging, however, did not confirm this zone. It is suspected that a lack of proper drill water circulation may have caused increased friction at the core barrel, falsely suggesting a zone of disturbance.

TX-8, 9, and 10 were drilled along the beach west of the site. Both TX-8 and 10 encountered zones of broken rock with what appeared to be minimal clay remnants from depths of 65.85 to 66.7 feet and 63.5 to 64.9 feet, respectively. Minimal loss of recovery was measured in both zones. Geophysical logging, however, did not recognize disturbed rock in either TX-8, 9, or 10.

TX-11 was drilled approximately 1060 feet southeast along dip direction of the intake tunnel fault exposure. This boring was the deepest of the TX series, drilled to a depth of 730 feet down from the shoreline bluff. No naturally disturbed rock was encountered in the entire borehole length. Three runs of core were disturbed by uncontrollable core barrel handling because of gas inflows. Hydrofract stress measurements were performed in this hole in test intervals between 394 and 718 feet.

1254 034

Angle hole TX-12 was drilled from approximately the same location as TX-7. The drill rig employed a wire-line, double barrel system. The double barrel was actually able to core the fault zone materials with very little loss in recovery from 376.4 to 380.0 feet. This boring confirmed the continuation of a 17 degree SE fault plane dip, approximately 230 feet horizontally southeast of the last confirmed fault zone occurrence in tunnel-boring TX-4. Cored fault zone materials included angular shale fragments within several grey, clayey, gouge seams, broken fractured rock, and rock laminae with multiple dips. TX-12 was completed at an angle depth of 480.0 feet.

After the completion of TX-12, TX-7 was reamed and extended 100 feet using the double barrel wire line system. A disturbed zone was encountered from 412.8 to 413.9 feet, vertical depth. Unlike TX-12 a gouge zone was not recovered. Increased drill rod vibration, a 100 psi increase in drill water pressure, 50 percent loss in recovery, and broken rotated rock, speckled with grey clay remnants suggested a zone of disturbance. If this zone represents the fault, its location marks an increase in fault plane dip between TX-12 and the extended TX-7.

Geologic logs of TX-series borings are attached as Appendix F.

4.1.3 SHORELINE RECONNAISSANCE

Traverses northeast and southwest of the plant area along the shoreline and headward in stream cuts emerging at the beach revealed no offsets or structural disturbance of the exposed lacustrine and till deposits. A boulder layer which occurs at the base of structureless lower till is not offset and maintains a constant elevation within the lake facing bluff. An absence of bedrock outcrops and maintenance of boulder layer elevation are demonstrative of the lack of surface faulting.

1241 035

4.1.4 VIDEO EXAMINATION OF LAKE BOTTOM FEATURES

The video survey of the Lake Erie bottom in the vicinity of the nodip projection of the fault did not indicate the presence of any long continuous fractures parallel to the projected fault trace. Those fractures which are noted show no evidence of lateral or vertical offset and seem to close with depth. Figure 20 shows a schematic diagram of the fracturing on the Lake Erie bottom.

4.1.5 DETAILED GEOLOGIC MAPPING IN THE INTAKE AND DISCHARGE TUNNELS

4.1.5.1 Stratigraphy

Chagrin shale at Perry, is on the order of 800 feet thick⁽⁷⁾ based on reported thicknesses of 500 feet at Cleveland and 1,200 feet at the Ohio-Pennsylvania border (see Figure 21). Accordingly, the sequence of strata exposed in the tunnels is assigned here to the stratigraphic center of the Chagrin and is considered representative of the unit. This placement is consistent with the absence, within the tunnels, of marginal lithologic sequences and fossiliferous strata.

In both tunnels, the strata dip westward to northwestward about 2 degrees (for the detailed mapping sections see Figures 30 and 32). Most of the units are quite persistent in down-tunnel directions, and because the tunnels are random exposures of the internal geometry of the Chagrin, there is reason to assume that the observed units and sequences are equally persistent from east to west, and that a part of the mapped sequence should appear in both tunnels. Inasmuch as attempts to establish a correlation between tunnels were unsuccessful, it is concluded that the strata exposed in the intake tunnel pass below the discharge tunnel, and that the described sections are separated by a very short interval of unexplored strata. These relationships and detailed descriptions of the mapped intervals are presented on Figures 22, 23, and 24.

1241 036

The Chagrin strata exposed in the tunnels were subdivided to provide a framework within which folding and faulting in the tunnels could be described and interpreted. Unit boundaries were selected according to their mapability across tunnel wall exposures smeared during excavation and subsequently stained and otherwise obscured by minor surficial weathering. There is no genetic significance implied in their selection.

Bedding characteristics and stratigraphic relationships were examined to determine depositional modes and the role of penecontemporaneous deformation in the genesis of the folds and faults. The characteristics considered most significant in their regard are: (1) the attitude of the strata; (2) their thickness; (3) their composition and texture; and (4) the detailed nature of their boundaries.

The near-horizontal attitude of the strata and their marked planarity indicate clearly that the immediate substrate during deposition was similarly flat and featureless, a relatively stable distal shelf environment considerably removed from a postulated northerly source of clastic detritus. Minimal sand-size material reached this part of the shelf, and sedimentary structures and bedforms related to sand deposition are nowhere apparent. There is scant evidence, for example, of bedload transport of detritus, and none whatsoever of either outbuilding or proximal deposition from density currents, any of which would have produced a geometry significantly different from the planar parallel configuration of the tunnel sequence. Virtually all sediment exposed in the tunnel reaching the site area must have been deposited from periodic suspension clouds by processes of vertical accretion.

Bedforms and stratigraphic patterns indicate that sedimentary cycles begin at the sharply defined upper boundaries of prominent siltstones or siltstone-shale bedsets. These commonly exhibit asymmetrical ripple marks and, very locally, are truncated to a limited extent; overall, they suggest modification by bottom currents of low velocity and constant direction. These apparently were

1241 037

effective in distributing the limited amounts of available silt over fairly wide areas, probably through ripple migration; but, for the most part, were not competent to substantially modify the deposits or entrain the silt once deposited. The presence of thin shale laminae within many siltstone beds suggests that even winnowing was at times an ineffective process. During such periods of maximum current intensity, suspended detrital clay and buoyant organic debris must have been carried farther basinward and incorporated in the more distal black shale equivalents of the Chagrin.

Although the siltstones lend themselves readily to megascopic and microscopic analyses and are revealing of process-related structures, shale is everywhere the dominant lithologic-type comprising the lower, thicker part of each cycle. These are mainly dark-gray, clay shales with planar to broadly wavy, very sharply defined laminae, 1 mm to 2 cm thick, of purplish to brownish, clay shale. The laminae, reportedly sideritic in composition, impart a "banded" aspect to the beds; there is no discernible disparity in texture between the shale types to indicate fluctuations in depositional processes. Instead, the "banding" likely reflects oscillations in geochemical parameters and possibly detrital clay mineral composition. The shales, therefore, are considered simple beds deposited under uniform sedimentological conditions, and rapid, spasmodic, or uneven deposition of mud are essentially ruled out by their internal structure. Additionally, the general absence of load structures at shale-siltstone boundaries suggests that the mud substrate was quite viscous at times of silt deposition and also that the basin was seismically inactive.

Thickness variations in these strata are restricted to the attenuation and pinch-out of some of the more prominent siltstone beds. These are sedimentary in origin, locally modified by compaction of the section. Their effects on the thickness of the mapping units is negligible.

The indicated depositional setting, dominated by the process of slow vertical accretion, winnowing, sublevation, and bypassing, virtually precludes the possibility of rapid sedimentation at or near the site during Chagrin sediment deposition. Localized buildups of clastic sediment and primary slopes steep

124d 038

enough to generate adjustments by slumping are clearly inconsistent with the conditions postulated. Moreover, had faulting occurred prior to total consolidation, the adjacent strata, given their clayey composition, would certainly have been thrown into a series of folds and pull-apart structures, lithologic boundaries would have been grooved and polished, and shale thicknesses would have been considerably affected. In particular, those strata between the main fault and the main splay (intake tunnel, Station 10+50 to Station 10+80) would certainly have been markedly distorted. None of these criteria for penecontemporaneous faulting are met in this instance. Instead, the strata are little affected to within very short distances of the fault itself where the bedforms exhibit brittle deformation as subsequently discussed.

4.1.5.2 Tunnel Structural Geology

Tunnel excavation for the intake and discharge tunnel structures exposed three limited zones of bedrock deformation in the Chagrin shale (Figures 14, 15, and 25). This deformation is characterized by low-angle thrusting, fracturing, and small-scale folding. Deformation in the intake tunnel extends from Station 10+85 to Station 10+55 (Figure 26). Similar deformation occurs in the discharge tunnel from Station 13+65 to Station 13+25 (Figure 27). In the discharge tunnel from Station 11+50 to Station 11+80 (Figure 28), an interval of disturbed rock is recognized. Figure 29 contains geologic maps of the intake and discharge tunnel deformation.

4.1.5.2.1 Intake Tunnel Structure

Bedrock deformation exposed in the intake tunnel extends from Station 10+85 to Station 10+55 (Figure 30). Deformation consists of a low-angle thrust fault which strikes and dips approximately N51E, 18S (Figure 31). Stratigraphic offset is 1.4 feet with the strata to the southeast, upthrown. The throw becomes slightly less (i.e., 0.8 feet) towards the crown of the tunnel.

1241 039

The brittle nature of this deformation is exemplified by the development of fractured and broken drag folds, kinks, and angular/flaggy fragments of siltstone and shale adjacent to and in the prominent gouge zone and dip-slip striations (Figure 30 and 31).

The gouge is light gray, plastic clay with angular fragments of siltstone and shale derived from the adjacent strata. (See Appendix G for laboratory testing of gouge samples.) Gouge development is greatest where the main fault component is inclined and thinnest where the fault is bedding parallel. Associated with thrusting are numerous thin (0.1 feet) splays of gouge along which the strata have been offset. Offsets are somewhat variable but are on the order of 0.1 feet to 0.3 feet. In all instances, these stringers/splays are initiated at the main fault zone and die into bedding planes away from the deformation.

Drag folding is both well developed and quite pronounced. Locally, a faint axial plane cleavage is developed at the fold hinges. Drag folds are asymmetric, northwest verging, and exhibit a distinct bedding plane parting facility. Thin seams of gouge occur in the hinge area and parallel to this facility. Orientations of drag fold axes are parallel to the strike of faulting.

Numerous striations are recognized on both the hanging wall and foot wall (Figure 31). Striations indicate the fault movement is dip slip and does not exhibit any strike-slip component. Striations are primarily developed along the bedding parallel sections of the fault but are also recognized in the inclined sections.

To the immediate south of the intake tunnel thrust, an asymmetric syncline is exposed (Figures 26 and 31). Based on limited exposure, deformation associated with folding dies out up section and increases down section. The east wall of the intake tunnel exhibits a greater degree of fold deformation than the west wall. This fold is characterized by bedding parallel flexural slip and minor northwest-dipping thrusting on the northwest limb of the fold (Figures 26 and 31). Offset is minimal (0.1 feet to 0.2 feet), with thrusts merging with bedding planes.

1241 040

Detailed examination of the intake tunnel fault (Figure 26) indicates that the hanging wall is apparently more deformed than the footwall; deformation is brittle in nature and appears to diminish up section.

4.1.5.2.2 Discharge Tunnel Structure

Two zones of bedrock deformation are exposed in the discharge tunnel (Figures 27 and 28). Both structures are the result of compression. The structure closest to the shoreline is very minor and essentially a kink fold with very minor displacement along the hinge line. The second and furthest offshore structure is similar to the intake tunnel fault.

The nearshore structure is located approximately at Station 11+70 (Figure 28). Most of the deformation was accommodated by abrupt monoclinial strata bending. The hinge line (plane of deformation) has a strike and dip of N16E, 35SE (Figure 25). Stratigraphic offset dies out below the tunnel crown into a fractured/flexed zone immediately overlain by flat-lying strata. At the invert, the stratigraphic offset (mostly attributable to monoclinial flexure) is approximately 0.4 feet with the southeastern strata upthrown. Distinctly zig-zag in character, the structure exhibits gouge, localized fracturing, and flexuring of adjacent strata (Figure 28).

The gouge is similar to that developed elsewhere in the tunnels but quite thin (0.1 feet). Apart from the variation in strike and displacement magnitude (Figure 25), the style and the sense of offset are similar to other zones of deformation exposed in the tunnels.

The main zone of deformation in the discharge tunnel extends from Station 13+25 to Station 13+60 (Figure 27). Deformation is remarkably similar in style and nature to the intake exposure. The discharge thrust strikes and dips N61E, 13SE with the strata to the southeast upthrown approximately 0.8 feet (Figure 29). Associated with faulting are drag folds, fracturing, and well developed gouge (Figure 32). The gouge is light gray, plastic, and contains angular, randomly oriented fragments of siltstone and shale derived from the adjacent strata. Gouge development, as in the intake tunnel, is a function

1241 041

of the geometry of the fault plane. The thinnest gouge zones occur where the fault is bedding parallel while the thickest zones occur where the fault plane steepens.

Drag folds are quite prominent, with a northwest-verging sense and fold axes parallel to the strike of the fault. Hinge areas of the drag folds show a slight axial plane cleavage and the development of bedding parallel flexural-slip gouge.

Fracturing is intense in the vicinity of Station 13+40 where the fault plane is essentially bedding parallel. Associated with this fracturing are numerous small gouge-filled offsets. Stratigraphic analysis indicates that the strata here have been overthickened slightly due to thrusting.

Numerous splays/stringers of gouge trend out from the fault zone and exhibit minor offsets (0.1 feet to 0.4 feet). These splays/stringers, which die into bedding, become more frequent toward the crown of the tunnel and account for the diminished offset along the fault plane.

Striations are recognized on both the hanging and footwalls. Striation orientations indicate a dip-slip motion with no evidence of a strike-slip component (Figure 33).

Based on structural style, orientation, and sense of offset, the two main thrusts exposed in the tunnels are apparently the same structure. Faulting is distinctly brittle with deformation confined to the immediate vicinity of the faulting (Figure 33). The small-scale thrust at Station 11+70 in the discharge tunnel may be an en echelon structure or a splay off the main fault. However, based on limited structural data, the latter is favored.

4.1.6 MICROCRACK ANALYSIS

Dr. Gene Simmons performed an analysis of microcracks observed within gouge obtained from the fault zone in the intake and discharge tunnels at the site.

1241 042

Dr. Simmons' complete report is included as Appendix A to this report. The following is a summary of the results of the Simmons' investigations.

Specimens of the gouge and the adjacent country rock were prepared in a form suitable for the examination of microcracks and elemental compositions of individual minerals by the SEM. Two types of cracks were observed. The first type is caused by unavoidable desiccation of the sample. Desiccation cracks occur subsequent to sampling and are unrelated to tunnel deformation and are recognized as such on the basis of criteria developed previous to the present studies. The second type of crack appears to be related to the last movement on the fault and always contains new mineral growths that extend completely across the crack.

Approximately 350 cracks of the type produced by faulting were examined in six samples. Every crack examined contained approximately one percent new mineral growth.

On the basis of previous observations of several thousand microcracks in a wide variety of rock types, healed microcracks appear to be ubiquitous in rocks. Evidently, the microcracks begin to heal immediately on forming. The degree of healing can be a measure of the amount of time that has been available for the microcrack to heal. The exact mathematical description of the function that relates degree of filling to elapsed time since the crack was formed is unknown, but is likely S-shaped and asymptotic to the zero and 100 percent values. Two data points have been obtained - one point at one million years (possibly two to five million years) from sandstone at the Satsop site,⁽⁸⁾ the other at 18.5 million years from shocked rock at Ries Crater, Germany.⁽⁹⁾

The rate of healing of microcracks is very likely a function of temperature, pressure, mineralogy, and the composition and flow rate of pore fluids. Fortunately, the conditions at the Perry site and at the Satsop site are quite similar, and the degree of filling of the cracks at each site are comparable. Therefore, the data obtained previously for the Satsop site form a suitable basis on which to estimate the age of the microfractures in the gouge zone at Perry.

1241 043

On the basis of a thorough examination of the microcracks in six representative samples of the gouge and country rock from the fault, or faults, in the intake tunnel and the discharge tunnel and from the fracture zone in the discharge tunnel, it is concluded that the time of last movement of each of these faults is approximately one million years and may be as old as two to five million years.

4.1.7 WATER ANALYSIS

Chemical analyses of tunnel faulting seepages indicate a salinity concentration ranging from 14.4 to 8.4 percent during the period of April 17, 1978 to March 6, 1979. Both the intake and discharge tunnel seepages indicated decreases in salinity, chloride, and sodium concentrations with time. No apparent trend for relatively low sulfate concentrations was established. Measurements of pH were uniform ranging between 7.2 and 8.0. Table 1 contains the results of these analyses.

Salts within Chagrin shale groundwater are not uncommon for northeastern Ohio. Compositionally, no salts are known within the Chagrin shale member of Ohio Shale formation. Salt bearing strata of the Salina Group occur more than 1650 feet below the tunnel. Even though tunnel faulting is not presumed to extend into the Salina salt beds, the impervious character of the Chagrin shale including the tunnel fault zones would tend to confine the upward flow of salt-saturated groundwater from a great depth. It is more probable that sediment pore water residuum has been diluted by meteoric recharge water in a manner originally suggested by L.U. DeSitter in 1947.⁽¹⁰⁾ This contention is supported by the isotopic ratio results subsequently discussed.

The isotopic ratios of D/H and $^{18}\text{O}/^{16}\text{O}$ were measured with a mass spectograph for three samples of water from the fault in the intake tunnel, one sample from the fault in the discharge tunnel, and two samples from Lake Erie. The three samples from the intake tunnel differ insignificantly from each other and from the sample from the discharge tunnel. The two lake samples differ insignificantly from each other. However, the waters from the fault(s) differ

1241 044

significantly from the lake water. All three water samples have a meteoric origin. A sulfur isotope analysis was attempted unsuccessfully on the waters from the fault and Lake Erie. The data obtained indicate a high sulfur content for the lake waters and essentially no sulfur in the waters from the fault.

The interpretation of the present set of data is that the 'fault water' is not Lake Erie water. Appendix B, prepared by Dr. Simmons, presents the details of the results for the hydrogen and oxygen isotope analysis.

4.2 GEOPHYSICAL STUDIES

4.2.1 EVALUATION OF PUBLISHED AND UNPUBLISHED GEOPHYSICAL DATA

A review has been made of the available published and unpublished geophysical data for the immediate site area of the Perry site. These data include shipborne, high resolution, seismic reflection surveying,^(11,6) shipborne magnetic data,⁽¹²⁾ aeromagnetic surveys,^(13,14) and gravity data.^(15,16)

The seismic reflection surveys indicate no evidence of either abrupt changes in the Paleozoic bedrock surface beneath the lake or disruptions of the overlying unconsolidated lake bottom sediments.^(15,11,6)

Several profiles which would have crossed the projection of the faults noted in the intake and discharge tunnels did not indicate vertical offset.⁽⁶⁾

A shipborne magnetic survey in the site area, which consisted of three north-south profile lines at 5-mile spacings and one east-west line, shows no evidence for any linear trends parallel to the projected trace of the intake and discharge faults.^(11,12)

Similarly, the aeromagnetic surveys which were parallel to the projected trace of the fault and widely spaced (flight line separation on the order of 5 to 10 miles) do not suggest any linear magnetic anomalies in the near-site area of the Perry plant.^(13,14)

1249 045

The shipborne gravity data reported by Wall consist of a single traverse in the site area.⁽¹⁵⁾ The relatively widely-spaced shipborne gravity data are interpreted by Wall as indicative of lithologic variations within the Precambrian basement and not indicative of structure.

Wall's interpretation is similar to Heiskanen and Uotila,⁽¹⁷⁾ who interpreted most of the gravity anomalies in Ohio as reflective or lithologic variations in the Precambrian basement.

4.2.2 MAGNETIC SURVEYS

The magnetic profiles taken from Lake Erie traverses (Figures 34 to 42) display a generally flat signature. All of the significant peaks appear to be related to cultural influences such as drill barges and metal pipes. There are no anomalies which are associated with the fault.

The land magnetic profiles (Figures 43 to 48) show generally erratic signatures which are attributed primarily to cultural sources. There is no fault-related magnetic signature.

4.2.3 BOREHOLE LOGS

Units which could be used as marker beds, as a result of either an anomalous velocity or radiation level, were not detected in the geologic section (Figures 49 and 50). This is probably because of the relative macroscopic homogeneity of the Chagrin shale as evidenced by the thinness of the individual beds within the Chagrin. Offset which could be associated with the fault could not be determined.

In borings TX-3, TX-4, and TX-6, velocity logs show low velocity values associated with the fault. No such velocity "lows" are observed outside the tunnel in either the down-dip (TX-7) or along the strike (TX-8, TX-9, TX-10) projection of the fault. Outside the fault zone, the measured velocity is

1248 046

10,500±fps; within the fault zone, the measured velocity value is approximately 6,000 fps. This lower velocity value at the fault zone is most likely because of the (PVC) casing material.

In the tunnel drill holes (TX-3, TX-4, and TX-6), a low level of gamma radiation can be associated with the fault. However, the signature is not very marked. It appears that certainly the low P-wave velocity values can, and possibly the low radiation levels may, be used as distinguishing characteristics of the fault.

4.2.4 IN-SITU VELOCITY MEASUREMENTS

The velocities determined vary from 10,000 to 11,000 fps for "P" waves (compressional) and 3,900 to 5,200 fps for "S" (shear) waves and are similar to those determined in the previous cross-hole study at the plant area.

Velocities determined from measurements across the fault in the intake tunnel are 10,500 fps for "P" waves and 5,250 fps for "S" waves. These values indicate a relatively intact, sound shale.

Velocities across the fracture zone in the discharge tunnel are 10,700 fps for "P" waves and 3,900 fps for "S" waves; again, these values indicate a sound material. The values across the fault in the discharge tunnel are similar; the velocities are 10,000 fps for "P" waves and 4,000 fps for "S" waves. These velocity values are also within the range of those reported in the initial studies for the plant area.

4.3 EVALUATION OF LOCAL SEISMICITY AROUND THE PERRY NUCLEAR POWER PLANT SITE

A detailed study of the local seismicity around the Perry site was made with some significant observations (see Appendix H). In brief, the local historical seismicity is low: less than 50 events over a period of a century and a half, and no intensity larger than Intensity V Modified Mercalli. In general,

1248 047

assigned intensities can be considered conservative, and epicentral coordinates relatively uncertain. This uncertainty results, in part, from soil amplification and population distribution which make it difficult in many cases to delineate a clear epicentral area. As a consequence of this epicentral uncertainty, apparent alignments, or clustering of epicenters have no reliable tectonic significance. Details on local seismicity evaluations are presented in Appendix H.

4.4 IN-SITU STRESS MEASUREMENTS

Data regarding the orientation and magnitude of the complete stress tensor were obtained for the test intervals between 394 and 718 feet in TX-11. The direction of σ_1 was consistent with stress orientations over a regional basis. The stress magnitudes (the horizontal stresses are the maximum and intermediate principal stresses) fall within the limits of stresses measured in other parts of northeastern and north central United States and in southern Canada. The vertical component corresponds closely to the anticipated overburden pressure.

At the shallower depths, the tendency for $\sigma_1 \sim \sigma_2 \sim \sigma_3$ is well defined and extrapolations of existing measurements to the surface are reasonable. No high stress magnitudes were experienced in either the tunnel or plant area excavations or concluded from measurements of extensometers installed in the bedrock walls of the emergency service water pump house. These conclusions regarding stresses in plant structure excavations are consistent with the extrapolation of the deeper in-situ borehole measurements. Below a depth of approximately 600 feet, both σ_{Hmin} and σ_{Hmax} show an increase in gradient, with the gradient for σ_{Hmax} being larger. Data conclusions and an overview of the hydraulic fracturing technique are attached as Appendix D.

1241 048

Based on structural style, orientation, and sense of offset, the thrust fault exposed in each tunnel is apparently the same feature or en echelon. Faulting is distinctly brittle with deformation confined to the immediate vicinity of the fault plane. The zigzag fracture pattern and accompanying evidences of flexure characterizing the more southerly discharge tunnel deformation may be an en echelon structure, but more probably represents a splay from the main fault.

Paleozoic Tectonics, Mesozoic-Tertiary Tectonics, and Pleistocene-Recent faulting mechanisms were considered. Regarding mid-Paleozoic deformation, the concept of soft sediment deformation can be ruled out by the brittle nature of observed deformation. The tunnel fault formed following lithification of the shale sequence. Notwithstanding interpretation regarding age, pre-Pleistocene tectonics are evaluated primarily in consideration of geometric data on tunnel fault strike and shallow dip. Alleghenian (Appalachian) orogenic compressional stresses propagated northwesterly, employing Salina salt bed decollements, would be technically feasible. Upward propagation of faulting at low dip angles, as with the tunnel faulting, would be compatible. Alternatively, southeasterly gravitational movement during late Paleozoic or early Mesozoic time was possible when overburden pressure and formation temperatures were about at peak values. Again, a majority of the lateral movement would be expected to occur upon the Salina salts. Relatively high loading conditions existing during glaciation with high stress gradients near ice sheet boundaries may have activated flowage deformation within the salt which resulted in underthrusting of the more competent overlying strata. Other mechanisms associated with deeper rooted deformation such as basement-block faulting and differential warping of Paleozoic strata would tend to produce normal faulting in overlying formations, not thrust faults.

Data regarding the age of faulting were derived from field and laboratory studies. An age determination from fault gouge mineralization could not be undertaken because none of the constituent minerals contained radioactive

1248 049

isotopes suitable for dating. However, on the basis of syn and/or post-deformational mineral growth extending completely across fault zone microcracks related to the last movement on the fault, Dr. Simmons concludes that the time of last movement for each of the tunnel fault segments is approximately one million years but may be as old as two to five million years or as young as 0.8 million years.

Comparisons of the Perry microcrack data to similar data from other locales were employed in age determinations. Allowances for variability in factors such as temperature, pressure, and chemical environment and uncertainty related to mineral growth rates could suggest a greater range in estimated formation time. Notwithstanding the foregoing consideration, it is not reasonable to postulate a Recent age for last fault movement. Microcrack mineral growth bridges, some of which are quite delicate, remained intact and unruptured during the period of historical seismicity.

During faulting, the orientation of the maximum principal stress was oriented normal to fault strike. In-situ stress measurements employing the hydrofracture technique demonstrate that the stress field orientation has changed since faulting. The maximum principal stress consistent with the prevailing regional stress field is parallel to fault strike. The magnitude of vertical stresses measured is as expected for calculated overburden pressure. Reorientation of the stress field must have occurred during Pleistocene time in response to glaciation. Deposits of three major stages are recognized in northeastern Ohio. No Nebraskan stage deposits have been identified in Ohio. It is not known which major ice advance or minor recessional-readvance cycle altered the stress field prevailing during the last fault movement. This method of qualitatively dating the last fault movement is in agreement with the microcrack study.

1241 050

Dr. Voight hypothesizes on the basis of maximum past consolidation pressure of the fault gouge that the associated overburden pressure was not substantial but on the order inferred from an ice sheet considerably thinner than that estimated for northeastern Ohio at the Laurentide maximum. On this basis the last fault movement is more likely associated with deglaciation-rebound than an ice sheet advance. However, rock-to-rock contacts across the fault zone, as well as the step-like pattern of faulting, were documented during detailed mapping of the deformed tunnel segments. Furthermore, Dr. Voight suggests from extrapolations of fault displacement data that approximately 70 feet of undeformed bedrock overlies the updip projection of faulting. Therefore, it is doubtful whether the fault gouge would have experienced maximum overburden loading during any of the major or minor glacial stage advances when ice thicknesses exceeded several thousand feet. Hence, the age of movement for the fault based on gouge consolidation tests is not reliable.

The most reasonable interpretation of all the data is that the tunnel deformation or at least the last movement on the fault was a Pleistocene event associated with glaciation. Candidate mechanisms include ice-sheet traction, differential down-bowing with glacial advance, differential rebound with glacial retreat, surficial stress-relief or "pop-up" and subsurface salt tectonics, the latter as previously discussed. More probable is glacio-isostatic uplift and surficial stress relief during deglaciation rebound. Recurrent movement on deeper seated pre-Pleistocene structures or faults, either by direct propagation or by an echelon deformation could have been possible. Both of the latter would have been activated by glacial ice loading or unloading. The conclusions of these investigations, the opinions of the independent reviewing geologists and lack of evidence to the contrary are consistent; the fault is not capable as defined in 10 CFR 100 Appendix A.

1241 051

REFERENCES

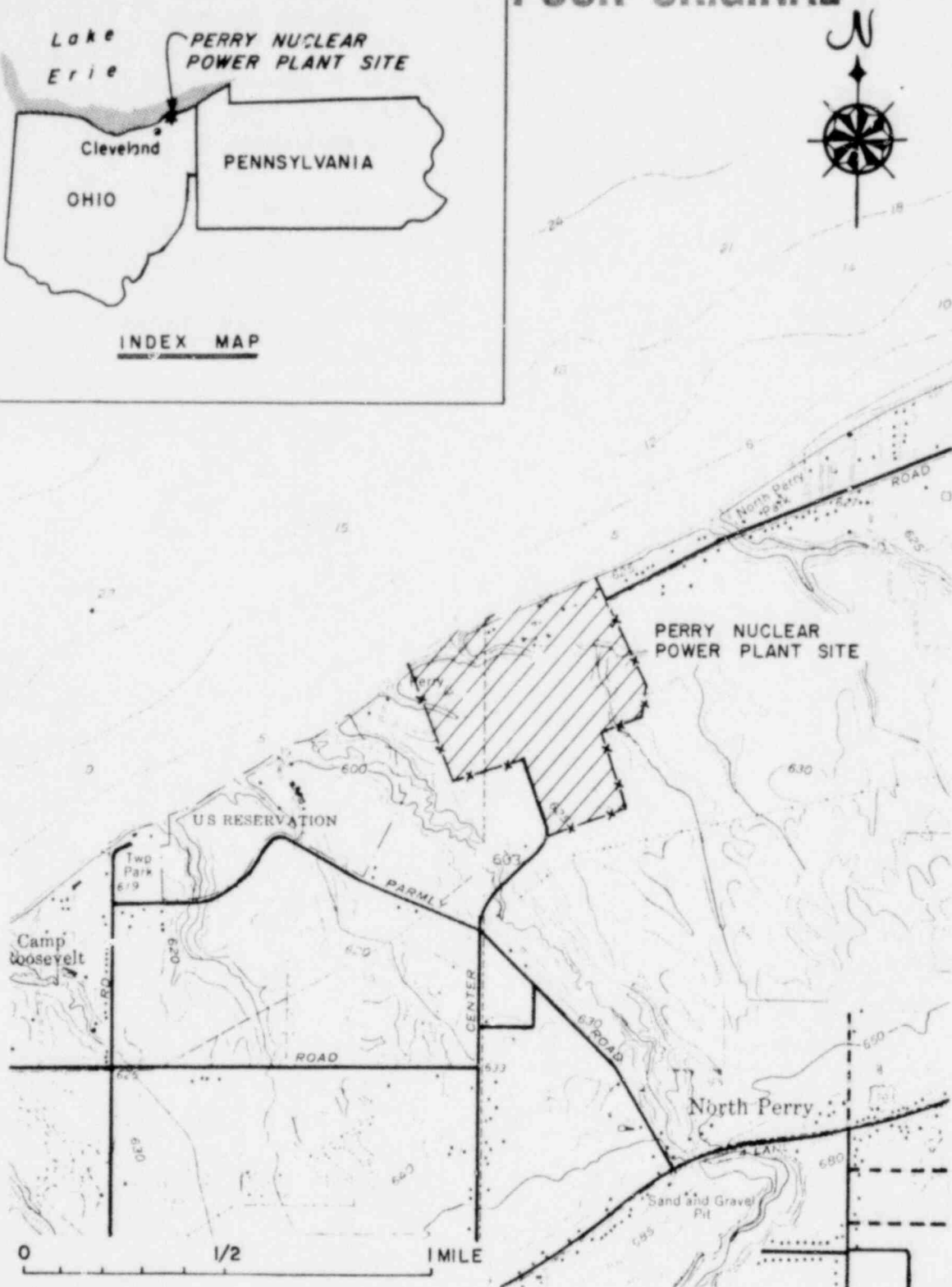
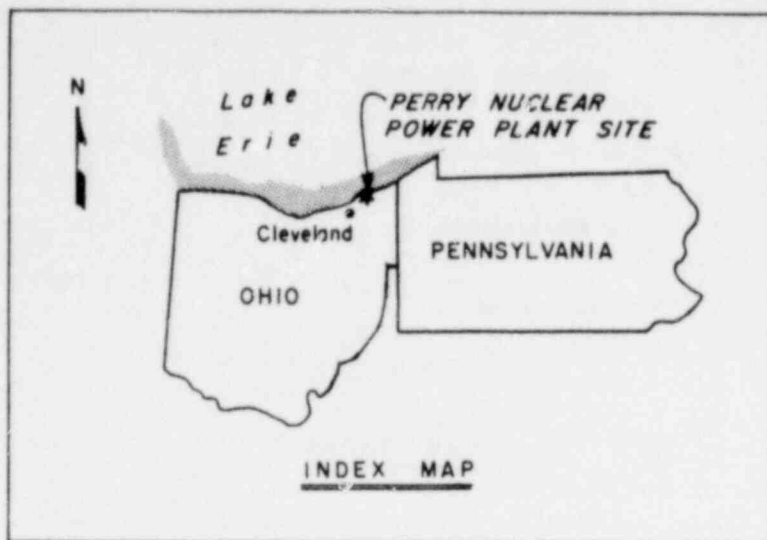
- (1) Stone and Webster Engineering Corporation, October 1978, Regional geology of the Salina Basin, Report of Geologic Project Manager - Salina Basin, Phase I August 1977 - January 1978, Vol. 1.
- (2) Heimlick, R. A., R. W. Manus, and C. H. Jacoby, 1974, General geology of the International Salt Mine, Cleveland, Ohio: in Heimlick, R. A. and R. M. Feldman, (eds), Selected field trips in northeastern Ohio: Ohio Department of Natural Resources, Division of Geological Survey, Survey Guidebook No. 2, p. 5-17., 59 p.
- (3) Jacoby, C. H., 1979, personal and written communications.
- (4) Richner, D. R., 1974, Minor discontinuities reported in the core description of Diamond Alkali Core Hole #202, Perry Township, Ohio, unpublished report.
- (5) Prosser, Charles S., 1912, The Devonian and Mississippian formations of northeastern Ohio: Ohio Geological Survey Bulletin, 15p.
- (6) Williams, S. Jeffress, 1978 and 1979, personal and written communications.
- (7) Cushing, H. P., F. Leverett, and F. R. Van Horn, 1931, Geology and mineral resources of the Cleveland District, Ohio: Geological Society of America Bulletin 818, p. 33-35.
- (8) Weston Geophysical Research, Inc., 1978, Feasibility of Dating the faults in the foundation of WNP 3 at the WNP 3 and 5 (Satsop) Site of Washington Public Power Supply System: report prepared for EBASCO Services Incorporated and submitted to Washington Public Power Supply System, 26 pp.
- (9) Padovani, E. R., M. L. Batzle, and G. Simmons, 1979, Characteristics of microcracks in asmples from the drill hole Nordlingen 1973 in the Ries Crater, Germany. Proceedings, Lunar Science Conference, 9th, in press.

1241 052

- (10) Blatt, Middleton and Murray, 1972, Origin of Sedimentary Rocks: Englewood, N.J., Prentice-Hall, p. 338.
- (11) Wall, R. E., 1968, A sub-bottom reflection survey in the Central Basin of Lake Erie: Geological Society of America Bulletin, v. 79, p. 91-106.
- (12) Peter, G. and R. E. Wall, 1961, Magnetic Total Intensity Measurements on Lake Erie: Lamont-Doherty Geophysical Observatory Technical Report, pp 9.
- (13) Ahern, J. L., 1975, Aeromagnetic reconnaissance survey of Lake Erie: Ohio State University, Columbus, Ohio, unpublished M. S. Thesis, 153 p.
- (14) Meyers, C. D., 1977, Aeromagnetic reconnaissance survey of Lake Erie: Ohio State University, Columbus, Ohio, unpublished M. S. Thesis, 172 p.
- (15) Wall, R. E., 1965, Geophysical Investigations in the Central Lake Erie Basin: University of Ohio, Unpublished Ph.d. Thesis, Columbus, 66 pp.
- (16) O'Hara, N. W., F. Mequid, and W. J. Hinze, 1974, Gravity and Magnetic Observations from the Lake Erie and Lake Ontario Region: Geological Society of America Abstracts with Programs, v. 6, p. 896.
- (17) Heiskanen, W. A., and U. A. Uotila, 1956, Gravity Survey of the state of Ohio: State of Ohio, Department of Natural Resources, Division of Geological Survey, Report of Investigations, No. 30, 34 p.

1241 053

POOR ORIGINAL



1241 054

LOCATION MAP, PERRY NUCLEAR POWER PLANT

FIGURE 1

POOR ORIGINAL

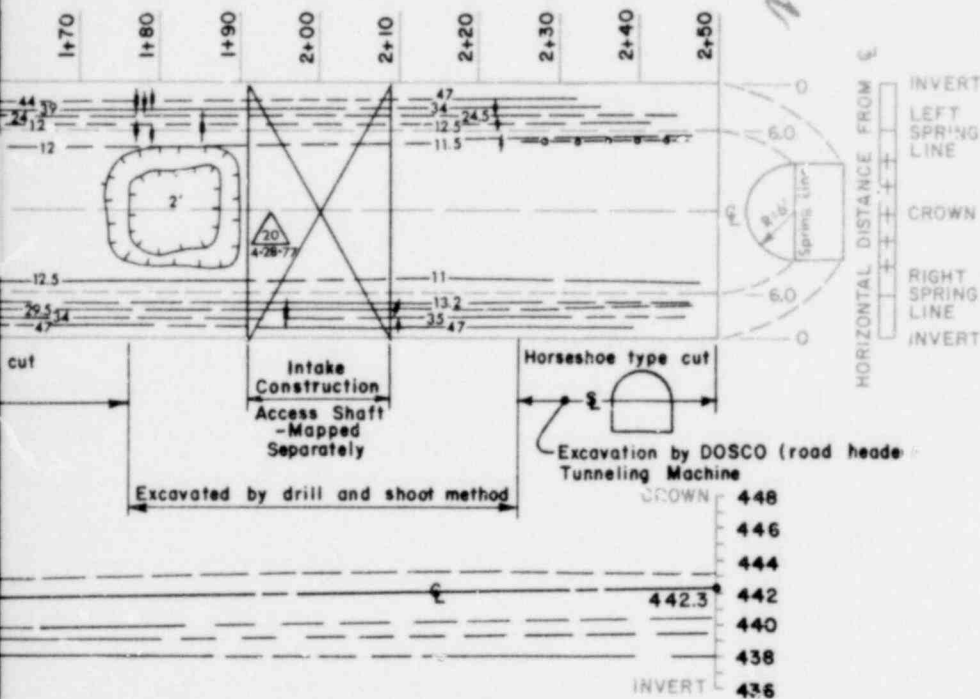
ING

RE

MUM

DATE

I thickness
inches
of



8-12 77	8-1 77	7-12 77	8-12 77
no. 4 no. 5 at crown		no. 4 no. 5 at crown	
Rock bolts in steel ribs, spaced by wire mesh		5 Rock bolts in steel ribs at 3.5'-4' centers spaced by wire mesh	
1/4" - 1"		1'-5"	
non-persistent 1'-5"		non-persistent 1'-10"	
No inflows		No inflows	
approx. 24' of lacustrine, approx. 35' of glacial till & approx. 116.7' of shale			

EXCAVATION PROGRESS
ESTIMATED ROCK
CONDITION (TERZAGHI NO.)
TEMPORARY SUPPORT
SYSTEM
BEDDING SPACING
FRACTURE SPACING
WATER CONDITION
DEPTH OF COVER

GEOLOGIC MAP OF TUNNEL EXCAVATIONS

FIGURE 2
SHEET 1 OF 24

1241 055

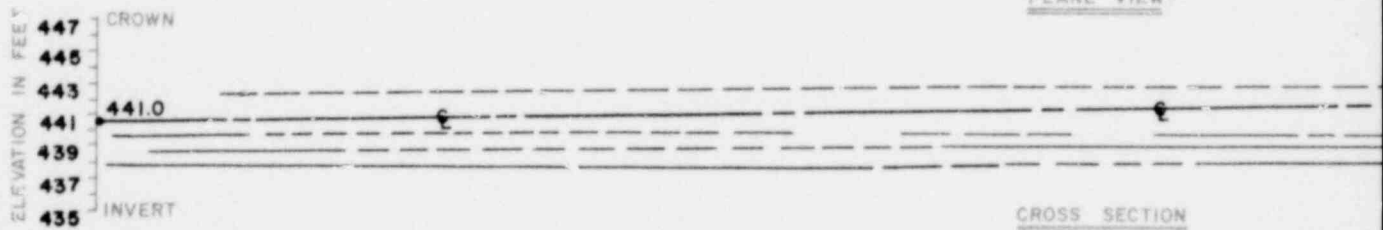
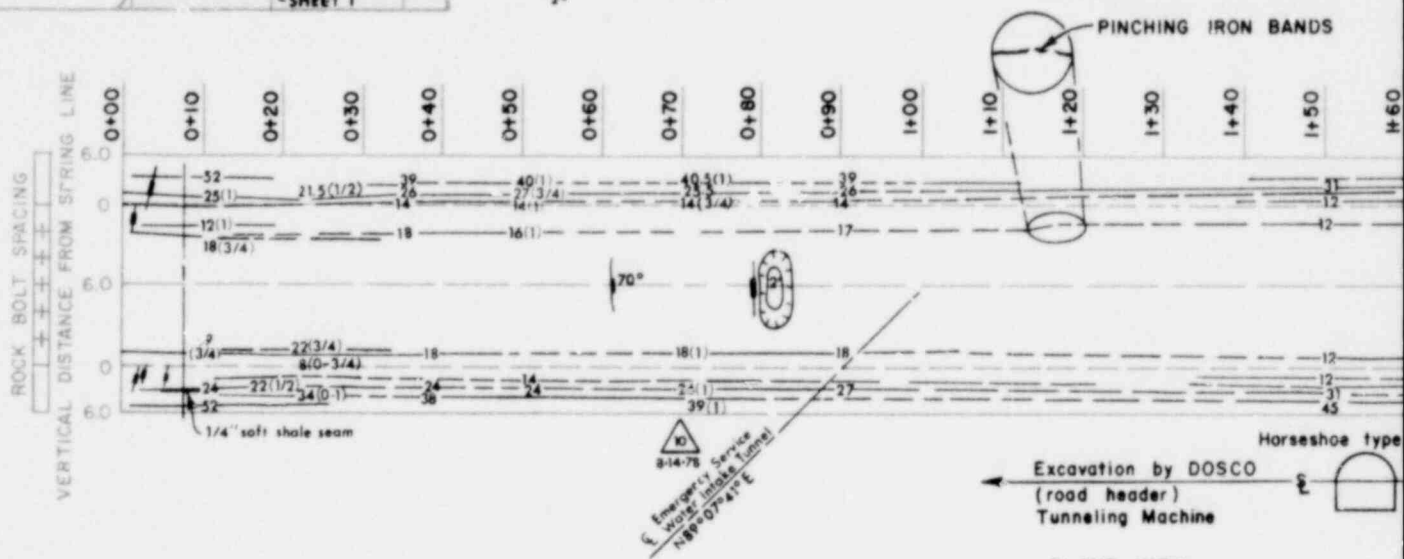
POOR ORIGINAL



- SYMBOLS**
- 6 (1/2)* — HARD, TAN, BROWN, CHERTY, IRON BED OR LAMINAE
 - - - 12 (0-2)* - - - DISCONTINUOUS IRON BED
 - - - 12 (1)* - - - HARD, LIGHT GREY, SANDY SHALE TO SILTSTONE BED
 - - - 10 (7 1/2 - 2)* - - - DISCONTINUOUS IRON BED WITHIN GREY BED
 - ↖ ↗ FRACTURE
 - / — FAULT
 - / — BEDDING PARTING
 - ↑ 75° VERTICAL JOINT
 - ↑ 75° INCLINED JOINT
 - / — BEDDING, STRIKE AND DIP

- / — MOISTURE ALONG BED PARTING
- / — SEEPAGE FROM FEATURE
- 2 OVEREXCAVATION OR OVERBREAK ZONE, MAXIMUM AMOUNT SHOWN
- △ 20 METHANE GAP, MAXIMUM PERCENT L.E.L. WITHIN OF OCCURRENCE

Note:
Number(s) in parentheses indicates bed Number preceding parenthesis indicates above or below spring line at station measurement.



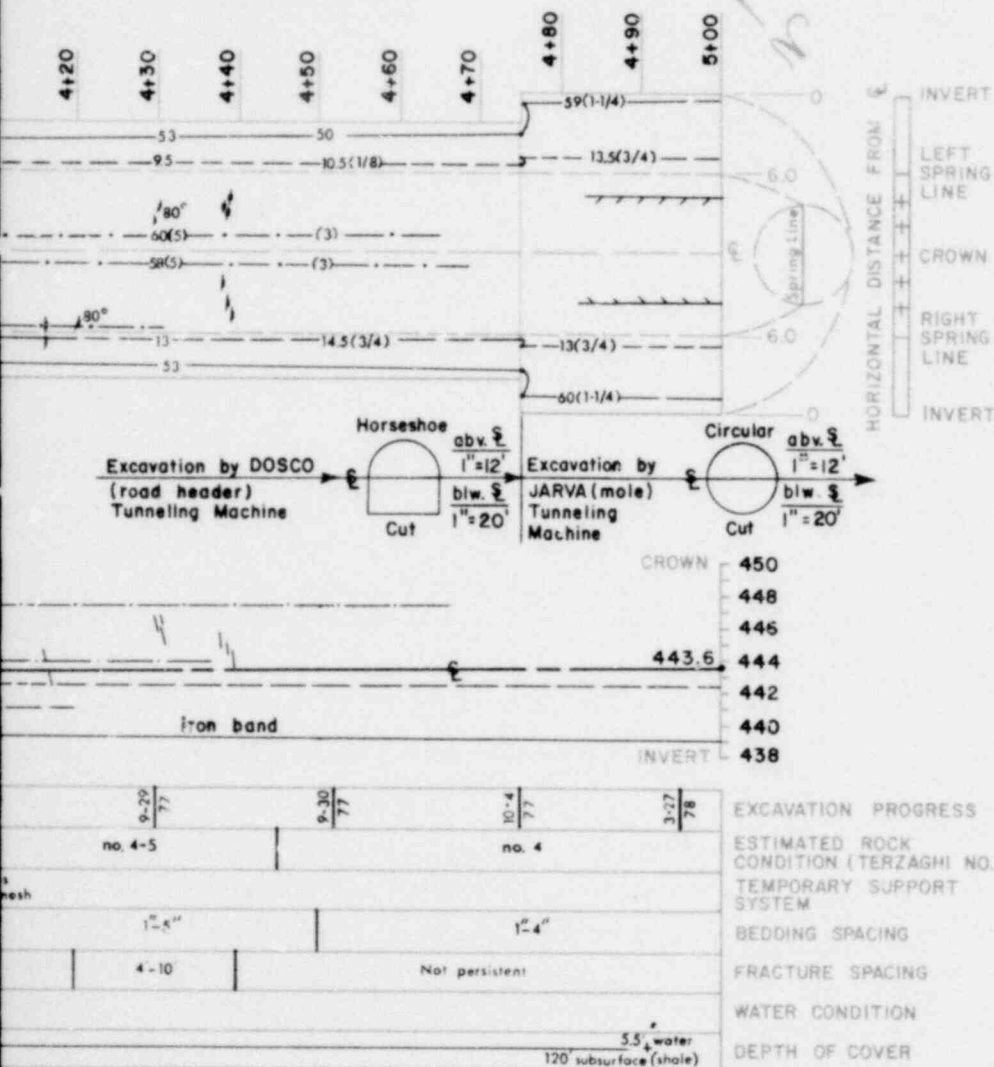
8-23/77	8-19/77	8-18/77	8-7/77	8-16/77	8-12/77	8-11/77	8-8/77	8-5/77	8-4/77
no. 4-5	4								5
5 Rock bolts in steel ribs with wire mesh between, roof surface coated w/cellite agent									
	2'-9"	2'-7"			2'-8"				
1'-3"	Bedding fractures only				Very widely spaced				
No inflow:									
approx. 24' of lacustrine, approx. 35' of glacial till									

1238 056

POOR ORIGINAL

ING
RE
MUM
M
DATE

Thickness
inches
of



GEOLOGIC MAP OF TUNNE EXCAVATIONS

FIGURE
SHEET 2 OF 24

1241 057

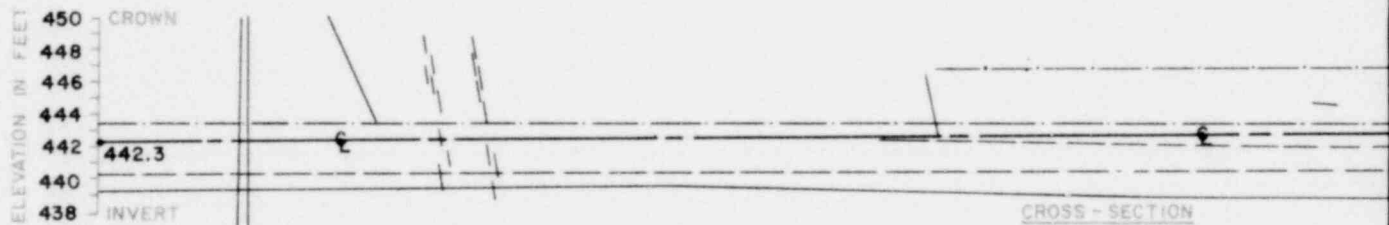
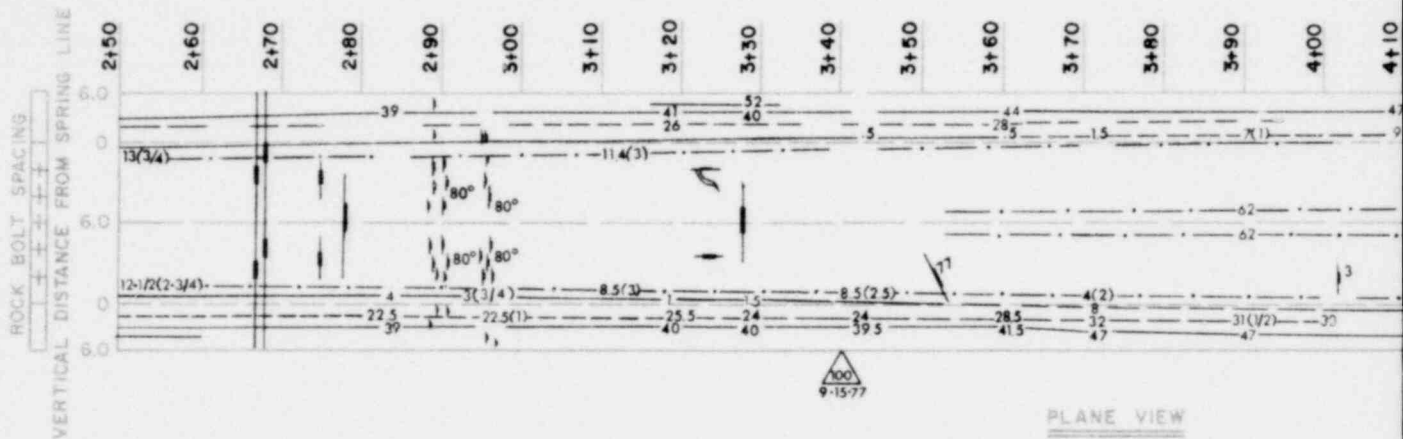
POOR ORIGINAL



- SYMBOLS**
- 6 (1/2)° — HARD, TAN, BROWN, CHERTY, IRON BED OR LAMINAE
 - 12 (0-2)° — DISCONTINUOUS IRON BED
 - 12 (1)° — HARD, LIGHT GREY, SANDY SHALE TO SILTSTONE BED
 - 10 (7) (0-2)° — DISCONTINUOUS IRON BED WITHIN GREY BED
 - FRACTURE ZONE
 - FAULT
 - BEDDING PARTING
 - VERTICAL JOINT
 - INCLINED JOINT
 - BEDDING, STRIKE AND DIP

- MOISTURE ALONG BEDDING PARTING
- SEEPAGE FROM FEATURE
- OVEREXCAVATION OR OVERBREAK ZONE, MAXIMUM AMOUNT SHOWN
- METHANE GAS, MAXIMUM PERCENT L.E.L. WITHIN OF OCCURRENCE

* Note: Number(s) in parentheses indicates bed. Number preceding parenthesis indicates above or below spring line at station measurement.



9-8 77	9-9 77	9-12 77	9-13 77	9-14 77	9-15 77	9-16 77	9-22 77	9-23 77	9-25 77	9-27 77
no. 4	no. 5	no. 4	no. 5	no. 4	no. 5	no. 4	no. 4	no. 4	no. 4	no. 4
1'-5"	1/2'-5"	1'-5"	2'-6"	1'-6"	1/2'-4"	3/4'-4"	1'-8"	1'-4"	1'-6"	1'-6"
1'-10"	1'-10"	2'-10"	1/2'-10"	10'	Not persistent	Not persistent	Not persistent	Not persistent	Not persistent	Not persistent
No inflows										
3' beach										
126' subsurface (shale)										

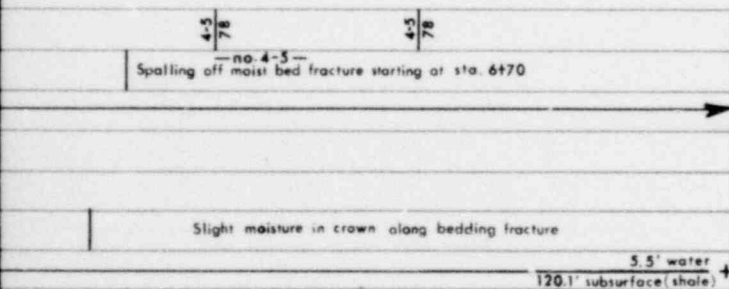
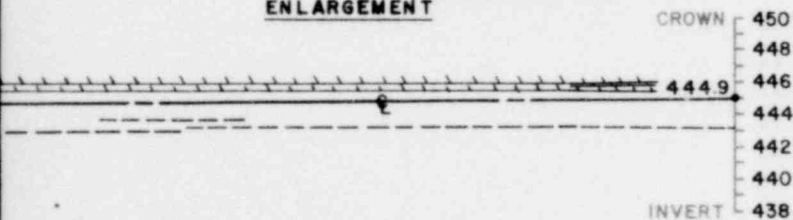
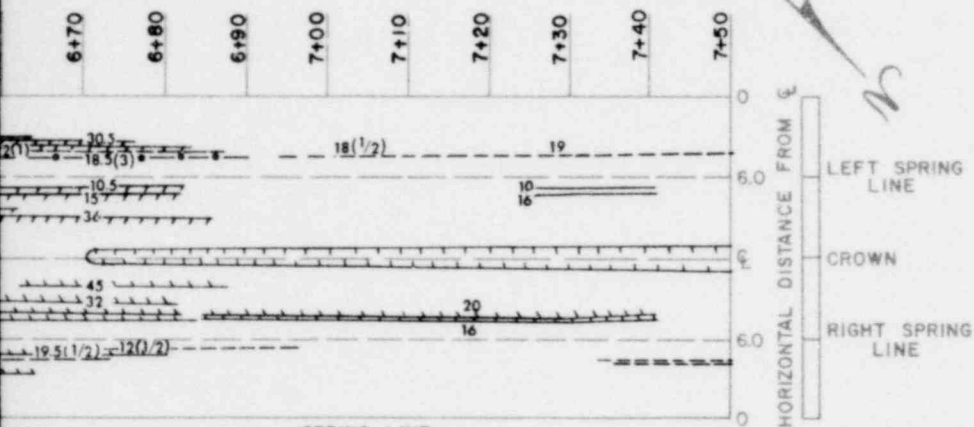
1233 058

POOR ORIGINAL

NG
E
MUM
M
ATE

thickness.
inches
of

ENLARGEMENT BELOW



1241 059

GEOLOGIC MAP OF TUNNEL EXCAVATIONS

FIGURE 2
SHEET 3 OF 24

POOR ORIGINAL

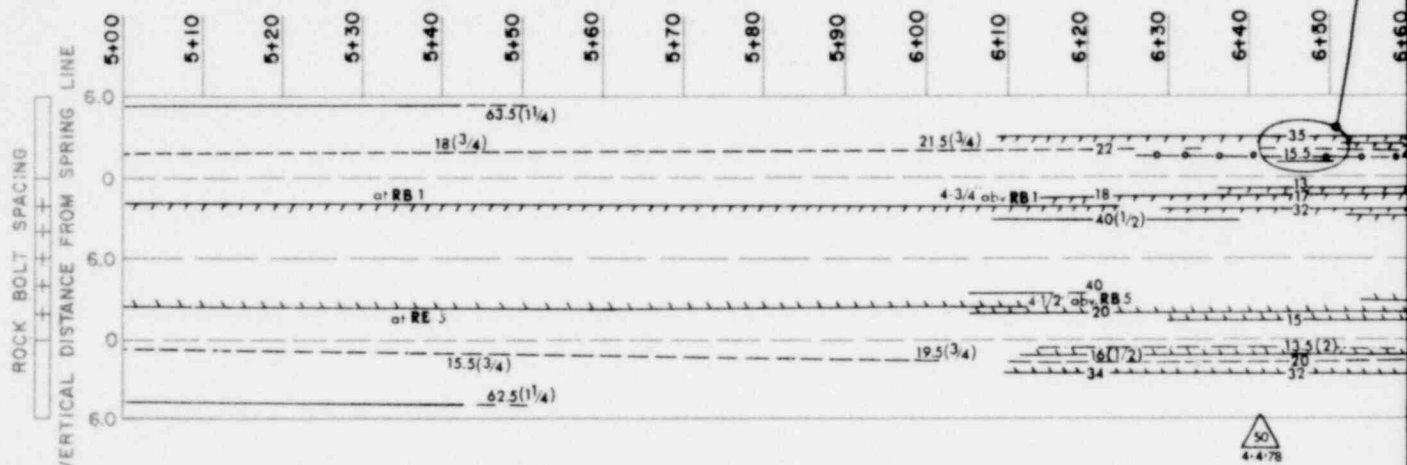


SYMBOLS

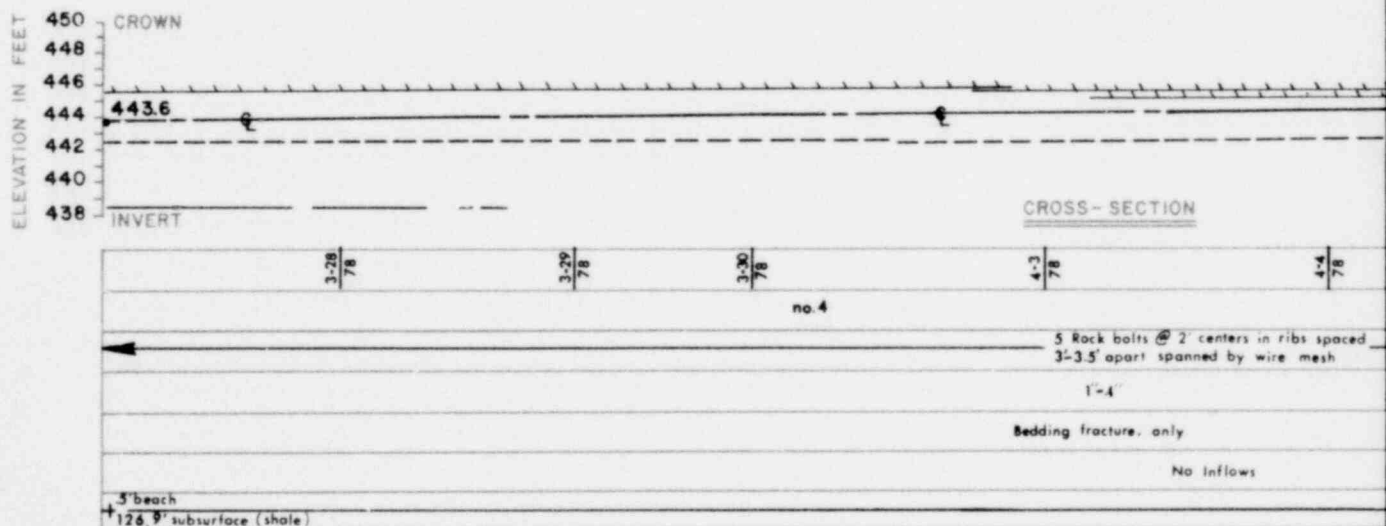
- $6(\frac{1}{4})^*$ HARD, TAN, BROWN, CHERTY, IRON BED OR LAMINAE
- $12(0-2)^*$ DISCONTINUOUS IRON BED
- $12(1)^*$ HARD, LIGHT GREY, SANDY SHALE TO SILTSTONE BED
- $10(7)(0-2)^*$ DISCONTINUOUS IRON BED WITHIN GREY BED
- FRACTURE
- FAULT
- BEDDING PARTING
- VERTICAL JOINT
- INCLINED JOINT
- BEDDING, STRIKE AND DIP

- MOISTURE ALONG BED PARTING
- SEEPAGE FROM FEATURE
- OVEREXCAVATION OR OVERBREAK ZONE, MAXIMUM AMOUNT SHOWN
- METHANE GAS, MAXIMUM PERCENT L.E.L. WITH DATE OF OCCURRENCE

*Note:
Number(s) in parentheses indicates bed
Number preceding parenthesis indicates
above or below spring line at station
measurement.



PLANE VIEW

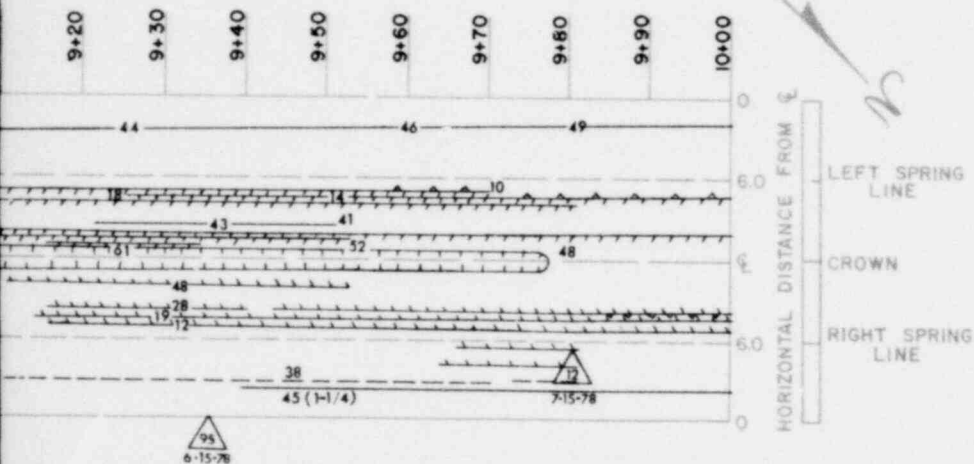


1233 060

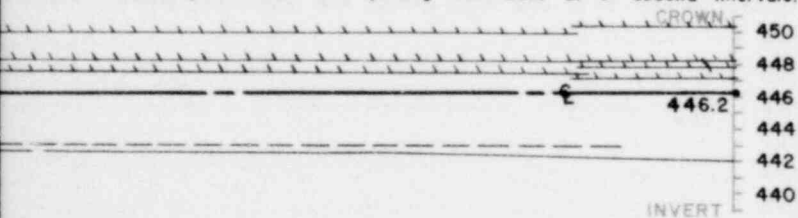
POOR ORIGINAL

NG
FE
MUM
M
ATE

Thickness
inches
of



At station 9+64 encountered brine groundwater and clay, 4/14/78. A 2" diameter probe yielded a full bore of inflow. By 4:45 A.M. inflow decreased volume. At 7:45 A.M. groundwater was spurting from bore at 3 second intervals.



4-13/78	na 4-5
1"-8"	2'-10"
Bedding fractures only	
near crown staining	1 * See Note Above
	Slight moisture along 20% of bedding fractures and rock bolts
	16.5' water
	116.8' subsurface (shale)

EXCAVATION PROGRESS
ESTIMATED ROCK
CONDITION (TERZAGHI NO.)
TEMPORARY SUPPORT
SYSTEM
BEDDING SPACING
FRACTURE SPACING
WATER CONDITION
DEPTH OF COVER

1248 061

GEOLOGIC MAP OF TUNNEL EXCAVATIONS

FIGURE 2
SHEET 4 OF 24

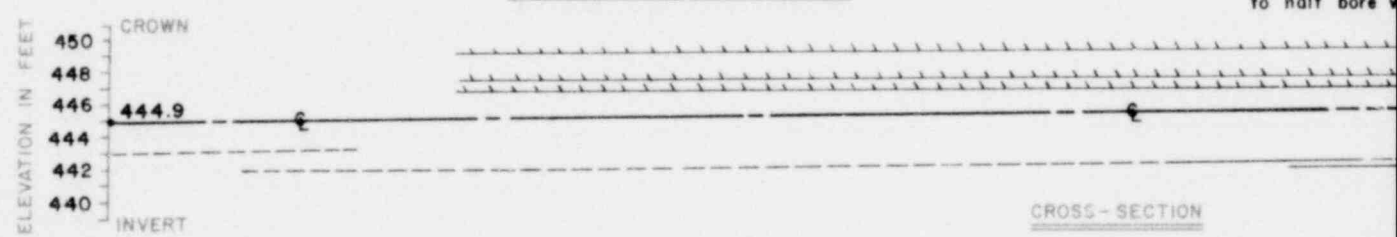
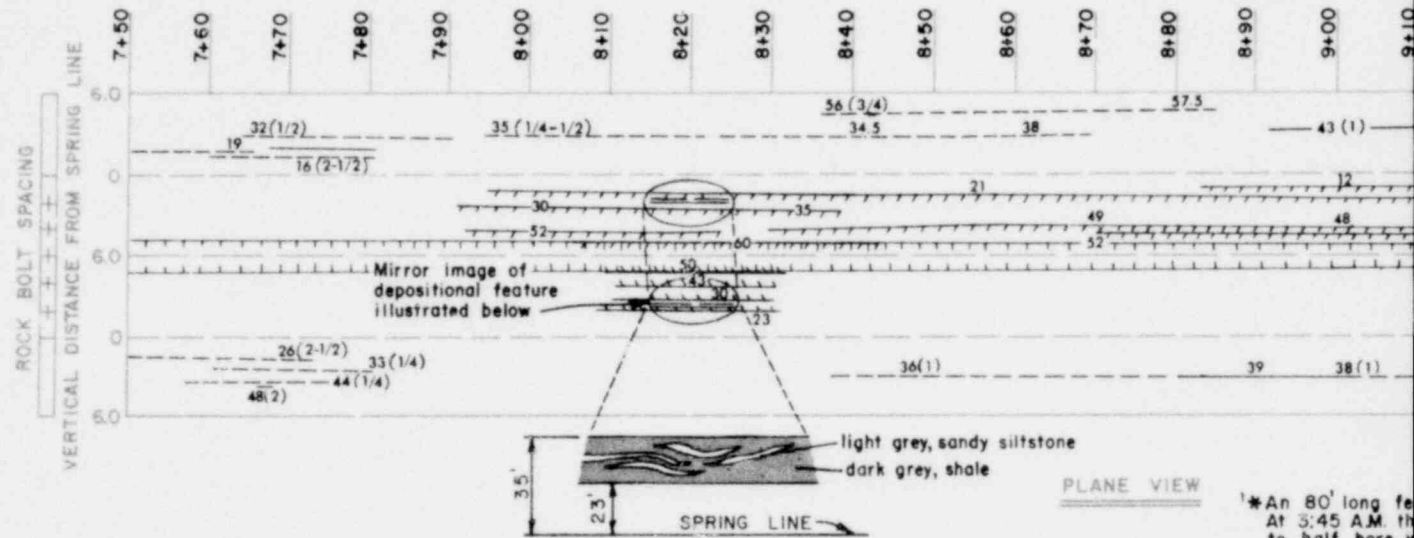
POOR ORIGINAL



- SYMBOLS**
- 6 (1/2)* — HARD, TAN, BROWN, CHERTY, IRON BED OR LAMINAE
 - - - 12 (0-2)* — DISCONTINUOUS IRON BED
 - - - 12 (1)* — HARD, LIGHT GREY, SANDY SHALE TO SILTSTONE B/D
 - - - 10 (7) (0-2)* — DISCONTINUOUS IRON BED WITHIN GREY BED
 - ⚡ — FRACTURE
 - — — — — FAULT
 - — — — — BEDDING PARTING
 - ↕ — VERTICAL JOINT
 - ↗ — INCLINED JOINT
 - — — — — BEDDING, STRIKE AND DIP

- — — — — MOISTURE ALONG BEDDING PARTING
- ↕ — SEEPAGE FROM FEATURE
- ⊞ — OVEREXCAVATION OR OVERBREAK ZONE, MAXIMUM AMOUNT SHOWN
- ⚠ — METHANE GAS, MAXIMUM PERCENT L.E.L. WITH DURATION OF OCCURRENCE

*Note: Number(s) in parentheses indicates bed thickness. Number preceding parenthesis indicates above or below spring line of station measurement.



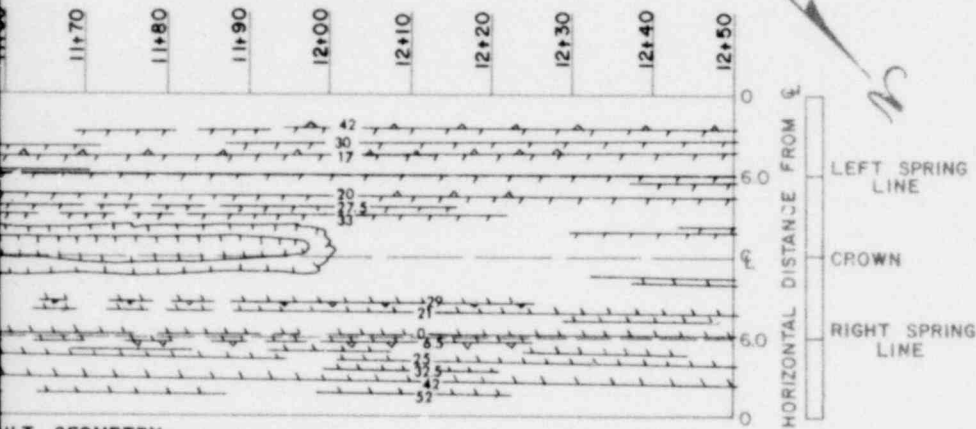
4-6	78	4-7	78	4-10	78	4-11	78	4-12
no. 4-5 Continued spalling along bedding fracture near crown								
5 Rock bolts @ 2' centers in ribs spaced 3-3.5 apart, spanned by wire mesh								
1'-4"			1'-7"					
Moisture along bedding fractures near crown						Moisture along bedding fracture		
Seepage out of rock bolts w/ iron								
5.5' water								
+ 120.1' subsurface (shale)								

1233 362

POOR ORIGINAL

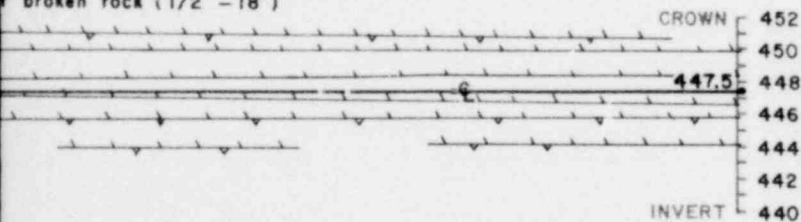
NG
RE
MUM
M
ATE

d thickness.
inches
of



ULT GEOMETRY

displacement - 22"
vertical displacement - 12"
N 47° E
prox. 17°
broken rock (1/2" - 18")



4.27 78	4.20 78
no 4-5	5 rock bolts at 2' centers in ribs at 3.5' centers, spanned by wire mesh
3'-3.5' centers spanned by wire mesh	Full shielding
14"	8"-15"
ictures only, spaced as above	
ght moisture along approx. 20% of bedding fractures and rock bolts	
	8.5' water
	109.3' subsurface (shale) +

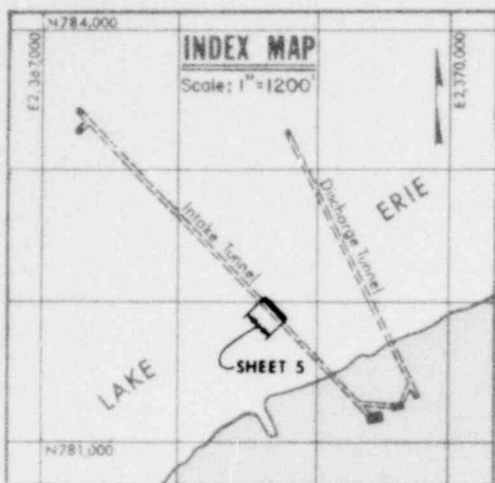
EXCAVATION PROGRESS
ESTIMATED ROCK
CONDITION (TERZAGHI NO.)
TEMPORARY SUPPORT
SYSTEM
BEDDING SPACING
FRACTURE SPACING
WATER CONDITION
DEPTH OF COVER

1241 063

GEOLOGIC MAP OF TUNNEL EXCAVATIONS

FIGURE 2
SHEET 5 OF 24

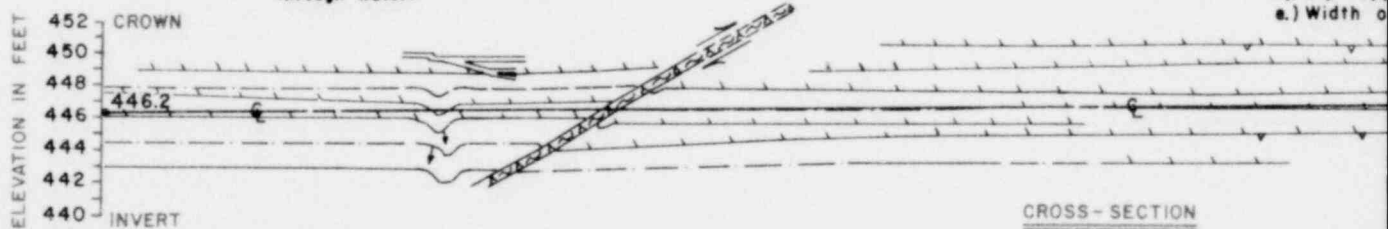
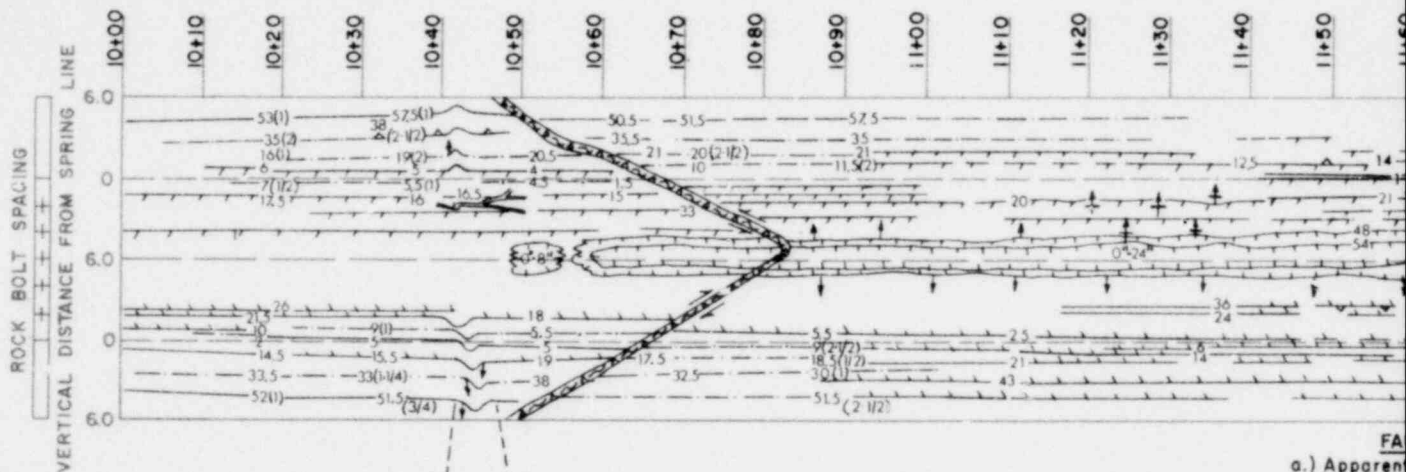
POOR ORIGINAL



- SYMBOLS**
- 6 (1/2)* HARD, TAN, BROWN, CHERTY, IRON BED OR LAMINAE
 - 12 (0-2)* DISCONTINUOUS IRON BED
 - 12 (1)* HARD, LIGHT GREY, SANDY SHALE TO SILTSTONE BED
 - 10 (7) (0-2)* DISCONTINUOUS IRON BED WITHIN GREY BED
 - ⚡ FRACTURE
 - ↔ FAULT (with sense of motion)
 - BEDDING PARTING
 - ⊥ VERTICAL JOINT
 - ↗ INCLINED JOINT
 - BEDDING, STRIKE AND DIP

- MOISTURE ALONG BED PARTING
- SEEPAGE FROM FEATURE
- 23 OVEREXCAVATION OR OVERBREAK ZONE, MAXIMUM AMOUNT SHOWN
- 20 4-28-77 METHANE GAS, MAXIMUM PERCENT L.E.L. WITHIN OF OCCURRENCE

*Note: Number(s) in parentheses indicates bed. Number preceding parenthesis indicates above or below spring line at station measurement.



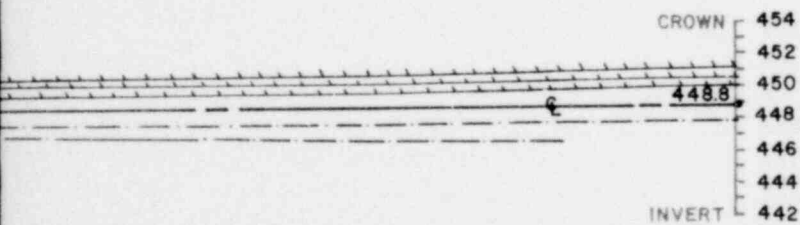
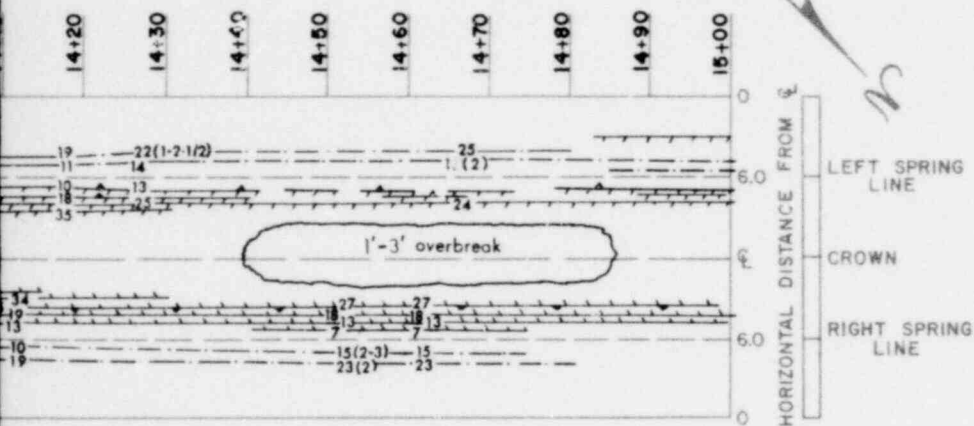
		4-19 78	no 5-6		4-20 78	4-21 78	4-24 78	4-25 78	4-26 78
no 5-6		0-24' of overbreak between rock bolt no 2-4							
5 rock bolts at 2' centers in steel ribs at 3'-3.5' centers spanned by wire mesh		5 rock bolts at 2' centers in steel ribs at							
2"-10"	1'-7"	2'-9"		Full shielding - Rock bolts in liner plates completely shield upper 3/8 of tunnel				approx. 6"	
10"	Bedding fractures & 1/2" to 18" thick, highly fractured fault zone w/gauge		Bedding fra						
No inflows	Slight seep, from fold	No inflows		Slight inflow from rock bolts				Sl	
7.5' water		Water dripping from shielding		2 inflows at approx. 1 gal./min.					
111.7' subsurface (shale)									

1233 064

POOR ORIGINAL

NG
RE
MUM
M
ATE

thickness.
inches
of



5.9 78	5.10 78	5.11 78
Shielding employed Cutting bit buried in overbreak		
Approx. 6"-10"		
Bedding spacing		
Amounts of moisture along crown		
14.5' water 107.2' subsurface shale		

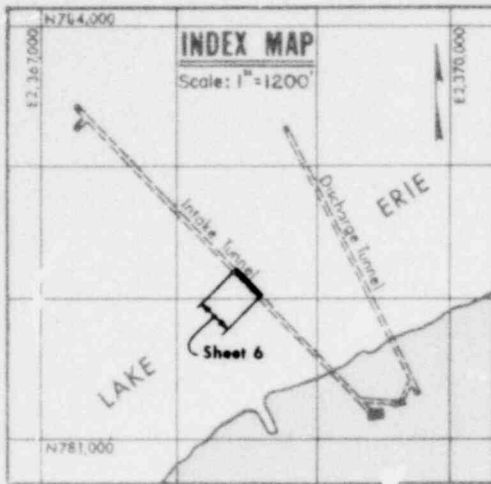
EXCAVATION PROGRESS
ESTIMATED ROCK
CONDITION (TERZAGHI NO.)
TEMPORARY SUPPORT
SYSTEM
BEDDING SPACING
FRACTURE SPACING
WATER CONDITION
DEPTH OF COVER

1241 065

GEOLOGIC MAP OF TUNNEL EXCAVATIONS

FIGURE 2
SHEET 6 OF 24

POOR ORIGINAL

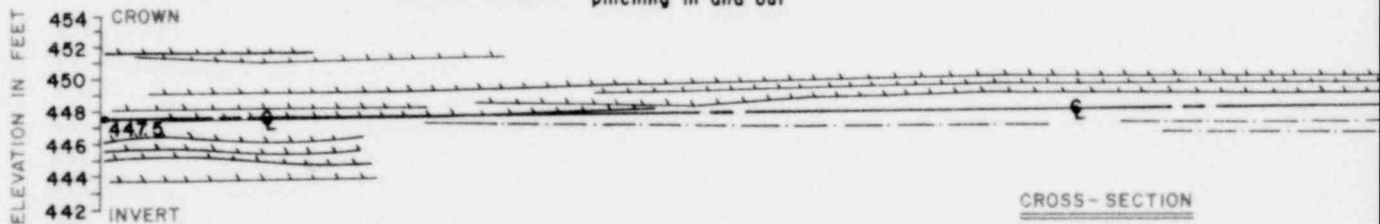
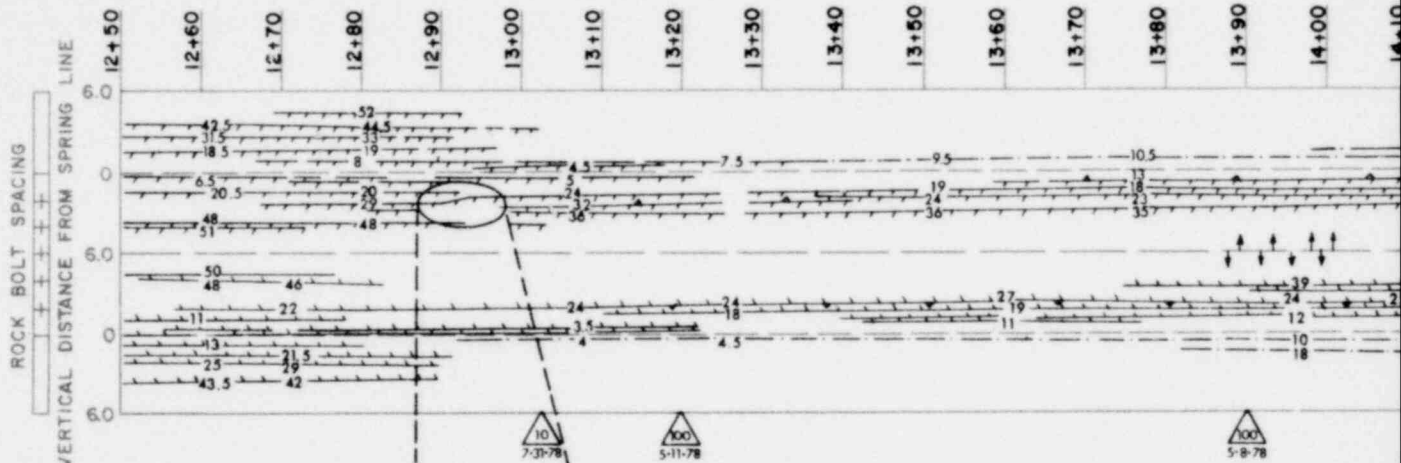


SYMBOLS

- 6 (1/2)* — HARD, TAN, BROWN, CHERTY, IRON BED OR LAMINAE
- - - 12 (0-2)* — DISCONTINUOUS IRON BED
- - - 12 (1)* — HARD, LIGHT GREY, SANDY SHALE TO SILTSTONE BED
- - - 10 (7)(0-2)* — DISCONTINUOUS IRON BED WITHIN GREY BED
- ⚡ — FRACTURE
- — — — — FAULT
- — — — — BEDDING PARTING
- ↕ — VERTICAL JOINT
- ↗ — INCLINED JOINT
- — — — — BEDDING, STRIKE AND DIP

- — — — — MOISTURE ALONG BED PARTING
- — — — — SEEPAGE FROM FEATURE
- ⬢ — OVER-CAVATION OR OVERBREAK ZONE, MAXIMUM AMOUNT SHOWN
- ⬢ — METHANE GAS, MAXIMUM PERCENT L.E.L. WITH D OF OCCURRENCE

*Note:
Number(s) in parentheses indicates bed
Number preceding parenthesis indicates
above or below spring line at station
measurement.



5-1 78	5-2 78	5-3 78	5-4 78	5-5 78	5-6 78
Rib bent 2"-6" between rock bolts no. 3-4		Rib bent 2"-6" between rock bolts no. 2-3		no. 4-5	
Approx. 8"-15"		Approx. 5"-15"		Rib bent 2"-6" between rock bolts no. 2-3	
No inflows		Approximately 20% of bedding fractures and rock bolts show minimal		Bedding fractures only, spaced as b	
+ 11.5 water					
+ 11.5 subsurface (shale)					

1238 066

POOR ORIGINAL

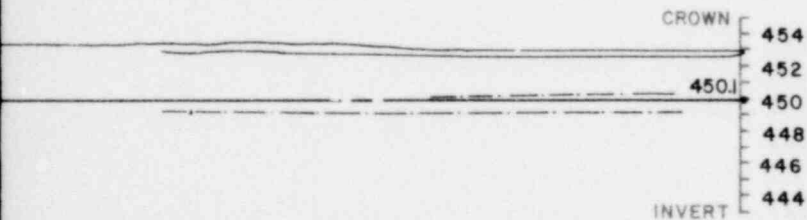
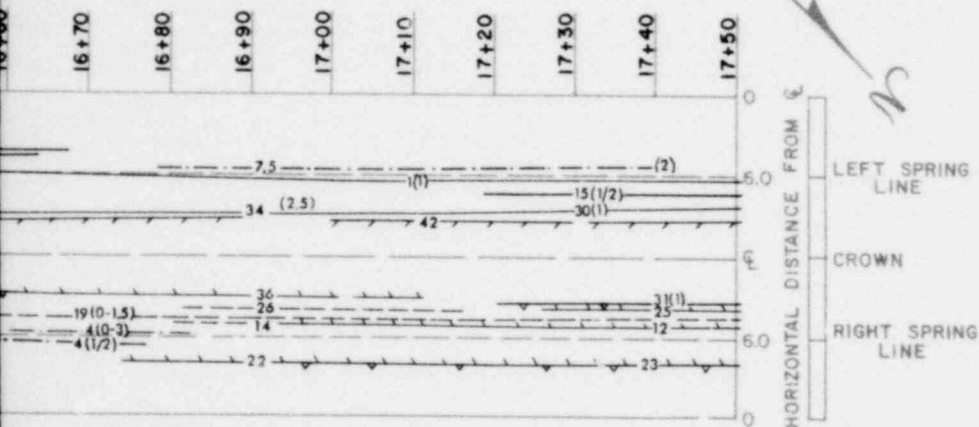
ING

RE

MUM

DATE

d thickness.
inches
of



5-18 78	5-10 78
no. 4-5	
by wire mesh	
6"-10"	
Approx. 10% of bedding fractures show moisture	
16.5' water 103.9' subsurface + (shale)	

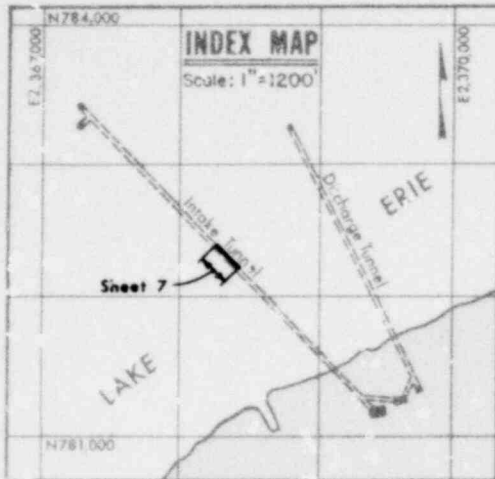
EXCAVATION PROGRESS
ESTIMATED ROCK
CONDITION (TERZAGHI NO.)
TEMPORARY SUPPORT
SYSTEM
BEDDING SPACING
FRACTURE SPACING
WATER CONDITION
DEPTH OF COVER

1248 067

GEOLOGIC MAP OF TUNNEL EXCAVATIONS

FIGURE 2
SHEET 7 OF 24

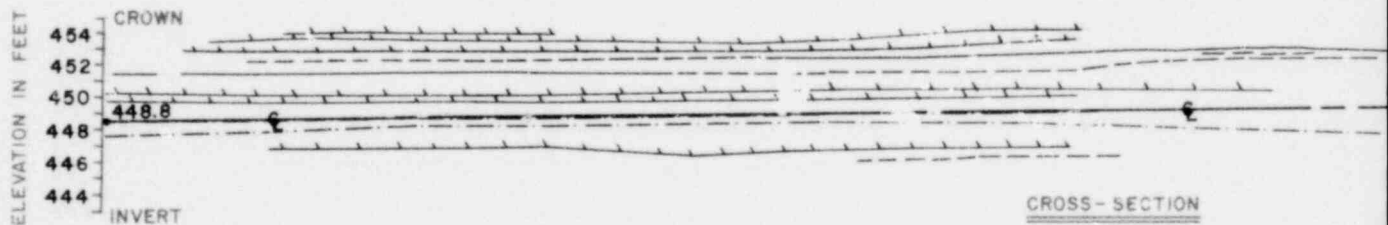
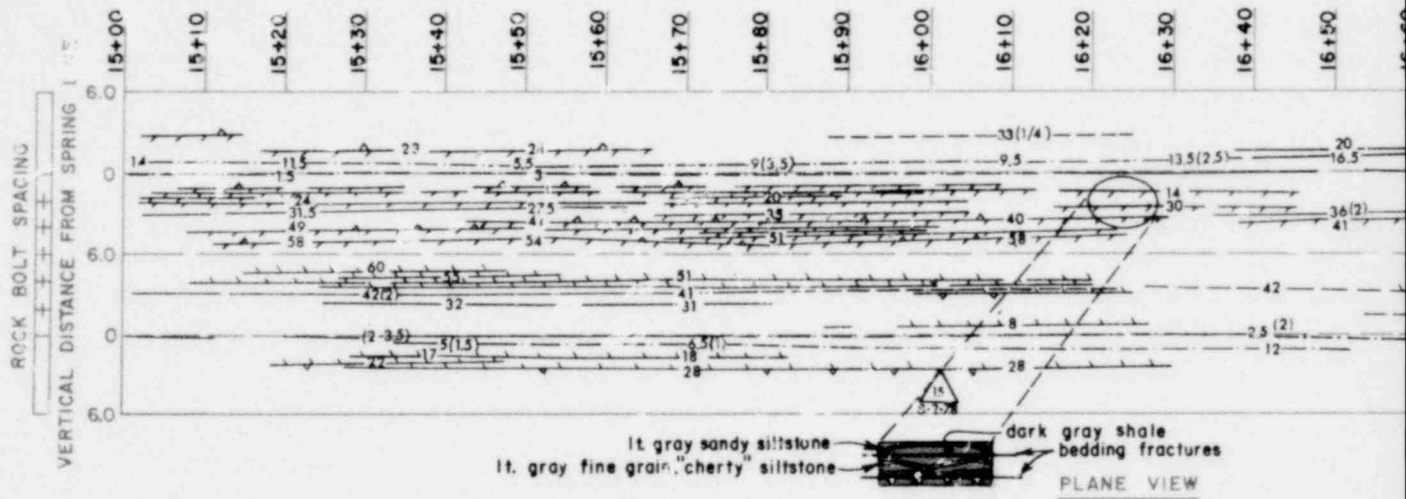
POOR ORIGINAL



- SYMBOLS**
- 6(1/2)* — HARD, TAN, BROWN, CHERTY, IRON BED OR LAMINAE
 - - - 12(0-2)* — DISCONTINUOUS IRON BED
 - - - 12(1)* — HARD, LIGHT GREY, SANDY SHALE & SILTSTONE BED
 - - - 10(7)(0-2)* — DISCONTINUOUS IRON BED WITHIN GREY BED
 - ⚡ — FRACTURE
 - FAULT
 - BEDDING PARTING
 - ↑ 75° — VERTICAL JOINT
 - INCLINED JOINT
 - BEDDING, STRIKE AND DIP

- MOISTURE ALONG BED PARTING
- SEEPAGE FROM FEATURE
- ⊞ — OVEREXCAVATION OR OVERBREAK ZONE, MAXIMUM AMOUNT SHOWN
- ⚠ — METHANE GAS, MAXIMUM PERCENT L.E.L. WITHIN OF OCCURRENCE

*Note:
Number(s) in parentheses indicates bed thickness.
Number preceding parentheses indicates distance above or below spring line of station measurement.



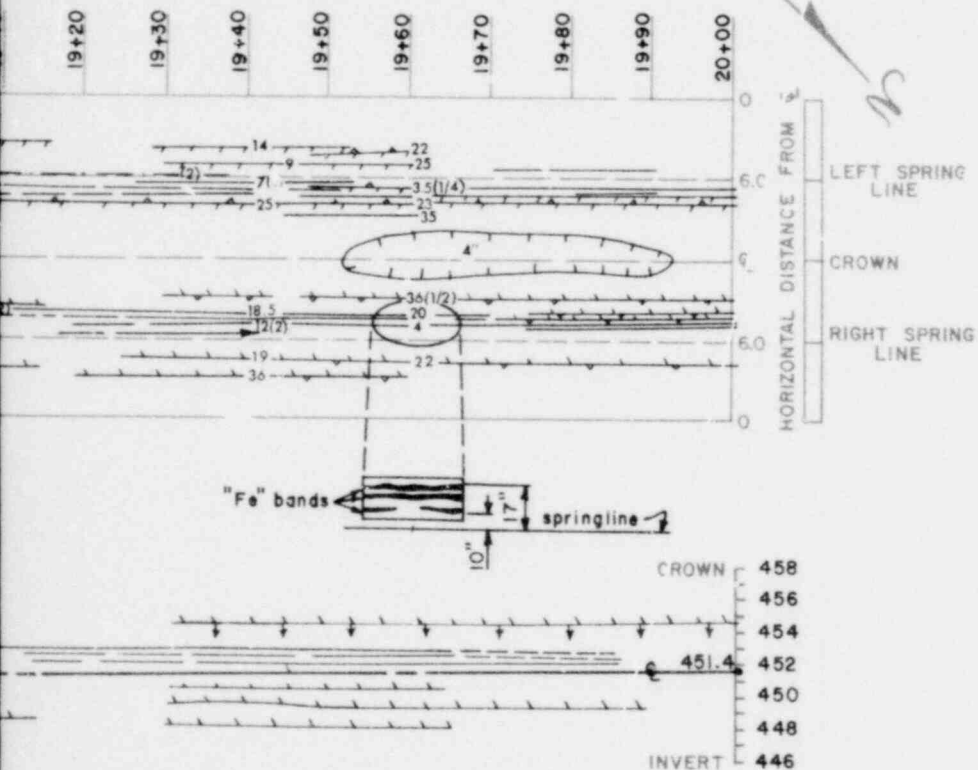
5-15/78	5-10/78	5-17/78
no. 4-5		
Slight scaling from crown along entire length of excavation (0'-2" overbreak)		
5 rock bolts at 2' centers in steel ribs at 3.5' to 4.0' centers, spanned		
Approx. 6"-10"	3'-9"	
Bedding fractures only		
Approx. 20% of bedding fractures show minimal moisture		
14.5' water		
107.2' subsurface (shale)		

1238 068

POOR ORIGINAL

ING
RE
MUM
W
ATE

thickness.
inches.
of



5-25 78	5-26 78
	Slight scaling from roof (0"-4") no. 4
	Same, ribs at 4.0' centers
	6" to 9"
	Slight moisture on approx. 60% of the excavation
	17.5' water
	101.5' subsurface (shale)

EXCAVATION PROGRESS
ESTIMATED ROCK
CONDITION (TERZAGHI NO.)
TEMPORARY SUPPORT
SYSTEM
BEDDING SPACING
FRACTURE SPACING
WATER CONDITION
DEPTH OF COVER

GEOLOGIC MAP OF TUNNEL EXCAVATIONS

FIGURE 2
SHEET 8 OF 24

1248 069

POOR ORIGINAL

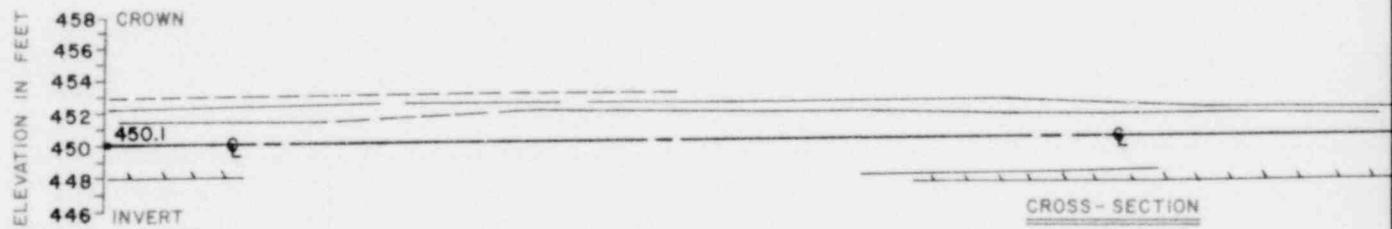
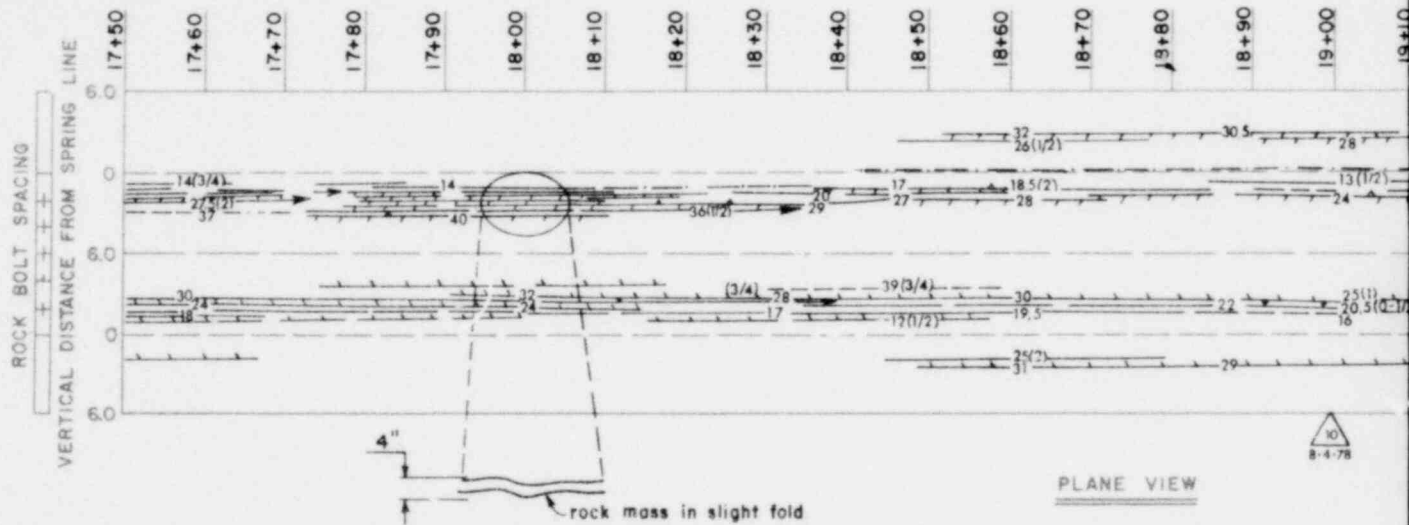


SYMBOLS

- 6 (1/2)* — HARD, TAN, BROWN, CHERTY, IRON BED OR LAMINAE
- 12 (0-2)* — DISCONTINUOUS IRON BED
- 12 (1)* — HARD, LIGHT GREY, SANDY SHALE TO SILTSTONE BED
- 10 (7) (0-2)* — DISCONTINUOUS IRON BED WITHIN GREY BED
- ⚡ FRACTURE
- ⚡ FAULT
- ⚡ BEDDING PARTING
- ⚡ VERTICAL JOINT
- ⚡ INCLINED JOINT
- ⚡ BEDDING, STRIKE AND DIP

- ⚡ MOISTURE ALONG BEDDING PARTING
- ⚡ SEEPAGE FROM FEATURE
- ⚡ OVEREXCAVATION OR OVERBREAK ZONE, MAXIMUM AMOUNT SHOWN
- ⚡ METHANE GAS, MAXIMUM PERCENT L.E.L. WITHIN ZONE OF OCCURRENCE

*Note:
Number(s) in parentheses indicates bed thickness.
Number preceding parenthesis indicates distance above or below spring line at station measurement.

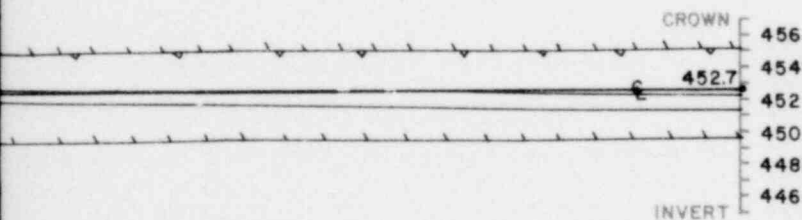
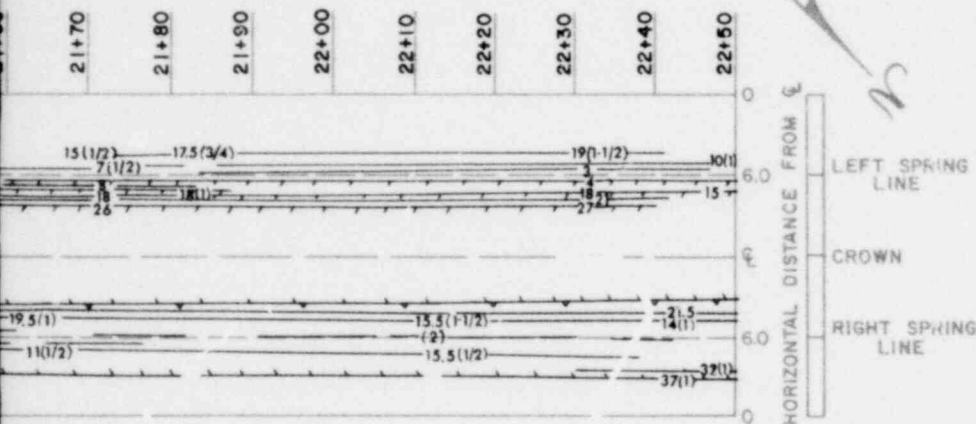


5-22 78	5-23 78	5-24 78
no. 4		
Slight scaling along crown for entire length (between rock bolt 2 & 4)		
5 rock bolts at 2.0' centers in steel ribs at 3.5' to 4.0' centers, spanned by wire mesh		
Approx. 6"		Approx. 4" to 10"
Bedding fractures only		
Traces of moisture along a couple bedding fractures		
16.5' water		
101.6' subsurface (shale)		

POOR ORIGINAL

NG
RE
MUM
M
ATE

d thickness.
inches
of



6-3/78
bolts at 2' centers in steel ribs at 3.5'-4.0' centers spanned by wire mesh
4"-9"
th
17.5' water
100.3' subsurface (shale) +

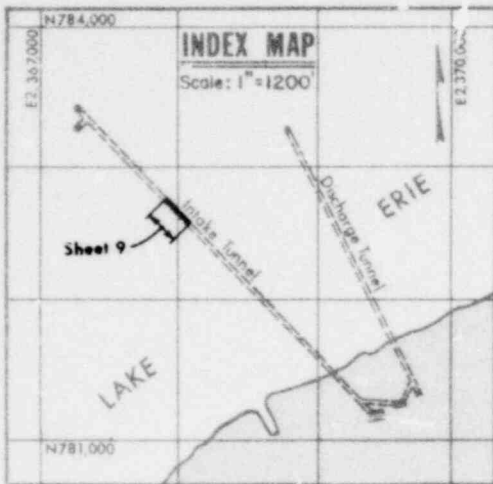
EXCAVATION PROGRESS
ESTIMATED ROCK
CONDITION (TERZAGHI NO.)
TEMPORARY SUPPORT
SYSTEM
BEDDING SPACING
FRACTURE SPACING
WATER CONDITION
DEPTH OF COVER

1248 071

GEOLOGIC MAP OF TUNNEL EXCAVATIONS

FIGURE 2
SHEET 9 OF 24

POOR ORIGINAL

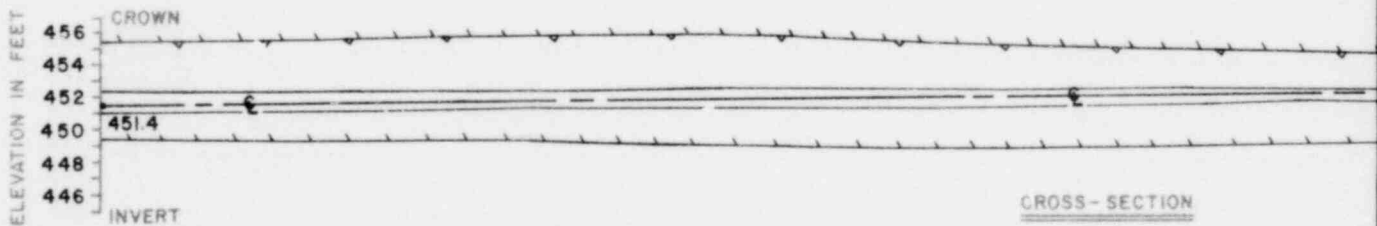
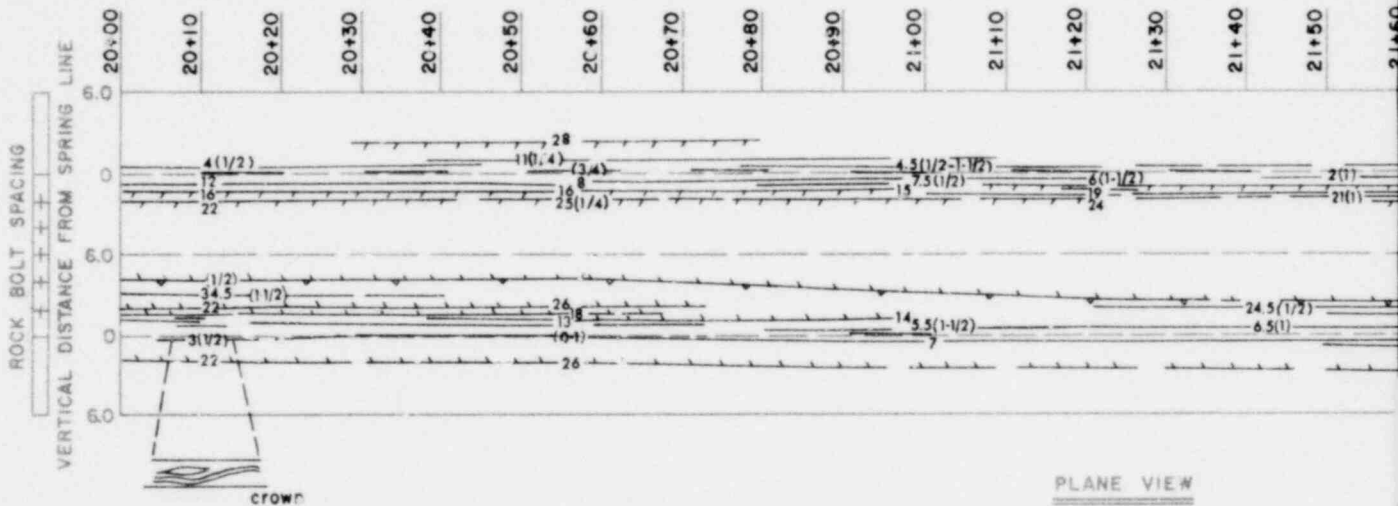


SYMBOLS

- 6(1/2)* — HARD, TAN, BROWN, CHERTY, IRON BED OR LAMINAE
- - - 12(0-2)* — DISCONTINUOUS IRON BED
- - - 12(1)* — HARD, LIGHT GREY, SANDY SHALE TO SILTSTONE BED
- - - 10(7/8-2)* — DISCONTINUOUS IRON BED WITHIN GREY BED
- ⚡ — FRACTURE
- — — — — FAULT
- — — — — BEDDING PARTING
- — — — — VERTICAL JOINT
- — — — — INCLINED JOINT
- — — — — BEDDING, STRIKE AND DIP

- — — — — MOISTURE ALONG BED PARTING
- — — — — SEEPAGE FROM FEATURE
- — OVEREXCAVATION OR OVERBREAK ZONE, MAXIMUM AMOUNT SHOWN
- △ — METHANE GAS, MAXIMUM PERCENT L.E.L. WITHIN OF OCCURRENCE

*Note: Number(s) in parentheses indicates bed Number preceding parenthesis indicates above or below spring line at station measurement.



5+30	5+31	6+1	6+2
7/8	7/8	7/8	7/8
no. 4			
5 rock bolts at 2' centers in steel ribs at 4' centers spanned by wire mesh			
5 rock			
6"-9"			
Bedding fractures only			
Slight moisture from open parting along east wall for entire length			
+17.5 water			
+101.6 subsurface (shale)			

1238 072

POOR ORIGINAL

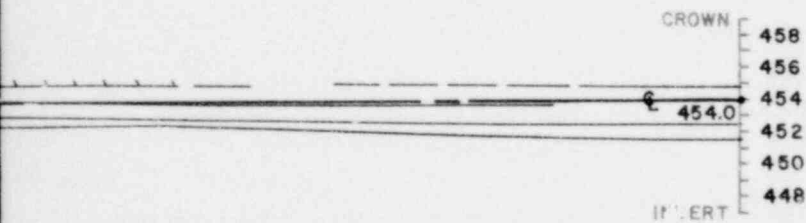
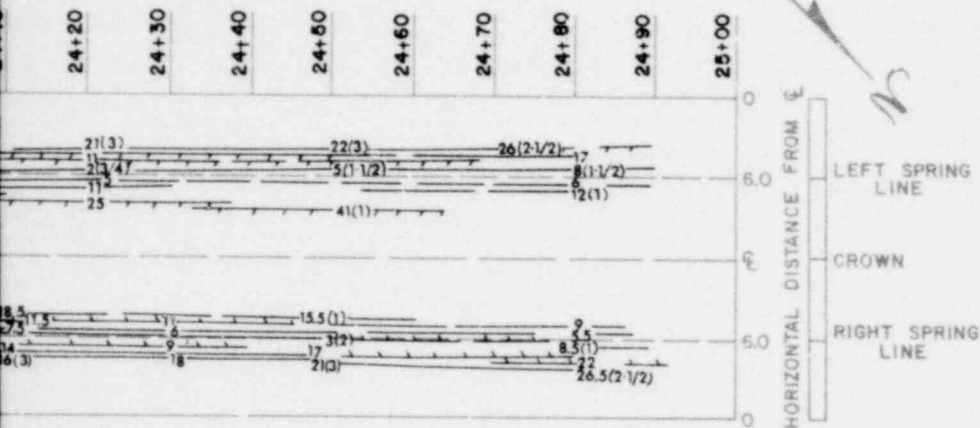
ING

RE

MUM

M
DATE

d thickness
inches
of



6.9	78
overbreak between rock bolts nos. 2 & 4, 1"-6" deep (max 3")	
by wire mesh	
3" - 9"	
No seepage	
18.5' water	
98.0' subsurface (shale) +	

EXCAVATION PROGRESS

ESTIMATED ROCK
CONDITION (TERZAGHI NO.)

TEMPORARY SUPPORT
SYSTEM

BEDDING SPACING

FRACTURE SPACING

WATER CONDITION

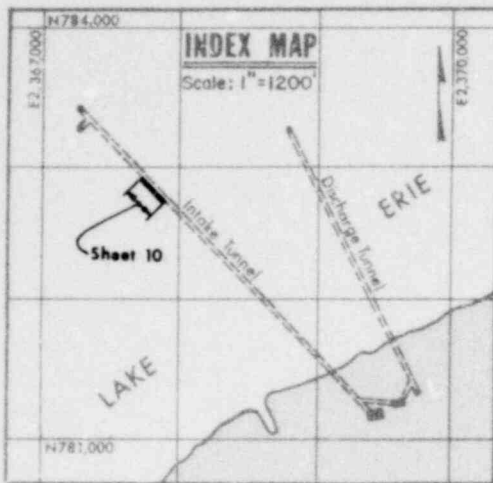
DEPTH OF COVER

1248 073

GEOLOGIC MAP OF TUNNEL EXCAVATIONS

FIGURE 2
SHEET 10 OF 24

POOR ORIGINAL

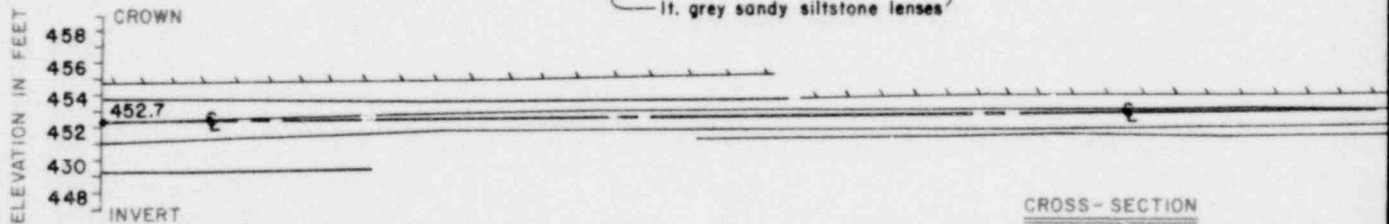
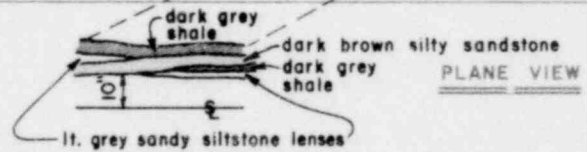
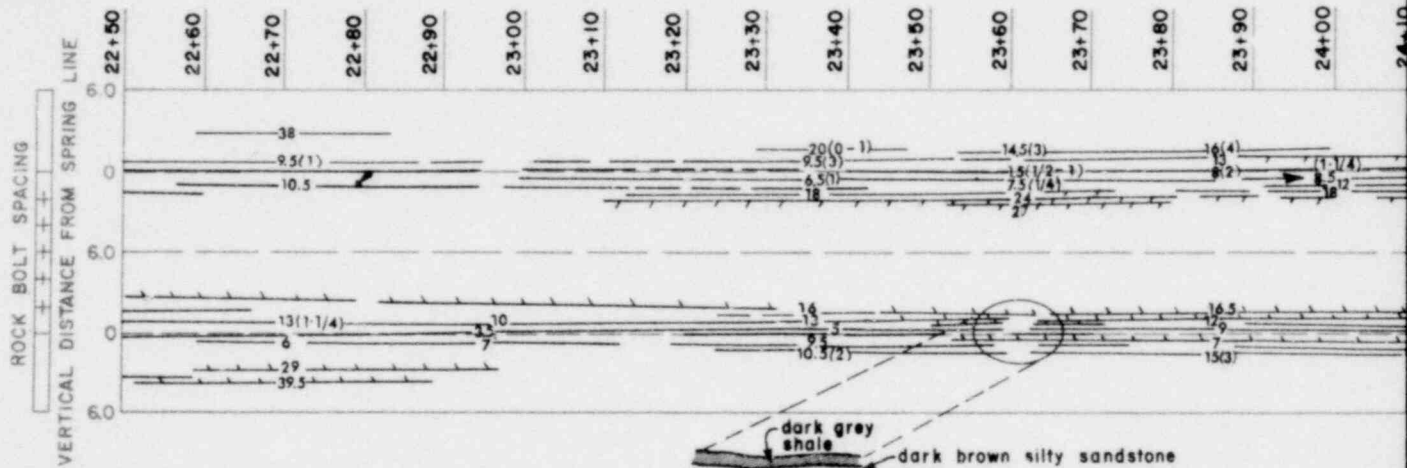


SYMBOLS

- 6 (1/2)* — HARD, TAN, BROWN, CHERTY, IRON BED OR LAMINAE
- - - 12 (0-2)* - - - DISCONTINUOUS IRON BED
- - - 12 (1)* - - - HARD, LIGHT GREY, SANDY SHALE TO SILTSTONE BED
- - - 10 (7/0-2)* - - - DISCONTINUOUS IRON BED WITHIN GREY BED
- ⚡ FRACTURE
- ⚡ FAULT
- BEDDING PARTING
- ↕ 75° VERTICAL JOINT
- ↗ 2° INCLINED JOINT
- BEDDING, STRIKE AND DIP

- MOISTURE ALONG BED PARTING
- SEEPAGE FROM FEATURE
- 2' OVEREXCAVATION OR OVERBREAK ZONE, MAXIMUM AMOUNT SHOWN
- 20 4 28-77 METHANE GAS, MAXIMUM PERCENT L.E.L. WITHIN OF OCCURRENCE

Note:
Number(s) in parentheses indicates the number preceding parenthesis indicates above or below spring line at station measurement.



CROSS-SECTION

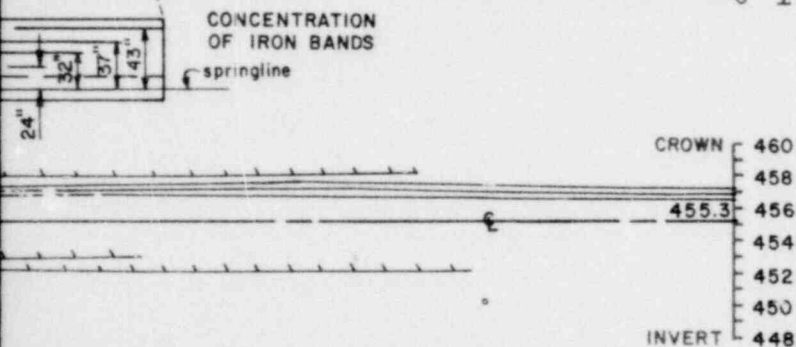
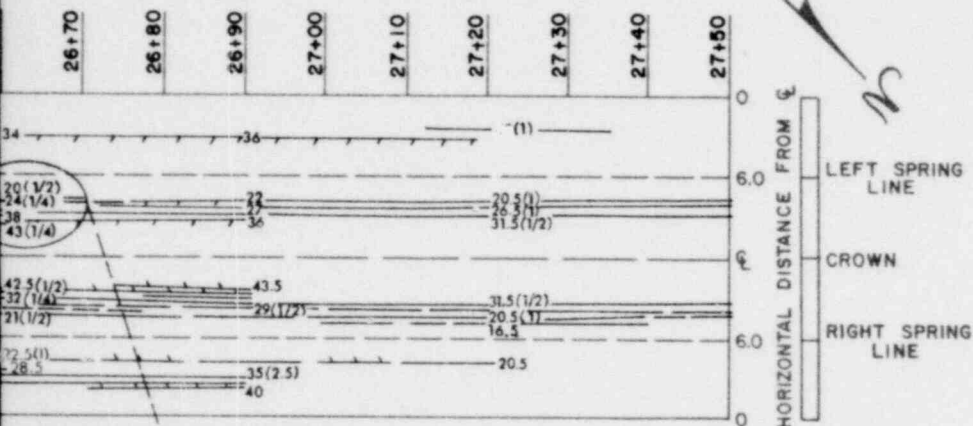
no. 4	0-6/78	0-7/78	0-8/78	no. 4
Slight overbreak between rock bolt nos. 2 & 4, 0"-6" deep (most >4")				
5 rock bolts at 2' centers in steel ribs at 3.5' to 4.0' centers, spanning				
3"-7"				
Bedding fractures only, spaced at or above				
Moist bedding fracture, above springline along east wall				
17.5' water				
100.3' subsurface (shale)				

1238 074

POOR ORIGINAL

NG
RE
MUM
M
ATE

thickness.
inches
of



along entire section, 0' - 6'	5 rock bolts at 2' centers in steel ribs at 3.5'-4.0' centers spanned by wire mesh
at	4' - 9'
No seepage	
	20.5' water + 24.7' subsurface (shale)

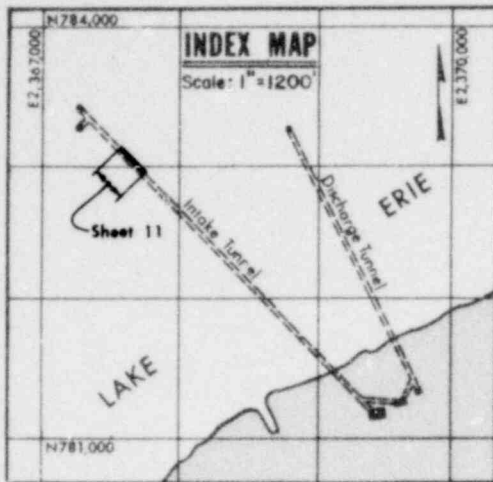
EXCAVATION PROGRESS
ESTIMATED ROCK
CONDITION (TERZAGHI NO.)
TEMPORARY SUPPORT
SYSTEM
BEDDING SPACING
FRACTURE SPACING
WATER CONDITION
DEPTH OF COVER

GEOLOGIC MAP OF TUNNEL EXCAVATIONS

1241 075

FIGURE 2
SHEET 11 OF 24

POOR ORIGINAL

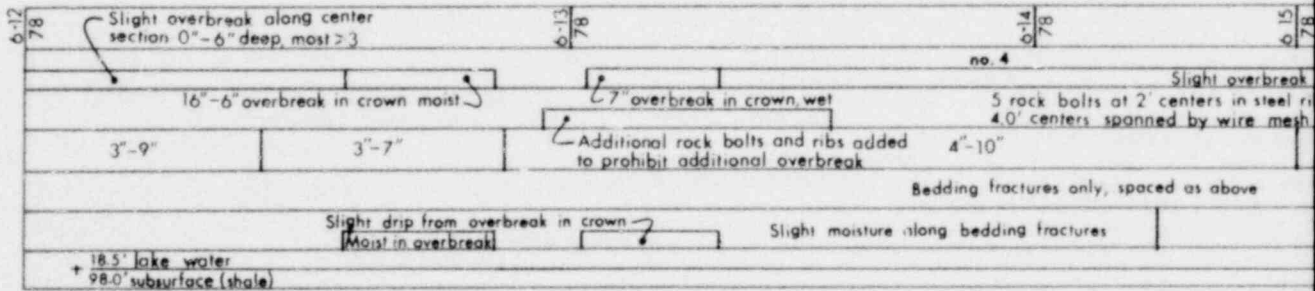
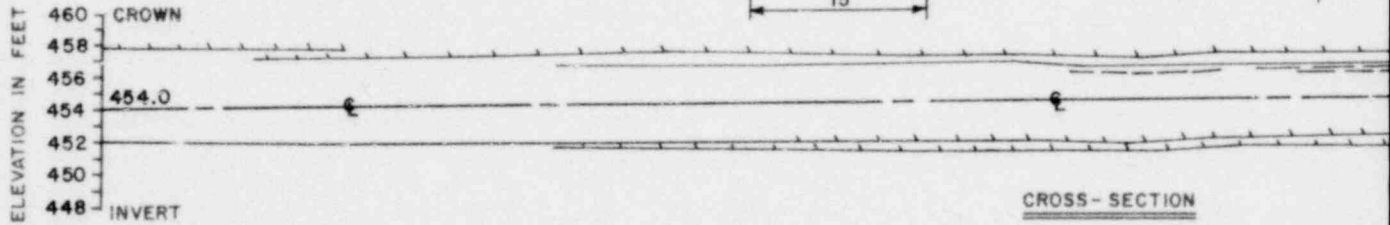
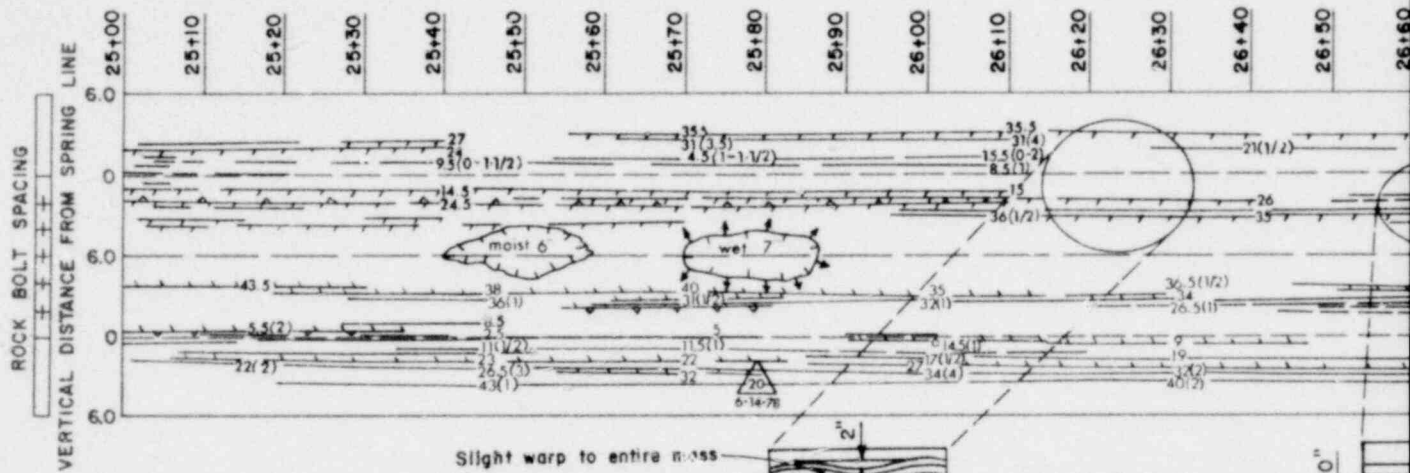


SYMBOLS

- 6 (1/2)* — HARD, TAN, BROWN, CHERTY, IRON BED OR LAMINAE
- - 12 (0-2)* - DISCONTINUOUS IRON BED
- - 12 (1)* - HARD, LIGHT GRAY, SANDY SHALE TO SILTSTONE BED
- - 10 (7X0-2)* - DISCONTINUOUS IRON BED WITHIN GREY BED
- ⚡ FRACTURE
- ⚡ FAULT
- BEDDING PARTING
- ↑ 75° VERTICAL JOINT
- ↗ 20° INCLINED JOINT
- BEDDING, STRIKE AND DIP

- MOISTURE ALONG BED PARTING
- SEEPAGE FROM FEATURE
- 2 OVEREXCAVATION OR OVERBREAK ZONE, MAXIMUM AMOUNT SHOWN
- 20 METHANE GAS, MAXIMUM PERCENT L.E.L. WITH D OF OCCURRENCE

*Note:
Number(s) in parentheses indicates bed
Number preceding parenthesis indicates
above or below spring line at station
measurement.

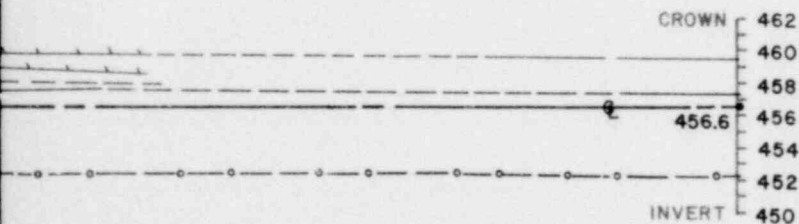
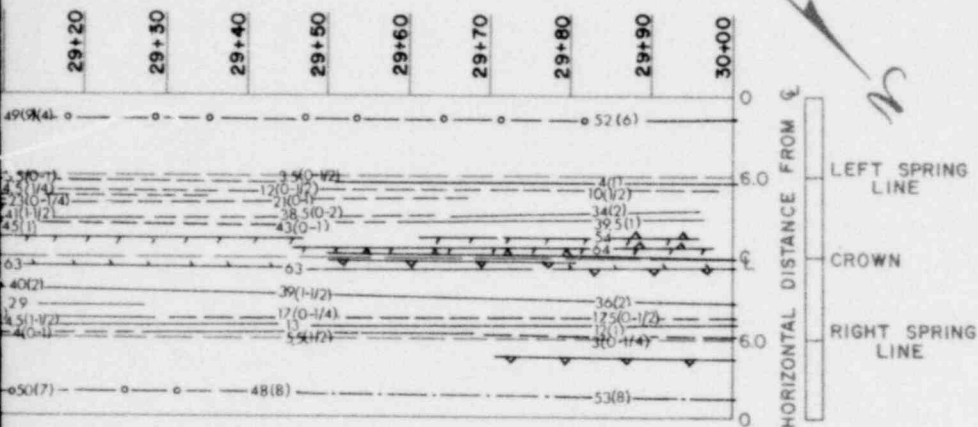


1238 076

POOR ORIGINAL

ING
RE
MUM
M
ATE

thickness
inches
of



6-11/78	5-22/78
entire section in crown	
5 rock bolts at 2' centers in steel ribs at 4' centers spanned by wire mesh	
Slight moisture from bedding fracture in crown	
22.5' water	
91.4' subsurface (shale)	

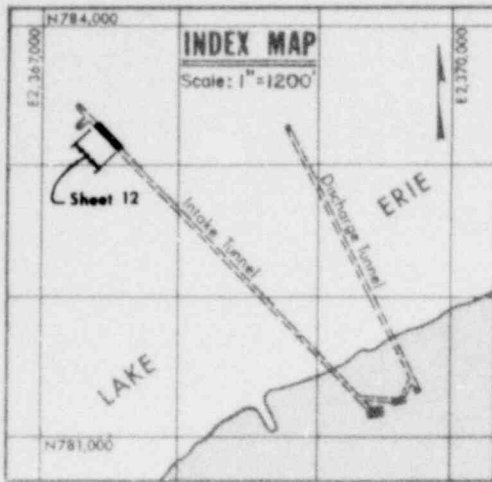
EXCAVATION PROGRESS
ESTIMATED ROCK
CONDITION (TERZAGHI NO.)
TEMPORARY SUPPORT
SYSTEM
BEDDING SPACING
FRACTURE SPACING
WATER CONDITION
DEPTH OF COVER

GEOLOGIC MAP OF TUNNEL EXCAVATIONS

FIGURE 2
SHEET 12 OF 24

1248 077

POOR ORIGINAL

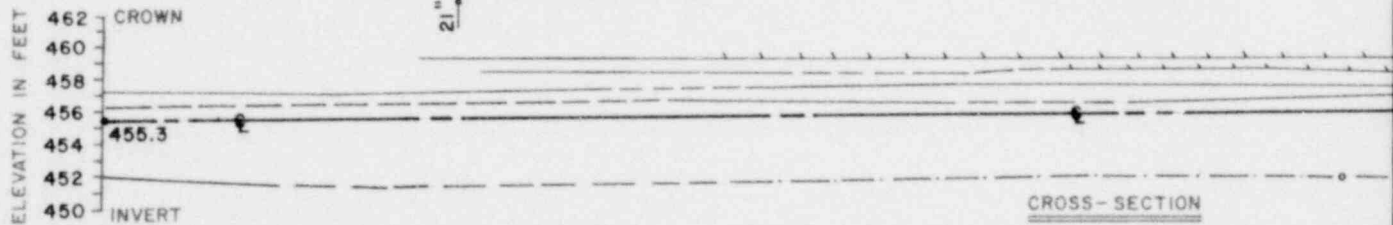
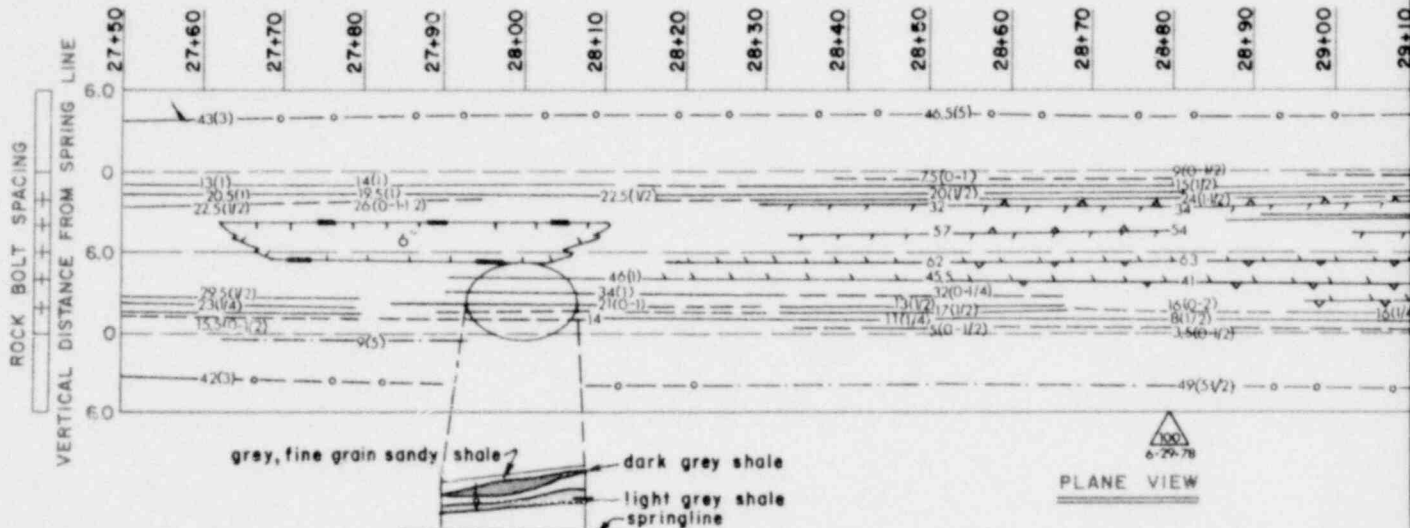


SYMBOLS

- 6 (1/2) — HARD, TAN, BROWN, CHERTY, IRON BED OR LAMINAE
- - - 12 (0-2) — DISCONTINUOUS IRON BED
- - - 12 (1) — HARD, LIGHT GREY, SANDY SHALE TO SILTSTONE BED
- - - 10 (X0-2) — DISCONTINUOUS IRON BED WITHIN GREY BED
- ⚡ — FRACTURE
- — — — — FAULT
- — — — — BEDDING PARTING
- ⊥ — VERTICAL JOINT
- ↗ — INCLINED JOINT
- — — — — BEDDING, STRIKE AND DIP

- — — — — MOISTURE ALONG BED PARTING
- ⬇ — — — — — SEEPAGE FROM FEATURE
- ⬆ — — — — — OVEREXCAVATION OR OVERBREAK ZONE, MAXIMUM AMOUNT SHOWN
- ⬆ — — — — — METHANE GAS, MAXIMUM PERCENT L.E.L. WITH D OF OCCURRENCE

Note:
Number(s) in parentheses indicates bed
Number preceding parenthesis indicates
above or below spring line at station
measurement.



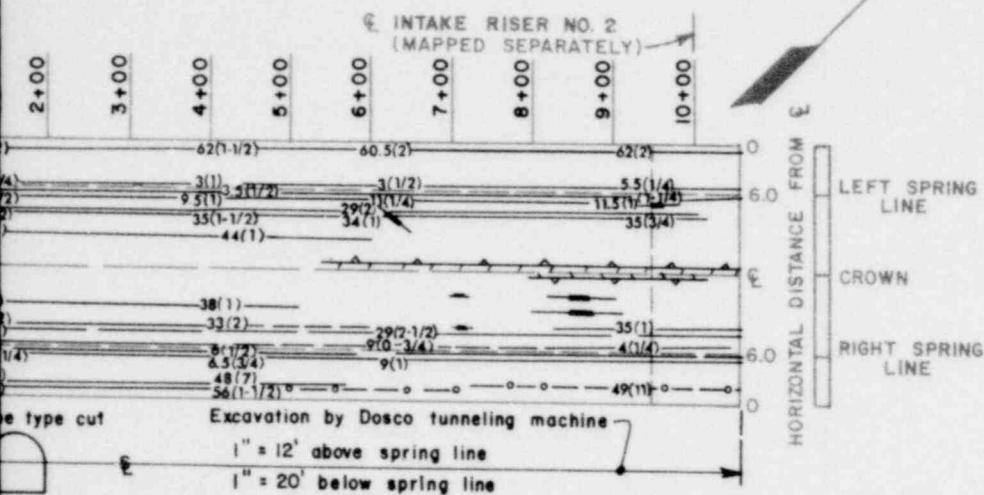
6-19 78	Overbreak 6" deep limited by vertical joints trending parallel to tunnel bearing	6-20 78	no. 4	Slight overbreak along
3 rock bolts at 3' centers in steel ribs at 4' centers spanned by wire mesh				
5 rock bolts at 2' centers in steel ribs at 4' centers spanned by wire mesh 3'-8"				
Bedding fractures only, spaced as above				
Slight moisture from all bedding fractures				
+ 20.5' water				
+ 94.7' subsurface (shale)				

1238 078

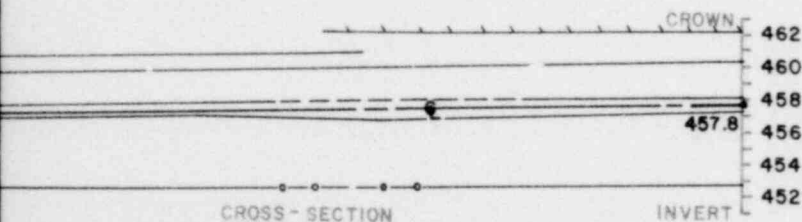
POOR ORIGINAL

ING
RE
IMUM
M
DATE

and thickness.
inches
of



PLANE VIEW B



CROSS-SECTION

10-12	10-13	10-15	10-17	10-18	10-19	10-20	10-24	10-25	10-26
78	78	78	78	78	78	78	78	78	78
no. 4									
rock bolts at 2' centers in steel ribs at 4'-4.5' centers, spanned by wire mesh									
3"-8" Vertical joints, trending parallel to tunnel bearing, spaced at 2'-4'									
Bedding fractures only, spaced as above									
No seepage									
Slight moisture from bedding parting in crown									
20.5' water									
91.2' subsurface (shale)									

EXCAVATION PROGRESS

ESTIMATED ROCK
CONDITION (TERZAGHI NO.)
TEMPORARY SUPPORT
SYSTEM

BEDDING SPACING

FRACTURE SPACING

WATER CONDITION

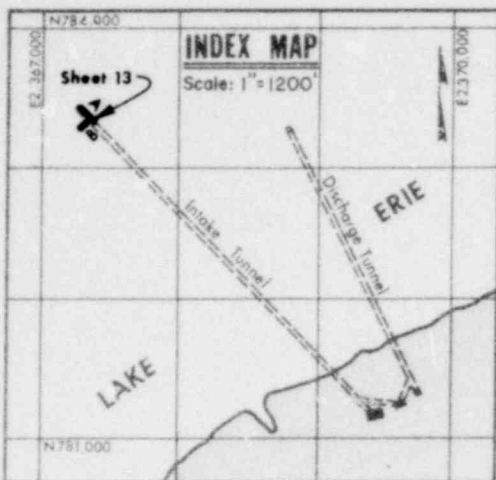
DEPTH OF COVER

1248 079

GEOLOGIC MAP OF TUNNEL EXCAVATIONS

FIGURE 2
SHEET 13 OF 24

POOR ORIGINAL

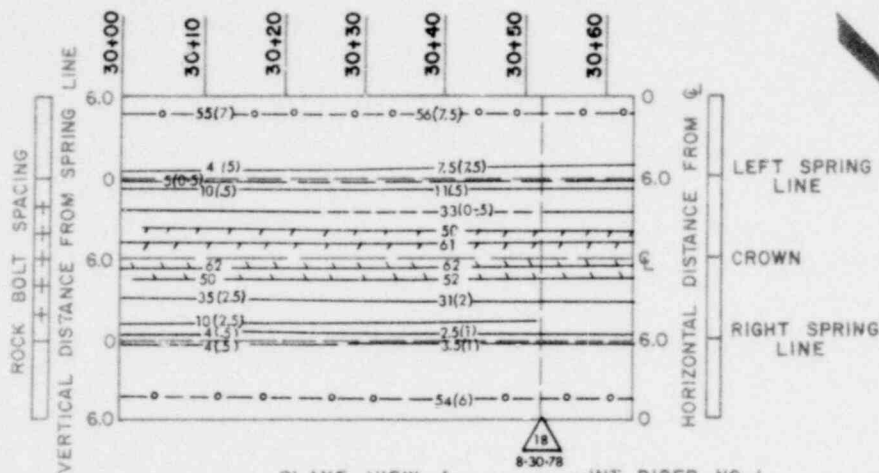


SYMBOLS

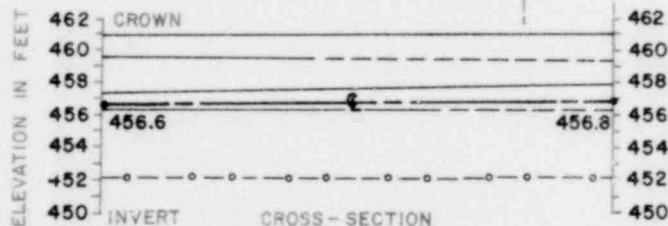
- 6(1/2)* — HARD, TAN, BROWN, CHERTY, IRON BED OR LAMINAE
- - 12(9-2)* - - DISCONTINUOUS IRON BED
- - 12(1)* - - HARD, LIGHT GREY, SANDY SHALE TO SILTSTONE BED
- - 10(7X0-2)* - - DISCONTINUOUS IRON BED WITHIN GREY BED
- ⚡ FRACTURE
- / — FAULT
- / — BEDDING PARTING
- / — VERTICAL JOINT
- / — INCLINED JOINT
- / — BEDDING, STRIKE AND DIP

- / — MOISTURE ALONG BEDDING PARTING
- / — SEEPAGE FROM FEATURE
- ⬢ OVEREXCAVATION OR OVERBREAK ZONE, MAXIMUM AMOUNT SHOWN
- ⚠ METHANE GAS, MAXIMUM PERCENT L.E.L. WITH OF OCCURRENCE

* Note:
Number(s) in parentheses indicates bed thickness in feet.
Number preceding parenthesis indicates stationing above or below spring line at station measurement.



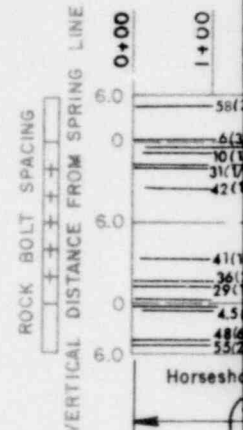
PLANE VIEW A
INT. RISER NO. 1 (MAPPED SEPARATELY)



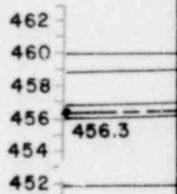
CROSS-SECTION

no. 4	
Slight overbreak along entire section	
5 rock bolts at 2' centers in steel ribs at 4' centers spanned by wire mesh	
4"-9"	
Bedding fractures only, spaced as above	
Slight moisture along all bedding fractures	
+ 22.5' lake water	22.5'
+ 91.5' subsurface (shale)	91.2'

- EXCAVATION PROGRESS
- ESTIMATED ROCK CONDITION (TERZAGHI NO.)
- TEMPORARY SUPPORT SYSTEM
- BEDDING SPACING
- FRACTURE SPACING
- WATER CONDITION
- DEPTH OF COVER



Horseshoe

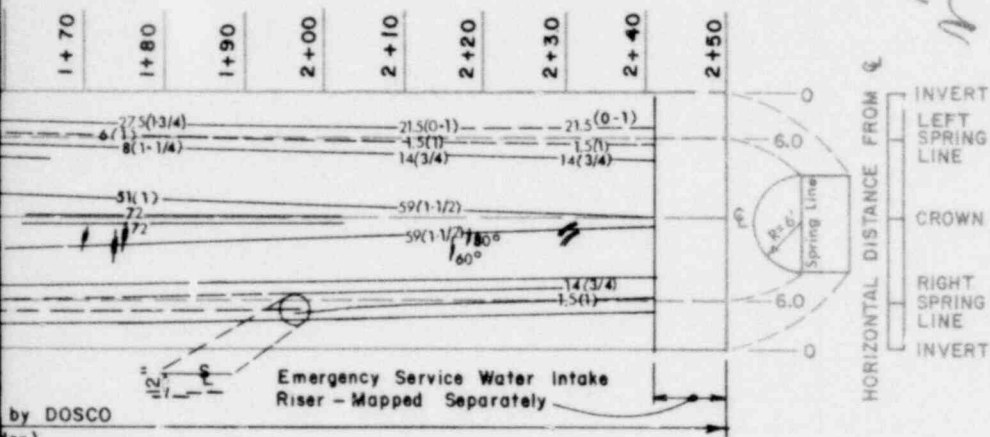


1238 080

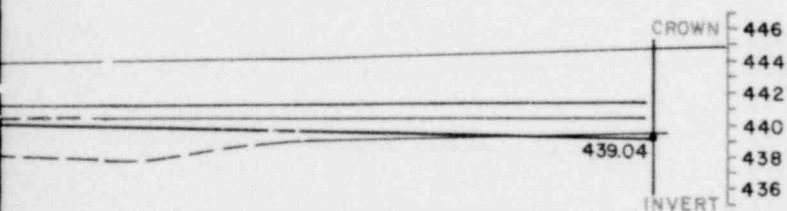
POOR ORIGINAL

ING
RE
IMUM
M
DATE

d thickness.
inches
of



by DOSCO
Machine



11-22	77	11-24	77
2" - 7"			
2" - 6"			
approx. 33.5' lacustrine, 27.5' glacial till			
121' of shale			

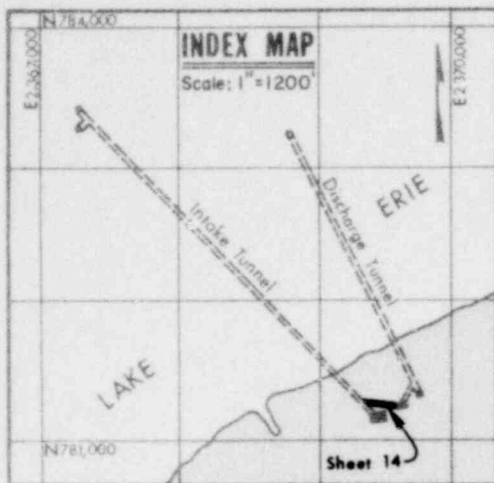
EXCAVATION PROGRESS
ESTIMATED ROCK
CONDITION (TERZAGHI NO.)
TEMPORARY SUPPORT
SYSTEM
BEDDING SPACING
FRACTURE SPACING
WATER CONDITION
DEPTH OF COVER

1248 081

GEOLOGIC MAP OF TUNNEL EXCAVATIONS

FIGURE 2
SHEET 14 OF 24

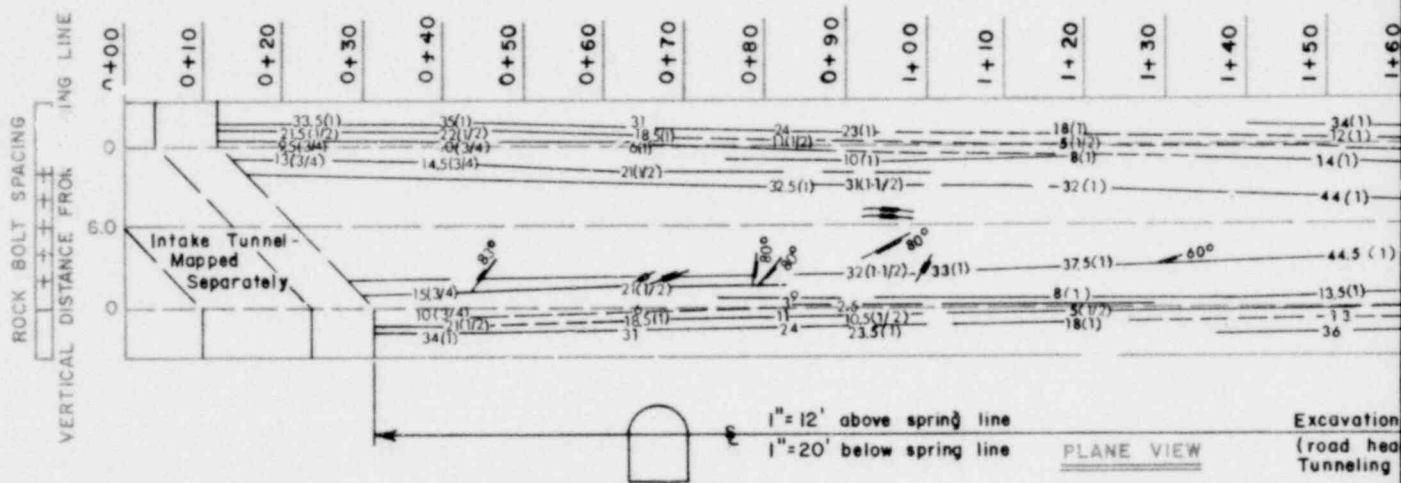
POOR ORIGINAL



- SYMBOLS**
- $\circ (1/2)$ HARD, TAN, BROWN, CHERTY, IRON BED OR LAMINAE
 - $12 (0-2)$ DISCONTINUOUS IRON BED
 - $12 (1)$ HARD, LIGHT GREY, SANDY SHALE TO SILTSTONE BED
 - $10 (7 \times 0-2)$ DISCONTINUOUS IRON BED WITHIN GREY BED
 - FRACTURE
 - FAULT
 - BEDDING PARTING
 - VERTICAL JOINT
 - INCLINED JOINT
 - BEDDING, STRIKE AND DIP

- MOISTURE ALONG BED PARTING
- SEEPAGE FROM FEATURE
- OVEREXCAVATION OR OVERBREAK ZONE, MAXIMUM AMOUNT SHOWN
- METHANE GAS, MAXIMUM PERCENT L.E.L. WITHIN OF OCCURRENCE

* Note: Number(s) in parentheses indicates bedrock thickness. Number preceding parenthesis indicates distance above or below spring line at station measurement.



ELEVATION IN FEET
CROWN
446
444
442
440
438
436
INVERT

CROSS SECTION

8-31	9-11	11-3	11-7	11-8	11-9	11-11	11-14	11-17
77	77	77	77	77	77	77	77	77
no. 4								
5 rock bolts at 2' centers in steel ribs at 3'-3.5' centers, spanned by w								
2'-6"	2"	1/2"-4"	3'-6"	3'-7"	2'-6"	1'-6"	3'-5"	
1'	Widely spaced 10' - 20'		1' - 10'		Widely spaced			
No seepage								
approx. + 33.5' of lacustrine and, 27.5' glacial till								
11.85' of shale								

1238 082

POOR ORIGINAL



SYMBOLS

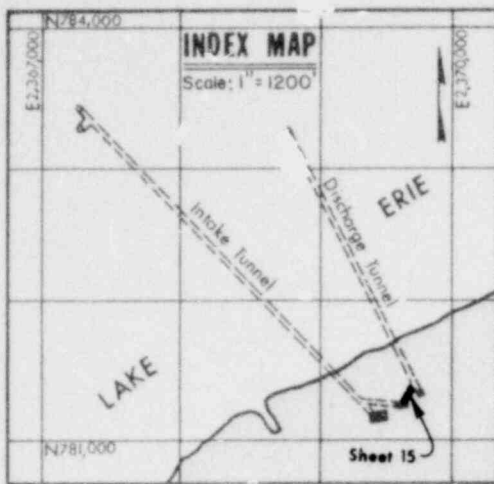
	HARD, TAN, BROWN, CHERTY, IRON BED OR LAMINAE
	DISCONTINUOUS IRON BED
	HARD, LIGHT GREY, SANDY SHALE TO SILTSTONE BED
	DISCONTINUOUS IRON BED WITHIN GREY BED
	FRACTURE
	FAULT
	BEDDING PARTING
	VERTICAL JOINT
	INCLINED JOINT
	BEDDING, STRIKE AND DIP
	MOISTURE ALONG BEDDING PARTING
	SEEPAGE FROM FEATURE
	OVEREXCAVATION OR OVERBREAK ZONE, MAXIMUM AMOUNT SHOWN

*Note:
Number(s) in parentheses indicates bed thickness.
Number preceding parenthesis indicates inches above or below spring line at station of measurement.

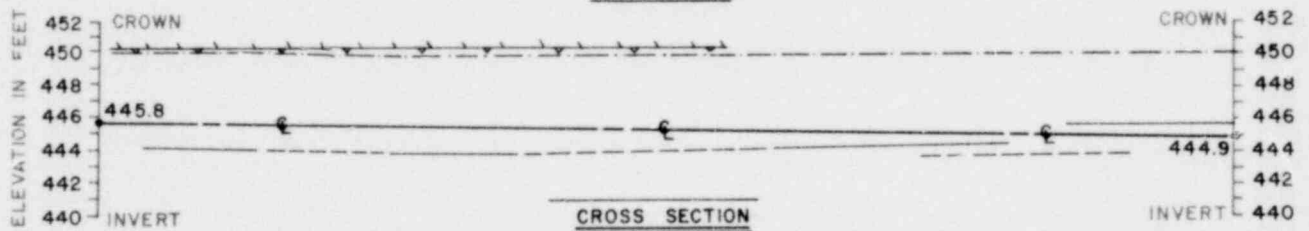
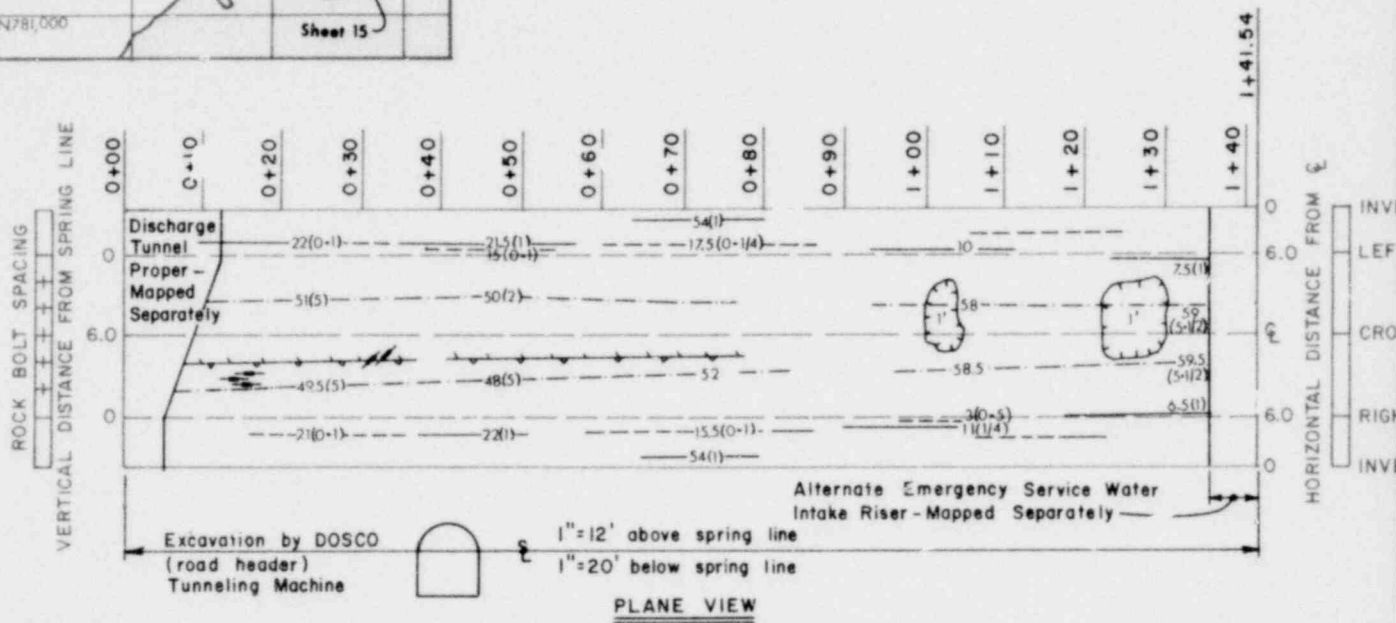
1241 083

GEOLOGIC MAP OF TUNNEL EXCAVATIONS

FIGURE 2
SHEET 15 OF 24



POOR ORIGINAL



1-4 78	1-6 78	1-11 78	1-13 78
no. 4			
5 rock bolts at 2' centers, in steel ribs at 3.0'-3.5' centers, spanned by wire mesh			
1/2"-5"	6"-2"	1"-8"	Approx. 1"-5" partings vague
7"-14"	Bedding fractures only, spaced as above		
Slight seepage from bedding parting along west wall			No inflows
Approx. 33.5' lacustrine, 27.5' glacial till		Approx. 33.5' lacustrine, 27.5' glacial till	
111.7' shale		113.1' shale	

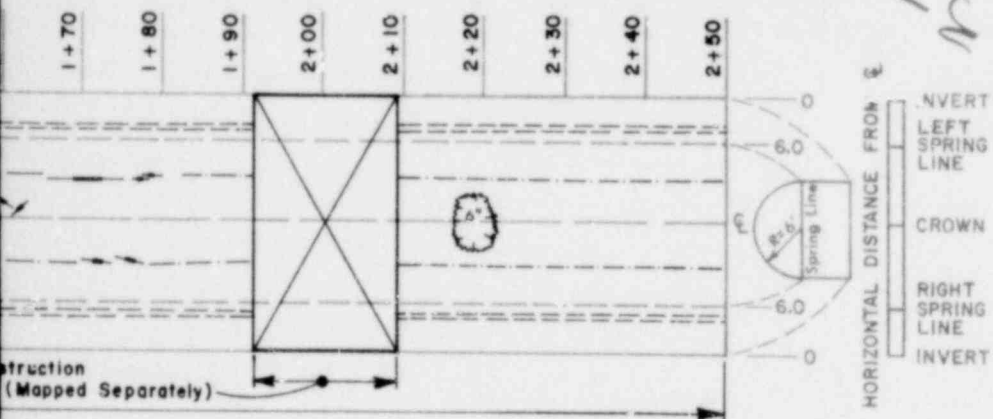
EXCAVATION
ESTIMATED
TEMPORARY
BEDDING
FRACTURE
WATER CO
DEPTH OF

1238 084

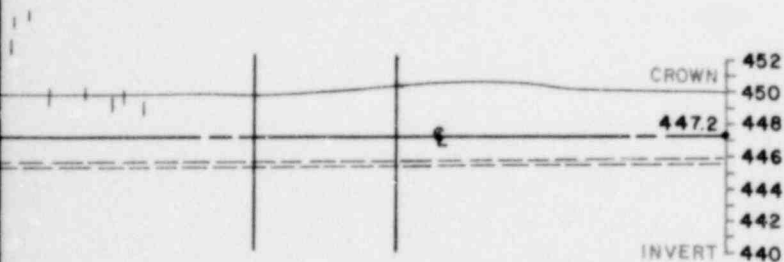
POOR ORIGINAL

INGS
RE
IMUM
IM
DATE

thickness,
inches
of



struction
(Mapped Separately)



12-10 77	12-12 77	10-28 77	10-20 77	10-28 77	12-10 77	1-29 76
no. 4-5						
1/2" - 6"						
1' - 4' Noticed substantial amount of moisture in downshaft, May be from melting ice						
Approx. 33.5' lacustrine + 27.5' glacial till & 109.8' shale						

EXCAVATION PROGRESS
ESTIMATED ROCK
CONDITION (TERZAGHI NO.)
TEMPORARY SUPPORT
SYSTEM
BEDDING SPACING
FRACTURE SPACING
WATER CONDITION
DEPTH OF COVER

1248 085

GEOLOGIC MAP OF TUNNEL EXCAVATIONS

FIGURE 2
SHEET 16 OF 24

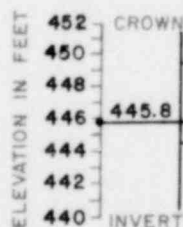
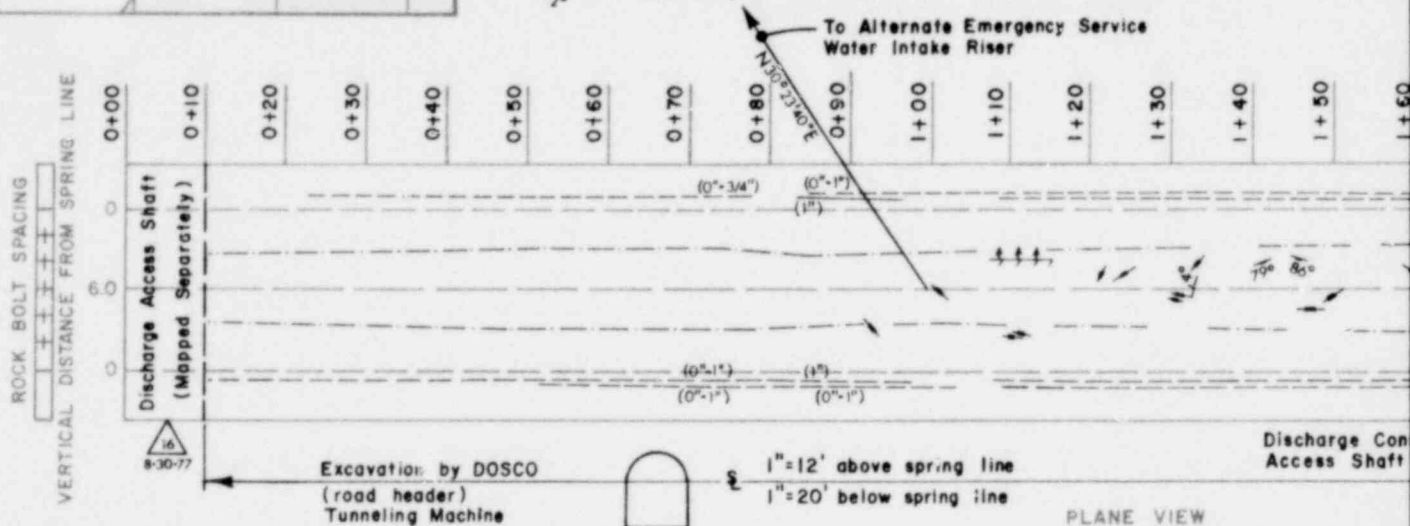
POOR ORIGINAL



- SYMBOLS**
- 5 (1/2)° — HARD, TAN, BROWN, CHERTY, IRON BED OR LAMINAE
 - 12 (0-2)° — DISCONTINUOUS IRON BED
 - 12 (1)° — HARD, LIGHT GREY, SANDY SHALE TO SILTSTONE BED
 - 10 (0-2)° — DISCONTINUOUS IRON BED WITHIN GREY BED
 - ⚡ FRACTURE
 - FAULT
 - BEDDING PARTING
 - VERTICAL JOINT
 - INCLINED JOINT
 - BEDDING, STRIKE AND DIP

- MOISTURE ALONG BED PARTING
- SEEPAGE FROM FEATURE
- OVEREXCAVATION OR OVERBREAK ZONE, MAXIMUM AMOUNT SHOWN
- △ METHANE GAS, MAXIMUM PERCENT L.E.L. WITHIN OF OCCURRENCE

* Note:
Number(s) in parentheses indicates:
Number preceding parenthesis indicates:
above or below spring line at station
measurement.



no. 4

2'-5"	1/2'-6"	1/2'-4"	2'-6"	1'-6"	1'-7"
1'-5'			5'-10'		
No seepage			Seepage out of parting 6 above springline on west wall		

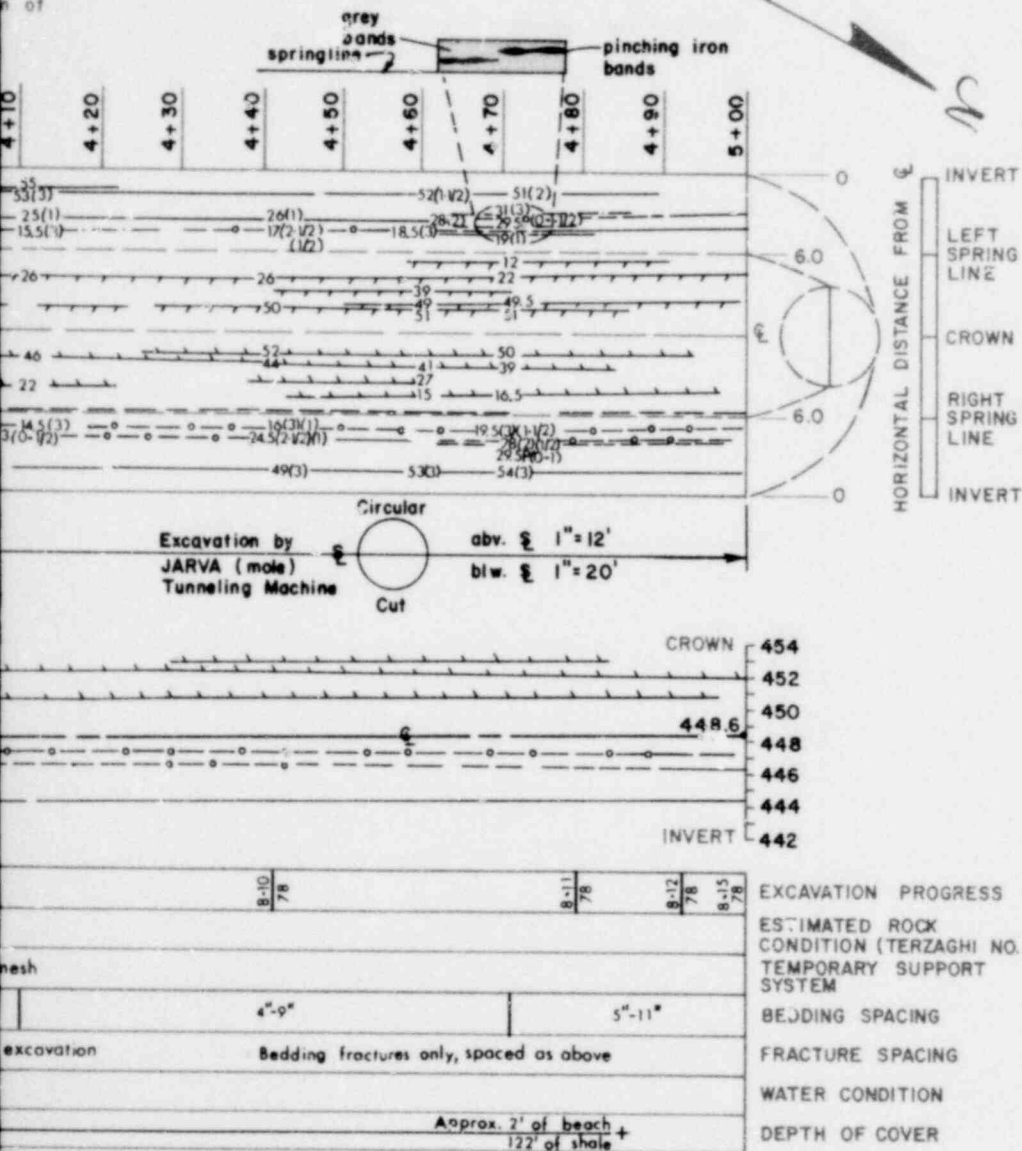
Approx. + 33.5' lacustrine
275' glacial till & 113.2' shale

1233 086

POOR ORIGINAL

DING
URE
IMUM

ed thickness.
s inches
n of

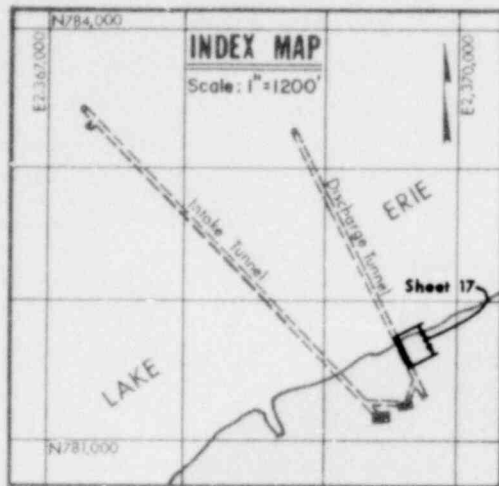


GEOLOGIC MAP OF TUNNEL EXCAVATIONS

FIGURE 2
SHEET 17 OF 24

1241 087

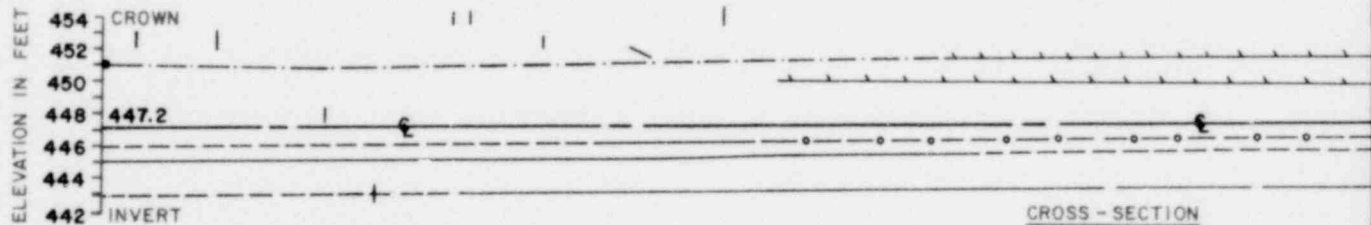
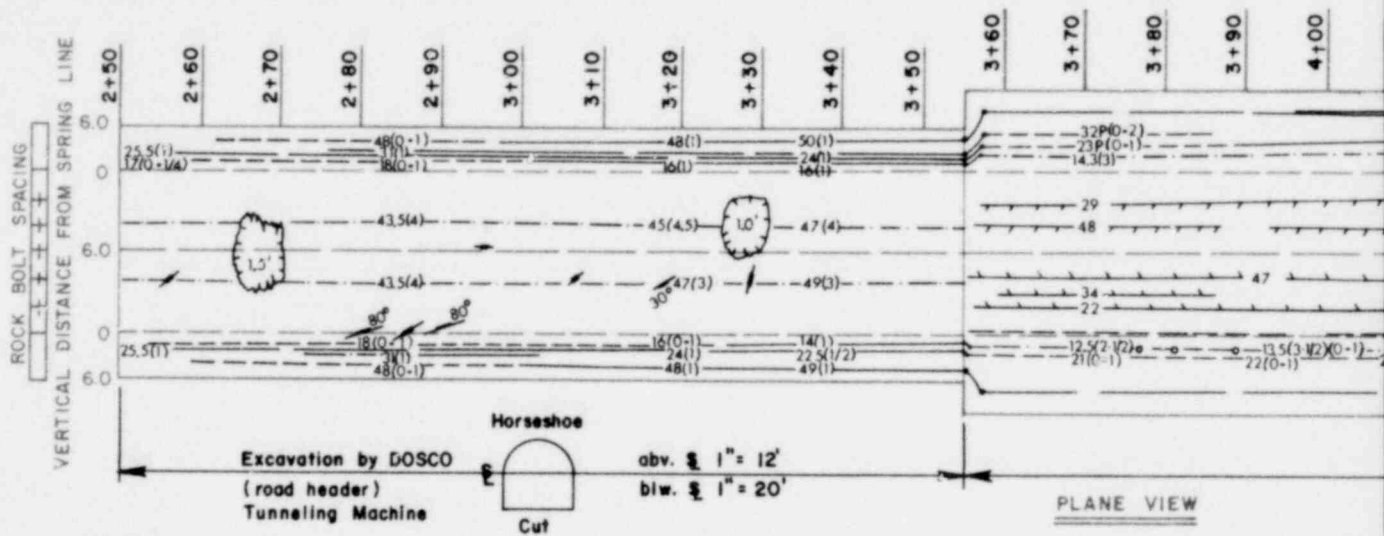
POOR ORIGINAL



- SYMBOLS**
- $\delta(1/2)^*$ HARD, TAN, BROWN, CHERTY, IRON BED OR LAMINAE
 - $12(0-2)^*$ DISCONTINUOUS IRON BED
 - $12(1)^*$ HARD, LIGHT GREY, SANDY SHALE TO SILTSTONE BED
 - $10(7)(0-2)^*$ DISCONTINUOUS IRON BED WITHIN GREY BED
 - FRACTURE
 - FAULT
 - BEDDING PARTING
 - VERTICAL JOINT
 - INCLINED JOINT
 - BEDDING, STRIKE AND DIP

- MOISTURE ALONG BEDDING PARTING
- SEEPAGE FROM FEATURE
- OVEREXCAVATION OR OVERBREAK ZONE, MAXIMUM AMOUNT SHOWN

* Note:
Number(s) in parentheses indicates
Number preceding parenthesis indicates
above or below spring line at station
measurement.



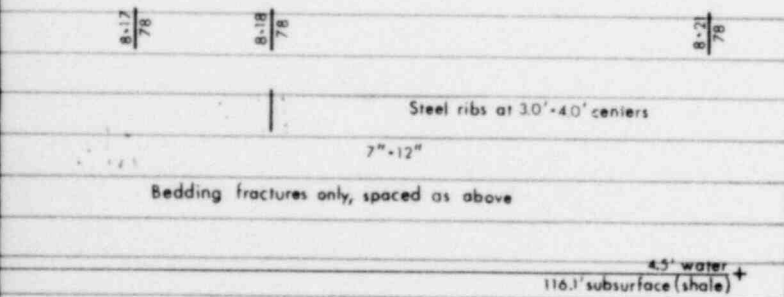
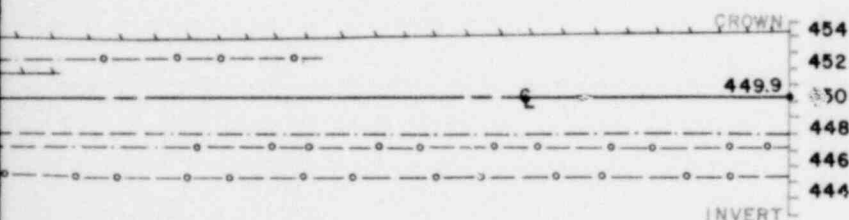
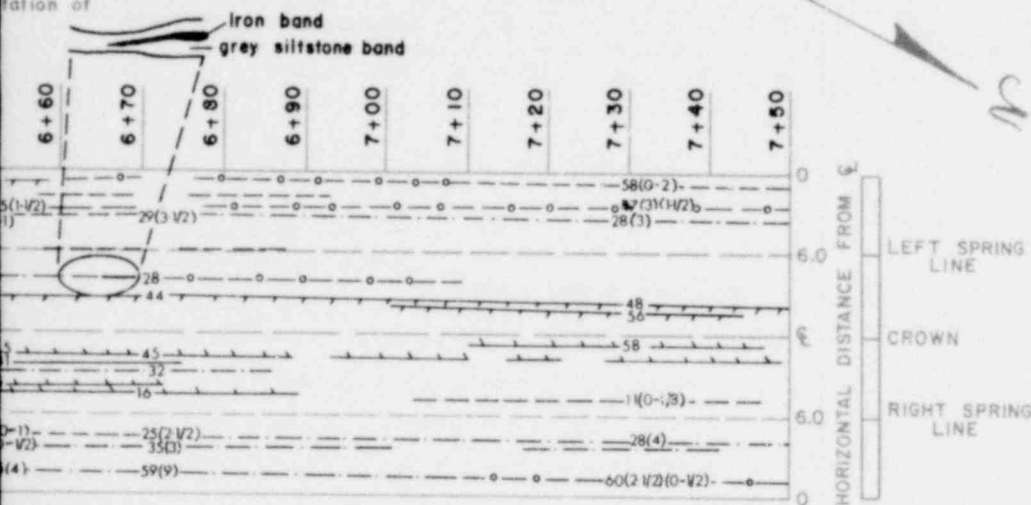
no. 4			
5 rock bolts at 2' centers in steel ribs at 3.0'-3.5' centers, spanned by wire			
1"-9"	1"-5"	1"-8"	5"-9"
Approx. 5'-10'	Approx. 8'	Approx. 11'	Jointing less apparent in smooth circular bore
No inflows			
+ Approx. 24' lacustrine & 34' glacial till 114.8' shale			

1238 088

POOR ORIGINAL

BEDDING
FEATURE
OR
MAXIMUM
MAXIMUM
TH DATE

es bed thickness.
icates inches
ation of



EXCAVATION PROGRESS

ESTIMATED ROCK
CONDITION (TENZAGHI NO.)

TEMPORARY SUPPORT
SYSTEM

BEDDING SPACING

FRACTURE SPACING

WATER CONDITION

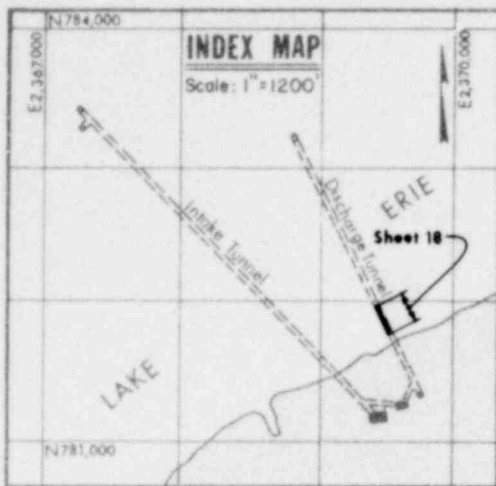
DEPTH OF COVER

1241 039

GEOLOGIC MAP OF TUNNEL EXCAVATIONS

FIGURE 2
SHEET 18 OF 24

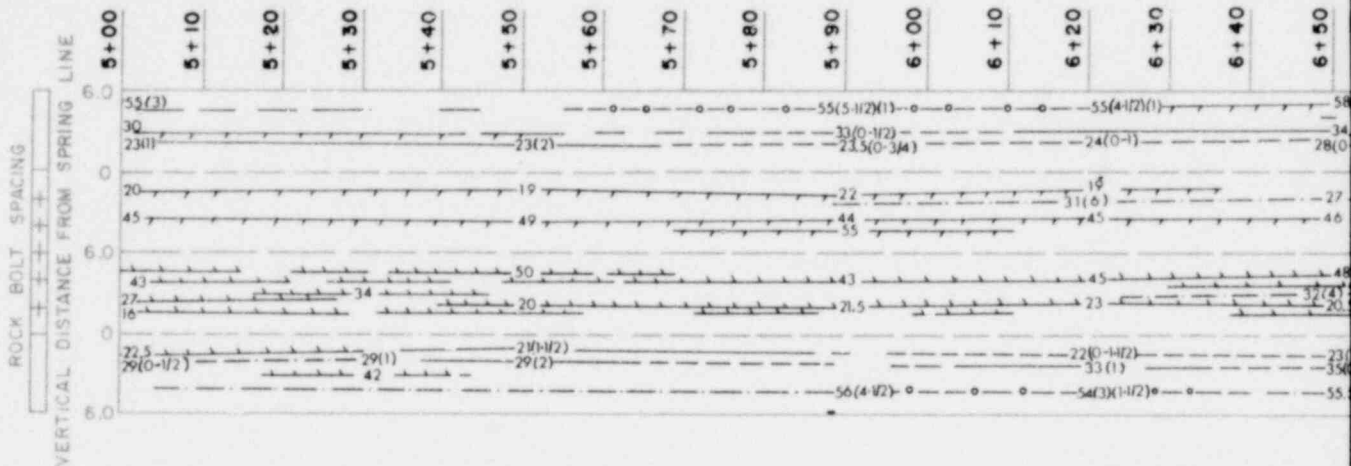
POOR ORIGINAL



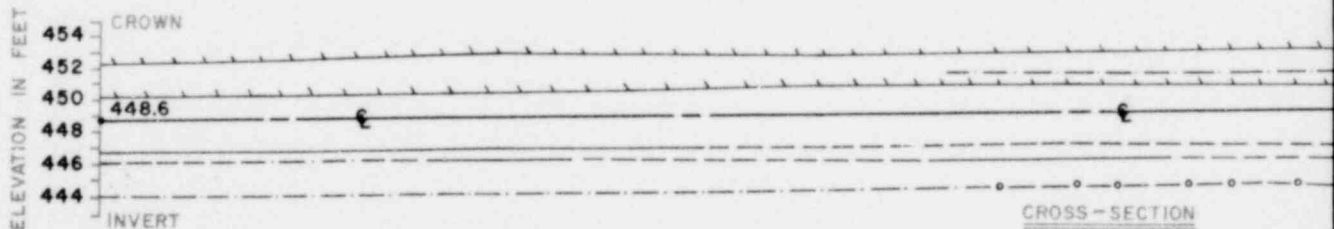
- SYMBOLS**
- 6(1/2)* — HARD, TAN, BROWN, CHERTY, IRON BED OR LAMINAE
 - 12(0-2)* — DISCONTINUOUS IRON BED
 - 12(1)* — HARD, LIGHT GREY, SANDY SHALE TO SILTSTONE BED
 - 10(7/10-2)* — DISCONTINUOUS IRON BED WITHIN GREY BED
 - ⚡ FRACTURE
 - / — FAULT
 - / — BEDDING PARTING
 - / — VERTICAL JOINT
 - / — INCLINED JOINT
 - / — BEDDING, STRIKE AND DIP

- / — MOISTURE ALONG PARTING
- / — SEEPAGE FROM F
- ⊠ OVEREXCAVATION OVERBREAK ZONE, AMOUNT SHOWN
- ⚠ METHANE GAS, M PERCENT L.E.L. W OF OCCURRENCE

* Note:
Number(s) in parentheses indicate
Number preceding parenthesis is
above or below spring line at
measurement.



PLANE VIEW



CROSS-SECTION

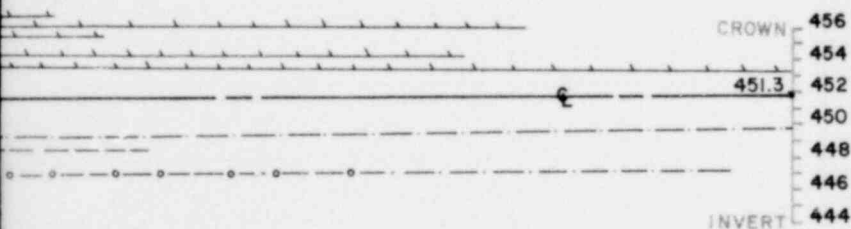
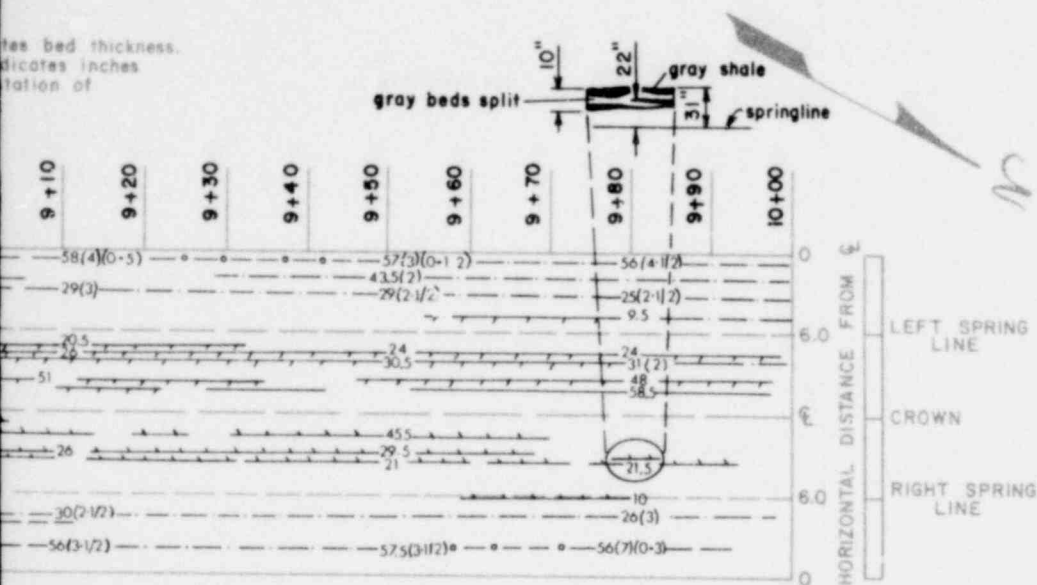
8-15 78	8-15 78
no. 4	
5 rock bolts at 2 centers in steel ribs at 3.5'-4.0' centers spanned by wire mesh	
5" - 11"	
Bedding fractures only, spaced as above	
No inflows	
+ Approx. 2' beach 121.9 subsurface (shale)	

1238 090

POOR ORIGINAL

BEDDING
FEATURE
OR
MAXIMUM
MAXIMUM
WITH DATE

tees bed thickness.
icates inches
tation of



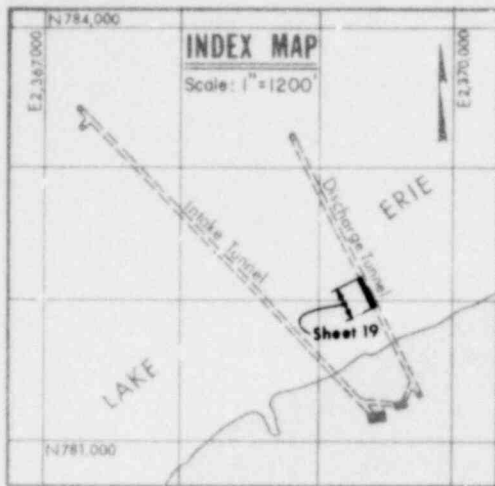
8-25 78	EXCAVATION PROGRESS
bed / wire mesh	ESTIMATED ROCK CONDITION (TERZAGHI NO.)
	TEMPORARY SUPPORT SYSTEM
	BEDDING SPACING
	FRACTURE SPACING
	WATER CONDITION
7.5' lake water 111.7' subsurface (shale)	DEPTH OF COVER

1248 091

GEOLOGIC MAP OF TUNNEL EXCAVATIONS

FIGURE 2
SHEET 19 OF 24

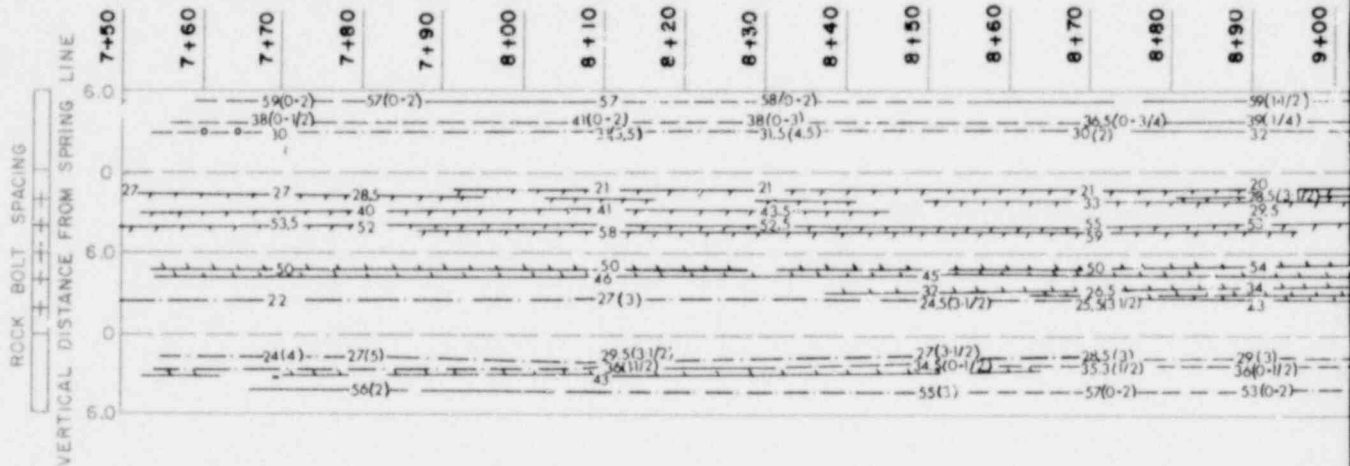
POOR ORIGINAL



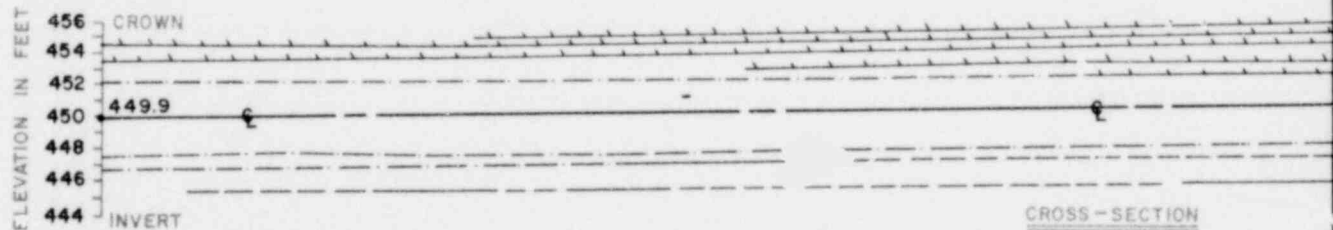
- SYMBOLS**
- 6 (1/2) — HARD, TAN, BROWN, CHERTY, IRON BED OR LAMINAE
 - 12 (0-2) — DISCONTINUOUS IRON BED
 - 12 (1) — HARD, LIGHT GREY, SANDY SHALE TO SILTSTONE BED
 - 10 (7/10-2) — DISCONTINUOUS IRON BED WITHIN GREY BED
 - ⚡ FRACTURE
 - FAULT
 - BEDDING PARTING
 - VERTICAL JOINT
 - INCLINED JOINT
 - BEDDING, STRIKE AND DIP

- MOISTURE ALONG PARTING
- SEEPAGE FROM F
- OVEREXCAVATION OVERBREAK ZONE AMOUNT SHOWN
- METHANE GAS, M PERCENT L.E.L. W OF OCCURRENCE

* Note:
Number(s) in parentheses indicate
Number preceding parenthesis in
above or below spring line at
measurement.



PLANE VIEW

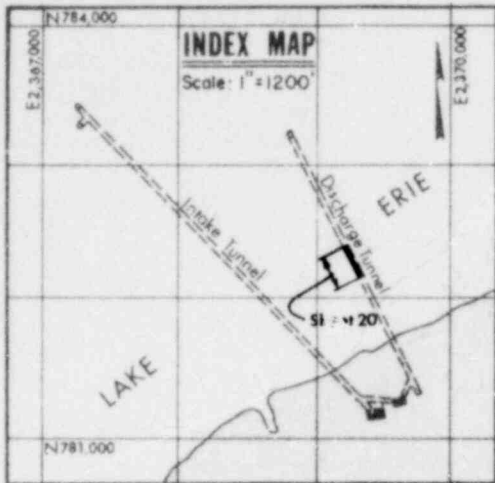


CROSS-SECTION



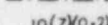


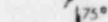
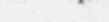


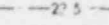
8+22	78	8+23	78	8+24	78
no. 4					
5 rock bolts at 2' centers in steel ribs at 3'-4' centers, spaced as above					
4"-12"					
Bedding fractures only, spaced as above					
No inflows					
+ 2' lake water					
116.1' subsurface (shale)					

1238 092

POOR ORIGINAL



SYMBOLS

- | | |
|---|---|
|  | HARD, TAN, BROWN, CHERTY,
IRON BED OR LAMINAE |
|  | DISCONTINUOUS IRON BED |
|  | HARD, LIGHT GREY, SANDY
SHALE TO SILTSTONE BED |
|  | DISCONTINUOUS IRON BED
WITHIN GREY BED |
|  | FRACTURE |
|  | FAULT |
|  | BEDDING PARTING |
|  | VERTICAL JOINT |
|  | INCLINED JOINT |
|  | BEDDING, STRIKE AND DIP |

MOISTURE ALONG PARTING

SEEPAGE FROM PARTING

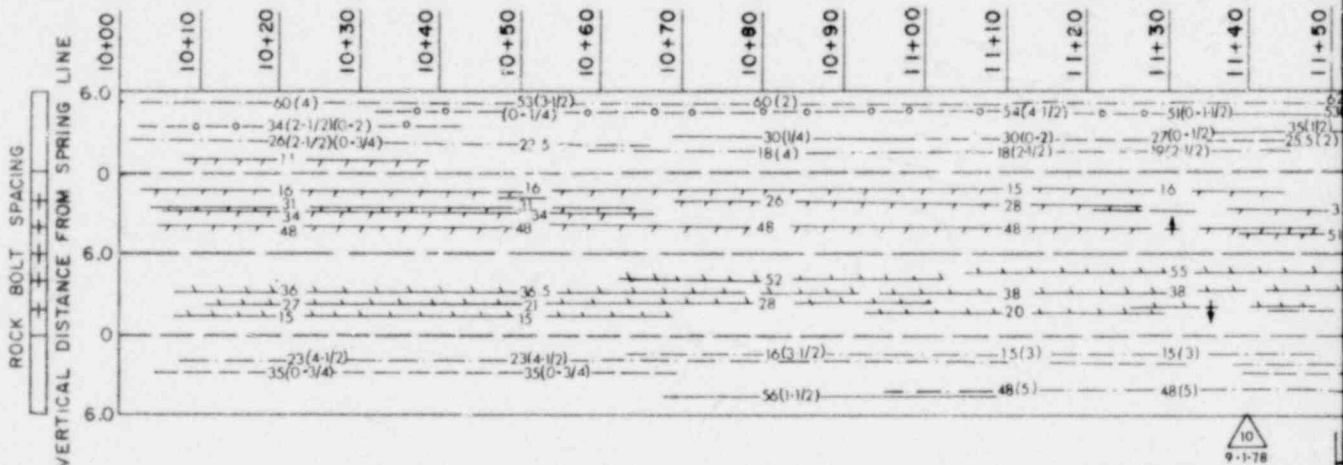
OVEREXCAVATION

OVERBREAK ZONE

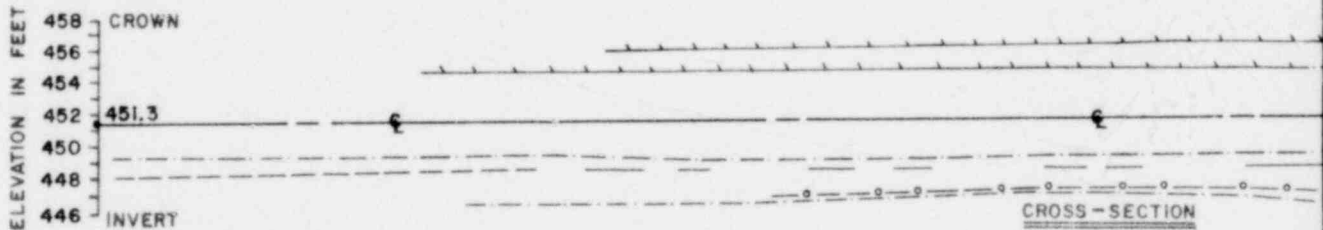
AMOUNT SHOWN

METHANE GAS, PERCENT L.E.L. OF OCCURRENCE

Note:
Number(s) in parentheses indicate
Number preceding parenthesis is
above or below spring line at
measurement.



PLANE VIEW



	no. 4	0"-4" of overbreak spalling from crown
5 rock bolts at 2' centers in steel ribs at 4.0'-4.5' centers, spanned		
3"-10"		
Bedding fractures only, spaced as above		
No inflows	Seepage from rock bolts	
+ 7.5' water + 111.7' subsurface (shale)		

1238 094

POOR ORIGINAL

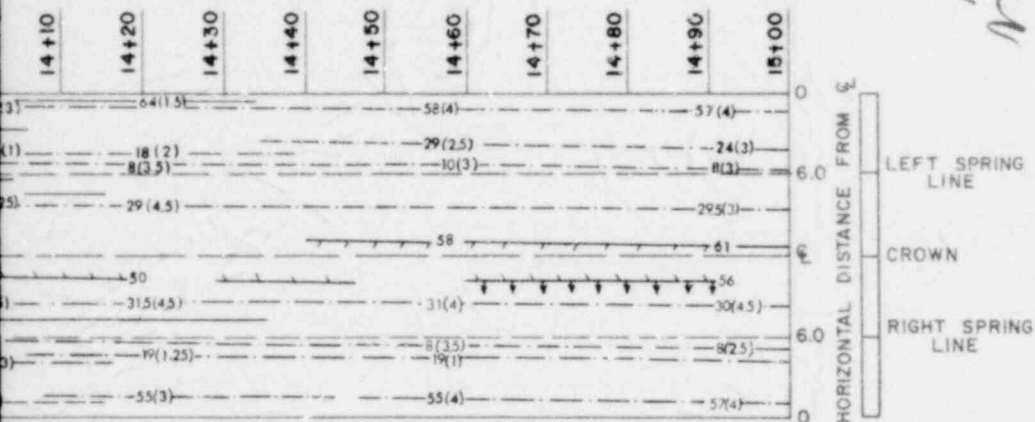
BEDDING

ATURE

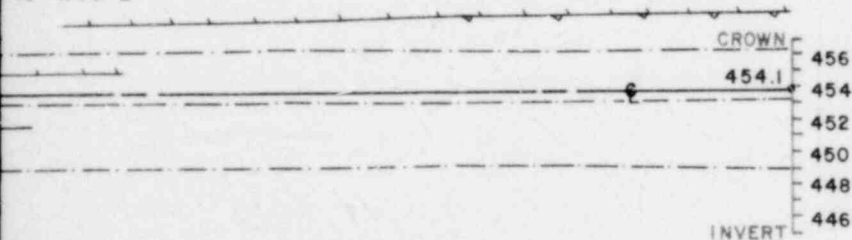
OR
MAXIMUM

MAXIMUM
TH DATE

es bed thickness.
icates inches
ation of



FAULT GEOMETRY
 parent displacement-12" to 25" d.) Dip approx. 16.5°
 dual vertical displacement-8-1/2" to 11-1/2" e.) Width of broken rock (1/2" to 24")
 like - N66°E



0.00	7.00	0.00	7.00
no. 4			
5	rock bolts at 2 centers in steel ribs at 3.5'-4' centers, spanned by wire mesh		
3'-9"			
Bedding fractures only, spaced as above			
14.5'	water		
101.9'	subsurface (shale)		

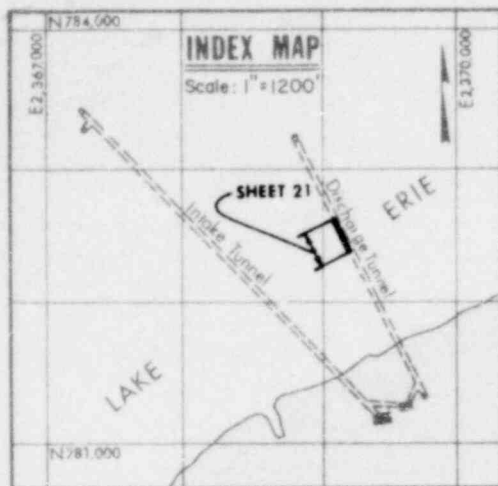
EXCAVATION PROGRESS
 ESTIMATED ROCK
 CONDITION (TERZAGHI NO.)
 TEMPORARY SUPPORT
 SYSTEM
 BEDDING SPACING
 FRACTURE SPACING
 WATER CONDITION
 DEPTH OF COVER

1248 095

GEOLOGIC MAP OF TUNNEL EXCAVATIONS

FIGURE 2
 SHEET 21 OF 24

POOR ORIGINAL

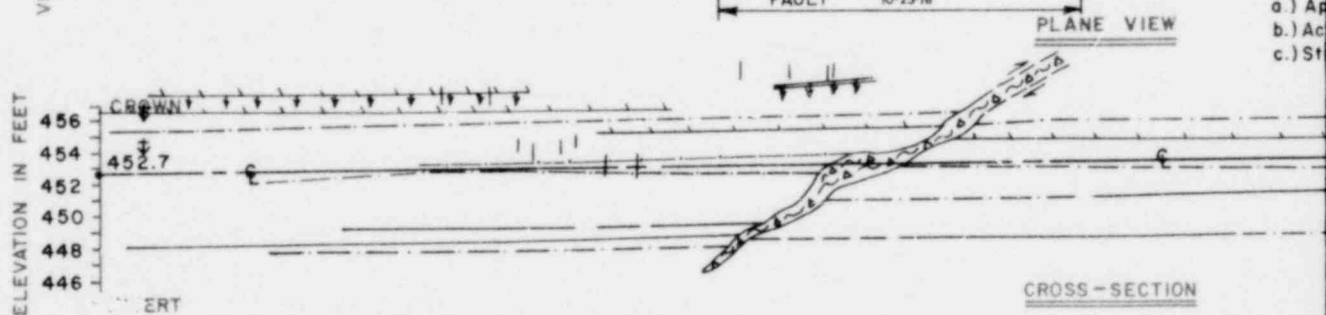
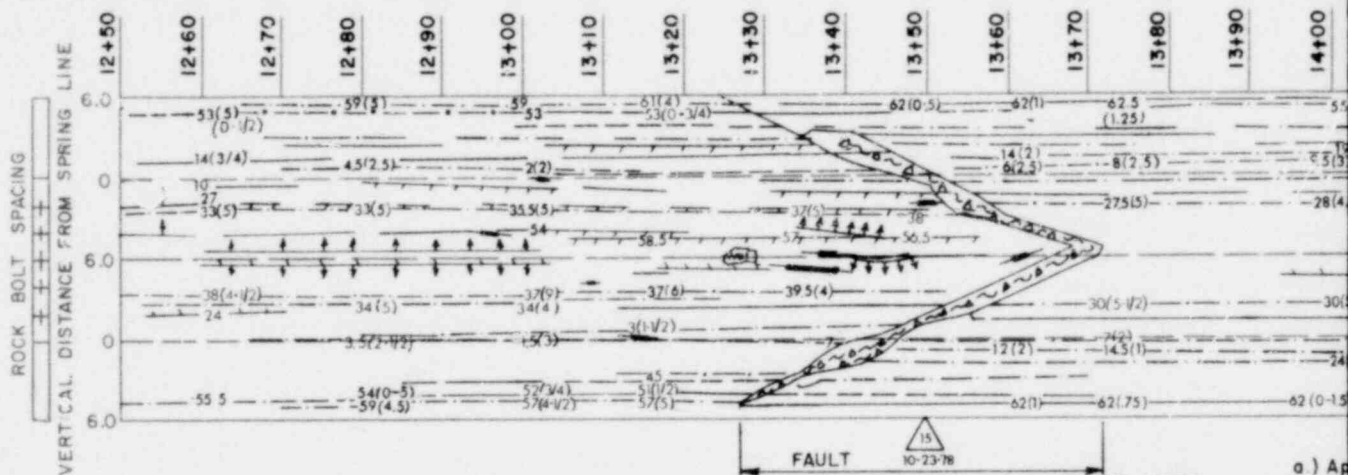


SYMBOLS

- 0(1/2) — HARD, TAN, BROWN, CHERTY, IRON BED OR LAMINAE
- 12(0-2) — DISCONTINUOUS IRON BED
- 10(7)(0-2) — HARD, LIGHT GREY, SANDY SHALE TO SILTSTONE BED DISCONTINUOUS IRON BED WITHIN GREY BED
- ⚡ FRACTURE
- ↗ FAULT (with sense of motion)
- BEDDING PARTING
- VERTICAL JOINT
- INCLINED JOINT
- BEDDING, STRIKE AND DIP

- MOISTURE ALONG PARTING
- SEEPAGE FROM F
- 2' OVEREXCAVATION (OVERBREAK ZONE, AMOUNT SHOWN)
- 20 METHANE GAS, MA PERCENT L.E.L. W OF OCCURRENCE

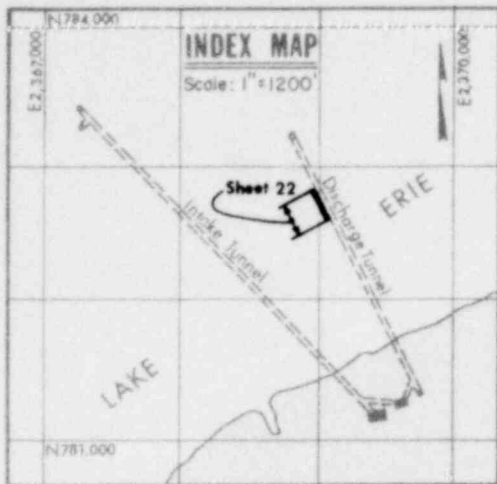
* Note:
Number(s) in parentheses indicate
Number preceding parenthesis in
above or below spring line at
measurement.



no. 4	no. 4-6
5 rock bolts at 2' centers in steel ribs at 3.5'-4' centers, spanned by wire mesh	Full shielding employed
3'-9"	Ribs at 2' centers
Bedding fractures spaced as above, joints widely spaced	Joint pairs shown at .5'-1.5' apart, otherwise bedding fractures at 3'-9"
Moist bedding fractures where indicated	Several minor inflows in fractured areas of fault hang wall
+ 8.5 water	Several dripping flows along shaft
+ 109.3 subsurface (shale)	two max. inflows of 0.1 gal./min.

1238 096

POOR ORIGINAL

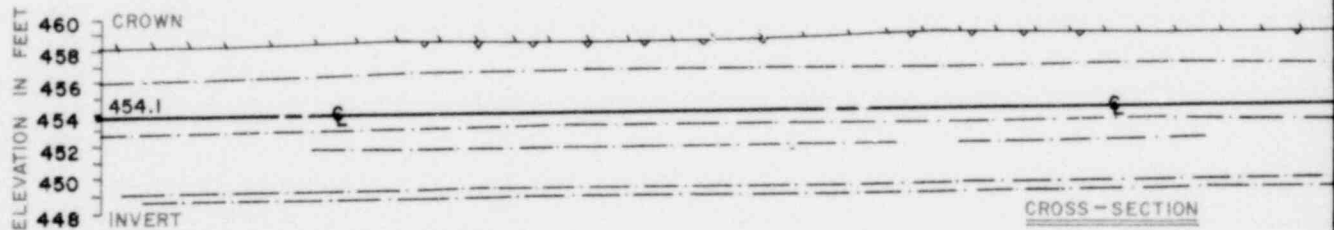
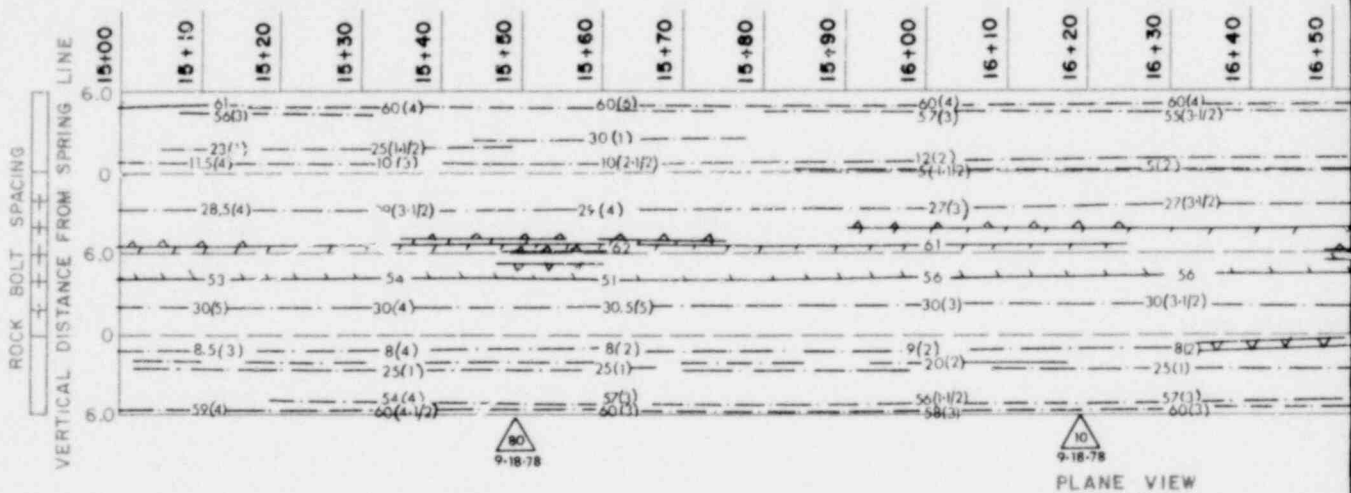


SYMBOLS

- 6(1/2)° — HARD, TAN, BROWN, CHERTY, IRON BED OR LAMINAE
- - - 12(0-2)° - - - DISCONTINUOUS IRON BED
- - - 12(1)° - - - HARD, LIGHT GREY, SANDY SHALE TO SILTSTONE BED
- - - 10(0-2)° - - - DISCONTINUOUS IRON BED WITHIN GREY BED
- ⚡ FRACTURE
- 75° — FAULT (with sense of motion)
- 70° — BEDDING PARTING
- 70° — VERTICAL JOINT
- 70° — INCLINED JOINT
- 70° — BEDDING, STRIKE AND DIP

- MOISTURE ALONG PARTING
- SEEPAGE FROM F
- OVEREXCAVATION OVERBREAK ZONE, AMOUNT SHOWN
- METHANE GAS, M PERCENT L.E.L. W OF OCCURRENCE

Note:
Number(s) in parentheses indicate
Number preceding parenthesis in
above or below spring line at
measurement.



9-12/78		9-13/78		9-14/78	
Slight overbreak along entire excavation (0"-6")					
5 rock bolts at 2' centers in steel ribs at 40'-45' centers spanned					
3"-9"		4"-9"			
Bedding fractures only, spaced as above					
Moisture from bedding parting		Moisture from bedding parting		Moisture from bedding parting	
+ 14.5' water					
+ 101.9' subsurface (shale)					

1238 098

POOR ORIGINAL

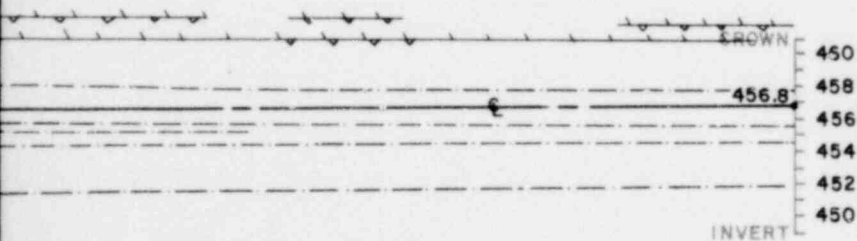
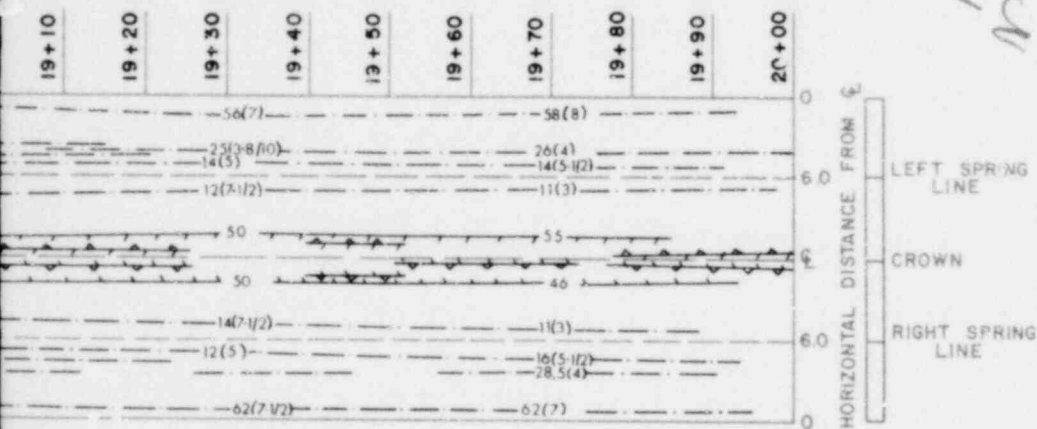
BEDDING

FEATURE

OR
MAXIMUM

MAXIMUM
WITH DATE

few bed thickness.
icates inches
tation of



EXCAVATION PROGRESS	9.22	78	9.25	78
ESTIMATED ROCK CONDITION (TERZAGHI NO.)				
TEMPORARY SUPPORT SYSTEM				
BEDDING SPACING				
FRACTURE SPACING				
WATER CONDITION				
DEPTH OF COVER				

d by wire mesh

4" - 12"

ng fractures only, spaced as above

Moisture from bedding partings

Moisture from bedding partings

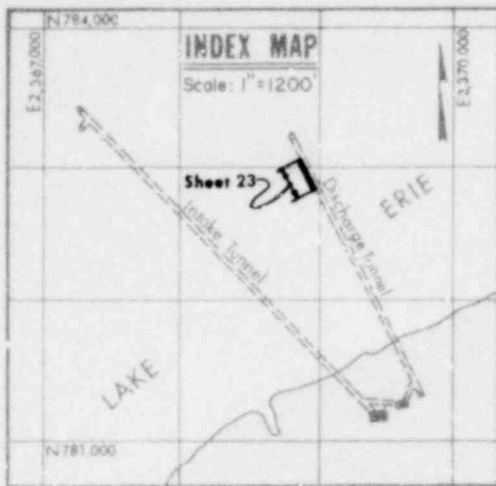
18.5' water

1248 099

GEOLOGIC MAP OF TUNNEL EXCAVATIONS

FIGURE 2
SHEET 23 OF 24

POOR ORIGINAL

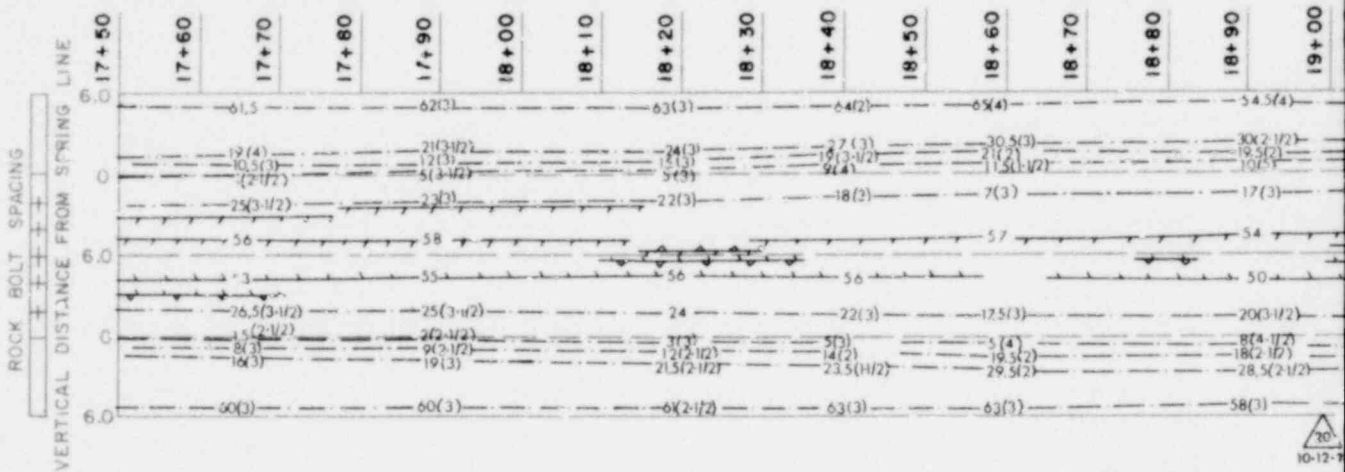


SYMBOLS

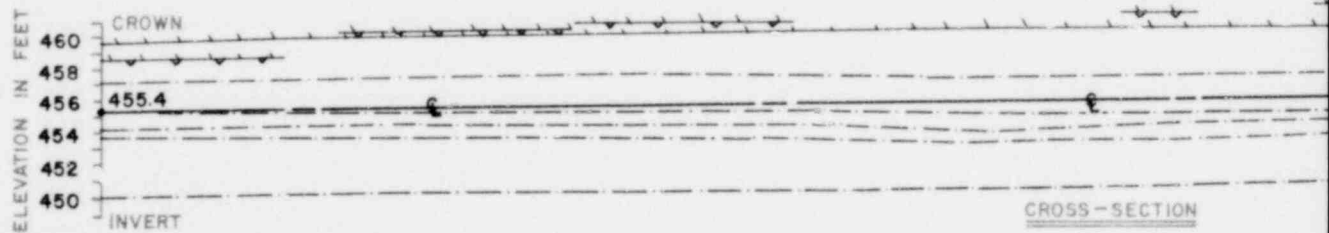
- $\delta(1/2)^{\circ}$ HARD, TAN, BROWN, CHERTY, IRON BED OR LAMINAE
- $12(0-2)^{\circ}$ DISCONTINUOUS IRON BED
- $12(1)^{\circ}$ HARD, LIGHT GREY, SANDY SHALE TO SILTSTONE BED
- $10(7XC-2)^{\circ}$ DISCONTINUOUS IRON BED WITHIN GREY BED
- FRACTURE
- FAULT
- BEDDING PARTING
- VERTICAL JOINT
- INCLINED JOINT
- BEDDING, STRIKE AND DIP

- MOISTURE ALONG PARTING
- SEEPAGE FROM FAULT
- OVEREXCAVATION OVERBREAK ZONE AMOUNT SHOWN
- METHANE GAS, PERCENT L.E.L. OF OCCURRENCE

* Note:
Number(s) in parentheses indicate Number preceding parenthesis in above or below spring line at measurement.



PLANE VIEW



CROSS-SECTION

9-20	78	9-21	78
no. 4			
5 rock bolts at 2' centers in steel ribs at 4.0'-4.5' centers, spanning			
3" x 10"			
Moisture from bedding partings			
Moisture from bedding partings			
15.5' water			
99.6' subsurface (shale)			

1238 100

POOR ORIGINAL



PRING LINE

PRING LINE

SYMBOLS

	HARD, TAN, BROWN, CHERTY, IRON BED OR LAMINAE
	DISCONTINUOUS IRON BED
	HARD, LIGHT GREY, SANDY SHALE TO SILTSTONE BED
	DISCONTINUOUS IRON BED WITHIN GREY BED
	FRACTURE
	FAULT
	BEDDING PARTING
	VERTICAL JOINT
	INCLINED JOINT
	BEDDING, STRIKE AND DIP
	MOISTURE ALONG BEDDING PARTING
	SEEPAGE FROM FEATURE
	OVEREXCAVATION OR OVERBREAK ZONE, MAXIMUM AMOUNT SHOWN

DGRESS

CONDITION (TERZAGHI NO.)

PPORT SYSTEM

Note:

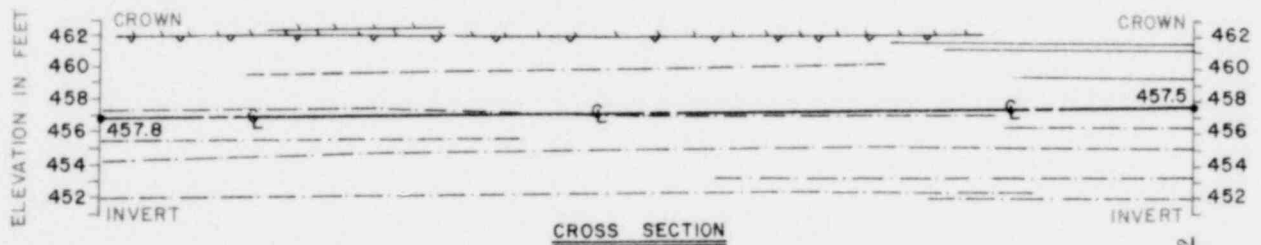
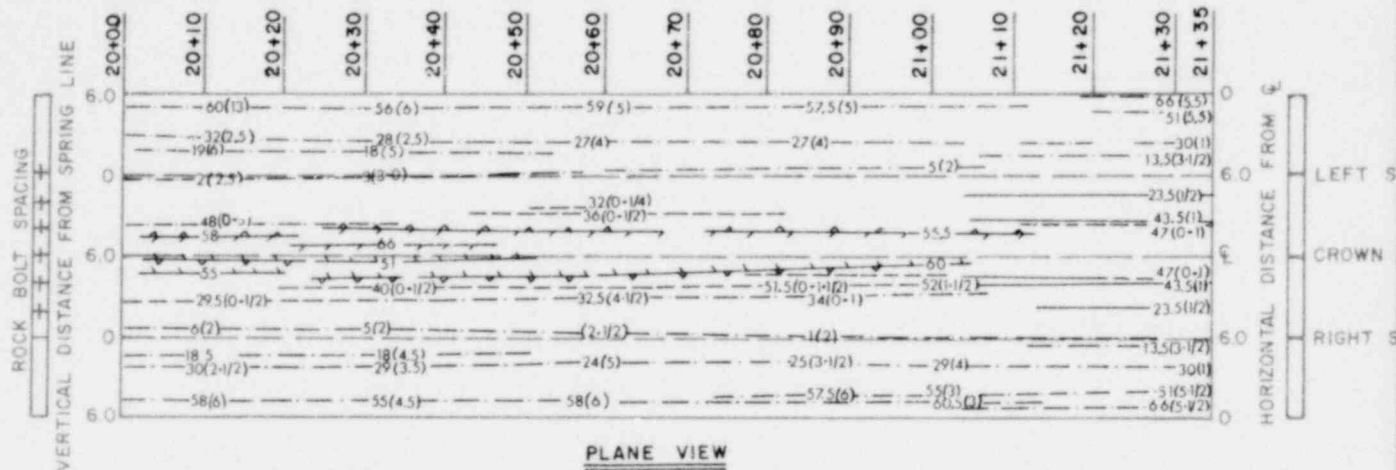
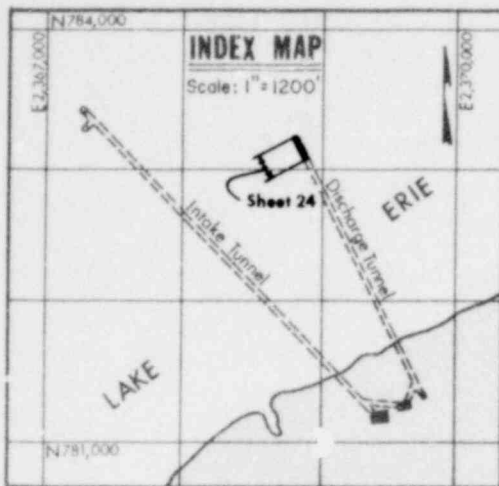
Number(s) in parentheses indicates bed thickness.
Number preceding parenthesis indicates inches above or below spring line at station of measurement.

GEOLOGIC MAP OF TUNNEL EXCAVATIONS

1240 101

FIGURE 2
SHEET 24 OF 24

POOR ORIGINAL



9.27	78	9.27	78	9.27	78
no. 4 Slight overbrenk along entire excavation (0"-3")					
5 rock bolts at 2 centers, in steel ribs at 4'-4.5' centers, spanned by wire mesh					
4'-11"					
Bedding partings only, spaced as above					
Slight moisture along bedding partings, where indicated					
+ 18.5' water			+ 19.5' water		
+ 95.2' subsurface (shale)			+ 93.5' subsurface (shale)		

EXCAVATION PR
ESTIMATED ROCK
TEMPORARY SU
BEDDING SPACIN
FRACTURE SPAC
WATER CONDITIO
DEPTH OF COVE

1238 102

POOR ORIGINAL

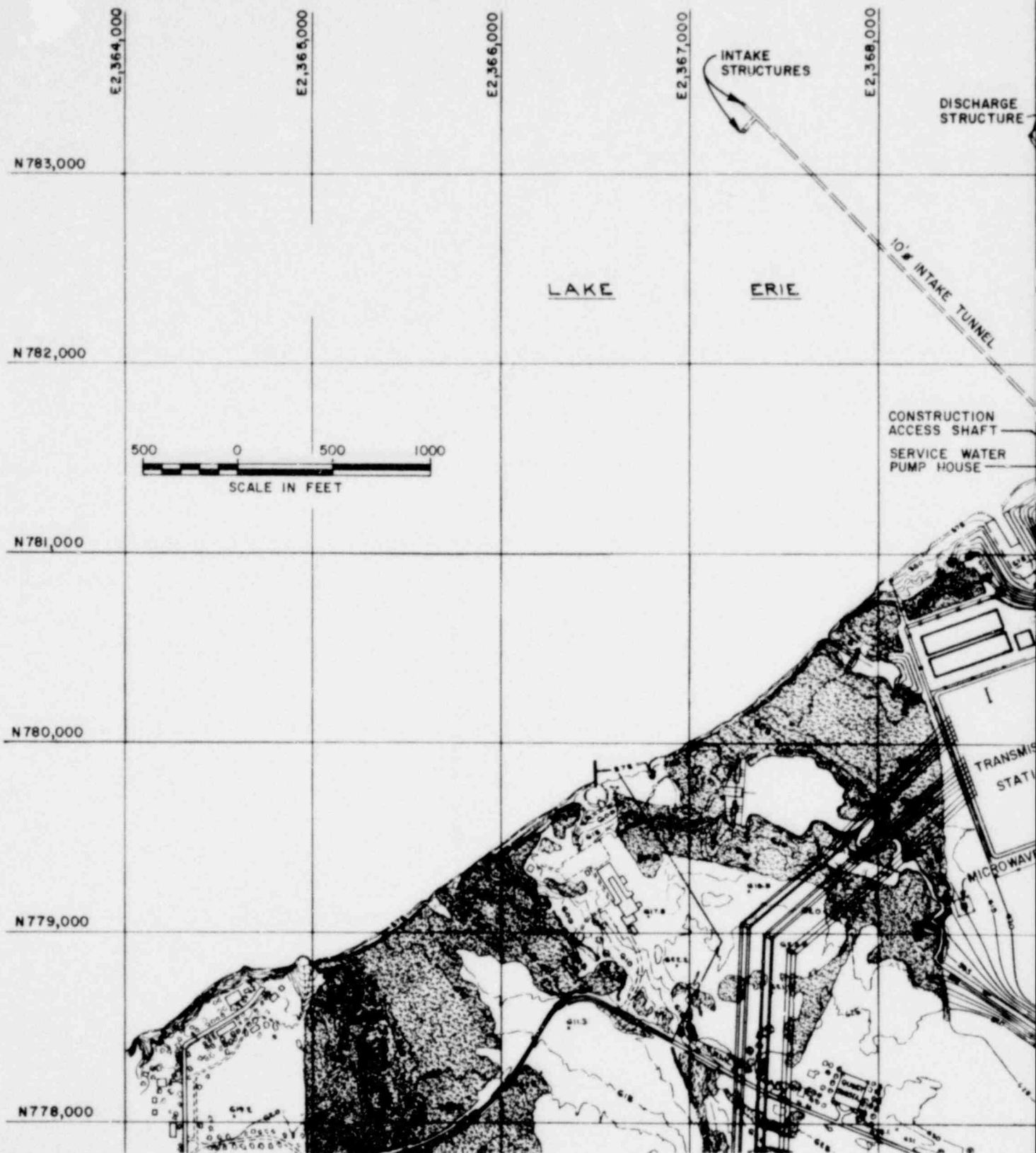


TUNNELING PLAN

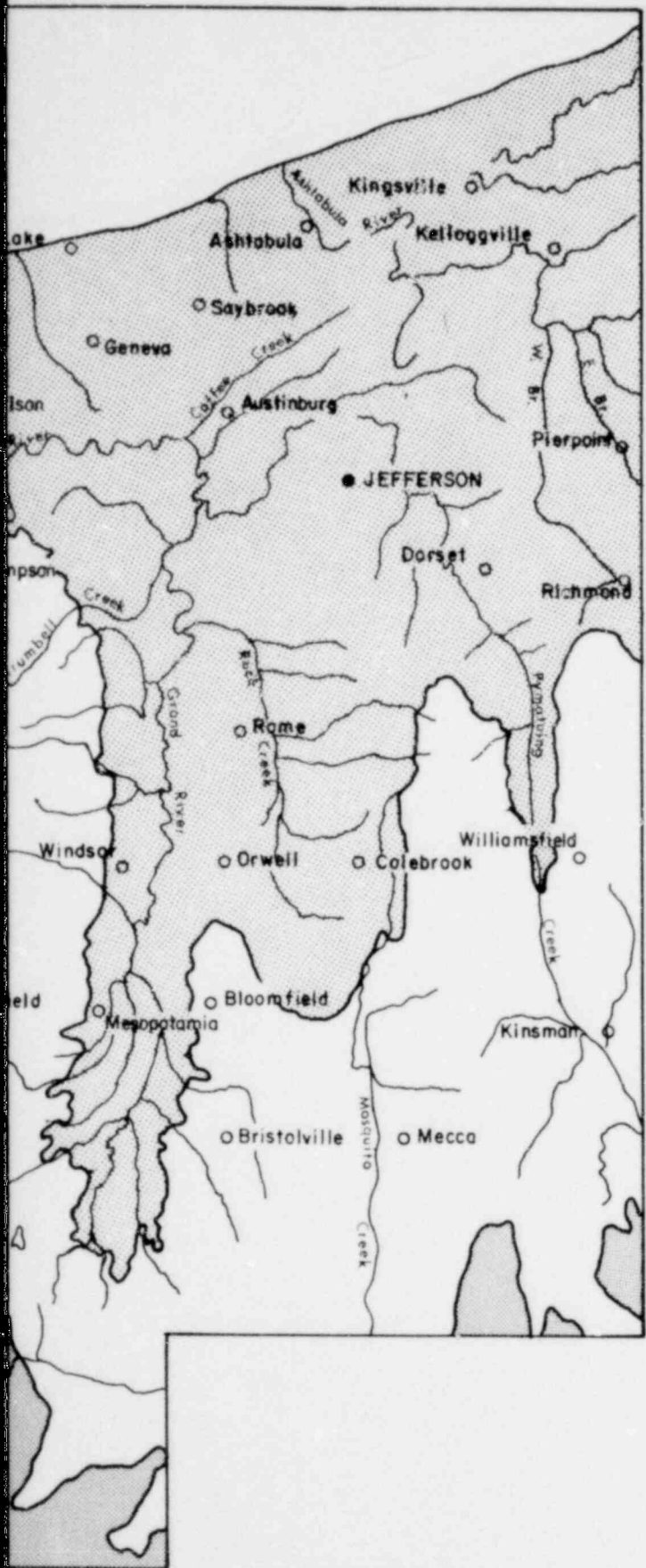
FIGURE 3

1248 103

POOR ORIGINAL

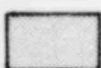


1238 104

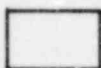


POOR ORIGINAL

LEGEND



POTTSVILLE & ALLEGHENY
(COAL, S.S., SH, L.S.)
PENNSYLVANIAN



WAVERLY & MAXVILLE
(SH, S.S., L.S.)
MISSISSIPPI



OLENTANGY & OHIO (SHALES)
DEVONIAN

1241 105

BEDROCK GEOLOGIC MAP OF
NORTHEASTERN OHIO

FIGURE 4

POOR ORIGINAL

ERIE

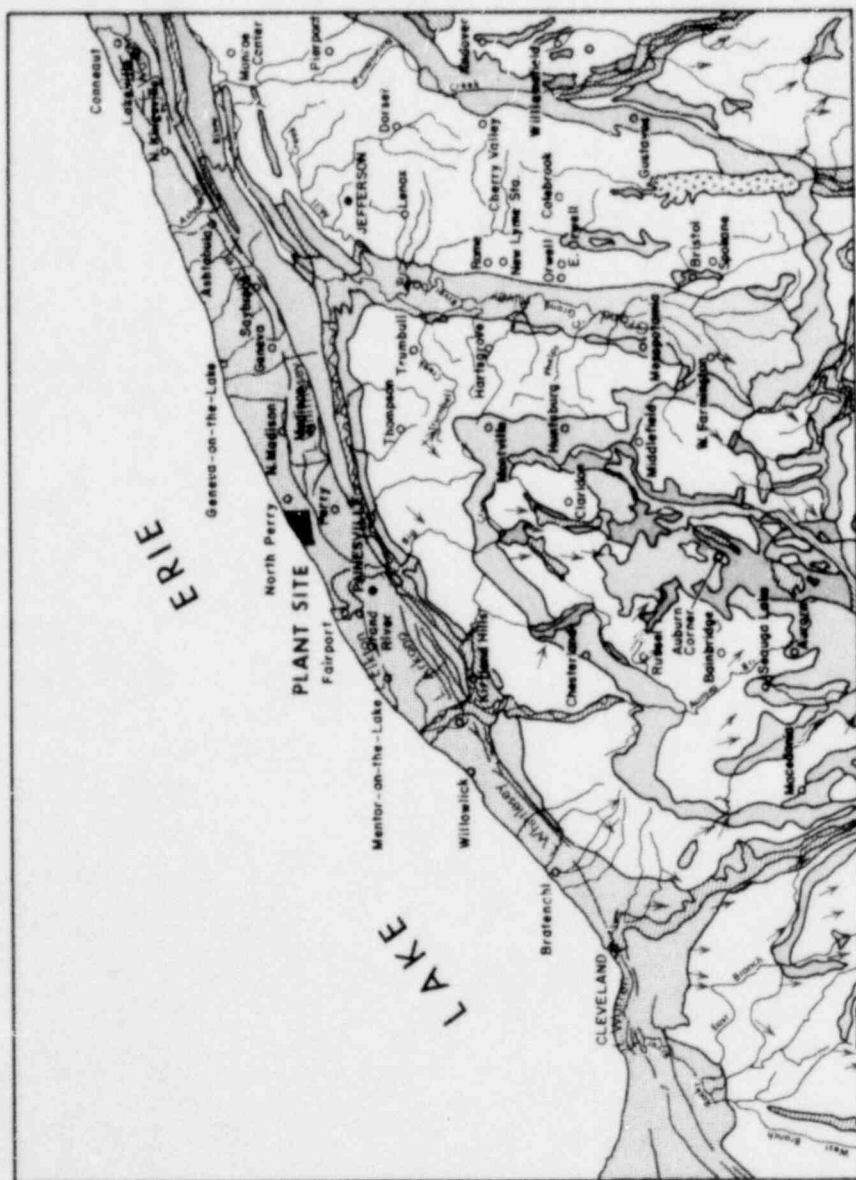
PLANT SITE



SCALE IN MILES

AFTER - BOWNOCKER 1965

1238 106



LEGEND

- GROUND MORaine - ILLINOIS
- LACUSTRINE DEPOSITS - WISCONSIN
- LACUSTRINE DEPOSITS - PRE-WISCONSIN
- ALLUVIUM - WISCONSIN
- OUTWASH - WISCONSIN
- KAMES AND ESKERS - WISCONSIN
- GROUND MORaine - WISCONSIN
- END MORaine - WISCONSIN
- BEACH DEPOSITS - WISCONSIN
- STRIATIONS

GLACIAL MAP - OHIO
PERRY NUCLEAR POWER PLANT 1 & 2
THE CLEVELAND ELECTRIC
ILLUMINATING COMPANY

POOR ORIGINAL

AFTER - GOLDTHWAIT, WHITE, FORSYTH 1961

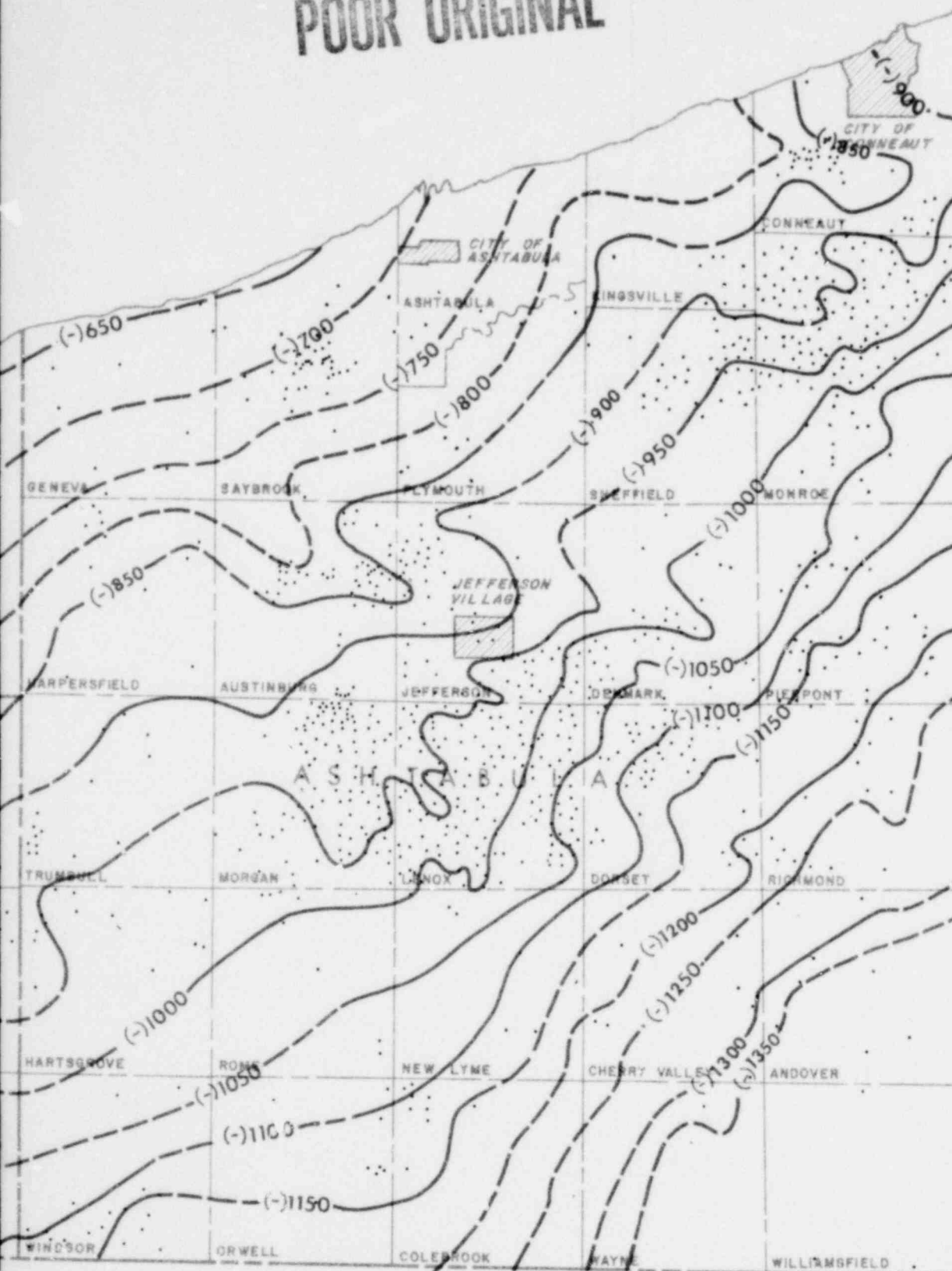


GLACIAL MAP OF NORTHEASTERN OHIO

FIGURE 5

125 107

POOR ORIGINAL



STRUCTURAL CONTOUR MAP -
TOP OF BIG LIME

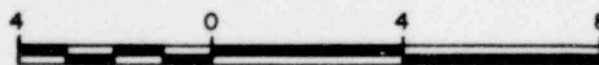
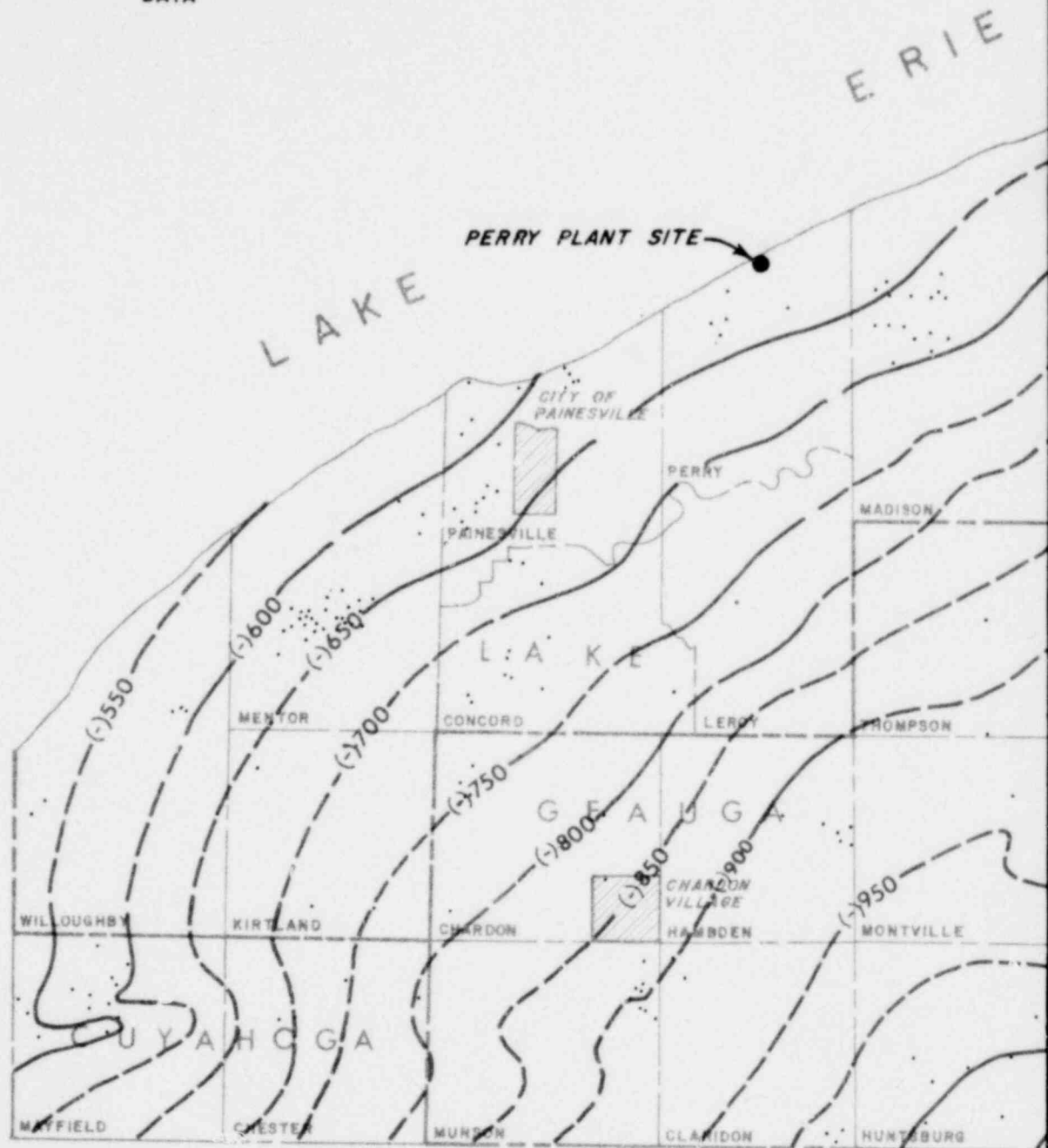
FIGURE 6

1241 108

POOR ORIGINAL

LEGEND

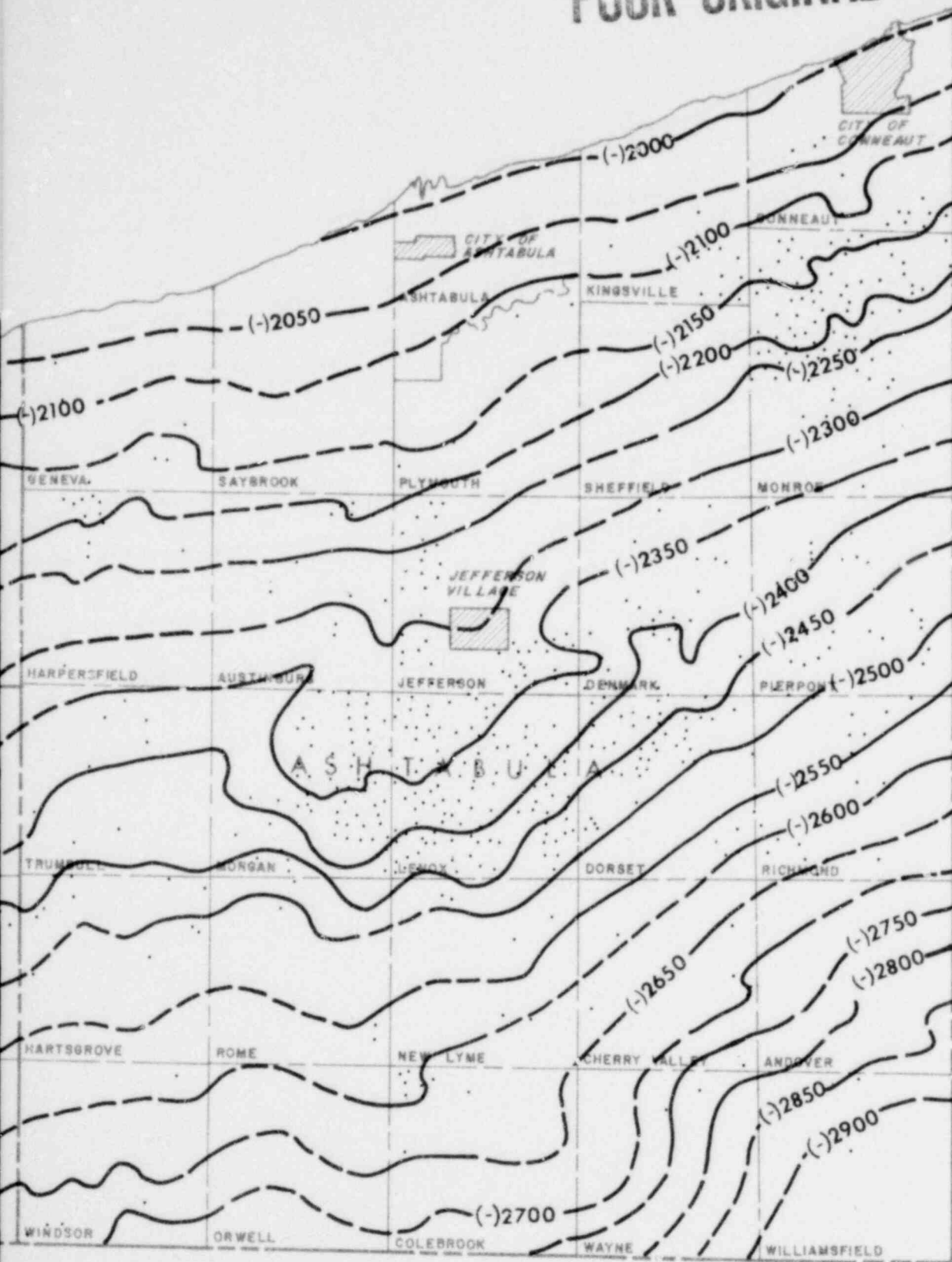
- LOCATION OF WELLS EVALUATED
FOR CONTOUR DATA
- CONTOUR LINE
- - - - CONTOUR IN AREA OF INFERRED
DATA



SCALE IN MILES

1238 109

POOR ORIGINAL



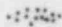


1241 110

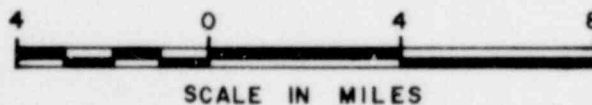
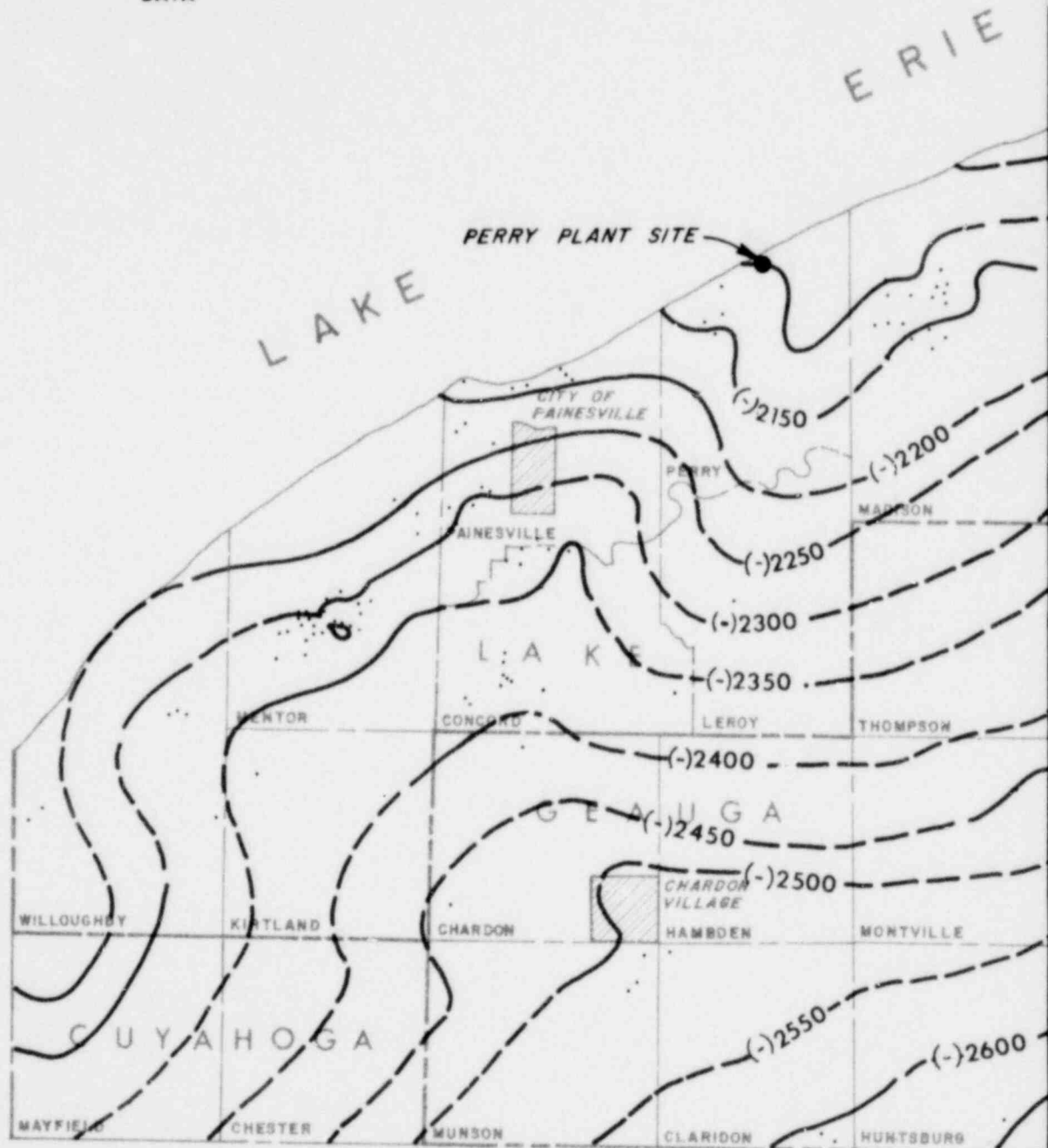
STRUCTURAL CONTOUR MAP -
TOP OF PACKER SHELL

FIGURE 7

POOR ORIGINAL

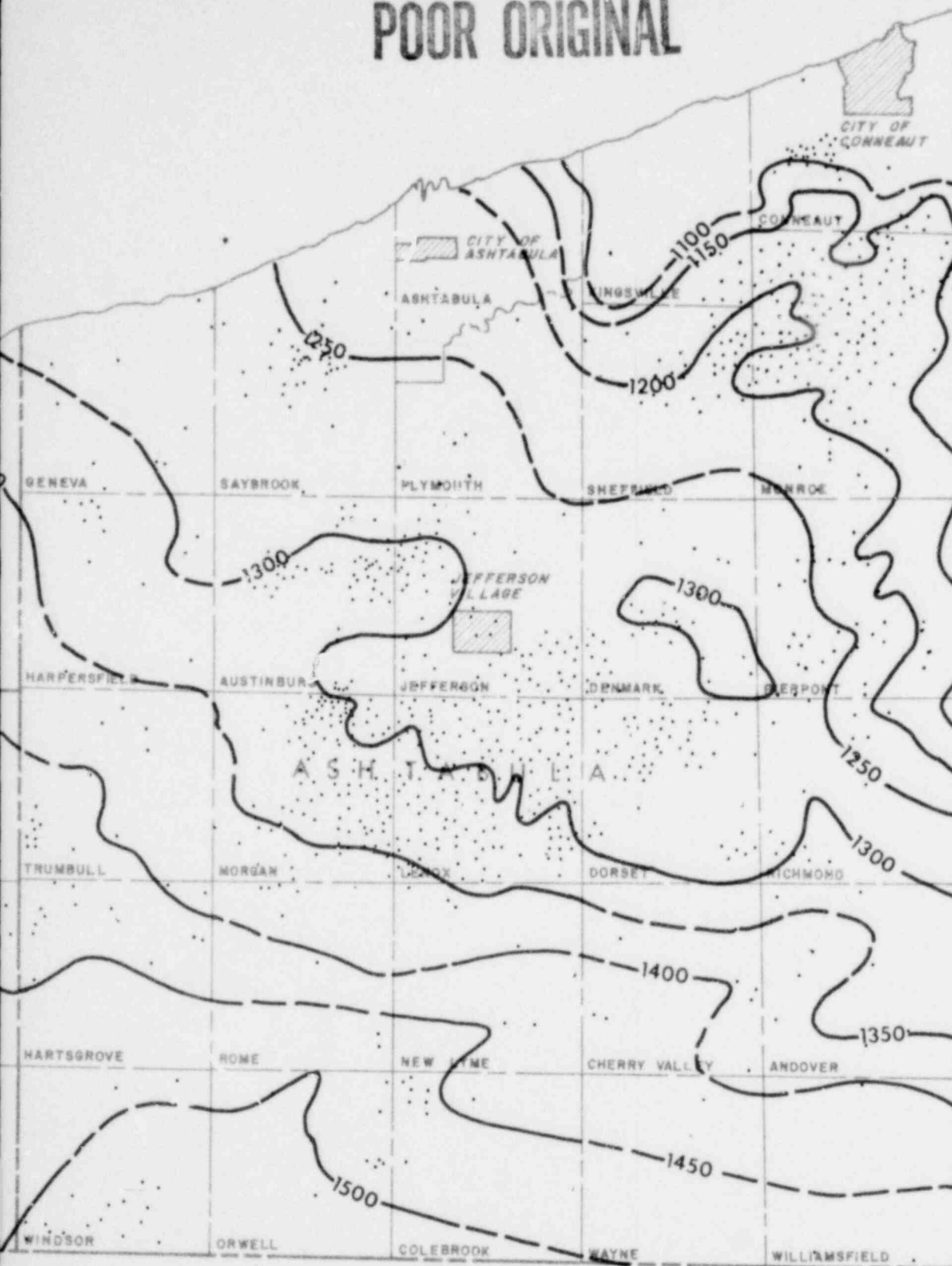
LEGEND

-  LOCATION OF WELLS EVALUATED FOR CONTOUR DATA
-  CONTOUR LINE
-  CONTOUR IN AREA OF INFERRED DATA



1238 111

POOR ORIGINAL



ISOPACH MAP OF BIG LIME
AND NIAGARAN SHALE

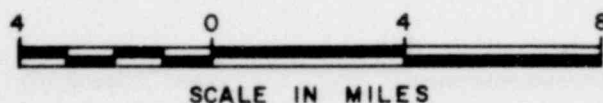
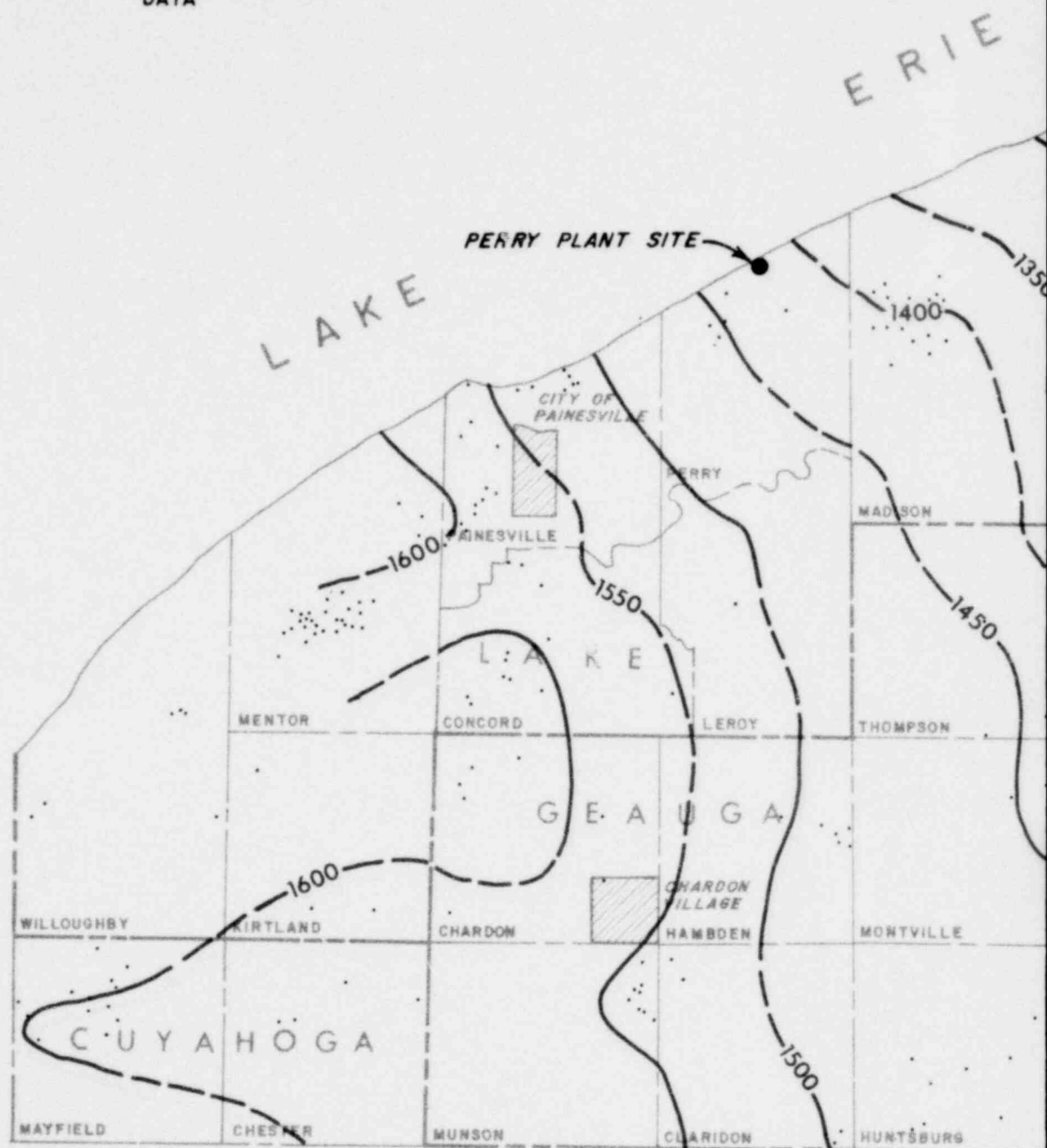
FIGURE 8

1254 112

POOR ORIGINAL

LEGEND

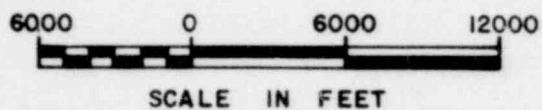
- LOCATION OF WELLS EVALUATED FOR CONTOUR DATA
- CONTOUR LINE
- - - - CONTOUR IN AREA OF INFERRED DATA






1238 113



POOR ORIGINAL



LEGEND

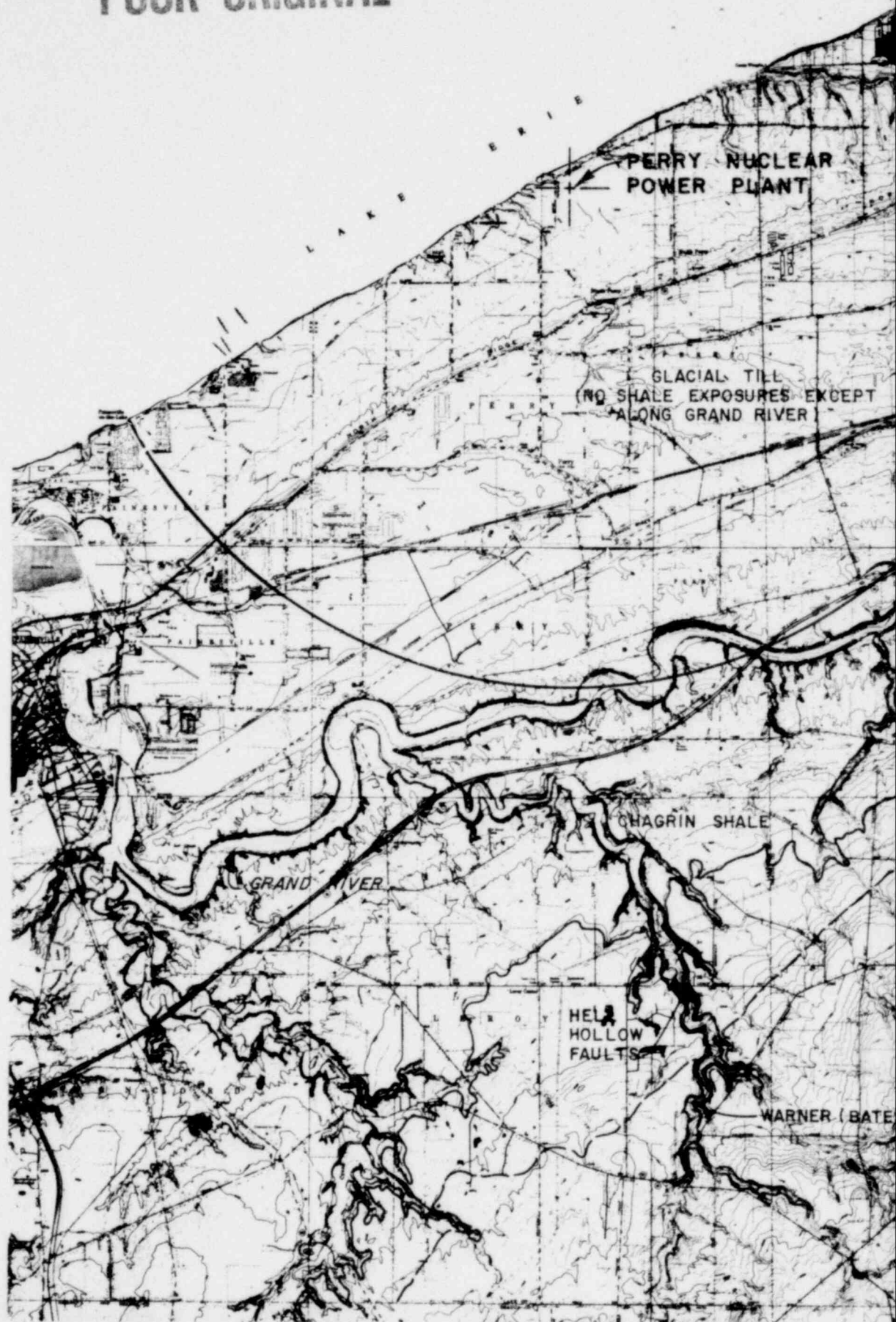
-  OBSERVED OUTCROPS
-  APPROXIMATE OUTCROP OF BEDROCK SHALE
-  APPROXIMATE OUTCROP OF BEREASANDSTONE

1248 114

FAULT AND OUTCROP LOCATION MAP

FIGURE 9

POOR ORIGINAL



NOTE:
 PLANNED EXCAVATION LIMITS ARE
 SHOWN BY DIAGONAL PATTERN,
 AND OVEREXCAVATION BY STIPPLED
 PATTERN.

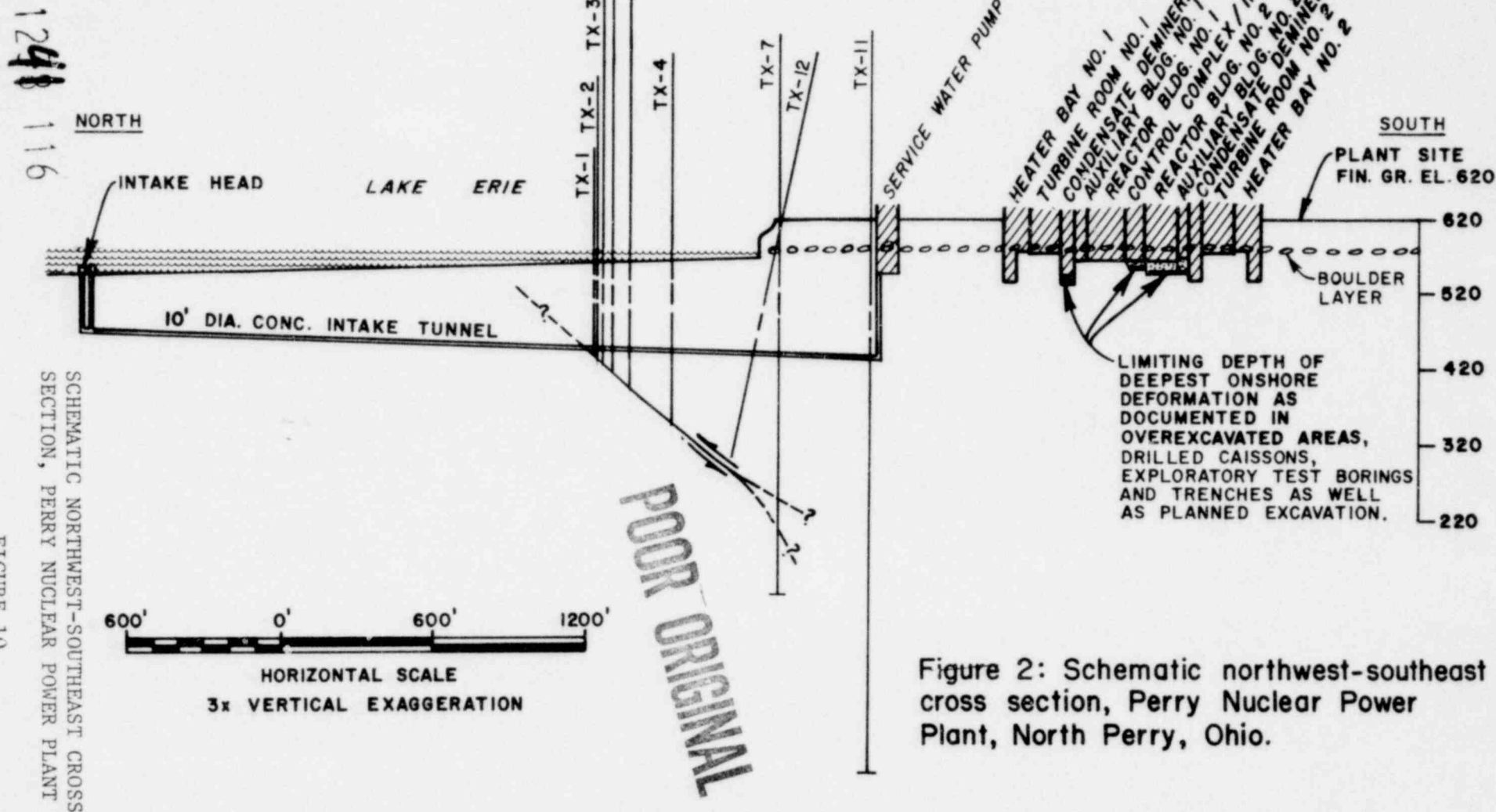


Figure 2: Schematic northwest-southeast cross section, Perry Nuclear Power Plant, North Perry, Ohio.

POOR ORIGINAL

E 2,366,000

E 2,367,000

E 2,368,000

E 2,369,000



1238 118

POOR ORIGINAL

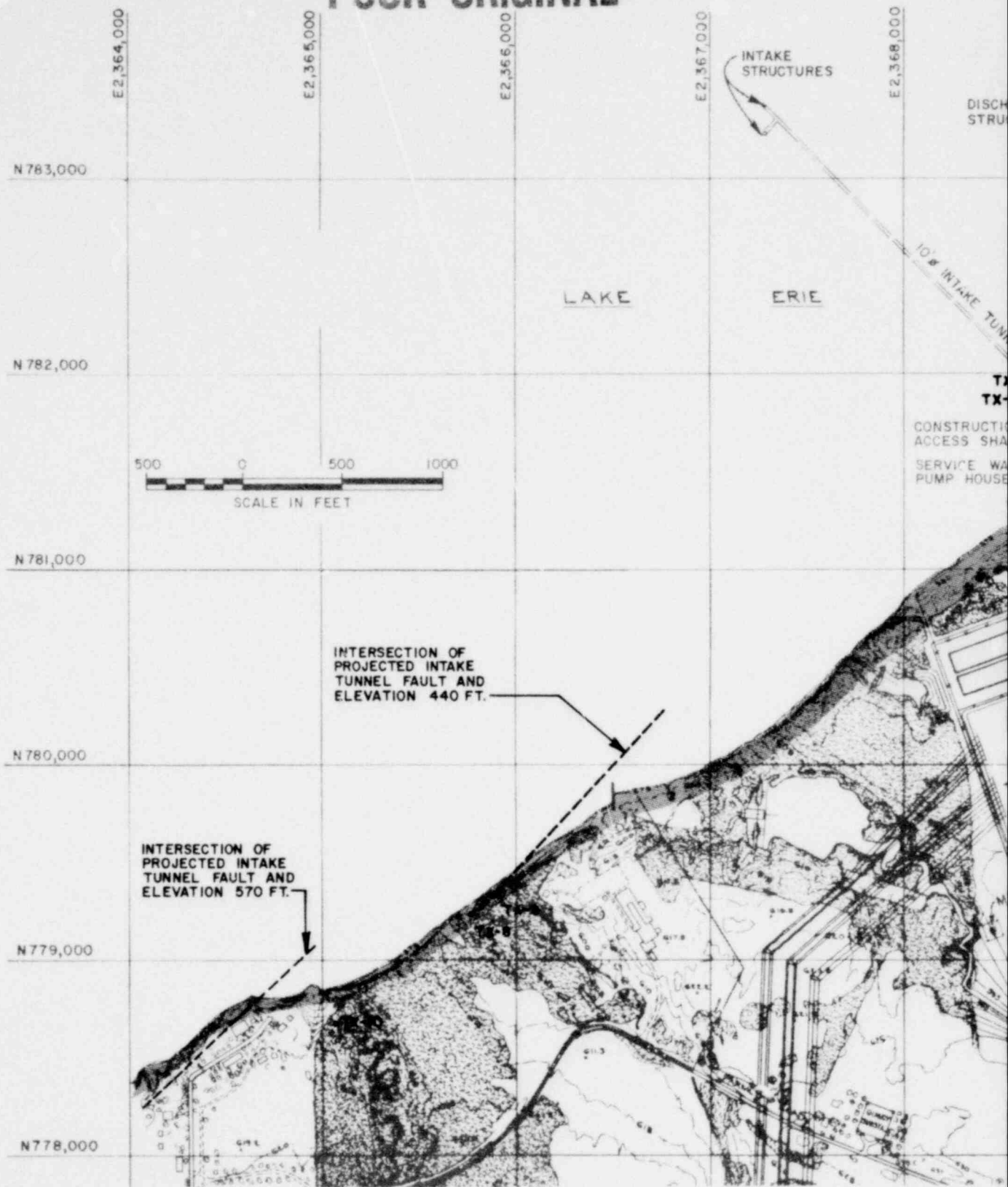


1248 119

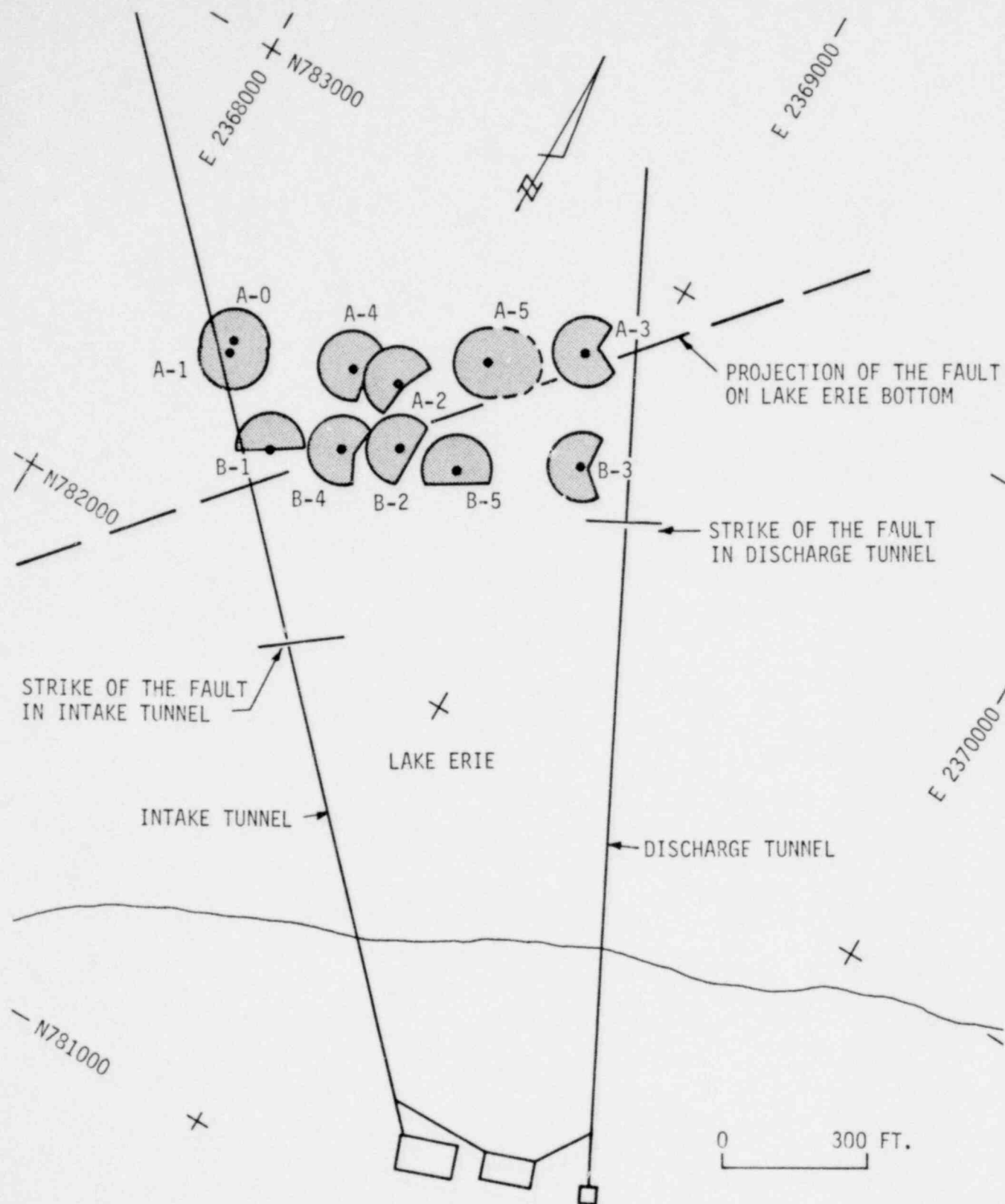
MAP OF SHORELINE SURVEY

FIGURE 12

POOR ORIGINAL



1238 120

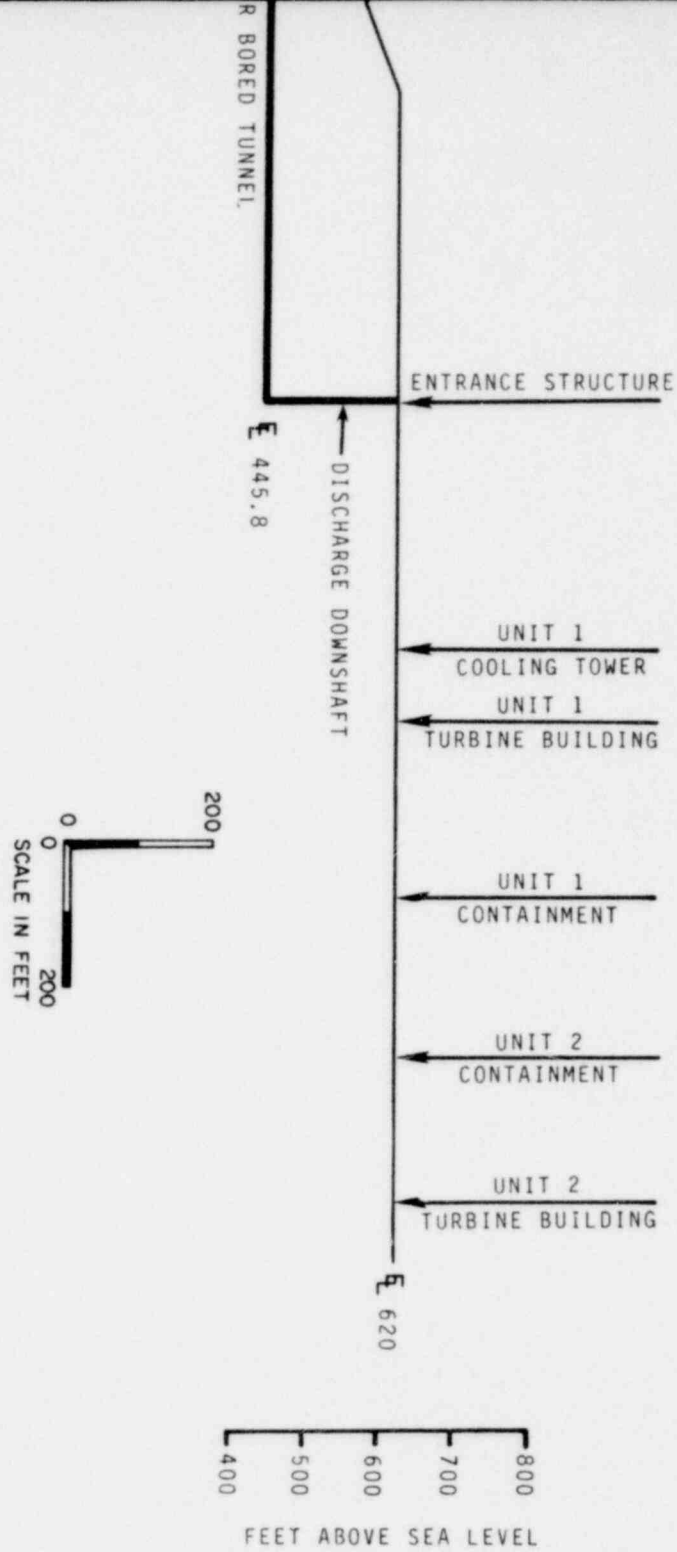


- = STATION LOCATION
- ◐ = AREA OF COVERAGE ABOUT EACH STATION

LOCATION MAP, VIDEO SURVEY
LAKE ERIE BOTTOM

FIGURE 13

LOCATIONS OF CENTERS OF POWER PLANT
BUILDINGS PROJECTED ONTO TUNNEL ALIGNMENT



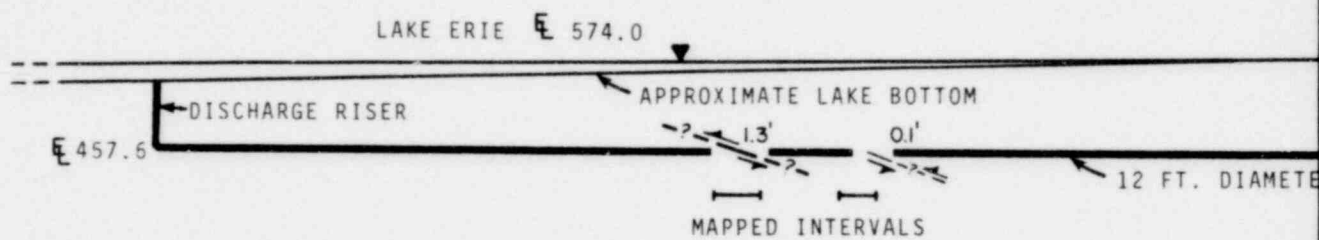
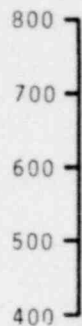
LONGITUDINAL SECTION, DISCHARGE TUNNEL.

FIGURE 14

1241 122

DISCHARGE TUNNEL HEADING N27°06'21"W

FEET ABOVE SEA LEVEL



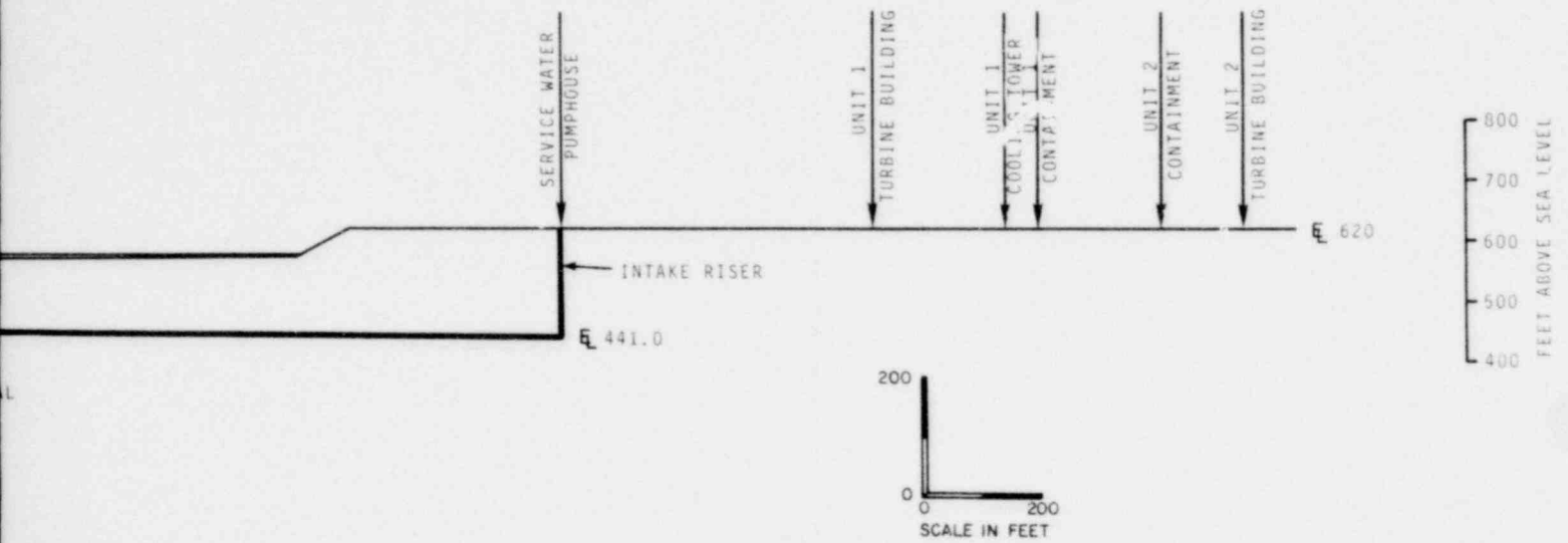
EXPLANATION



THRUST FAULT, DASHED AND QUESTIONED WHERE PROJECTED. ARROWS INDICATE DIRECTION OF RELATIVE MOVEMENT. DISPLACEMENT IN FEET AND TENTHS.

1238 123

LOCATIONS OF CENTERS OF POWER PLANT
BUILDINGS PROJECTED ONTO TUNNEL ALIGNMENT

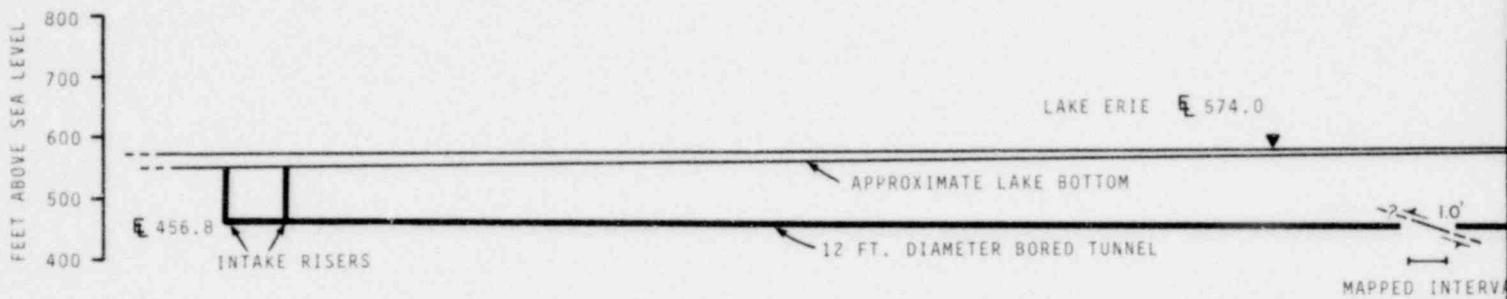


124 124

LONGITUDINAL SECTION, INTAKE TUNNEL

FIGURE 15

INTAKE TUNNEL HEADING N44°12'41"W

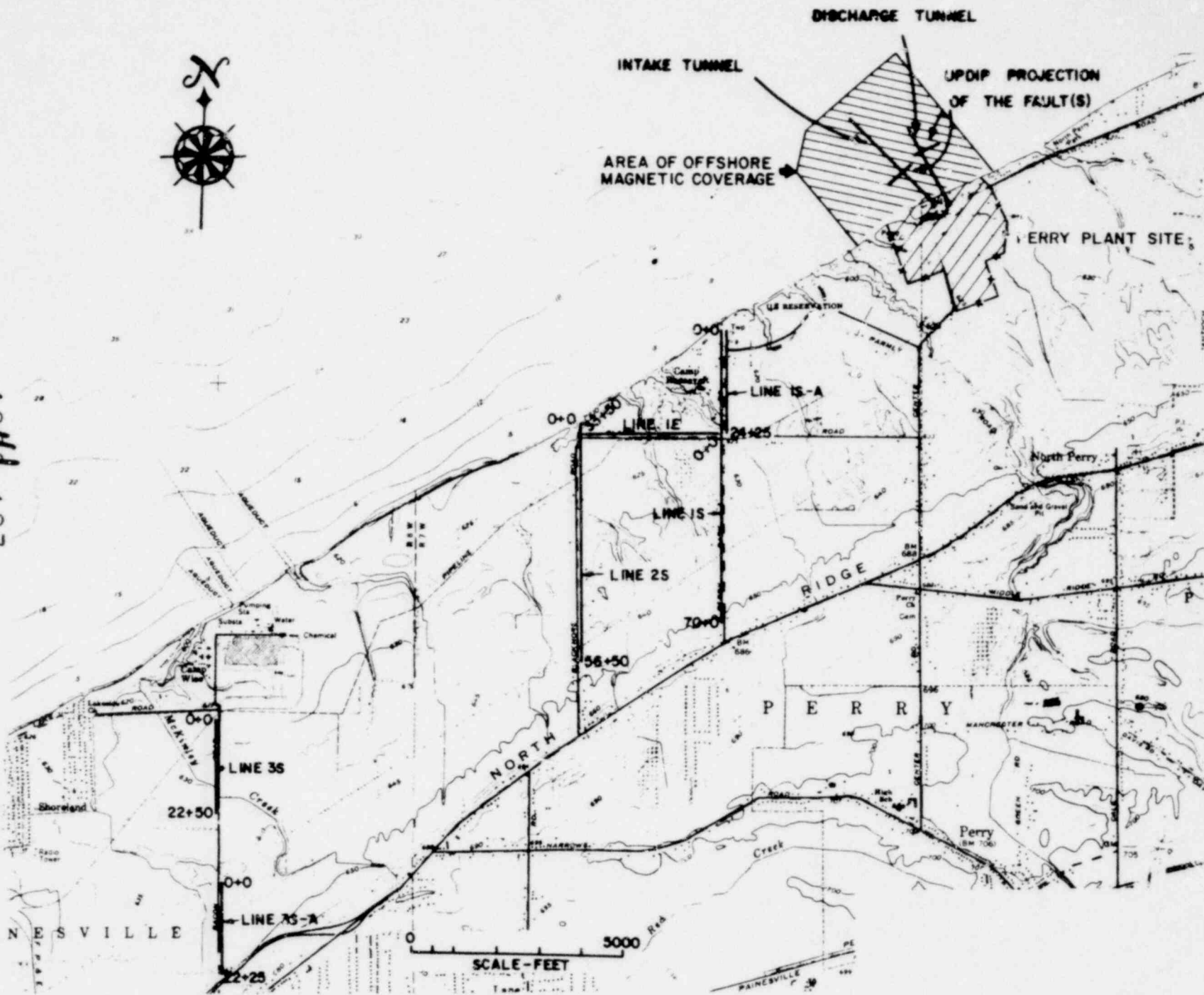


EXPLANATION

7' 10' THRUST FAULT, DASHED AND QUESTIONED WHERE PROJECTED. ARROWS INDICATE DIRECTION OF RELATIVE MOVEMENT. DISPLACEMENT IN FEET AND TENTHS.

1233 125

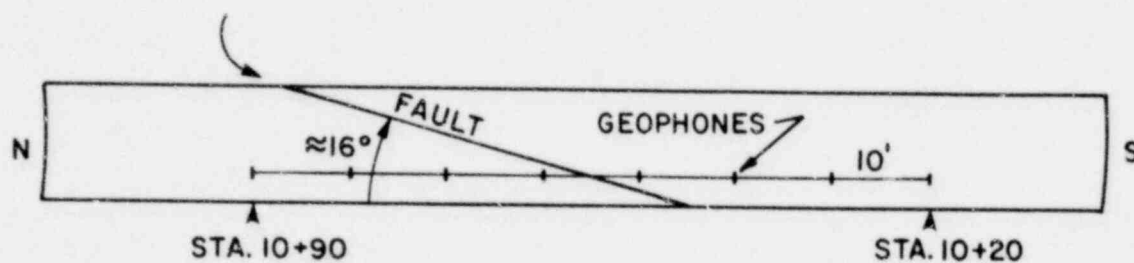
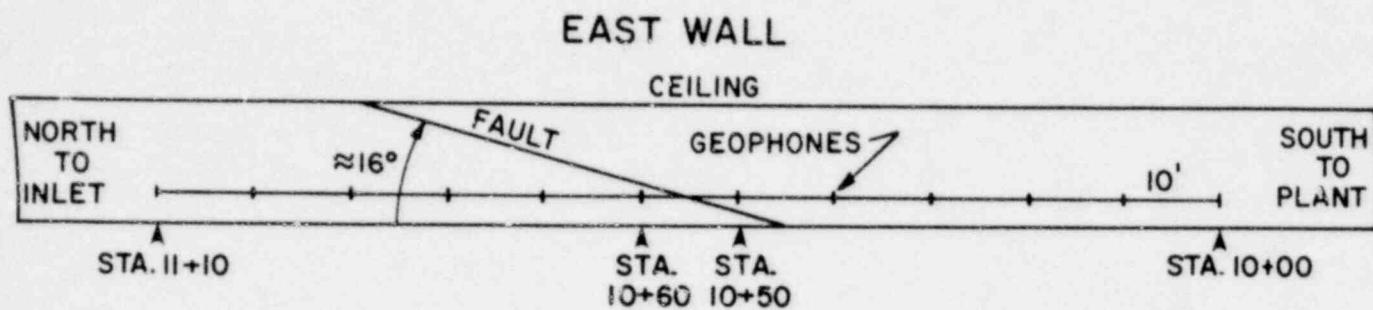
1248 127



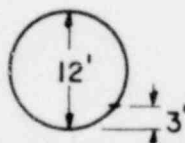
POOR ORIGINAL

LOCATION MAP, ONSHORE MAGNETIC SURVEY

FIGURE 17



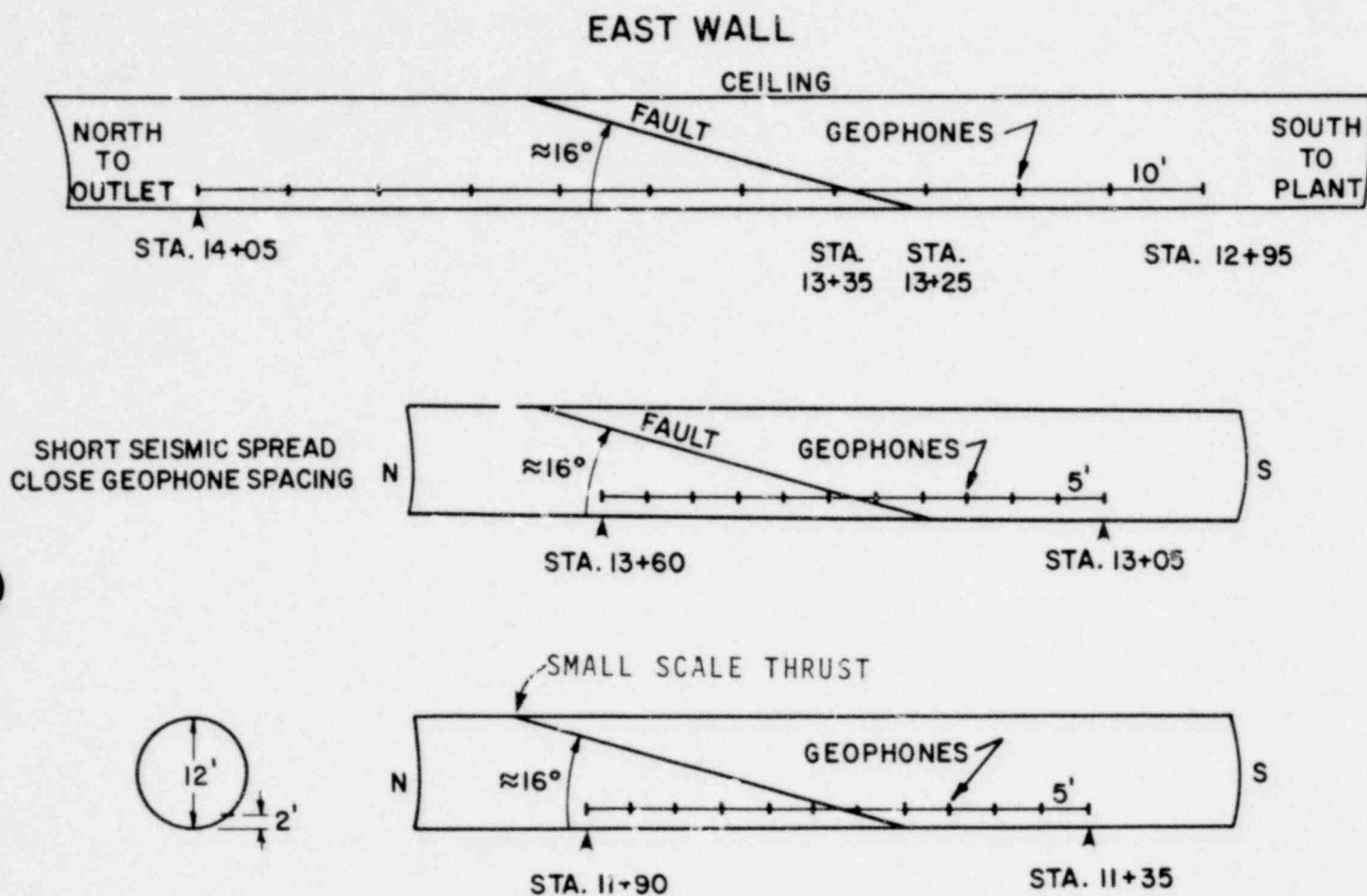
3 ELEMENT GEOPHONE
AT EACH STATION



1248 128

LOCATION MAP,
SEISMIC SPREADS, INTAKE TUNNEL

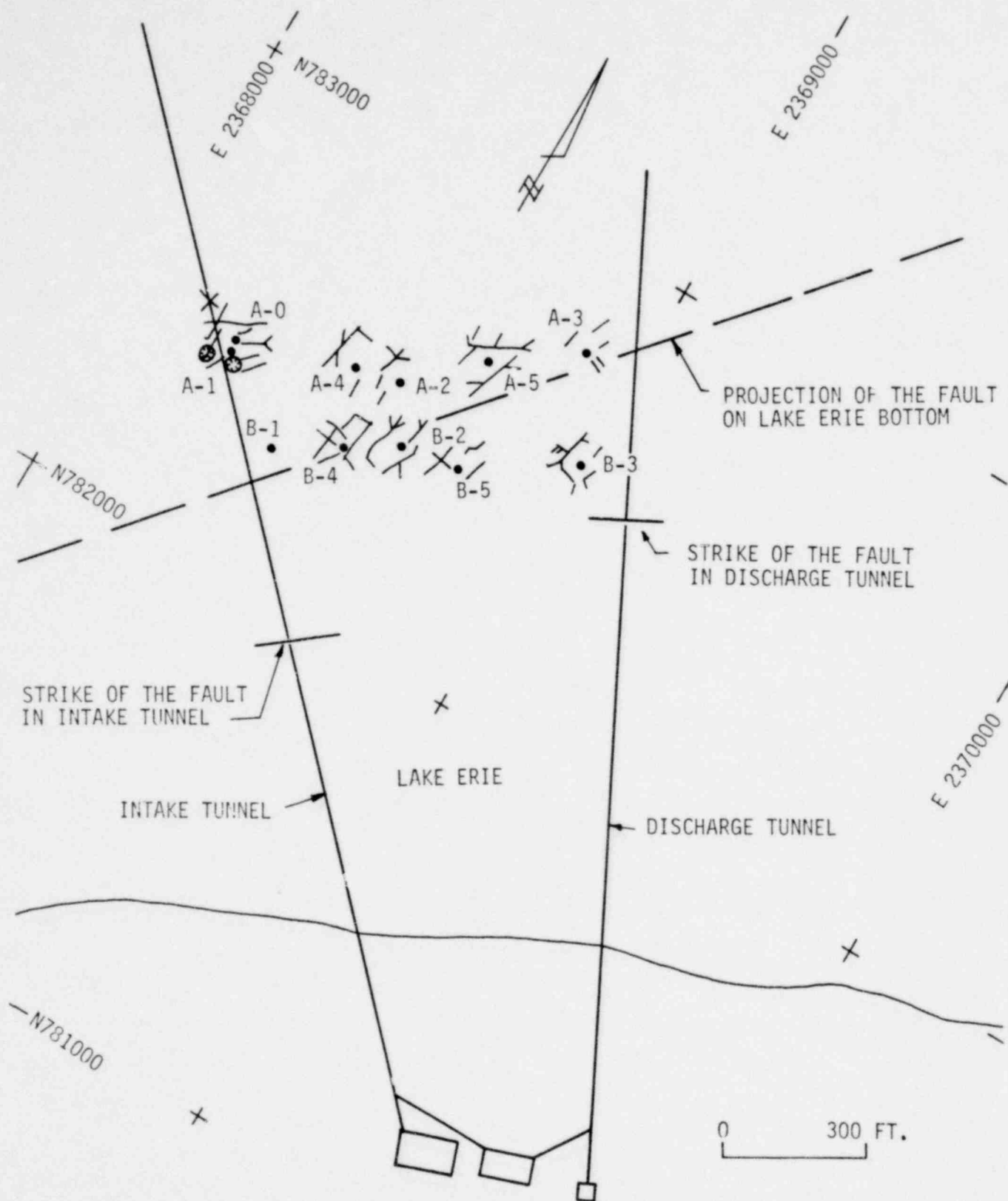
FIGURE 18



1248 129

LOCATION MAP,
SEISMIC SPREADS, DISCHARGE TUNNEL

FIGURE 19



• = STATION LOCATION

— = FRACTURE

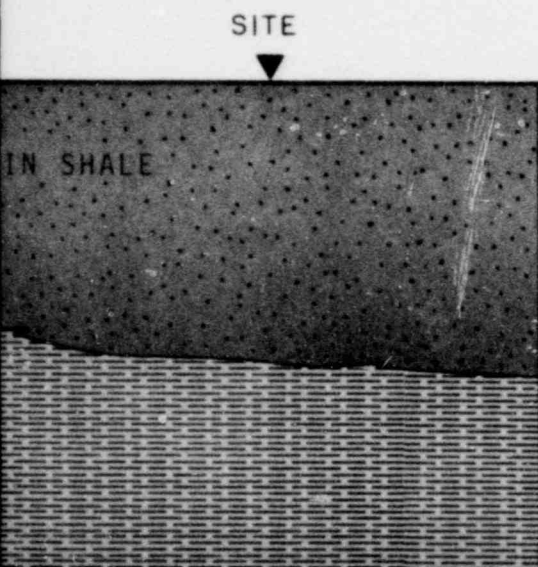
⊗ = SHALLOW DEPRESSION
IN BEDROCK SURFACE

SCHEMATIC MAP, LAKE BOTTOM FRACTURES

FIGURE 20

1241 130

POOR ORIGINAL

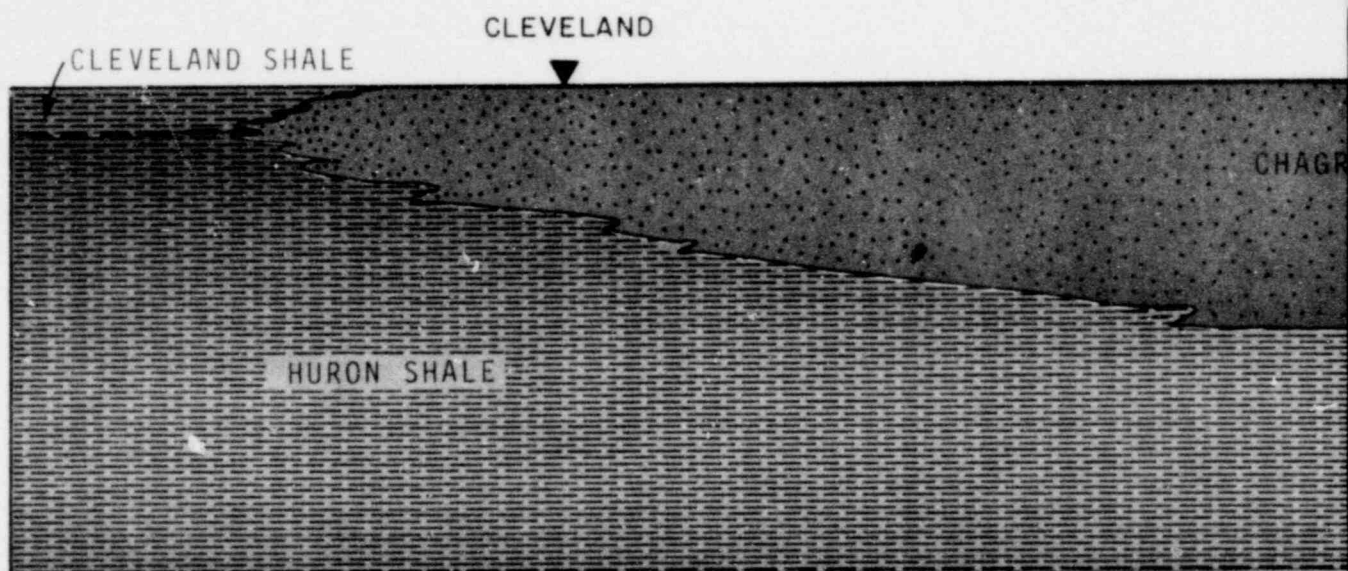


1248 131

SKETCH OF FACIES RELATIONSHIPS AMONG
THE HURAN, CHARGRIN, & CLEVELAND SHALES

FIGURE 21

POOR ORIGINAL



NOTE: SECTION ORIENTED NORTHEASTERLY.

1238 132

POOR ORIGINAL

EXPLANATION



SILTSTONE.



SILTSTONE LAMINA, DASHED WHERE BEDDING PLANE CONTINUOUSLY MAPPED BUT SILTSTONE LITHOLOGY PINCHED OUT.



SHALE.



IRONSTONE CONCRETIONS.

- 448.0 UNIT A: CLAY SHALE: DARK GRAY, WITH BLOCKY TO CONCHOIDAL FRACTURE; WITH CLOSELY SPACED GROUPS OF LATERALLY PERSISTENT, PLANAR, HAIR-THIN LAMINAE OF LIGHT-GRAY SILTSTONE.
- UNIT B: CLAY SHALE: DARK GRAY, WITH BLOCKY FRACTURE, WITH UPPER, MEDIAL, AND BASAL ZONES, ABOUT 1 CM THICK, OF LIGHT-GRAY HARD SILTSTONE. UPPER SILTSTONE THICKENS NORTHWARD AT EXPENSE OF UNDERLYING SHALE.
- UNIT C: CLAY SHALE AND SILTSTONE: FLAT BLACK, SOOTY APPEARING CLAY SHALE UNDERLAIN BY PINCHING-AND-SWELLING, LIGHT-GRAY, SHALE-LAMINATED SILTSTONE UP TO 4.5 CM THICK. SILTSTONE LAMINATION IS FORM CONCORDANT. NORTHWARD, THE BASE OF C IS A BEDDING SURFACE, A SERIES OF SILTSTONE LENSES, AND A CONTINUOUS BED.
- 446.0 UNIT D: CLAY SHALE: SAME AS UNIT C EXCEPT UNDERLAIN BY PERSISTENT PLANAR BED, LESS THAN 1 CM THICK, OF LIGHT-GRAY SILTSTONE INTERLAMINATED WITH GRAY SILTY SHALE. BASAL SILTSTONE VERY HARD.
- UNIT E: CLAY SHALE: DARK GRAY, SOFT, LUSTERLESS, NON-FISSILE. UPPER ONE-THIRD CONTAINS NUMEROUS DISCONTINUOUS LAMINAE OF LIGHT-GRAY SILTSTONE UP TO 2 MM THICK. BASE OF UNIT IS LATERALLY PERSISTENT ZONE, 2 TO 3 CM THICK, OF INTERLAMINATED LIGHT-GRAY SILTSTONE AND GRAY SILTY SHALE; LAMINATION WITHIN THIS ZONE IS FORM CONCORDANT.
- UNIT F: CLAY SHALE AND SILTSTONE: DARK-GRAY, LUSTERLESS CLAY SHALE WITH BLOCKY FRACTURE. BASE OF UNIT IS 4 TO 8 CM-THICK ZONE OF CONVOLUTED, INTERLAMINATED LIGHT-GRAY SILTSTONE TO VERY FINE-GRAINED SANDSTONE, AND GRAY SILTY SHALE. CORES OF CONVOLUTIONS LOCALLY SIDERITIC. LOWER ONE-HALF OF UNIT CONTAINS TWO PROMINENT PLANES INTERVALS OF INTERLAMINATED SILTSTONE AND SILTY SHALE. SILTSTONE LAMINAE UNCOMMON IN UPPER PART OF UNIT.
- 444.0 UNIT G: CLAY SHALE: DARK GRAY TO BLACK, WITH BLOCKY TO CONCHOIDAL FRACTURE; WITH SEVERAL PLANAR TO BROADLY WAVY LAMINAE, ABOUT 1 MM THICK, OF BROWNISH-BLACK (SIDERITIC) CLAY SHALE NEAR BASE OF UNIT, WITH SEVERAL DISCONTINUOUS SILTSTONE LAMINAE, ABOUT 1 MM THICK, NEAR CENTER OF THE UNIT.
- UNIT H: CLAY SHALE, SILTSTONE, & IRONSTONE. UPPERMOST 9 TO 10 CM IS WAVY BEDDED ZONE OF HARD, FLAT, LIGHT-GRAY SILTSTONE. UNDERLYING SHALE SAME AS UNIT G, WITH TWO DISCONTINUOUS BROADLY WAVY LAMINAE OF LIGHT-GRAY SILTSTONE (AS SHOWN). BASE OF SHALE CONTAINS CLOSELY SPACED IRONSTONE CONCRETIONS 2 TO 5 CM THICK AND 5 TO 15 CM IN DIAMETER.
- 442.0

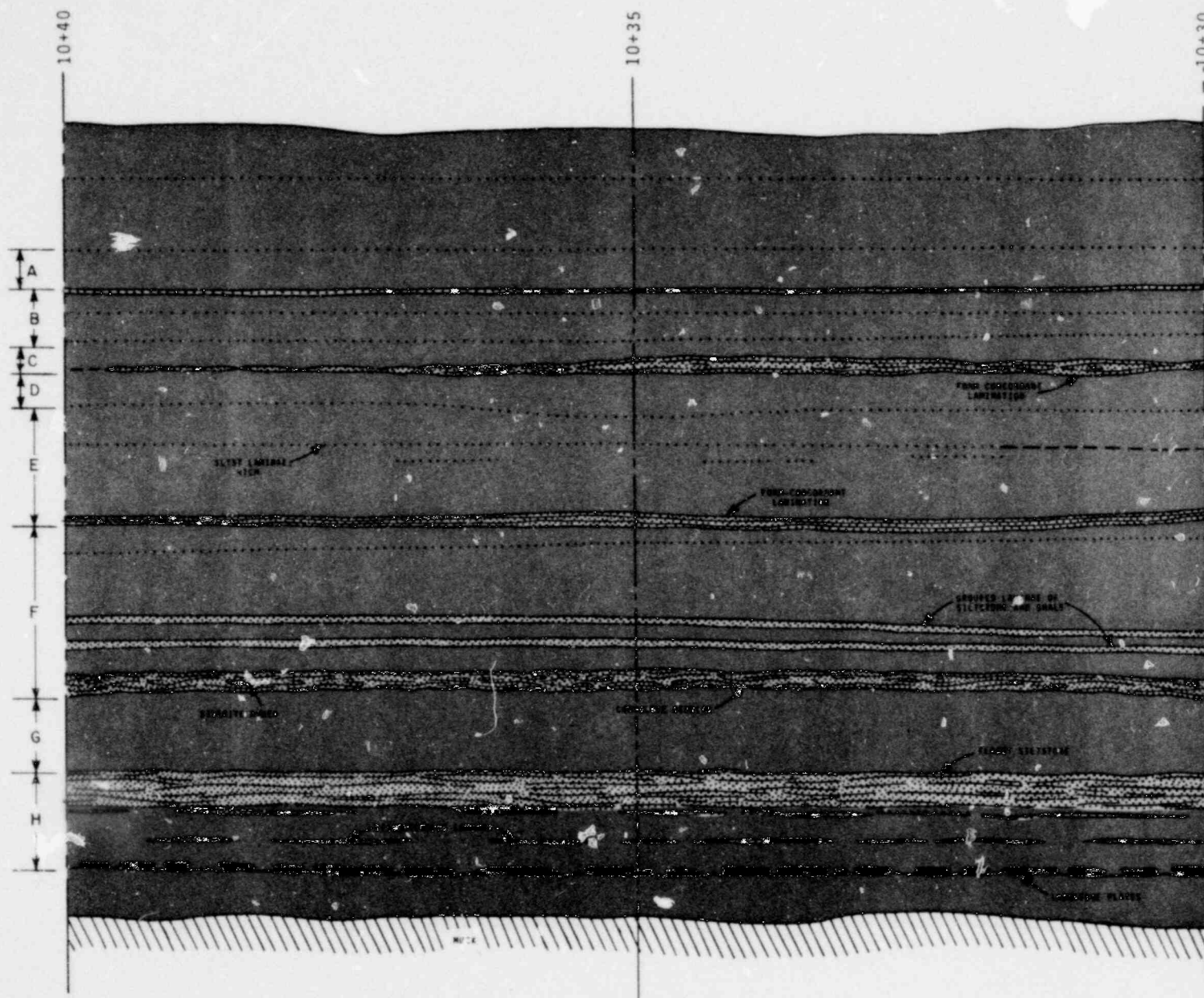
DETAILED STRATIGRAPHIC SECTION,
INTAKE TUNNEL
EAST WALL STATION 10+30-10+40

FIGURE 22

124 133

POOR ORIGINAL

INTAKE TUNNEL EAST WALL



1238 134

POOR ORIGINAL

EXPLANATION



SILTSTONE.



SILTSTONE LAMINA, DASHED WHERE BEDDING PLANE CONTINUOUSLY MAPPED BUT SILTSTONE LITHOLOGY PINCHED OUT.



SHALE.



IRONSTONE CONCRETIONS.

KK GRAY, WITH BLOCKY FRACTURE; WITH SEVERAL PLANAR PARALLEL LAMINAE OF BROWNISH-BLACK (SIDERITIC?) CLAY SHALE. TOP OF UNIT IS 1 CM-THICK ZONE OF INTERLAMINATED SILTSTONE AND SILTY SHALE; BASAL CM IS BROADLY WAVY, INTERLAMINATED BROWNISH-BLACK CLAY SHALE, LIGHT-GRAY SILTSTONE, AND SUBORDINATE CLAY SHALE. SILTSTONES IN LOWER PART PINCH AND SWELL, RANGE FROM 2 TO 8 MM IN THICKNESS; UPPER SILTSTONE OF THIS BEDSET BECOMES MUCH THICKER NORTH OF STATION 13+55.

KK GRAY, WITH BLOCKY TO CONCHOIDAL FRACTURE; WITH ONE PROMINENT MEDIAL SILTSTONE ZONE, ABOUT 1 CM THICK. SCONTINUOUS PARALLEL LAMINAE, TO 2 MM THICK, OF LIGHT-GRAY SILTSTONE AND BROWNISH-BLACK (FERRUGINOUS?) CLAY SHALE VERY COMMON ABOVE MEDIAL SILTSTONE. SINGLE SCONTINUOUS SILTSTONE LAMINA NEAR BASE OF UNIT. UNIT N-UNIT M BOUNDARY IS A BEDDING SURFACE AT STATION 11+55, A PROMINENT SILTSTONE PARATES UNITS N AND M.

SILTSTONE: DARK GRAY, MASSIVE, WITH BLOCKY TO CONCHOIDAL FRACTURE; MEDIAL ZONE OF SILTSTONE CONSISTS OF BROADLY WAVY INTERLAMINATIONS OF LIGHT-GRAY SILTSTONE AND BROWNISH-GRAY SILTY SHALE, OVERLAIN BY A SINGLE DISCONTINUOUS (LENTICULAR) BED OF LIGHT-GRAY SILTSTONE. (FERRUGINOUS?) CLAY SHALE AS VERY THIN DISCONTINUOUS PARALLEL LAMINAE ABOVE MEDIAL SILTSTONE, AND AS PLANAR CONTINUOUS PARALLEL LAMINAE IN LOWER PART OF UNIT. LOWER ONE-HALF HAS "BANDING" ASPECT.

SILTSTONE: LOWER ONE-HALF IS CLAY SHALE, DARK GRAY, WITH NUMEROUS BROWNISH-GRAY, FERRUGINOUS(?), BROADLY WAVY LAMINAE, WITH "BANDING" ASPECT, BLOCKY FRACTURE. UPPER ONE-HALF IS GRAY CLAY SHALE WITH SEVERAL BROADLY WAVY SILTSTONE BEDS TO 3 CM IN THICKNESS; UPPER BEDS SCONTINUOUS, LOWER BEDS CONTINUOUS, ALL CHANNELS PRESENT AS SHOWN.

SILTSTONE, AND IRONSTONE: DARK-GRAY, LIGHTLY SILTY CLAY SHALE WITH CONCHOIDAL FRACTURE; WITH NUMEROUS BROADLY WAVY THIN LAMINAE OF BROWNISH-GRAY FERRUGINOUS(?) CLAY SHALE. UPPERMOST 8 CM IS WAVY BEDDED ZONE OF FLAGGY, THINLY INTERLAMINATED SILTSTONE AND SHALY SILTSTONE WITH PARTINGS OF DARK-GRAY SHALE, SOUTHWARD. THE TOP OF THIS SILTSTONE IS RIPPLE-MARKED. SILTSTONE, UP TO 3 CM THICK, HAS STRAIGHT-CRESTED CURRENT RIPPLES AT TOP. BASE OF UNIT CONTAINS BED OF CLOSELY SPACED IRONSTONE CONCRETIONS ABOUT 1.5 CM THICK.

SILTSTONE: DARK GRAY CLAY SHALE, WITH NUMEROUS THIN LAMINAE, 1 TO 2 MM THICK, OF DARK BROWNISH-GRAY FERRUGINOUS(?) CLAY SHALE. UPPERMOST 1 CM IS WAVY BEDDED ZONE OF FLAGGY, THINLY INTERLAMINATED LIGHT-GRAY SILTSTONE AND SOFT, DARK-GRAY SHALE; ALL LOAD CASTS COVER BASE OF MANY SILTSTONE LAMINAE. MICRO-RIPPLES OCCUR LOCALLY ON TOPS OF SILTSTONE LAMINAE. SOUTHWARD. UNIT J CONTAINS A MEDIAL PINCHING AND SWELLING BED OF SILTSTONE.

SILTSTONE, AND IRONSTONE: SAME SEQUENCE AS UNIT K, EXCEPT AS INDICATED GRAPHICALLY.

MEASURED AND DESCRIBED AT STATIONS K THROUGH O WERE MEASURED AT STATION 13+25.

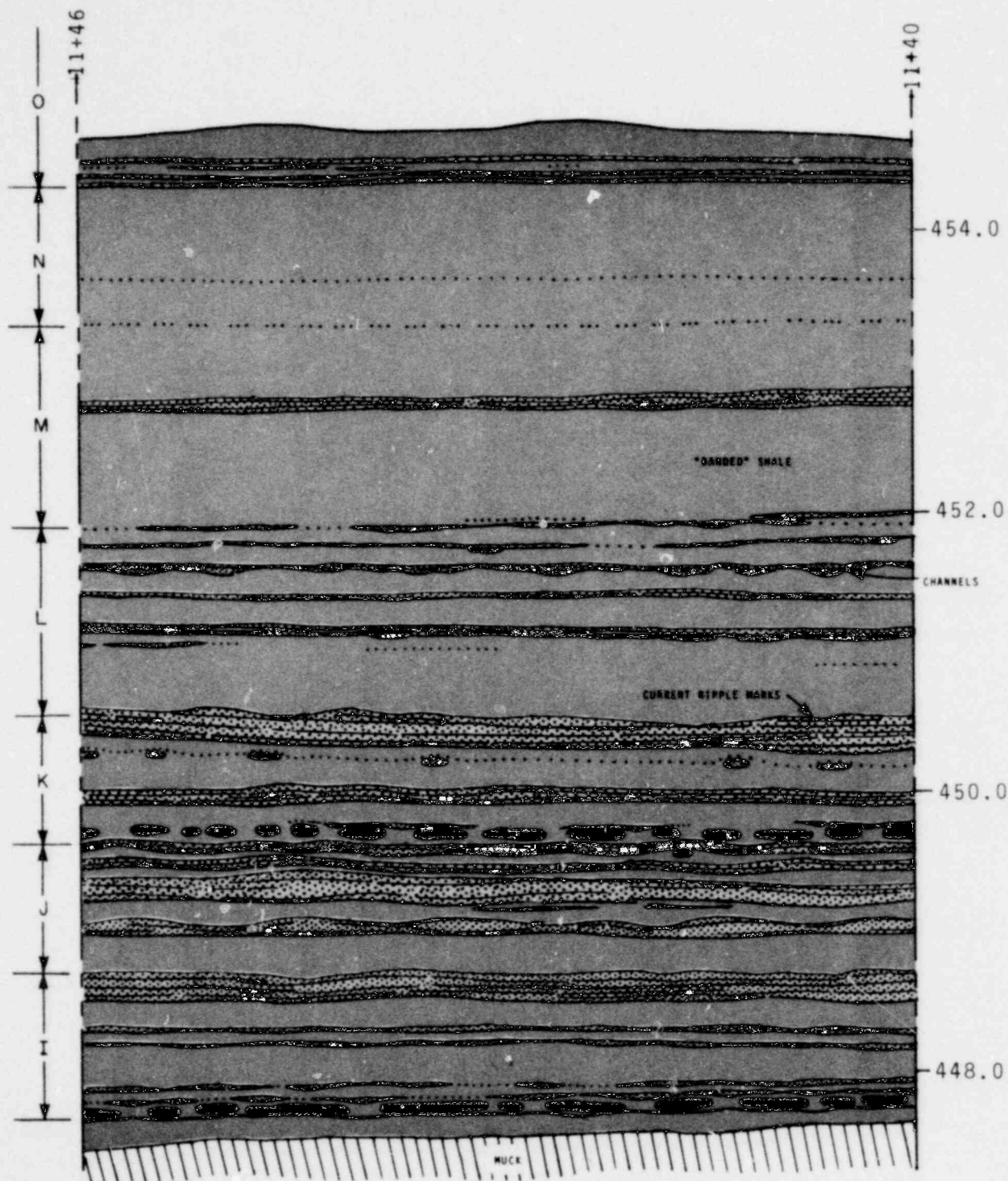
1240 135

DETAILED STRATIGRAPHIC SECTION,
DISCHARGE TUNNEL
EAST WALL STATION 11+40-11+46

FIGURE 23

POOR ORIGINAL

DISCHARGE TUNNEL EAST WALL



UNIT O: CLAY SHALE: DA
WT
LA
CL
SU
R
BR
GR
LO
FR
ME
MI

UNIT N: CLAY SHALE: DA
FR
SI
DI
I
SI
IF
CO
DI
BA
TH
ST
SE

UNIT M: CLAY SHALE AND SI
BL
ME
OF
OF
SI
BO
FO
TH
LA
AN
LA
BA

UNIT L: CLAY SHALE AND SI
SI
DA
BR
AS
ON
SE
UP
DI
SM

UNIT K: CLAY SHALE, SILT
SU
CO
BR
BR
SH
BO
TH
SH
OF
ME
TH
RI
CO
TH

UNIT J: CLAY SHALE AND SI
TH
FE
TH
SI
SM
SI
OD
LA
UN
AN

UNIT I: CLAY SHALE, SILT
AR
I

NOTE: UNITS I AND J WERE
STATION 11+40; UN
AND DESCRIBED AT

1238 136

POOR ORIGINAL

EXPLANATION



FAULT GOUGE ZONE. GRAY, PLASTIC CLAY GOUGE MATRIX WITH AGGREGATE OF RANDOMLY ORIENTED SILTSTONE AND SHALE FRAGMENTS.



SILTSTONE.



SILTSTONE LAMINA, DASHED WHERE BEDDING PLANE CONTINUOUSLY MAPPED BUT SILTSTONE LITHOLOGY PINCHED OUT.



SHALE.



IRONSTONE CONCRETIONS.

ARK GRAY, WITH BLOCKY FRACTURE; WITH SEVERAL PLANAR PARALLEL LAMINAE OF BROWNISH-BLACK (SIDERITIC?) CLAY SHALE. TOP OF UNIT IS 1 CM-THICK ZONE OF INTERLAMINATED SILTSTONE AND SILTY SHALE; BASAL 1 CM IS BROADLY WAVY, INTERLAMINATED BROWNISH-BLACK CLAY SHALE, LIGHT-GRAY SILTSTONE, AND SUBORDINATE GRAY CLAY SHALE. SILTSTONES IN LOWER PART PINCH AND SWELL, RANGE FROM 2 TO 8 MM IN THICKNESS; UPPER-MOST SILTSTONE OF THIS BEDSET BECOMES 1 CM THICKER NORTH OF STATION 13+55.

ARK GRAY, WITH BLOCKY TO CONCHOIDAL FRACTURE; WITH ONE PROMINENT MEDIAL SILTSTONE ZONE, ABOUT 1 CM THICK. DISCONTINUOUS PARALLEL LAMINAE, 1 TO 2 MM THICK, OF LIGHT-GRAY SILTSTONE AND BROWNISH-BLACK (FERRUGINOUS?) CLAY SHALE VERY COMMON ABOVE MEDIAL SILTSTONE; SINGLE DISCONTINUOUS SILTSTONE LAMINA NEAR BASE OF UNIT. UNIT N-UNIT M BOUNDARY IS A BEDDING SURFACE AT THIS STATION; NORTHWARD FROM STATION 11+55, A PROMINENT SILTSTONE SEPARATES UNITS N AND M.

SILTSTONE: DARK GRAY, MASSIVE, WITH BLOCKY TO CONCHOIDAL FRACTURE; MEDIAL ZONE OF SILTSTONE CONSISTS OF BROADLY WAVY INTERLAMINATIONS OF LIGHT-GRAY SILTSTONE AND BROWNISH-GRAY SILTY SHALE, OVERLAIN BY A SINGLE DISCONTINUOUS (LENTICULAR) BED OF LIGHT-GRAY SILTSTONE. FERRUGINOUS(?) CLAY SHALE AS VERY THIN DISCONTINUOUS PARALLEL LAMINAE ABOVE MEDIAL SILTSTONE, AND AS PLANAR CONTINUOUS PARALLEL LAMINAE IN LOWER PART OF UNIT. BASAL ONE-HALF HAS "BANDED" ASPECT.

SILTSTONE: LOWER ONE-HALF IS CLAY SHALE, DARK GRAY, WITH NUMEROUS DARK BROWNISH-GRAY, FERRUGINOUS(?) BROADLY WAVY LAMINAE, WITH "BANDED" ASPECT, BLOCKY FRACTURE. UPPER ONE-HALF IS GRAY CLAY SHALE WITH SEVERAL BROADLY WAVY SILTSTONE BEDS 1 TO 3 CM IN THICKNESS; UPPER BEDS DISCONTINUOUS, LOWER BEDS CONTINUOUS. SMALL CHANNELS PRESENT AS SHOWN.

STONE, AND IRONSTONE: DARK-GRAY, LIGHTLY SILTY CLAY SHALE WITH CONCHOIDAL FRACTURE; WITH NUMEROUS BROADLY WAVY THIN LAMINAE OF BROWNISH-GRAY FERRUGINOUS(?) CLAY SHALE. UPPERMOST 6 CM IS WAVY BEDDED ZONE OF FLAGGY, THINLY INTERLAMINATED SILTSTONE AND SHALY SILTSTONE WITH PARTINGS OF DARK-GRAY SHALE; SOUTHWARD THE TOP OF THIS SILTSTONE IS RIPPLE-MARKED. SILTY SILTSTONE, UP TO 3 CM THICK, HAS STRAIGHT-CRESTED CURRENT RIPPLES AT TOP. BASE OF UNIT CONTAINS BED OF CLOSELY SPACED IRONSTONE CONCRETIONS ABOUT 1.5 CM THICK.

SILTSTONE: DARK GRAY CLAY SHALE, WITH NUMEROUS THIN LAMINAE, 1 TO 2 MM THICK, OF DARK BROWNISH-GRAY FERRUGINOUS(?) CLAY SHALE. UPPERMOST 5 CM IS WAVY BEDDED ZONE OF FLAGGY, THINLY INTERLAMINATED LIGHT-GRAY SILTSTONE AND SOFT, DARK-GRAY SHALE. SMALL LOAD CASES COVER BASE OF MANY SILTSTONE LAMINAE; MICRO-RIPPLES SCUR LOCALLY ON TOPS OF SILTSTONE LAMINAE. SOUTHWARD UNIT J CONTAINS A MEDIAL PINCHING AND SWELLING BED OF SILTSTONE.

STONE, AND IRONSTONE: SAME SEQUENCE AS UNIT K, EXCEPT AS INDICATED GRAPHICALLY.

MEASURED AND DESCRIBED AT STATIONS K THROUGH O WERE MEASURED AT STATION 13+25.

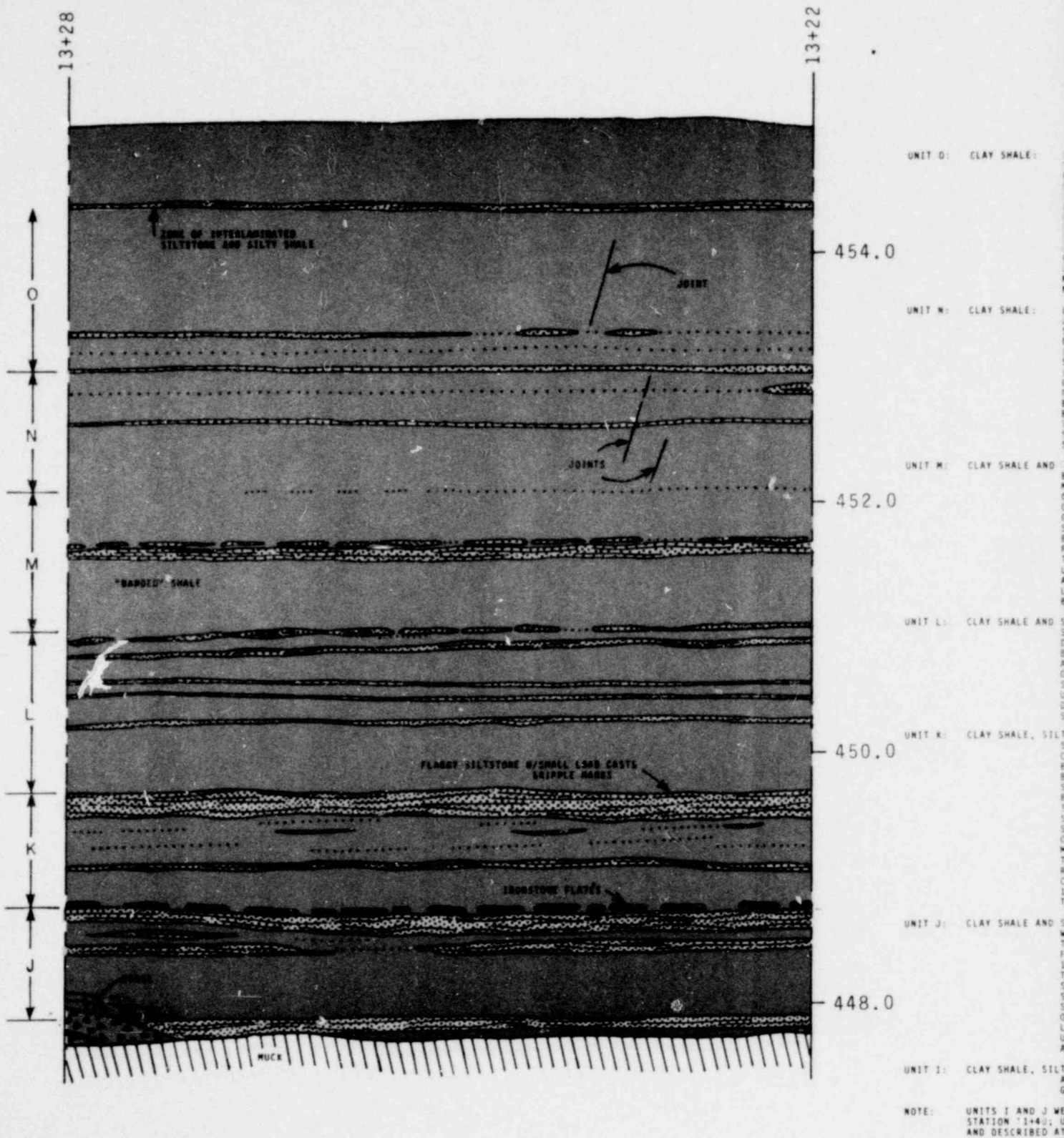
124B 137

DETAILED STRATIGRAPHIC SECTION,
DISCHARGE TUNNEL
EAST WALL STATION 13+22-13+28

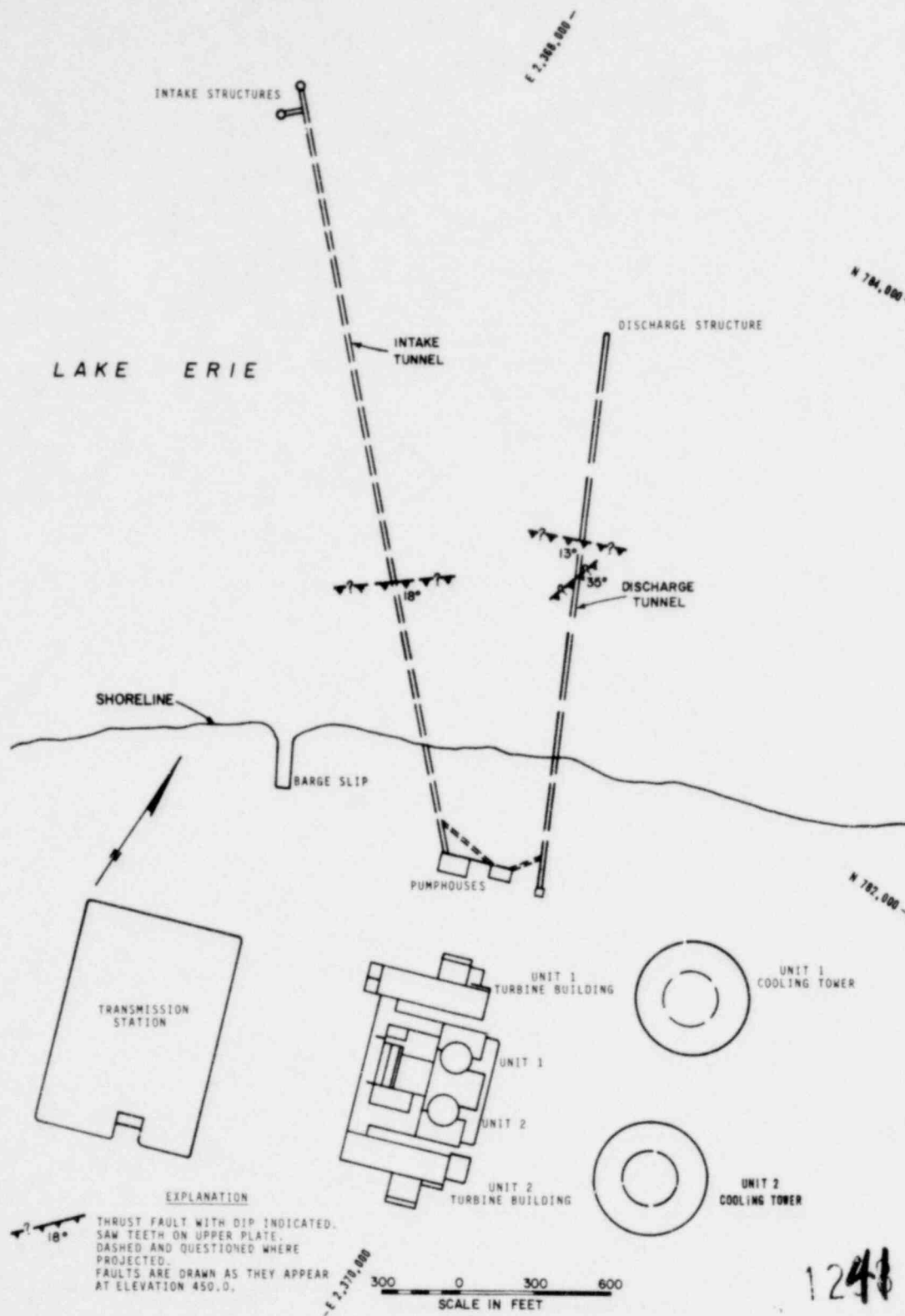
FIGURE 24

POOR ORIGINAL

DISCHARGE TUNNEL EAST WALL



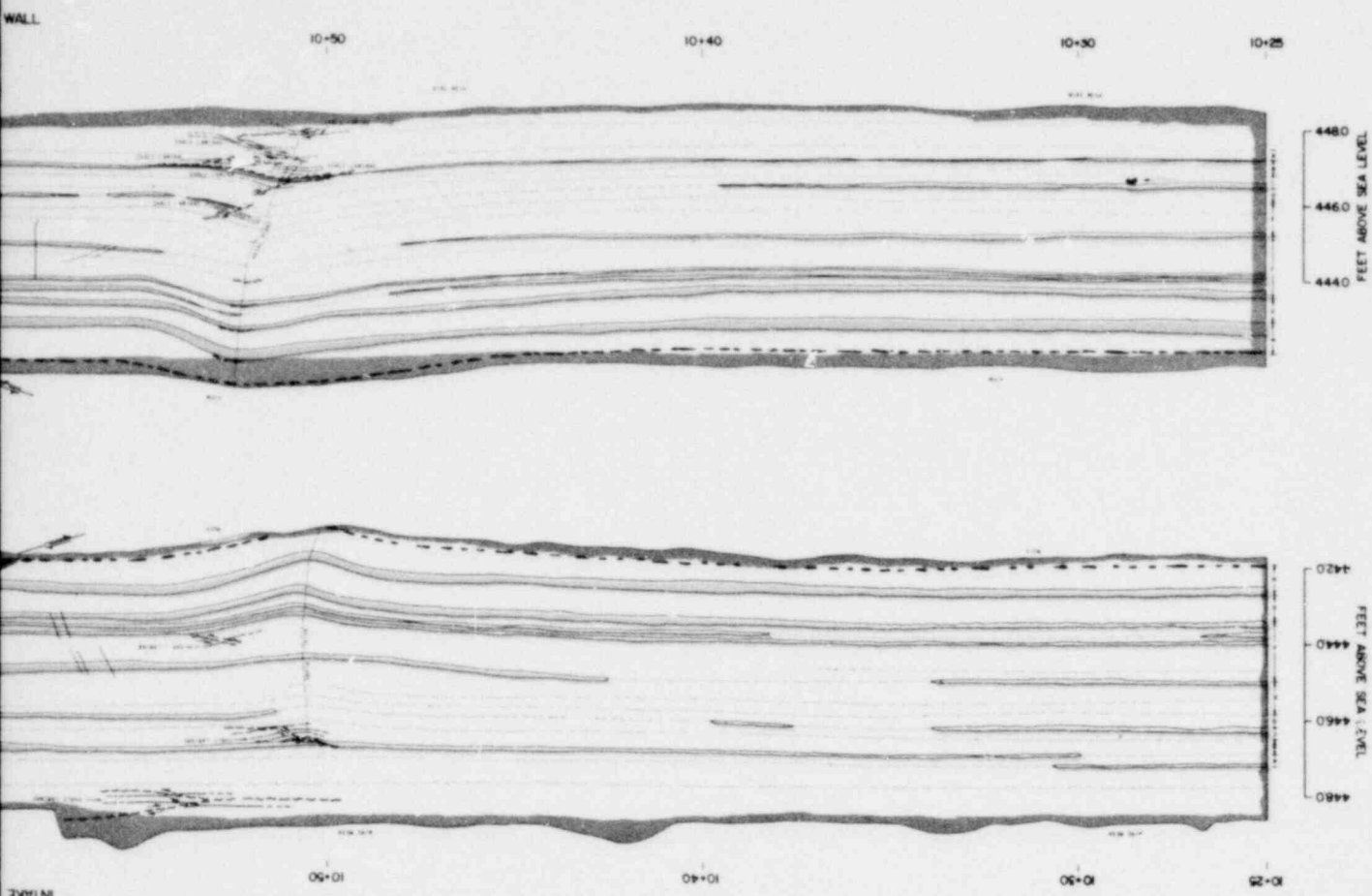
1238 138



GEOLOGIC STRUCTURE MAP,
INTAKE & DISCHARGE TUNNEL FAULTS

FIGURE 25

POOR ORIGINAL

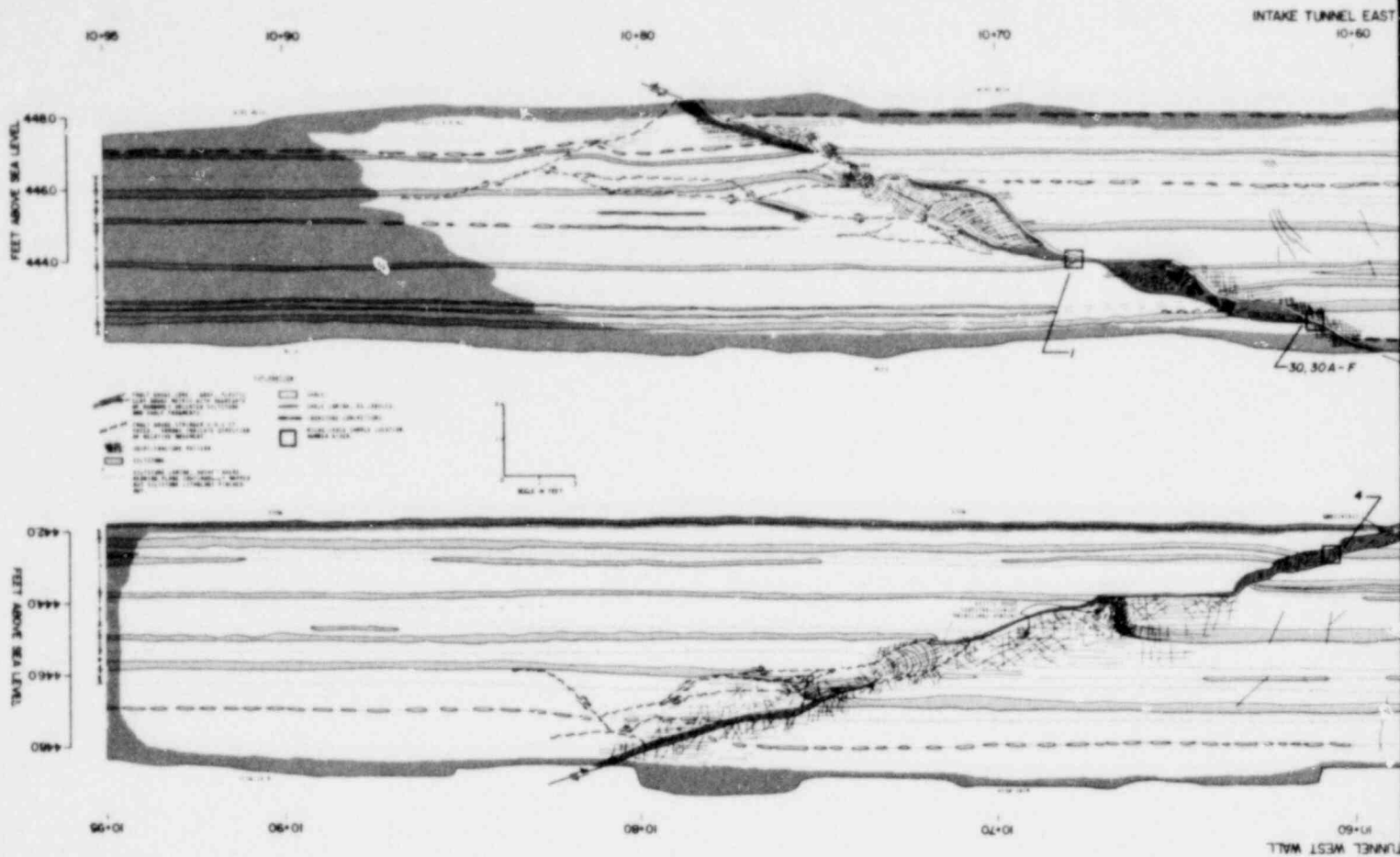


1248 140

INTAKE TUNNEL WALL MAPS,
STATIONS 10+25-10+95

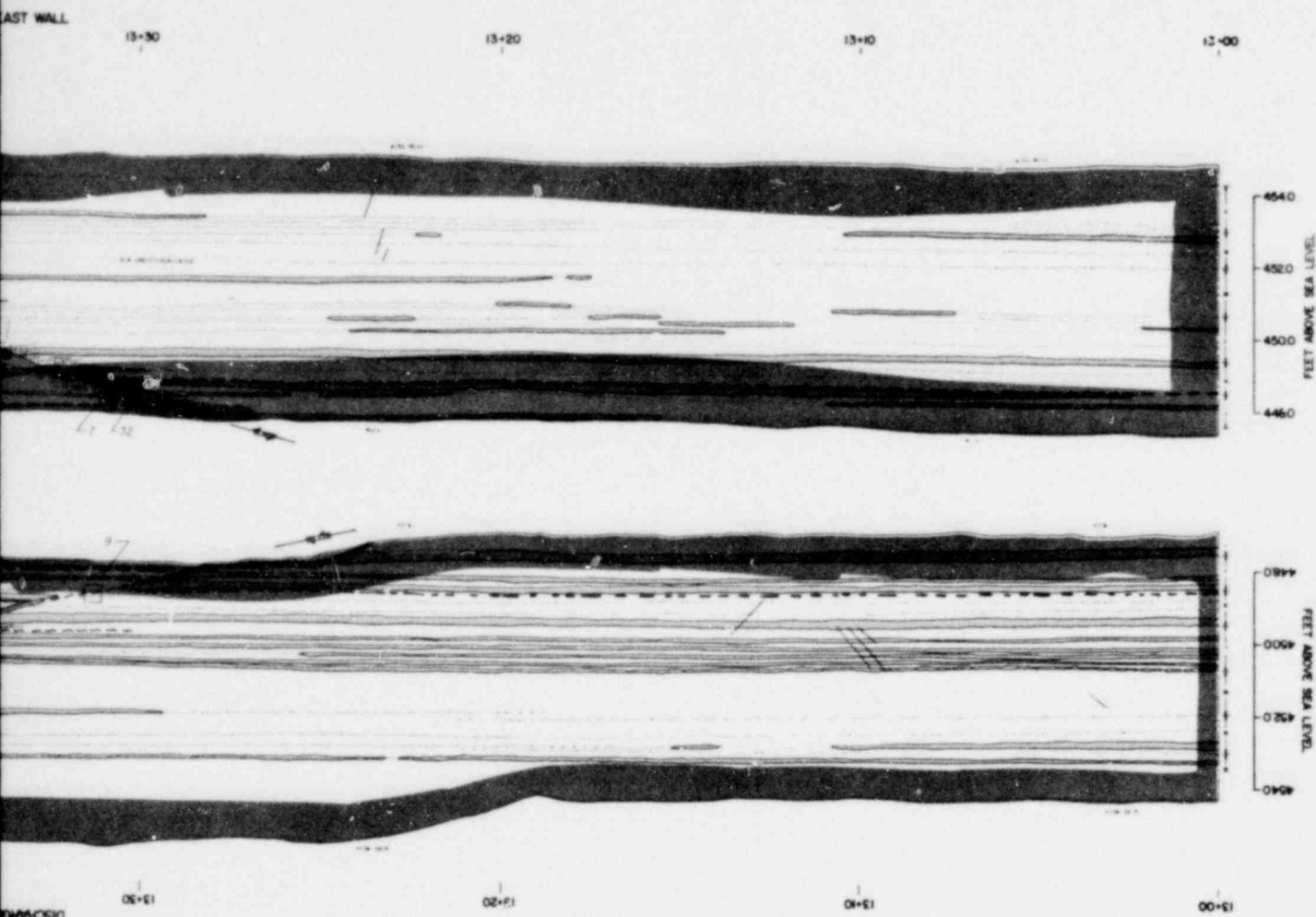
FIGURE 26

POOR ORIGINAL



1238 141

POOR ORIGINAL



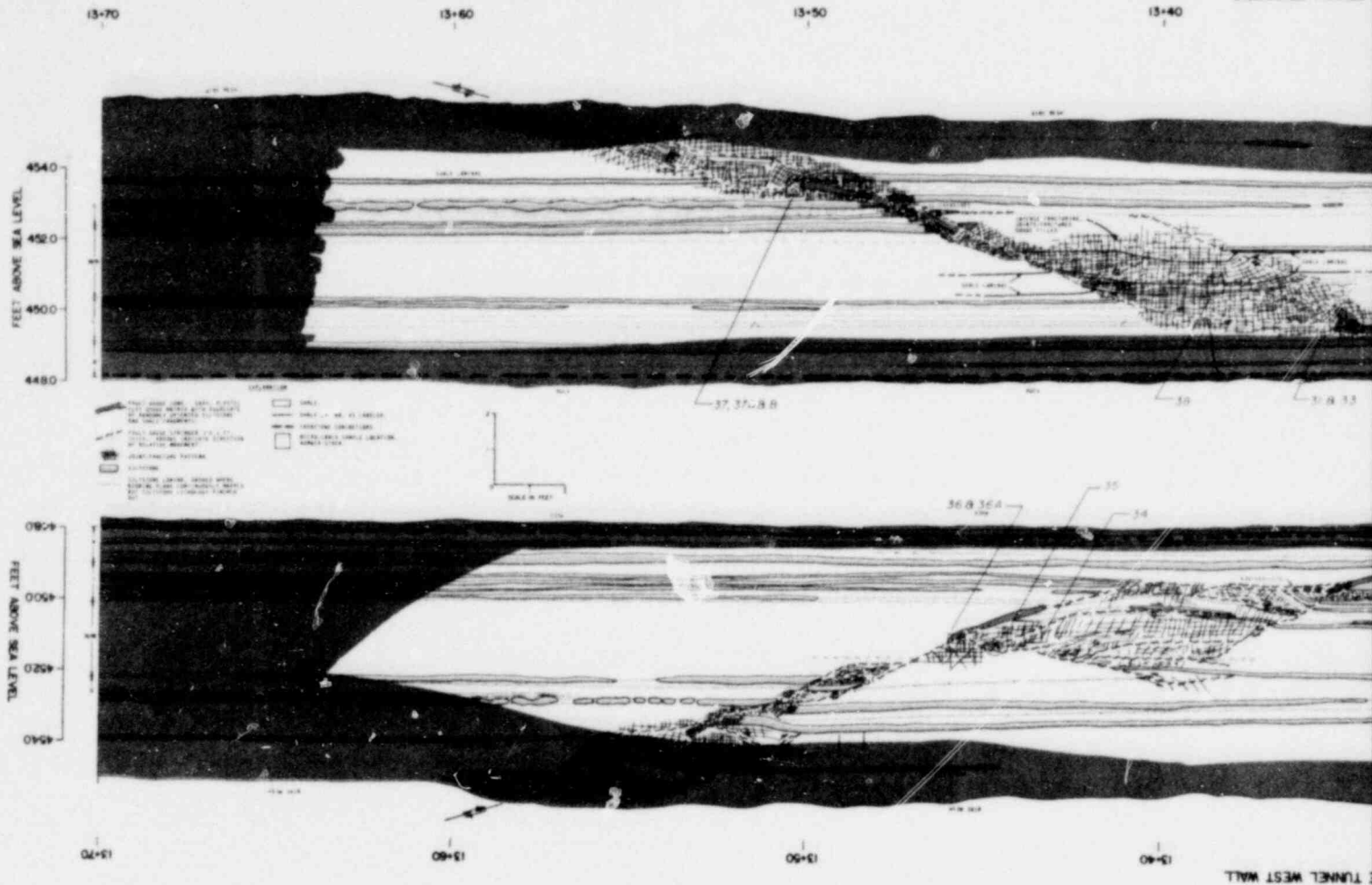
1248 142

DISCHARGE TUNNEL WALL MAPS,
STATIONS 13+00-12+00

FIGURE 27

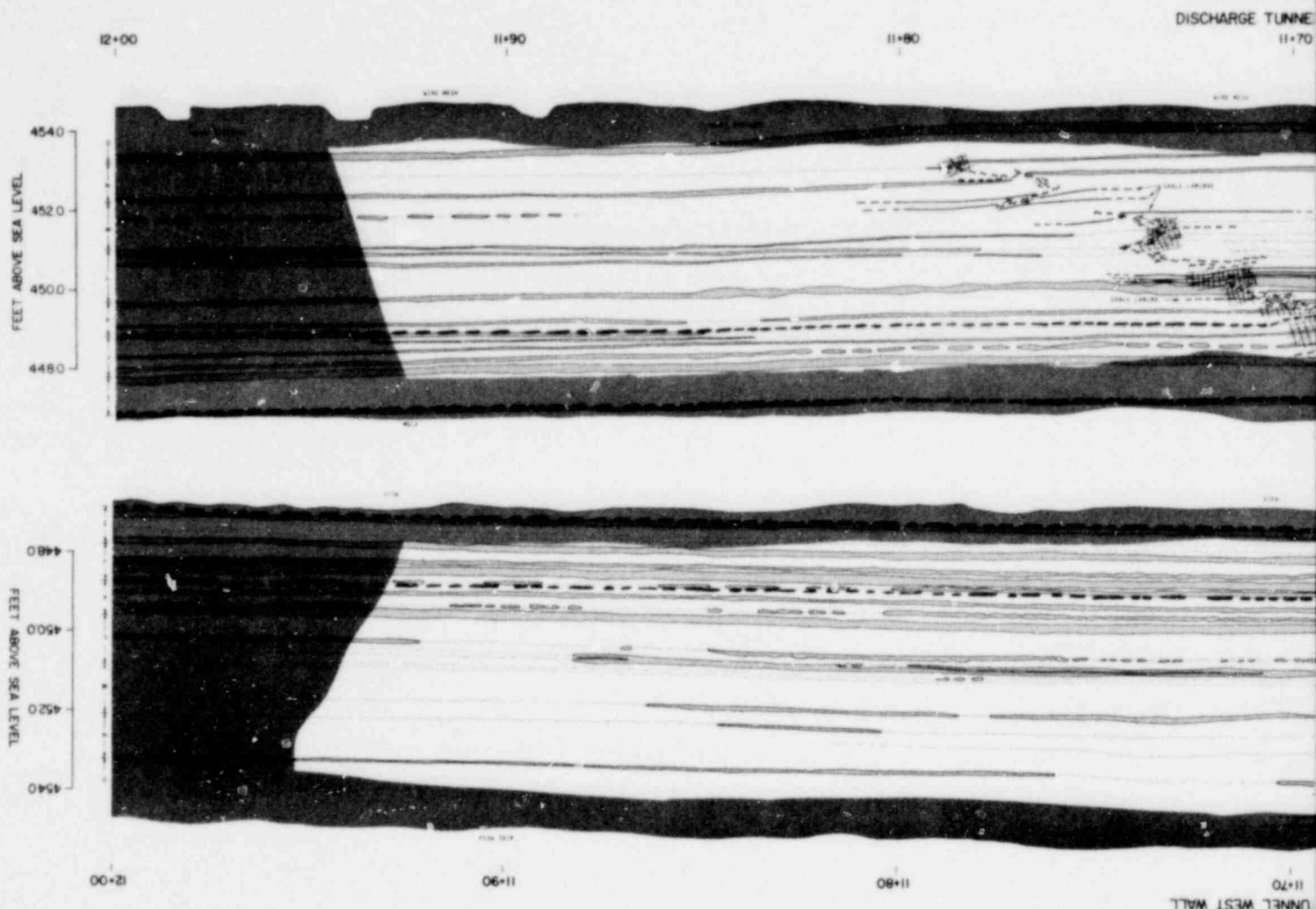
POOR ORIGINAL

DISCHARGE TUNNEL

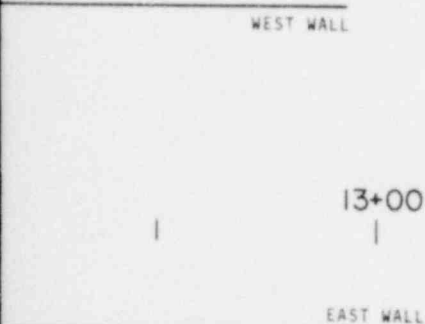
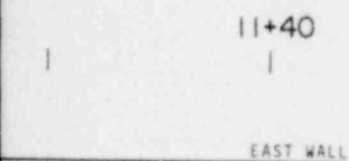
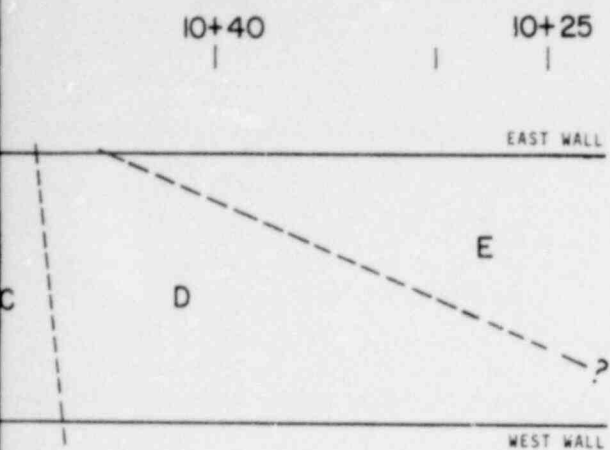


1238 143

POOR ORIGINAL



1233 145



EXPLANATION

A

STRATIGRAPHIC UNITS: A, B, C, D, E, K, L. UNITS K AND L ARE SUBDIVIDED INTO UPPER AND LOWER SECTIONS AS INDICATED BY SUBSCRIPT.



THRUST FAULT SHOWING DISPLACEMENT AND DIP

STRATIGRAPHIC UNIT CONTACT.



SEVERELY FRACTURED ROCK.



SYNCLINAL FOLD AXIS.

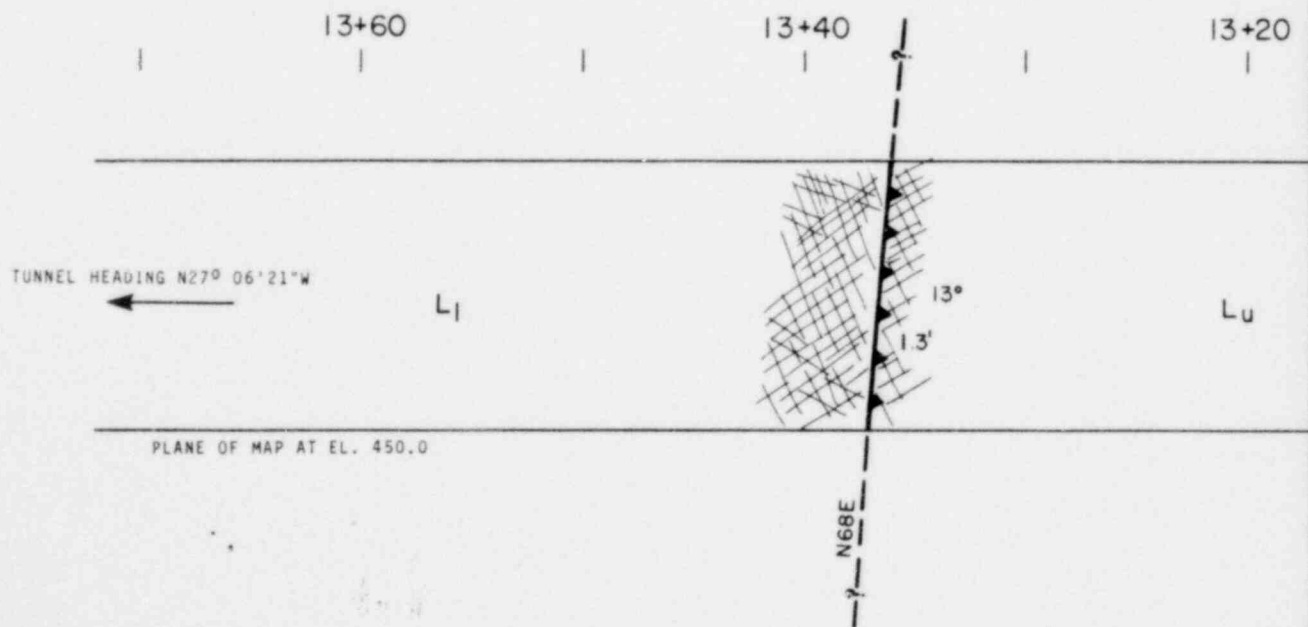
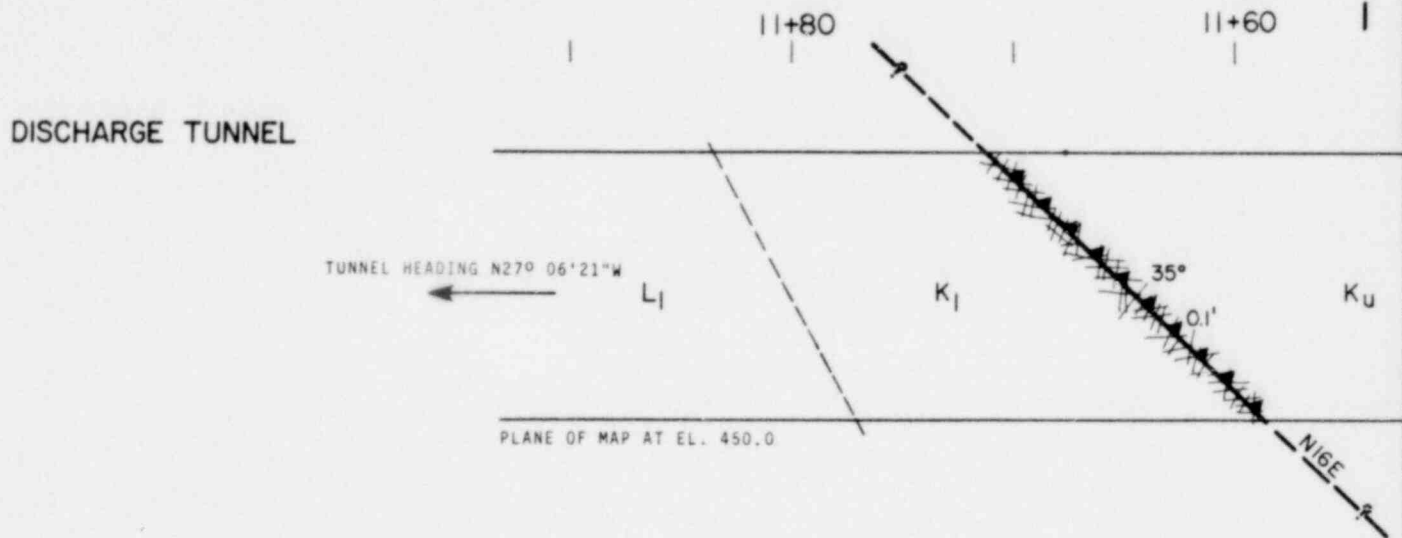
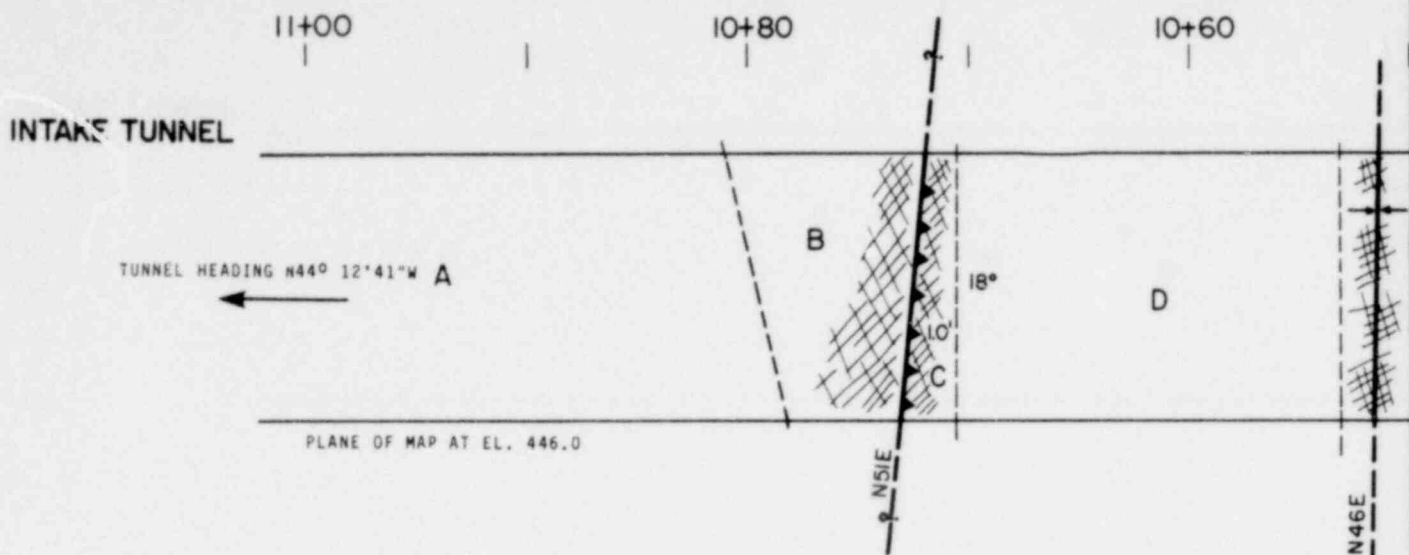
NOTES: 1. SEE FIGURES 22, 23, AND 24 FOR STRATIGRAPHIC UNIT RELATIONSHIPS.

2. MAPS COMPILED FROM INTAKE AND DISCHARGE TUNNEL WALL MAPS, SEE FIGURES 26, 27, AND 28.

GEOLOGIC MAPS,
INTAKE & DISCHARGE TUNNELS

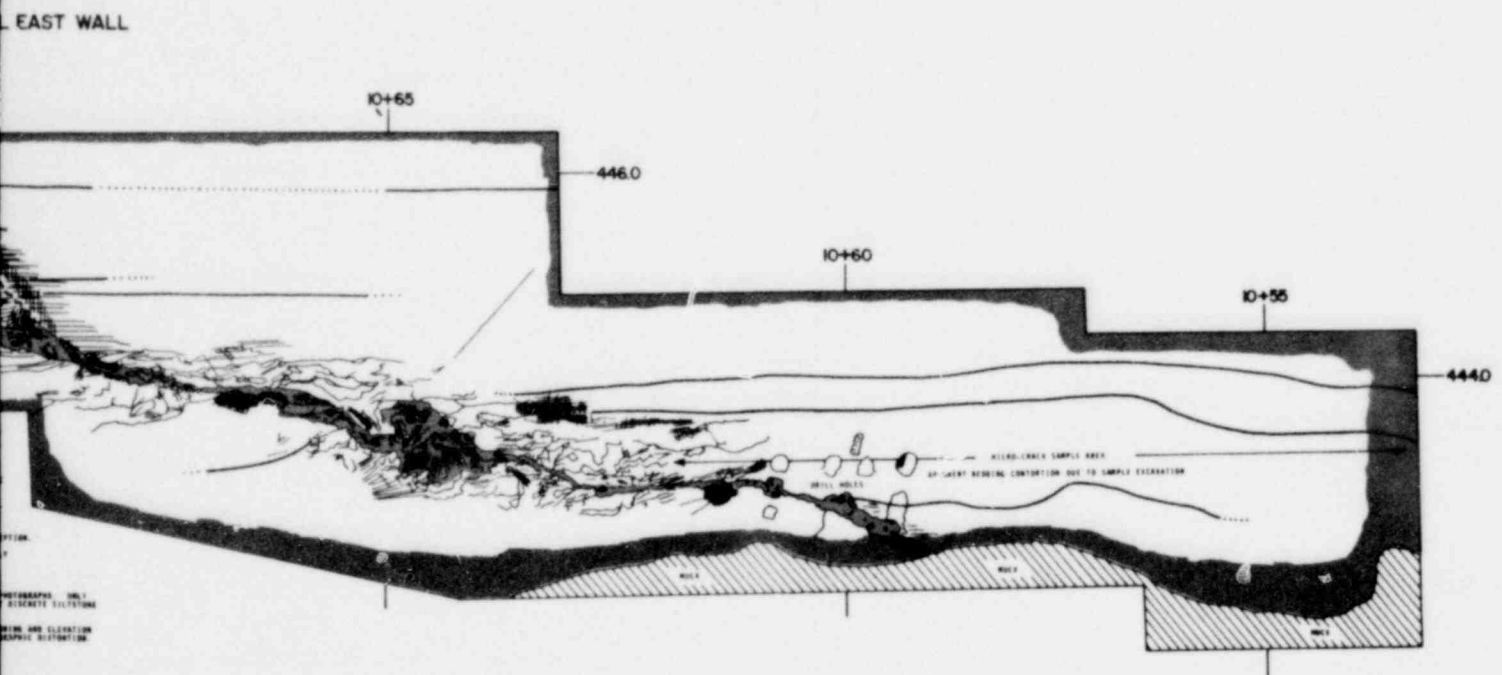
FIGURE 29

1248 146



1238 147

POOR ORIGINAL

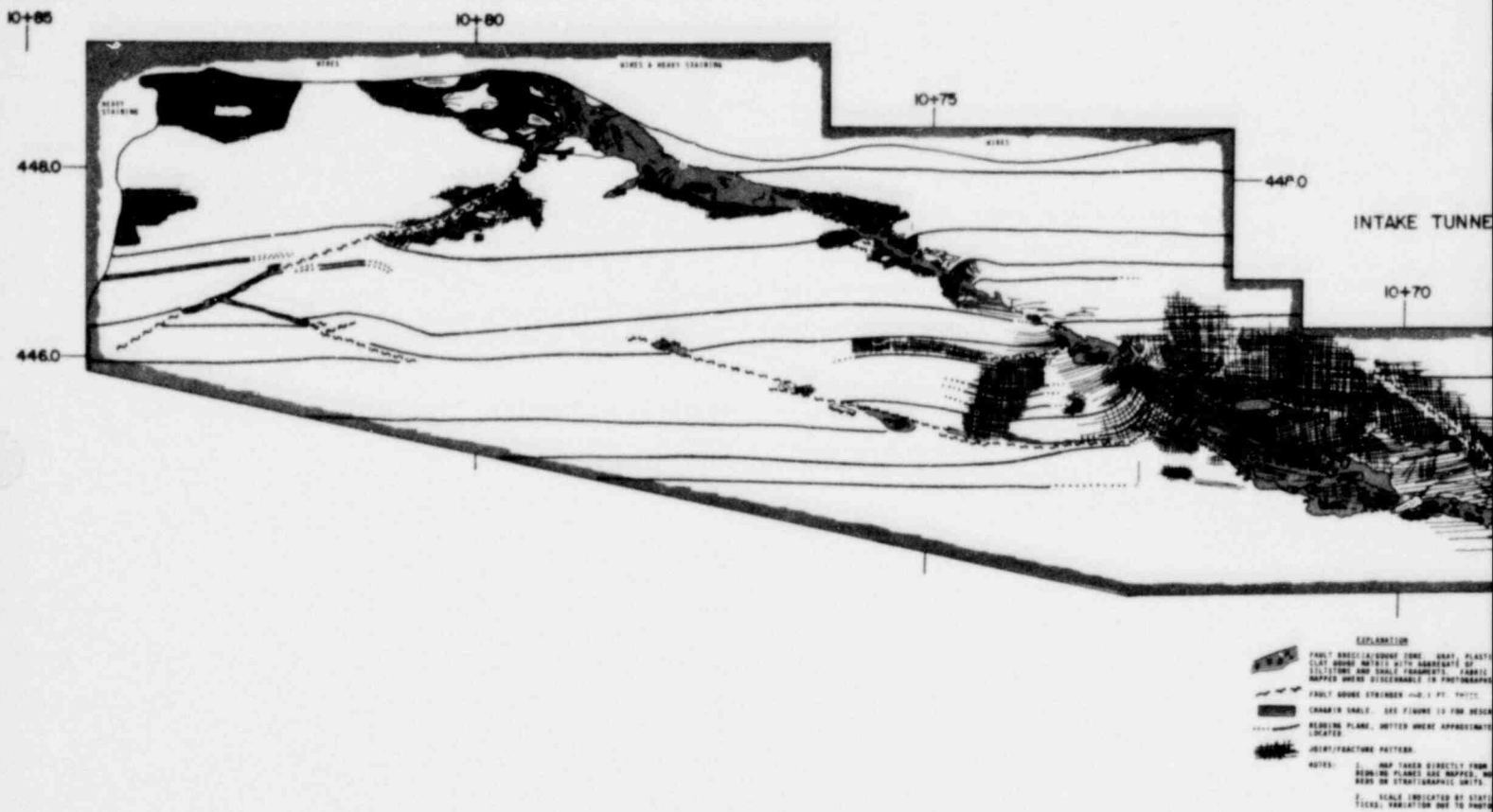


1244 148

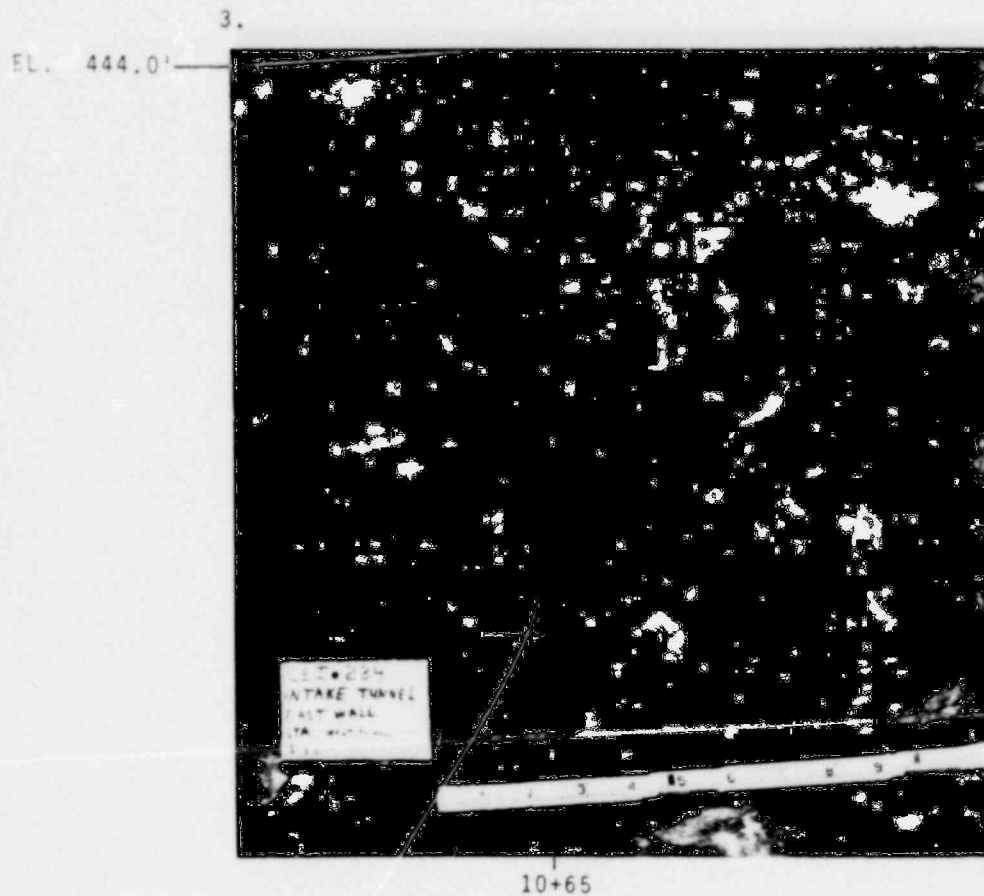
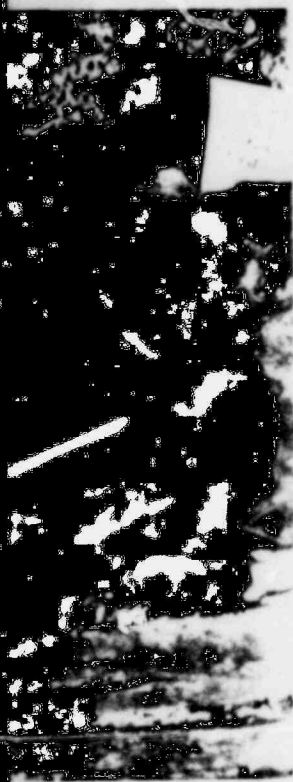
DETAILED MAP, INTAKE TUNNEL FAULT

FIGURE 30

POOR ORIGINAL



POOR ORIGINAL



TUNNEL, STATION 10+61.
N37°W PARALLEL TO NAIL.

FRACTURED AND DRAGGED STRATA; EAST WALL INTAKE TUNNEL,
STATION 10+65.

1241 150

PHOTOGRAPHS, STRUCTURAL DETAILS,
INTAKE TUNNEL

FIGURE 31

POOR ORIGINAL

1.



EL. 448.0'

EL. 446.0'

10+51

ASYMMETRIC FOLD; STATION 10+51, EAST WALL INTAKE TUNNEL.
NOTE FAULTED NW LIMB OF FOLD.

2.



10+61

STRIATIONS; WEST WALL INTAKE
STRIATIONS ON FOOTWALL, TREND

1238 151

—

[illegible]

1

FIGURE 32

12

	FAULT BRECCIA/SANDSTONE CLAY GOUGE MATRIX WITH ILLITE/MICA AND TALC MAPPED WHERE DISCERNABLE
	APPROXIMATE TRACE OF FAULTED IN PHYLLOSILICATE TRACE OF FAULT ZONE
	FAULT GOUGE STRINGER
	CHARCOAL SAMPLE SEE
	BUDDING PLANT, BOTTLE LOCATED
	JOINT/FRACTURE PATTERN

```

NOTES:  1.  MAP 1
          DESIGN PL
          REFS ON ST

          2.  SCALE
          FEET, VARS

          3.  QA 51
          COMBINED BR
          REQUIRED 1

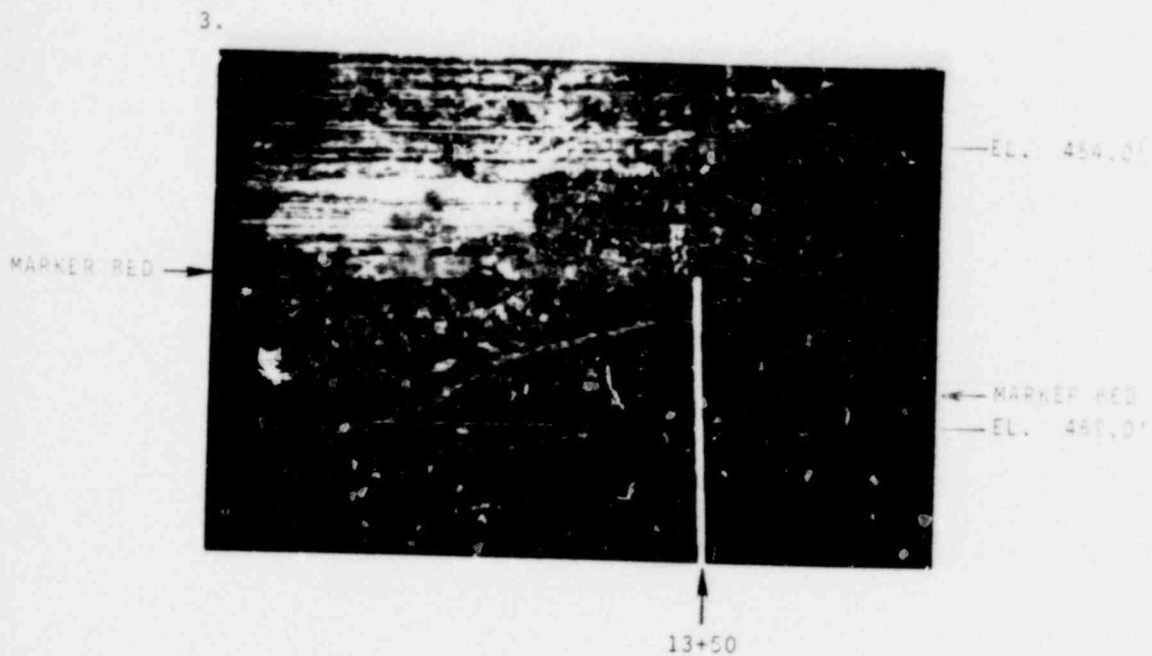
```

1238 153

421

21

POOR ORIGINAL



DISCHARGE TUNNEL.

DRAG FOLDS, KINKING AND FAULT SPLAYS; STATION 13+50 WEST WALL DISCHARGE. SCALE GIVEN BY STATIONING AND RULE.

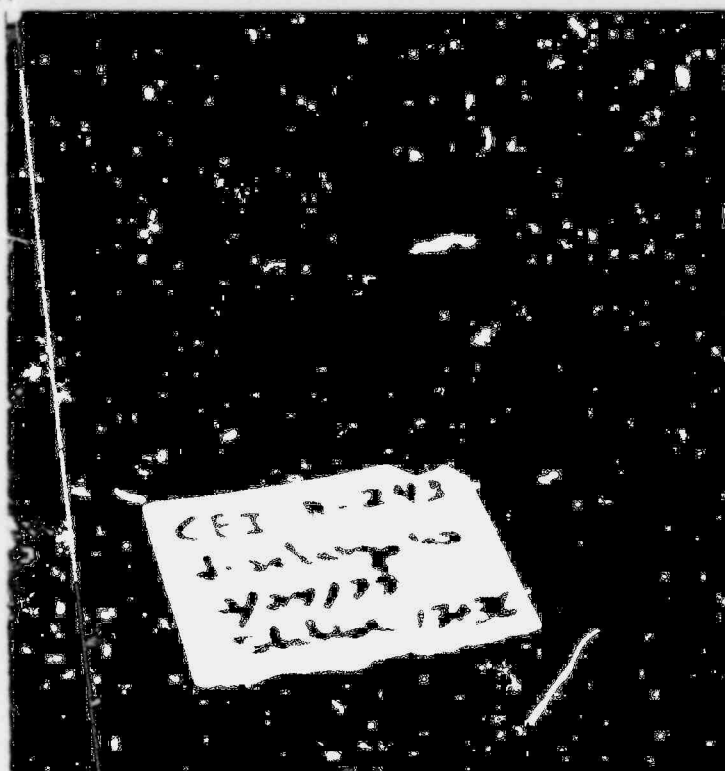
1248 154

PHOTOGRAPHS, STRUCTURAL DETAILS,
DISCHARGE TUNNEL

FIGURE 33

POOR ORIGINAL

1.

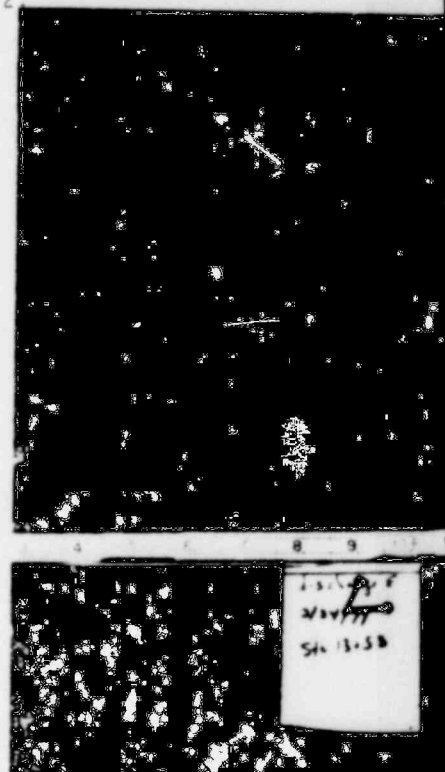


— GOUGE

13+36

STRIATIONS AND GOUGE; WEST WALL DISCHARGE TUNNEL, STATION 13+36.
STRIATIONS TREND N22°W PARALLEL TO NAIL (TWO INCHES LONG).
NOTE ANGULAR SHALE AND SILTSTONE FRAGMENTS IN GOUGE.

2.

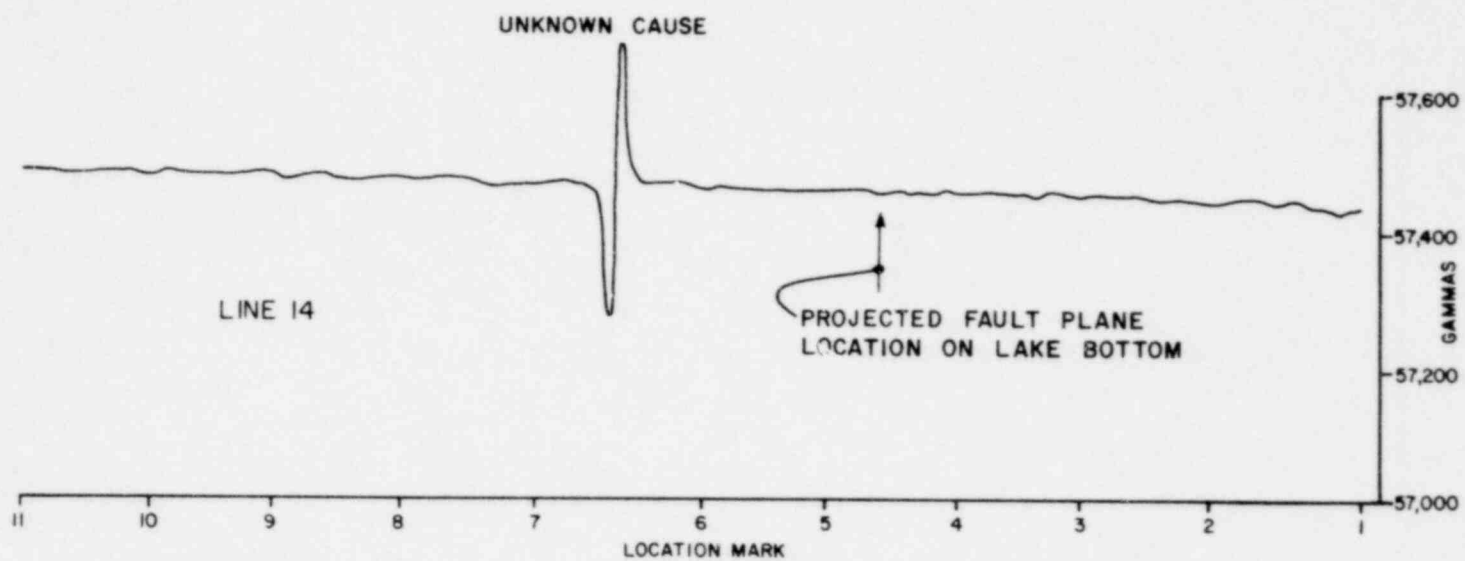


13+53

DRAG FOLD; STATION 13+53, EAST WALL

1238 155

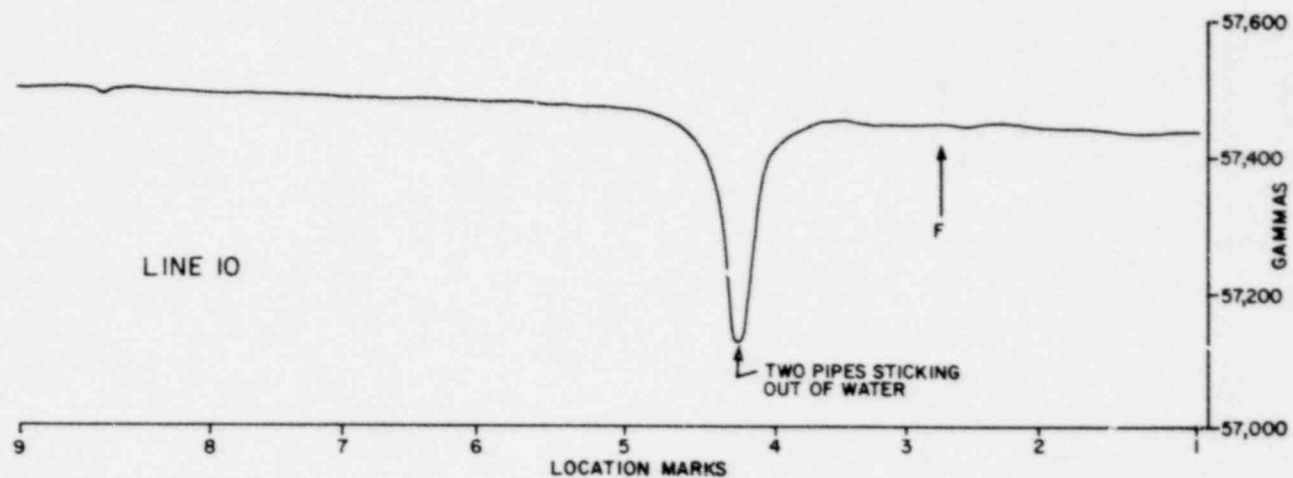
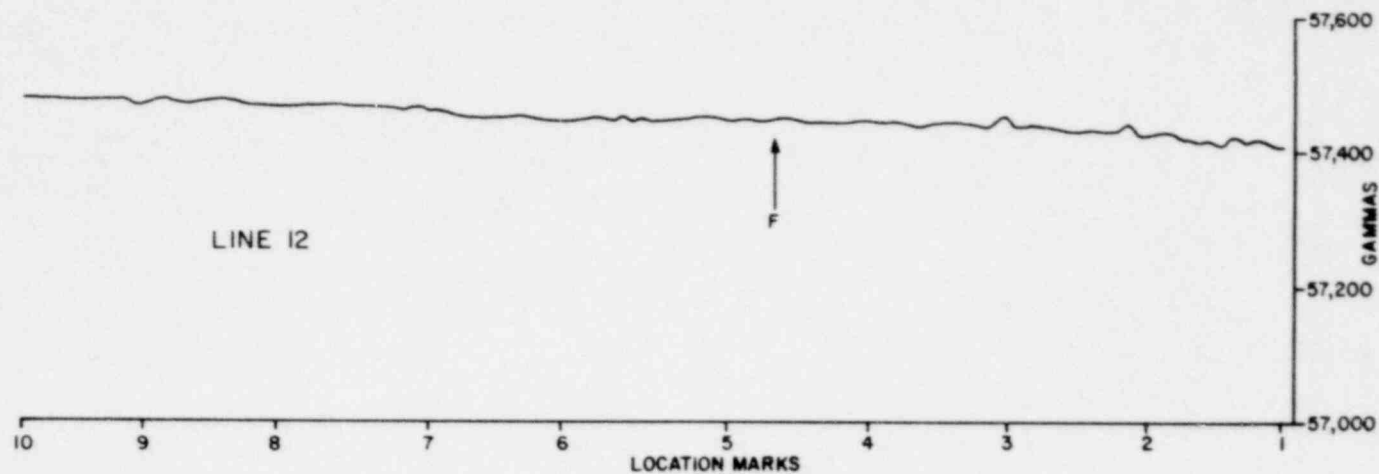
NOTE: MARK SEPARATION APPROXIMATELY 1000'



OFFSHORE FOR SHIPBORNE
MAGNETIC PROFILE 14

FIGURE 34

NOTE: MARK SEPARATION APPROXIMATELY 1000'

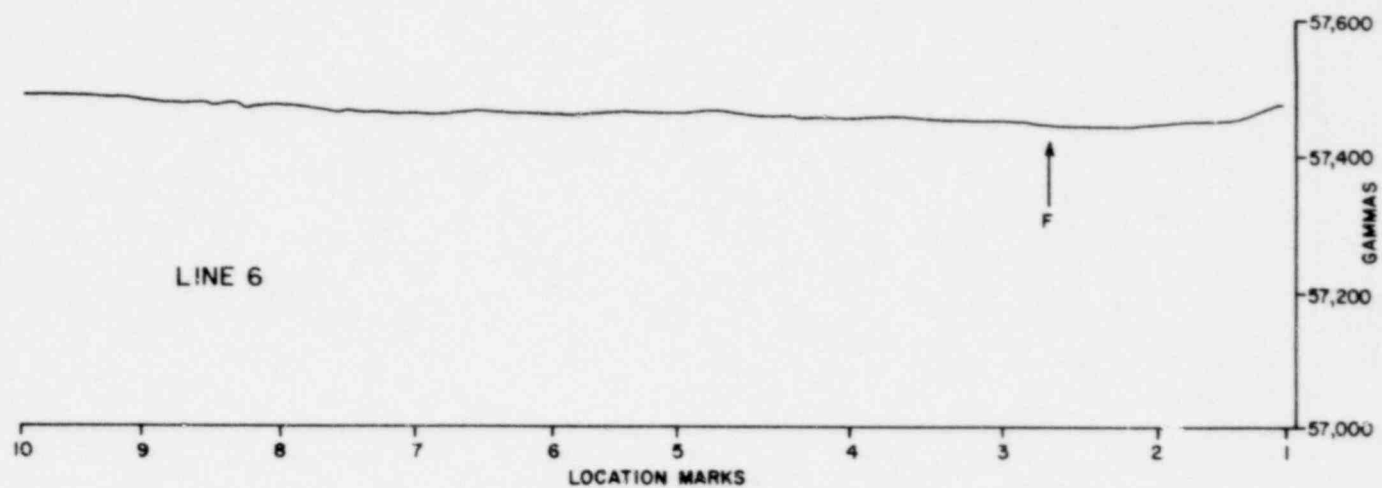
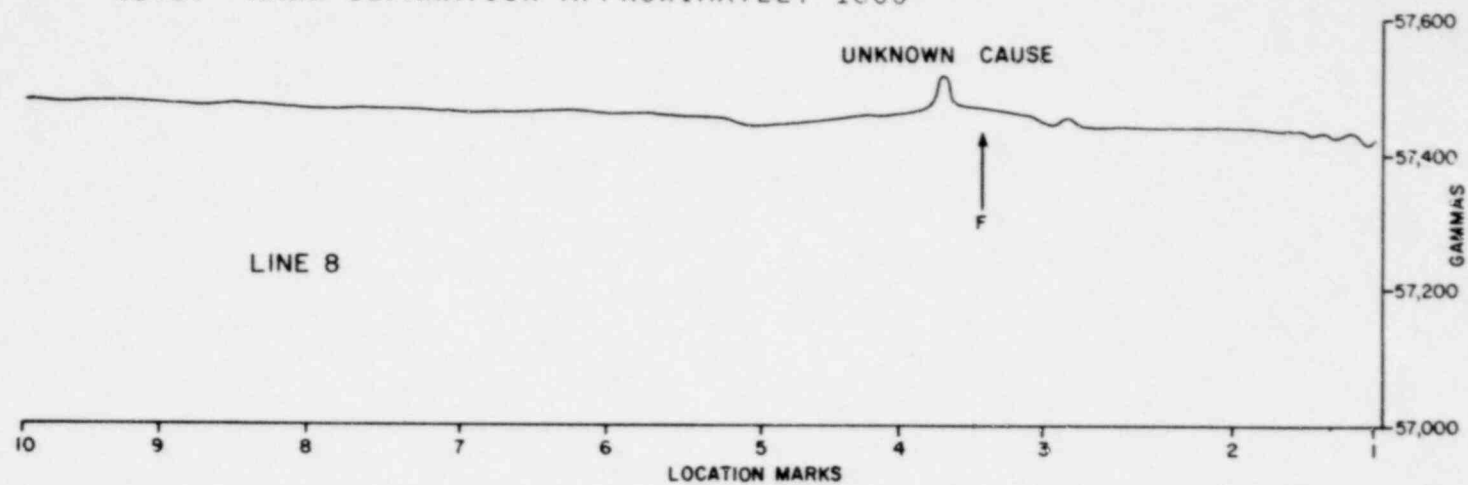


EXPLANATION

↑ PROJECTED FAULT LOCATION ON
LAKE BOTTOM.

OFFSHORE FOR SHIPBORNE
MAGNETIC PROFILES 10 AND 12
FIGURE 35

NOTE: MARK SEPARATION APPROXIMATELY 1000'



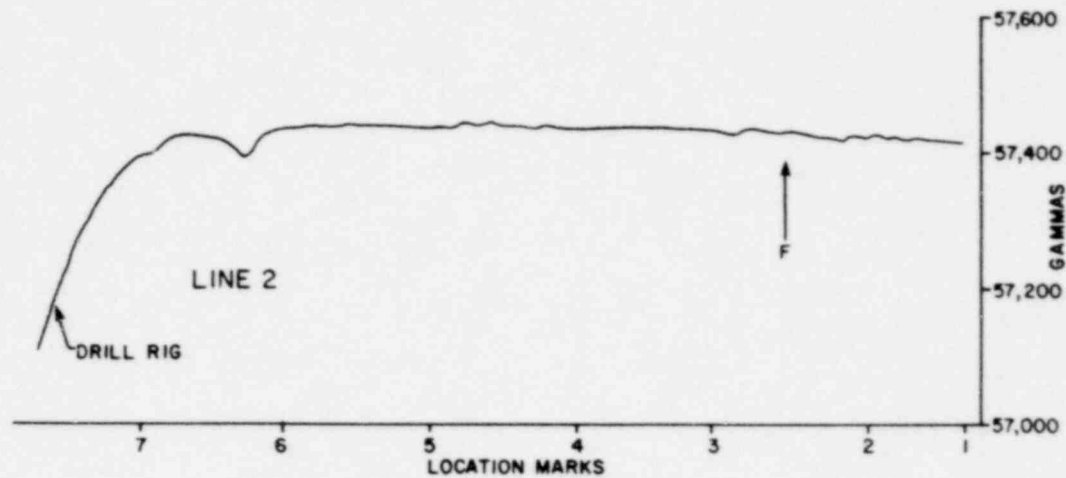
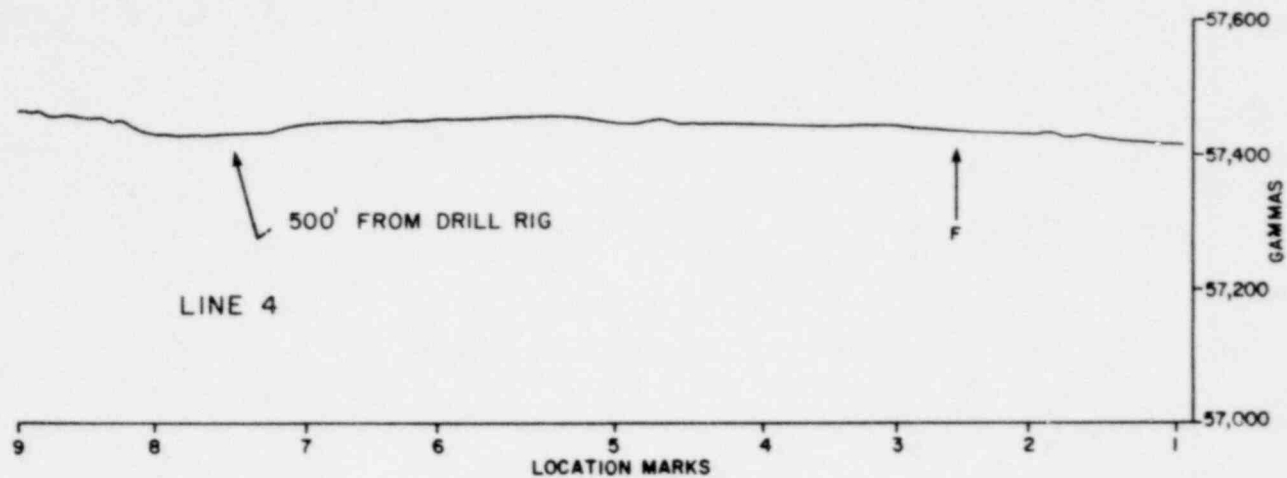
EXPLANATION

↑ PROJECTED FAULT LOCATION ON
LAKE BOTTOM.

124158

OFFSHORE FOR SHIPBORNE
MAGNETIC PROFILES 6 AND 8

NOTE: MARK SEPARATION APPROXIMATELY 1000'



EXPLANATION

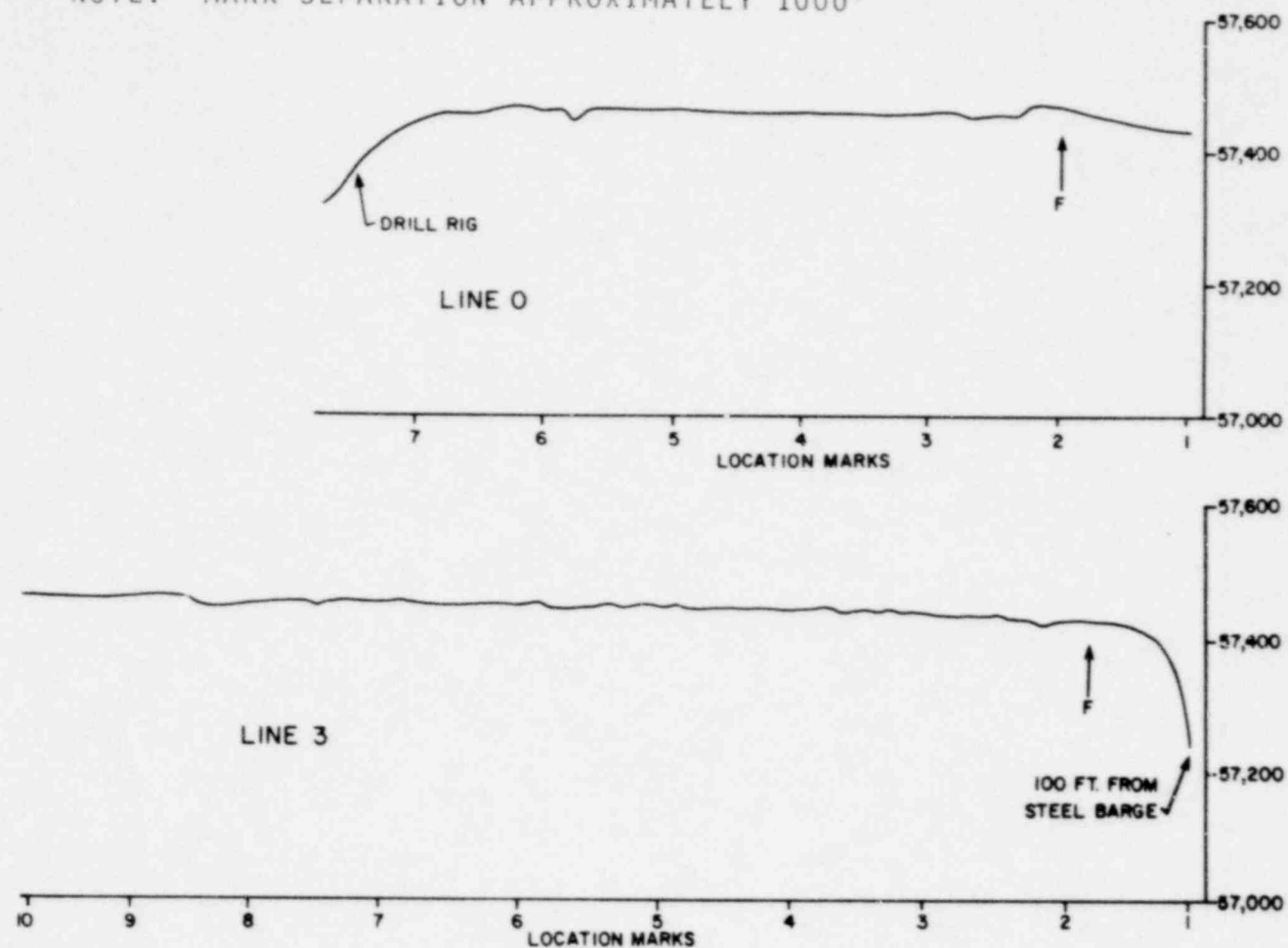
↑ PROJECTED FAULT LOCATION ON
LAKE BOTTOM.

1248 159

OFFSHORE FOR SHIPBORNE
MAGNETIC PROFILES 2 AND 4

FIGURE 37

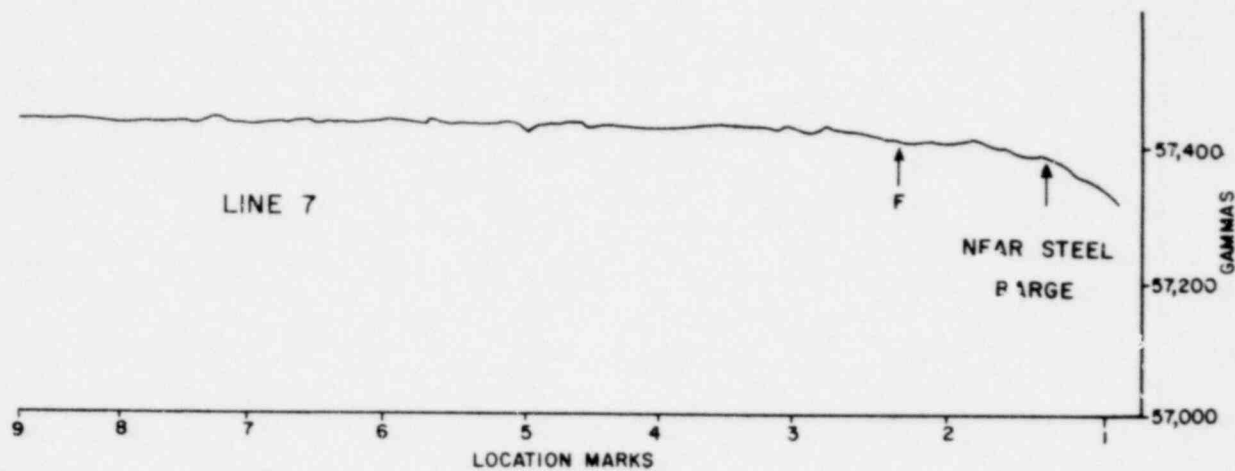
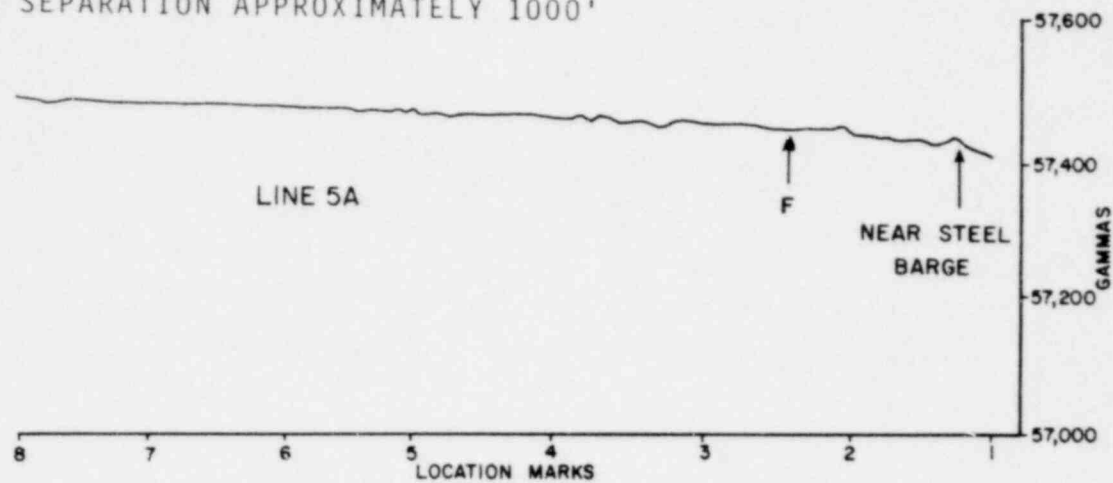
NOTE: MARK SEPARATION APPROXIMATELY 1000'



EXPLANATION

↑ PROJECTED FAULT LOCATION ON
LAKE BOTTOM.

NOTE: MARK SEPARATION APPROXIMATELY 1000'



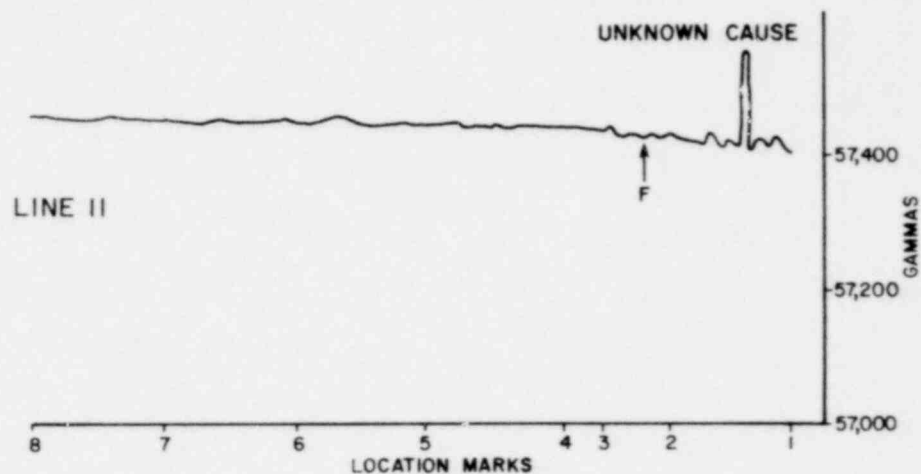
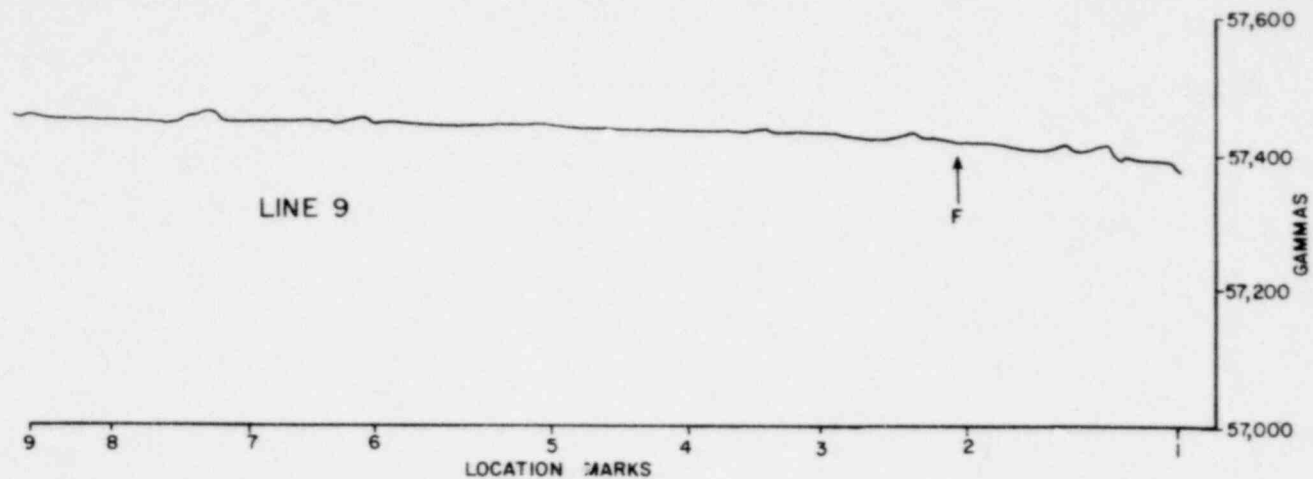
EXPLANATION

↑ PROJECTED FAULT LOCATION ON LAKE BOTTOM.

1241 161

OFFSHORE FOR SHIPBORNE
MAGNETIC PROFILES 5A AND 17

NOTE: MARK SEPARATION APPROXIMATELY 1000'



EXPLANATION

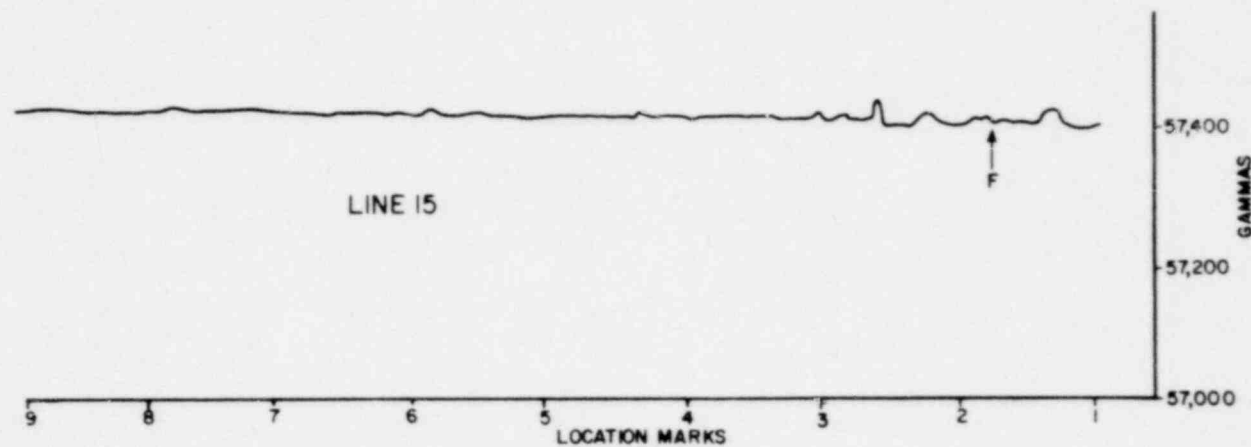
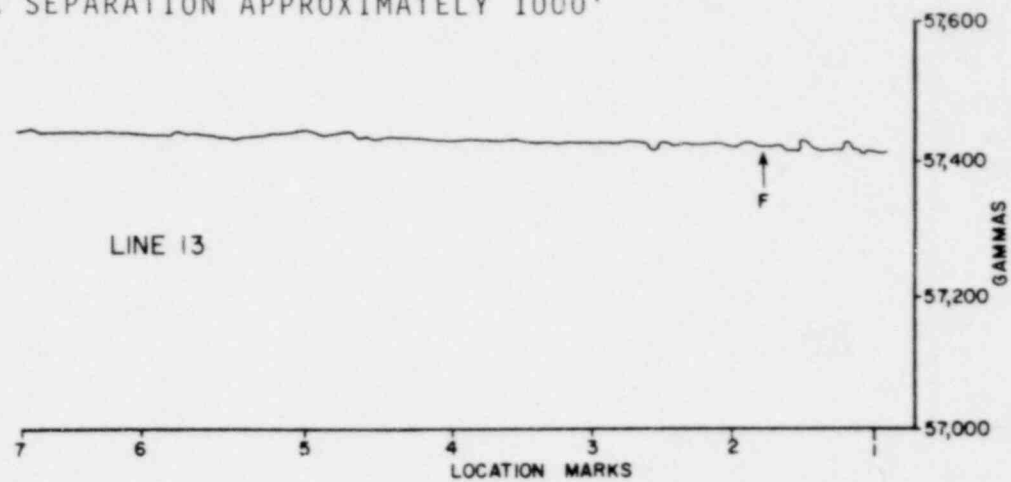
↑ PROJECTED FAULT LOCATION ON LAKE BOTTOM.

12/11/162

OFFSHORE FOR SHIPBORNE
MAGNETIC PROFILES 9 AND 11

FIGURE 40

NOTE: MARK SEPARATION APPROXIMATELY 1000'



EXPLANATION

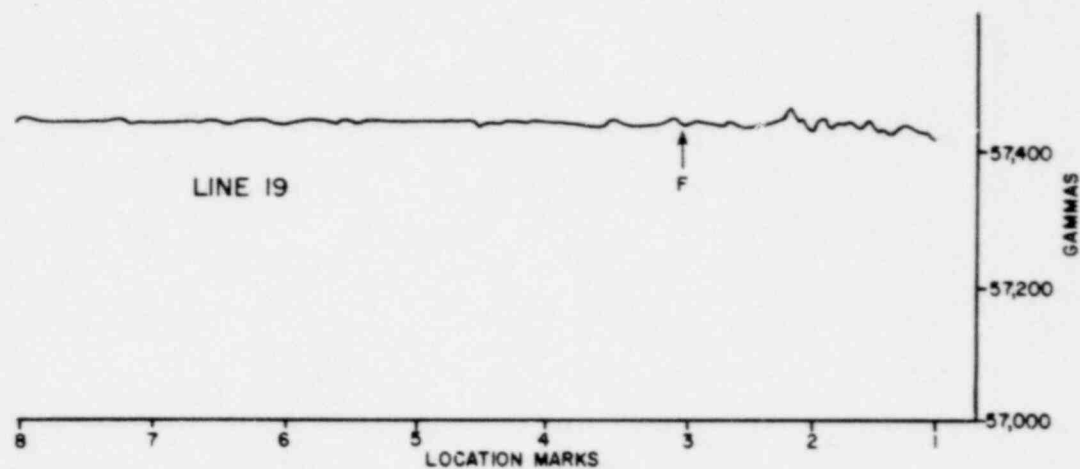
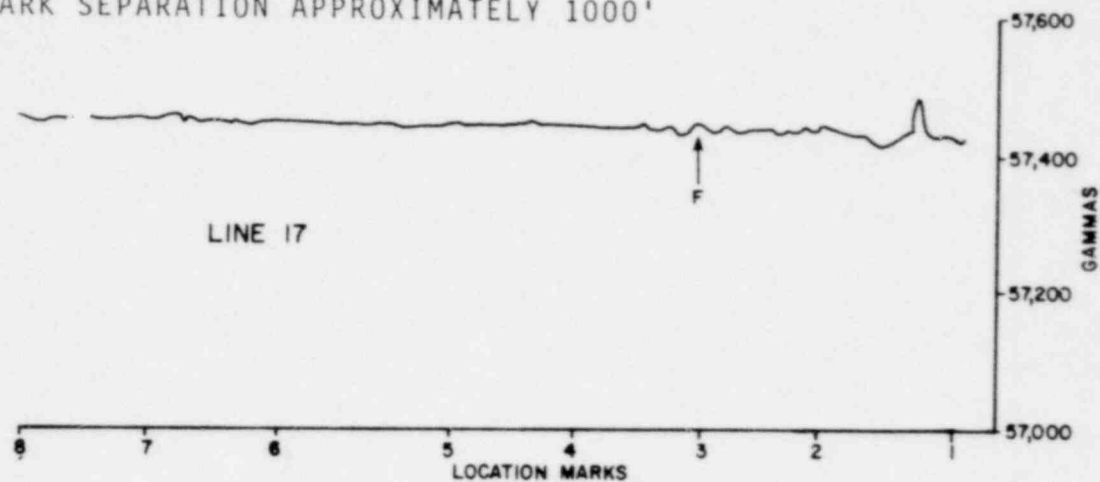
↑ PROJECTED FAULT LOCATION ON LAKE BOTTOM.

1241 163

OFFSHORE FOR SHIPBORNE
MAGNETIC PROFILES 13 AND 15

FIGURE 41

NOTE: MARK SEPARATION APPROXIMATELY 1000'

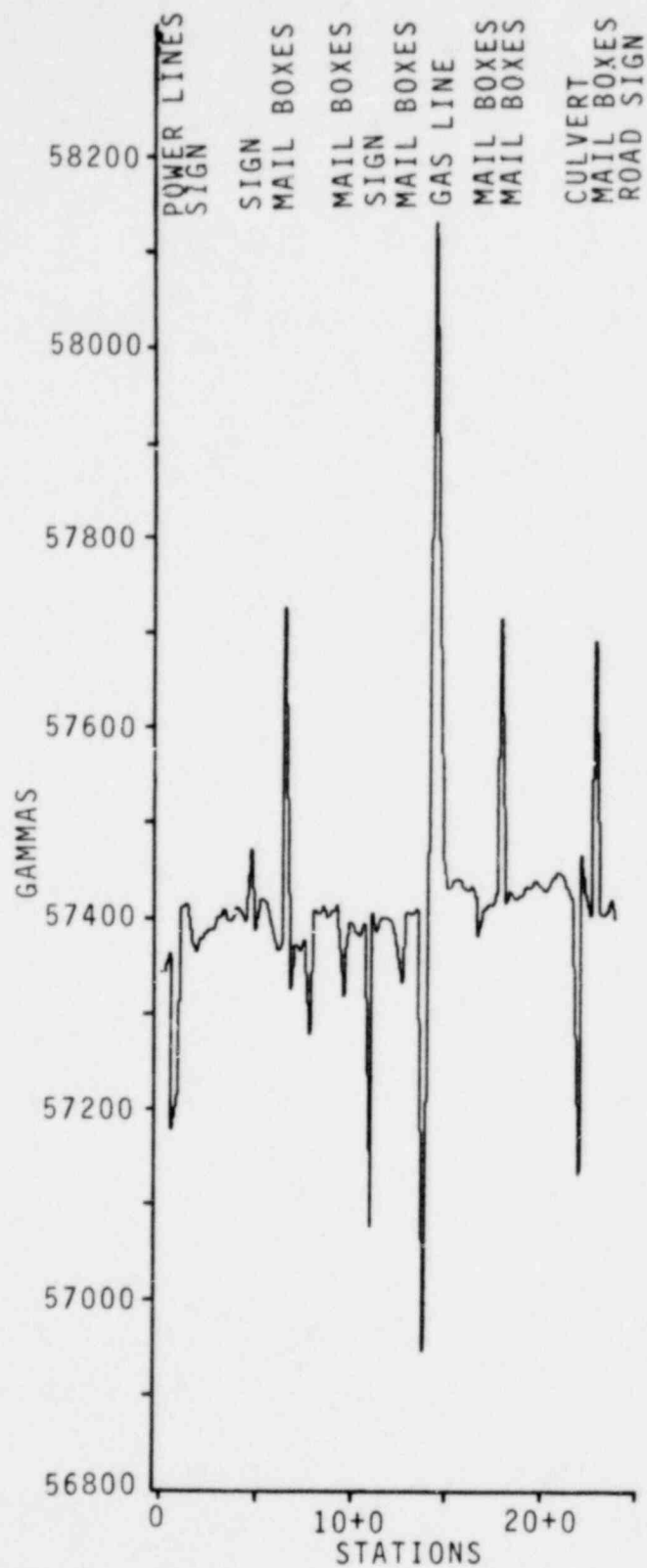


EXPLANATION

↑ PROJECTED FAULT LOCATION ON
LAKE BOTTOM.

1241 164

OFFSHORE FOR SHIPBORNE
MAGNETIC PROFILES 17 AND 19

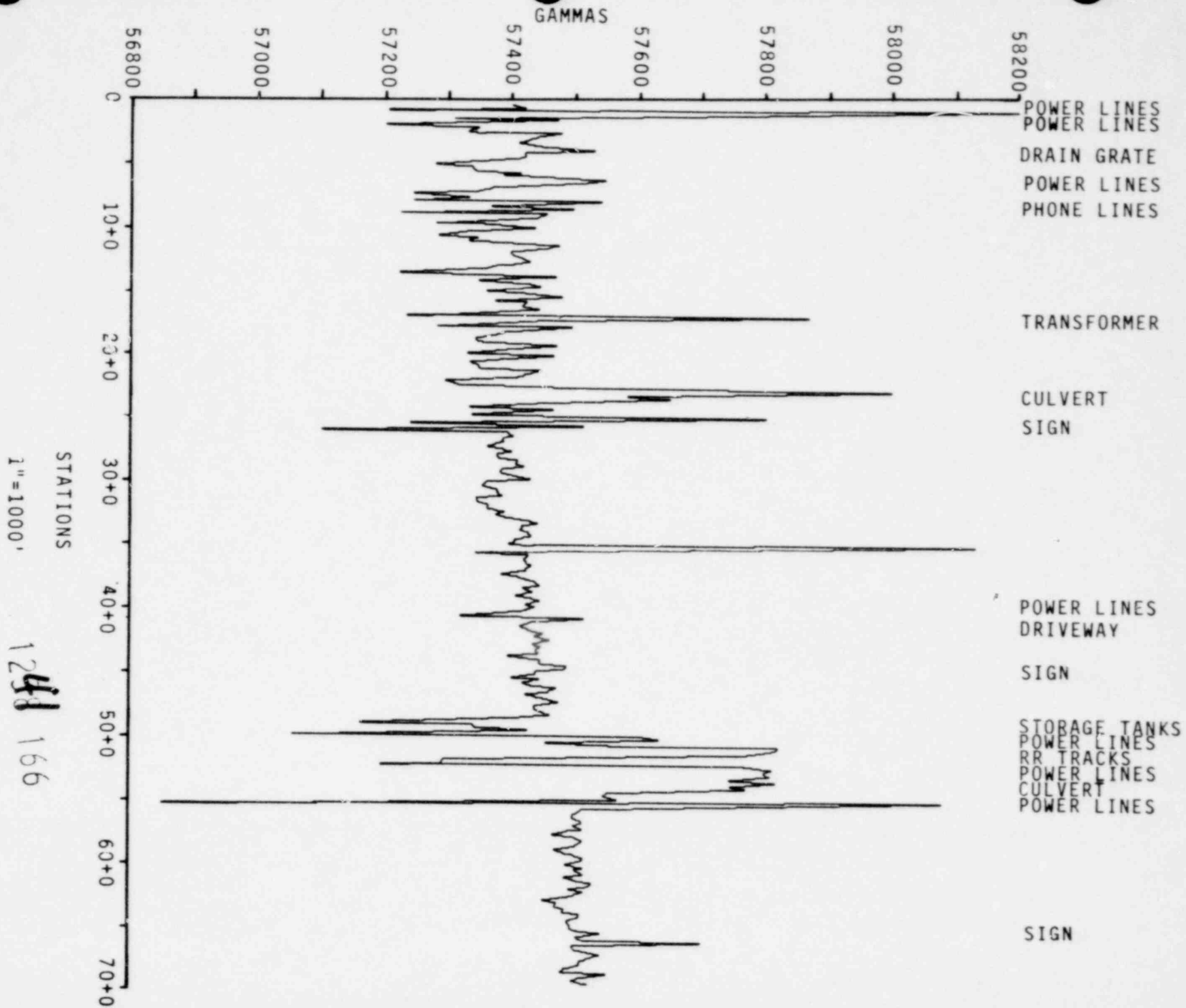


1241 165

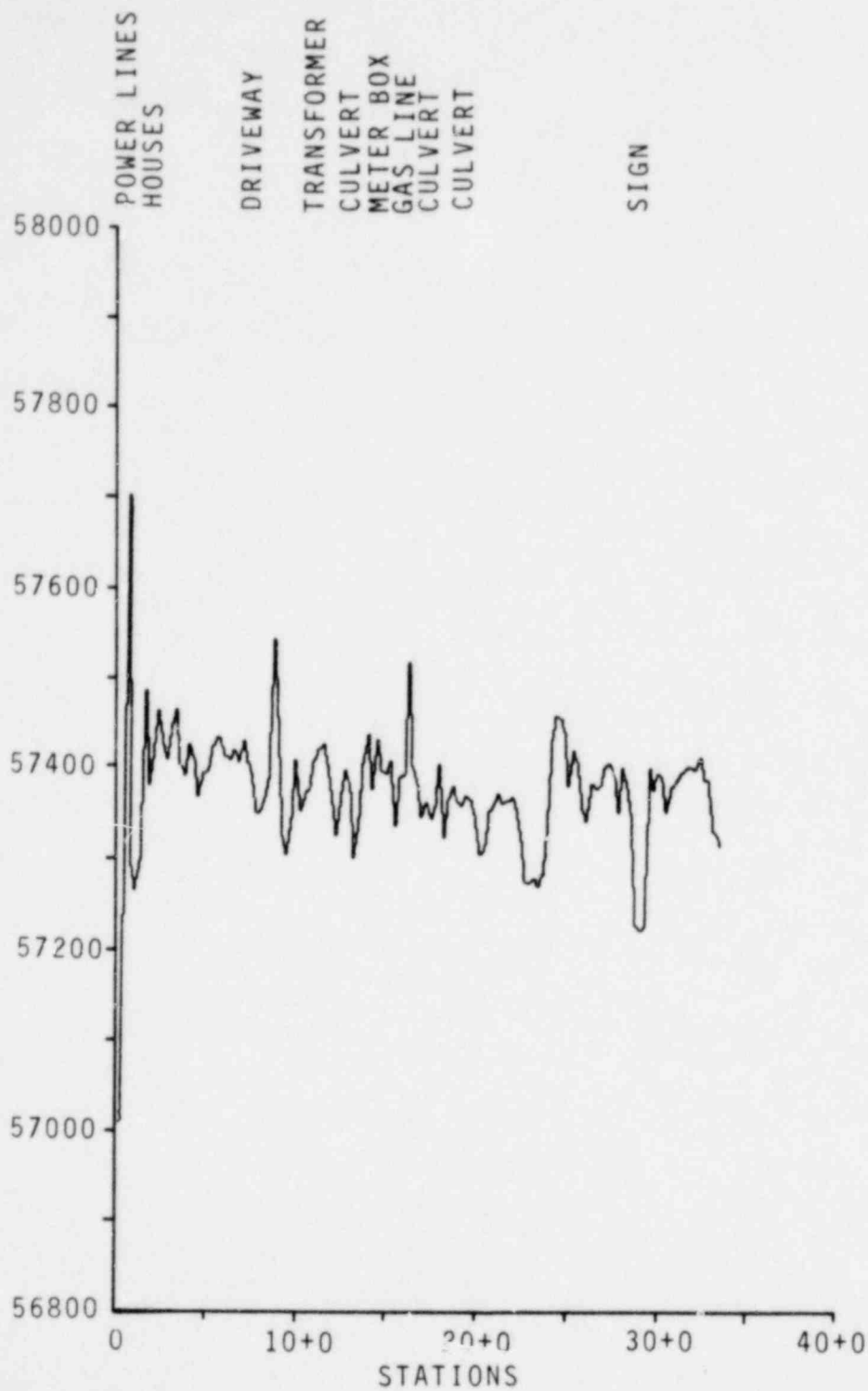
1"=1000'

ONSHORE FOR LAND MAGNETIC PROFILE 1S-A

FIGURE 43



ONSHORE FOR LAND MAGNETIC PROFILE IS

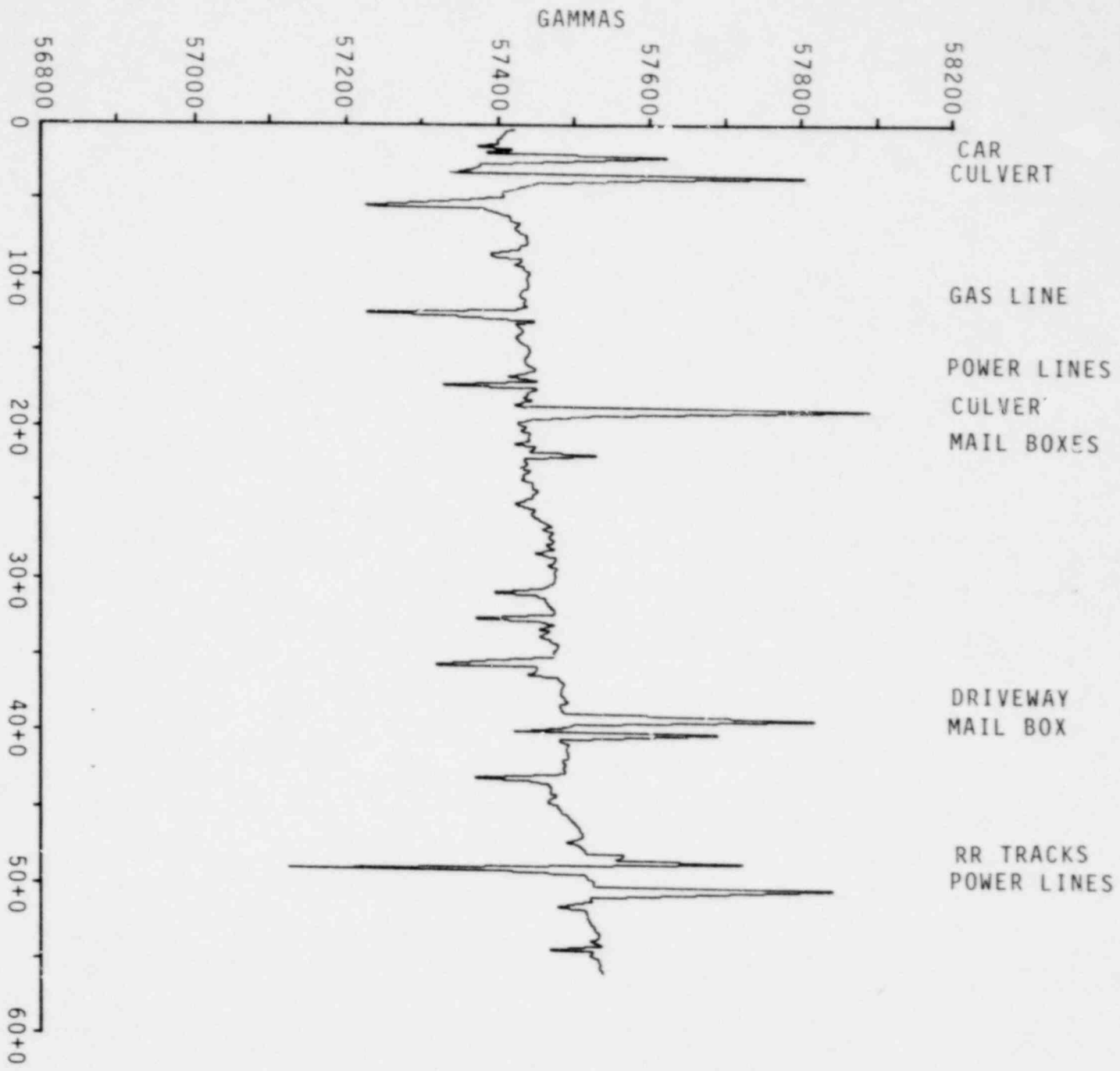


1"=1000'

1241 167

ONSHORE FOR LAND MAGNETIC PROFILE 1E

FIGURE 45

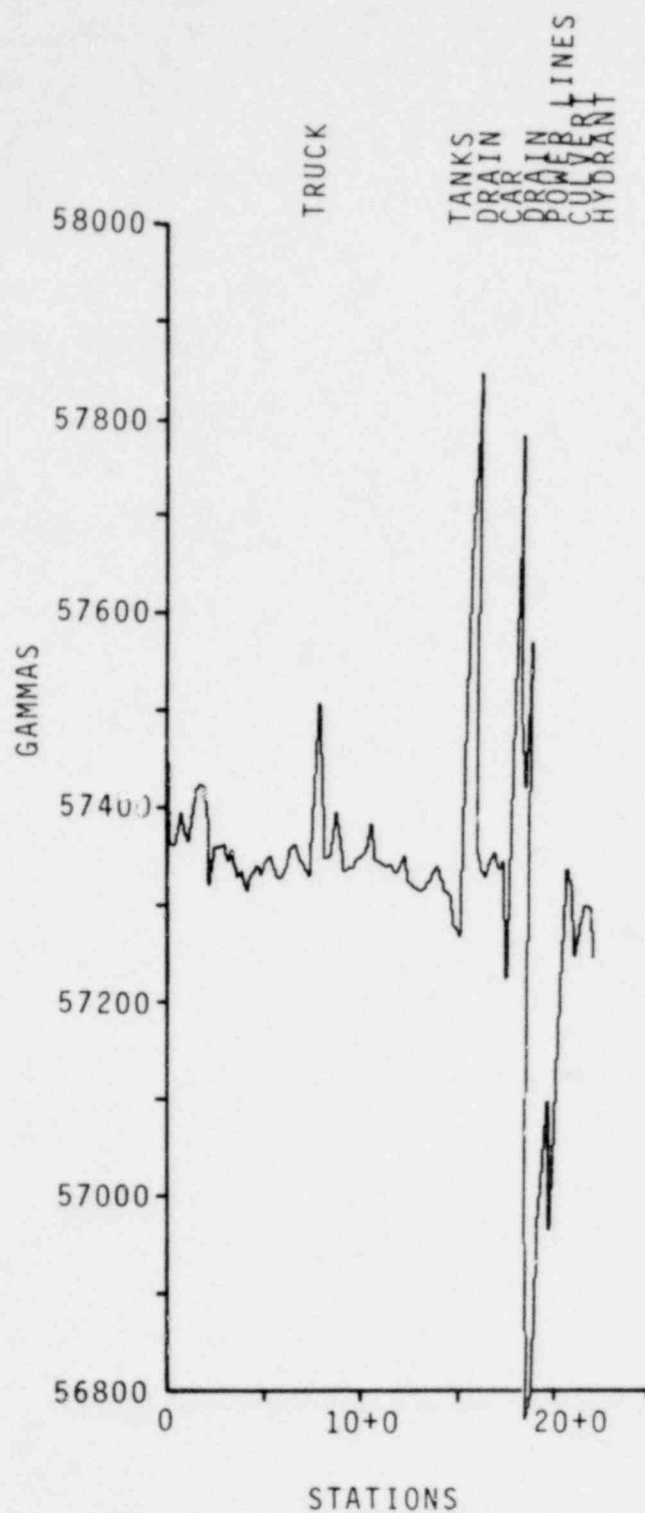


1" = 100'

1241 168

ONSHORE FOR LAND MAGNETIC PROFILE 2S

FIGURE 46

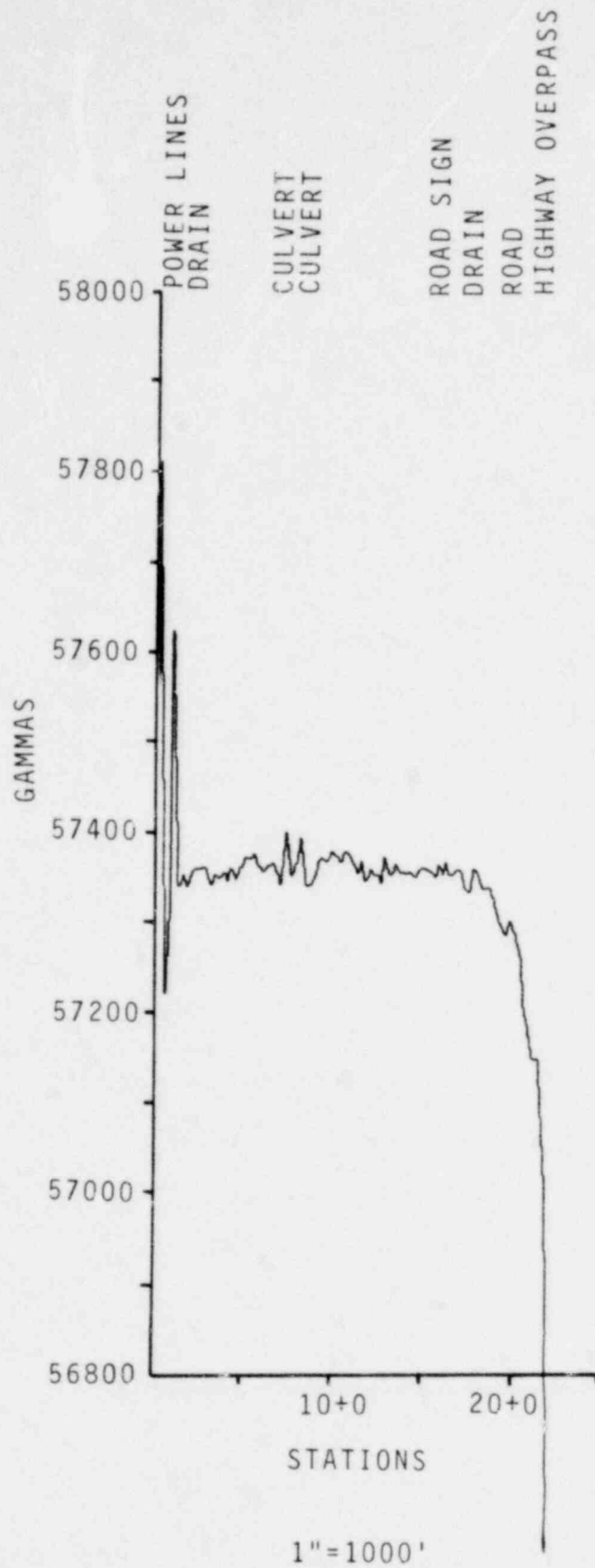


1"=1000'

1291 169

ONSHORE FOR LAND MAGNETIC PROFILE 3S

FIGURE 47

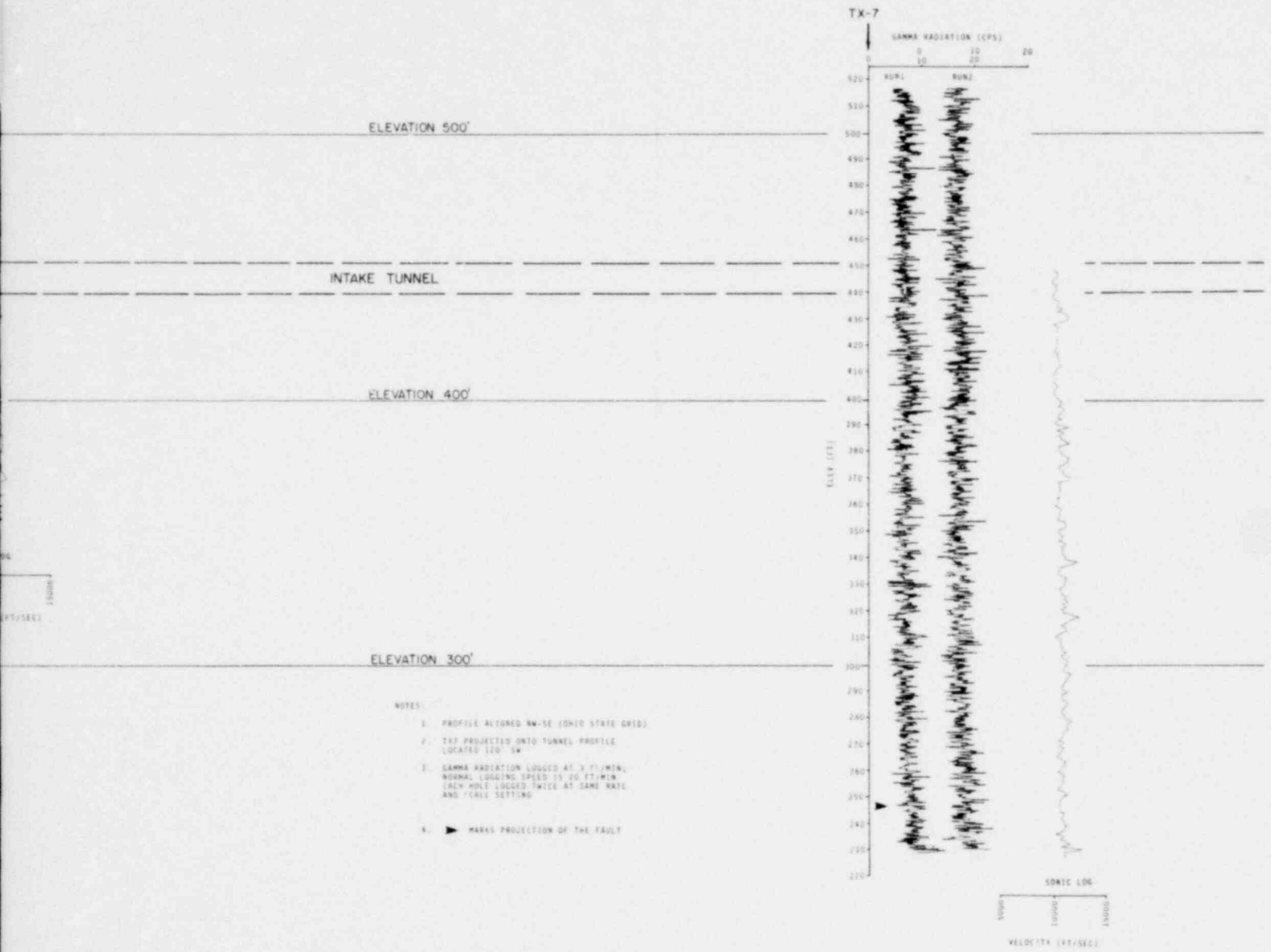


1248 170

ONSHORE FOR LAND MAGNETIC PROFILES 3S-A

FIGURE 48

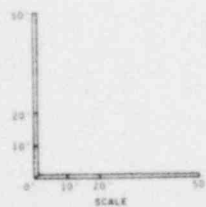
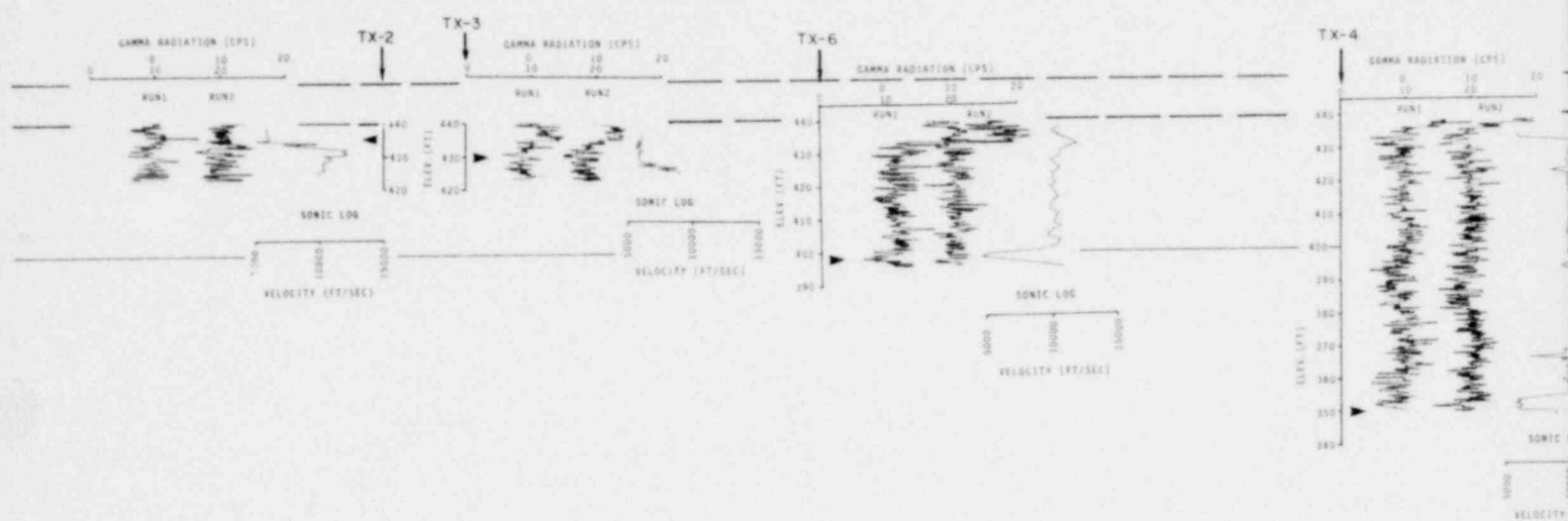
POOR ORIGINAL



1241 171

BOREHOLE LOGS - GAMMA/SONIC,
TX BORINGS 2,3,4,5,6,7

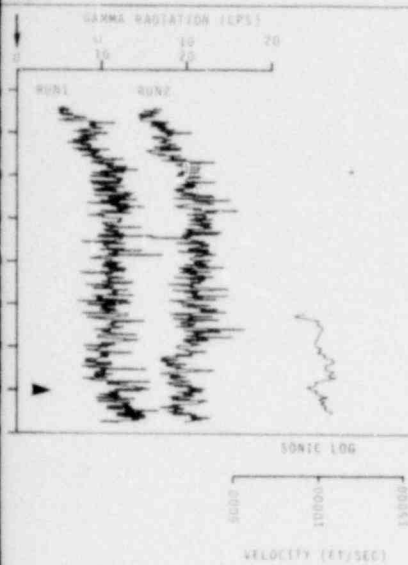
POOR ORIGINAL



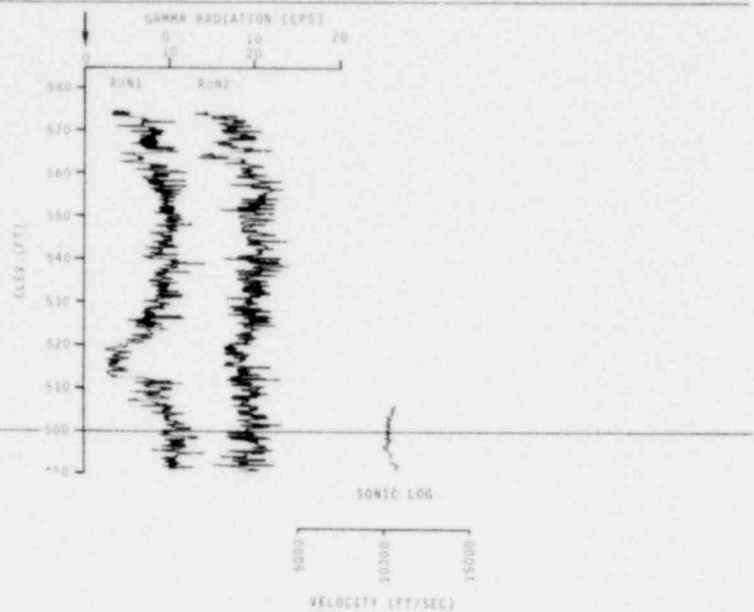
1238 172

POOR ORIGINAL

X-8



TX-9



NOTES:

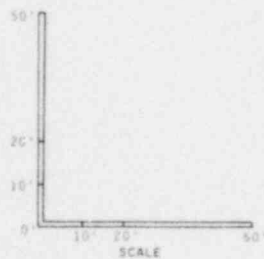
1. PROFILE ALIGNED APPROXIMATELY SW-NE (OHIO STATE GRID)
2. GAMMA RADIATION LOGGED AT 3 FT/MIN; NORMAL LOGGING SPEED IS 20 FT/MIN. EACH HOLE LOGGED TWICE AT SAME RATE AND SCALE SETTING
3. ► MARKS PROJECTION OF THE FAULT

1248 173

BOREHOLE LOGS - GAMMA/SONIC,
TX BORINGS 8,9,10

FIGURE 50

POOR ORIGINAL



1238 174

1241 175

APPENDIX A
A STUDY OF THE MICROCRACKS ASSOCIATED WITH FAULTING
AT THE PERRY NUCLEAR POWER PLANT SITE

by Dr. Gene Simmons

April 1979

1248 176

A STUDY OF THE MICROCRACKS ASSOCIATED WITH FAULTING

AT THE PERRY NUCLEAR POWER PLANT SITE

1.0 INTRODUCTION

A small fault was discovered during the excavation of the intake tunnel for the emergency cooling water at the Perry nuclear site. Samples of the fault gouge and adjacent shale were collected in July 1978 by Dr. Gene Simmons and Weston personnel. Those samples were examined briefly with the scanning electron microscope (SEM) using techniques for the study of microcracks that have been recently developed by Dr. Simmons and colleagues. A report on the preliminary findings of that investigation was submitted to the Nuclear Regulatory Commission on November 1, 1978.

During the excavation of the tunnel for the discharge of emergency cooling water at the Perry nuclear site, a fault was intersected at approximately the location of the projection along strike of the fault present in the intake tunnel. In addition, a small fracture zone was recognized approximately 200 feet south of the fault. Samples were obtained in October 1978, January 1979, and March 1979 by Dr. Simmons and Weston personnel.

2.0 SUMMARY AND CONCLUSIONS

Specimens of the gouge and the adjacent country rock were prepared in a form suitable for the examination of microcracks and elemental compositions of individual minerals in the SEM. Two types of cracks were observed. The first type, due to the desiccation of the sample, appears to be unavoidable, but is readily recognizable on the basis of objective criteria developed previous to the present studies. The second type of crack appears to be related to the last movement on the fault and always contains new mineral growths that extend completely across the crack.

Approximately 350 cracks of the type produced by faulting were examined in six samples. Every crack examined contained approximately one percent new mineral growth.

On the basis of previous observations of several thousand microcracks in a wide variety of rock types, healed microcracks appear to be ubiquitous in rocks. Evidently, the microcracks begin to heal immediately on forming. The degree of healing can be a measure of the amount of time that has been available for the microcrack to heal. The exact mathematical description of the function that relates degree of filling to elapsed time since the crack was formed is unknown, but is likely S-shaped and asymptotic to the zero and 100 percent values. Two data points have been obtained - one point at 1 million years (possibly 2 to 5 million years) from sandstone at the Satsop site, the other at 18.5 million years from shocked rock at the Ries Crater, Germany.

The rate of healing of microcracks is very likely a function of temperature, pressure, mineralogy, and the composition and flow rate of pore fluids. Fortunately, the conditions at the Perry site and at the Satsop site are quite similar, and the degree of filling of the cracks at each site are comparable. Therefore, the data obtained previously for the Satsop site are a suitable basis on which to estimate the age of the microfractures in the gouge zone at Perry.

On the basis of a thorough examination of the microcracks in six representative samples of the gouge and country rock from the fault, or faults, in the intake tunnel and the discharge tunnel and from the fracture zone in the discharge tunnel, it is our conclusion that the time of last movement of each of these faults is conservatively estimated at approximately 1 million years and may be as old as 2 to 5 million years.

3.0 BASIS OF METHOD

Displacement of rock along fault surfaces, in the laboratory as well as in the field, appears to produce microfractures. For examples of representative laboratory studies, reference is made to the work of Griggs and Handin (1960), Conrad and Friedman (1976), Jackson and Dunn (1974). The examination of natural specimens from faults by Engelder (1974), Swain and Jackson (1976), and Stearns (1972) demonstrates the applicability of the laboratory results to rock in situ.

Work done during the past decade on microcracks (Simmons and Richter, 1976; Richter and Simmons, 1977; Simmons et al., 1975; Batzle and Simmons, 1976, 1977; and Wang and Simmons, 1978) has shown clearly that healed and partially healed microcracks in rocks are ubiquitous. Apparently, the microcracks began to heal immediately upon forming.

The degree of healing, as measured by the volume percentage of new mineral growth that fills the microcracks, is an indication of the amount of time that has elapsed since the formation of the microcrack. The general form of the function that relates degree of filling to elapsed time, shown on Figure 1, can be deduced in the following manner. The initial rate is low because of the difficulty of nucleation. The final rate is low because the transfer of fluid from residual cavities (i.e., fluid inclusions) must occur by diffusion of water through solid phases. Thus, the functional form of the curve is asymptotic at both zero percent filling and at one hundred percent filling. During the intermediate phase, the rate is controlled by both the availability and fluid phase. Because the rate of many processes is described adequately by an Arrhenius-type relation (Kingery et al., 1976, Chapter 9), we suggest that the rate of sealing of microcracks is described satisfactorily by

$$\ln(c/c_0) = K(t - t_0)$$

$$K = A \exp(-Q/RT) \quad (1)$$

where c/c_0 is the volume fraction of filling

K is the reaction rate

1241 178

t is time

A and Q are experimentally determined constants

R is the gas constant

T is absolute temperature.

At the present time, we have two data points that appear to lie on the curve during the intermediate period. They are shown on Figure 2 and are connected with a straight line. Both data points lie in the intermediate region because in each case the new mineral growth had extended completely across the open microcracks, but an open channelway still exists throughout the microcracks. Additional confidence is derived from the observation that apparent degree of filling of a 0.2 mybp crack shown by Swain and Jackson (1976, Figure 4) is very small.

The data for the low end of the curve were obtained on a sample of sandstone from the Satsop site (Weston Geophysical Research, Inc., 1978). The cracks were produced during the compaction phase of the sandstone. The stratigraphic unit (the Montesano formation) that was deposited above the sandstone was dated on the basis of fossils (Rau, 1967) as at least 1 million years and possibly 2 to 5 million years. Because the creation of compaction fractures must have ceased when the unit began uplift, the youngest age for any compaction-induced fracture must be the age of the youngest overlying formation, approximately 1 million years. The minerals that were examined in the study of the sample from Satsop included quartz, feldspar, and pyroxene. These minerals, as a group, contain Al, Si, Fe, K, Ca, Na, and Ti. The maximum depth of burial was approximately 3,000 to 3,500 feet. The thermal gradient at the site was probably 15° to 25° C/km. Therefore, the maximum temperature to which the sample had been exposed was probably 20° to 30°C, an estimate that is consistent with, but somewhat higher than, the temperature estimated from the metamorphic grade of the organic material contained in the sandstone.

The data for the high end of the curve are based on data reported by Padovani *et al.* (1979) for a series of core samples from the 3,500-foot hole drilled in the Ries Crater, Germany. The Ries Crater and the microcracks in the rocks from the Ries Crater were produced when a meteorite hit the earth 18.5 million years ago. The age was obtained with radiometric techniques. Figure 3 shows a typical crack in the mineral amphibole partially filled with grains of the mineral chlorite. Cracks were observed in quartz and feldspar also. The degree of filling was highest in quartz, intermediate in feldspar, and lowest in amphibole. The host grains for the partially sealed microcracks contained the elements Al, Si, Fe, Mg, K, Ca, Na. The thermal gradient at the present time in the Ries Crater is 15° to 25°C/km. Thus, the maximum temperature at present to which the samples *in situ* have been exposed is approximately 20° to 25°C.

The time required for nucleation in the cracks in the rocks from the Ries Crater may have been very short. The meteorite impact produced a

high temperature associated with the shock waves that lasted a few microseconds to perhaps a few milliseconds. In addition, a significant volume of the rocks in the vicinity of the impact and sampled by the drill would have been exposed to a temperature that might have been as high as 100° to 200°C for intervals of time of the order of hundreds or perhaps thousands of years. The higher temperatures would likely have shortened greatly the amount of time required for the nucleation of the new mineral growths in individual microcracks. We have included the uncertainty of this effect in the error bar that is shown for this data point on Figure 3 by indicating that the degree of filling might appear to be too large for a sample whose age is 18.5 million years, but which used 5 million years for the nucleation time.

4.0 PROCEDURES

4.1 SAMPLE COLLECTION

The samples for this study were collected with methods designed to minimize, or perhaps prevent completely, the creation of open microfractures in the material which had very low strength. Two different techniques were used. In the first technique, we used a jackhammer to line-drill a large block of rock. The concept for this procedure was that the jackhammer would damage material relatively near the drilled holes which could then be removed and discarded. The procedure, illustrated on Figure 4, appears to have been successful for several samples but was not successful for all samples. Some samples simply disintegrated within a few days after collection.

In the second procedure, we used a small masonry saw to remove completely, the specimen from the rock mass in situ. A series of photographs on Figure 5 illustrates the second technique. This procedure, though rather time consuming for large samples, was highly successful.

4.2 SPECIMEN PREPARATION

The rock and gouge while in situ contain free water in the cracks and pores. The examination of the material in the SEM requires that the free water be removed. Therefore, a major problem in the preparation of the specimens for the examination with the SEM is the removal of the free water without creating open microfractures or destroying any delicate structures that existed in the microcracks while the material was still in situ. This problem appears to have been overcome completely in our specimen preparation (as judged on the basis that no open microfracture without new mineral growth was observed and that many microcracks with delicate structures of new mineral growth were observed). We used Buehler isomet diamond saws operated at very low speeds, drying furnaces kept at temperatures below 45°C, and epoxies that cure at room temperature.

4.3 SEM PROCEDURES

The procedures for the examination of specimens in the scanning electron microscope are described for general specimens by Hearle et al. (1972) and for rock samples by Simmons and Richter (1976), Richter and Simmons

(1977), and Batzle and Simmons (1976, 1977). We include here only a brief description of the procedures. The SEM consists of an electron source, focussing and rastoring coils, a moveable stage for supporting the specimen, various detectors, and associated electronics for amplifying, displaying, and recording the detected signal. The major systems of an SEM are shown on Figure 6 schematically. A typical image is shown on Figure 7. Unlike a photographic image, the SEM image is generated sequentially in time by the detection and recording of the intensity of the image at individual points. The intensity is controlled by the composition of the material at the point, the topographic roughness of the surface of the material at the point, and (to a lesser extent) by the crystallographic orientation of the material at the point.

The detector in the scanning electron microscope may be sensitive to secondary electrons, backscattered electrons, or x-rays. Most of the work done on the Perry samples was done with secondary electrons or with the x-ray detector. With the x-ray detector, one also uses associated electronics to measure the energy spectrum of the x-rays that are emitted by the specimen. Because each element produces x-rays with characteristic energies, the spectrum of energies can be used to obtain semiquantitative estimates of the elemental composition of the specimen. Typical spectra are shown on Figure 8.

5.0 SAMPLE LOCATIONS

Representative samples of the various faults were collected from the intake tunnel and the discharge tunnel. Samples of the fracture zone in the discharge tunnel were also collected. The sample locations are shown on the intake and discharge tunnel wall maps (Figures 17, 18, and 19) of the main body of Weston Geophysical's text.

6.0 RESULTS

6.1 DESCRIPTION OF GOUGE

The gouge zone contains lithic fragments set in a matrix of clay-sized (1 to 4 microns) grains. A typical image is shown on Figure 9. The texture and minerals of the lithic fragments are identical to those of the adjacent country rock. The gouge matrix contains the same clay mineral (illite) as the country rock and also contains gypsum and feldspar. Crystals of NaCl, observed in the gouge zone but not in the country rock, are believed to have crystallized from saline water after collection.

6.2 MICROCRACKS

Two types of cracks were observed in the samples from the Perry site. One set, termed desiccation cracks, was produced during the drying of the specimen and appears to be unavoidable. The other set, termed fault-cracks, was not produced during the drying of the sample and appears to have been produced by the last movement of the fault.

Desiccation cracks had been observed previously in other samples. On Figure 10, an example of desiccation cracks in clay-like minerals (chlorite in this case) are shown for a specimen described by Wang and Simmons (1978). These cracks developed during examination of the specimen.

with the SEM. They were actually observed during the time that they formed; hence, their origin is known unequivocally. Desiccation cracks have distinct characteristics: (1) they are relatively wide in comparison with their lengths; (2) their walls are very irregular, but opposite walls would fit exactly when restored to the contacting position; (3) they are relatively short (typically a few microns); and (4) they are often curved. The criteria for the recognition of desiccation cracks are unambiguous. An example of desiccation cracks in the Perry samples is shown on Figure 11 and may be compared with the cracks on Figure 10.

Examples of the other type of cracks observed in the Perry samples are shown on Figures 12, 13, and 14. These cracks are typical representatives of approximately 350 cracks that were examined in the Perry samples. Every individual crack in the set of 350 cracks contained new mineral growths that spanned completely the fracture. No open microcrack without new mineral growth was observed - except, of course, the desiccation cracks.

6.3 AGE OF MICROCRACKS

The age of the microcracks can be obtained from the degree of filling, approximately one percent. The value is the same as the value for the compaction fractures in the sandstone at the Satsop site. If the factors that control rate of fracture filling are approximately the same for the two sites (as they are), then the ages of the cracks are the same. The factors are compared in Table 1, and we conclude that they are quite similar for the two sites. Therefore, the age of the microcracks associated with faulting at the Perry site is approximately 1 million years.

Although our estimates of the several parameters that affect the rate of healing of microfractures are similar for the Perry and Satsop sites, they are not identical. Therefore, some possible error exists in the estimate of the date of last fracturing for the Perry site. In our opinion, and based on our experience of working on microcracks in a variety of rocks during the past 10 years, the date might be as young as 0.8 million years and as old as 5 million years.

6.4 SLICKENSIDES

Samples that contained slickensides were examined with the SEM. A typical image is shown on Figure 15. The grooves appear to have been created by grains of pyrite that were embedded in a surface that moved with respect to another adjacent surface. The mineral pyrite was identified on the basis of elemental composition (FeS) and crystal morphology (octahedra).

7.0 REFERENCES

- Batzle, M. L. and G. Simmons, 1976, "Microfractures in Rocks from Two Geothermal Areas," Earth Planete. Sci. Lett., 30, 71-93.
- Batzle, M. L. and G. Simmons, 1977, "Geothermal Systems: Rocks, Fluids, Fractures," in The Earth's Crust: Its Nature and Physical Properties, Geophys. Monogr. Ser., Vol. 20, edited by J. G. Heacock, AGU, Washington, DC, 233-242.

- Conrad, R. E. and M. Friedman, 1976, "Microscopic Feather Fractures in the Faulting Process," Tectonophysics, 33, 187-198.
- Engelder, J. T., 1974, "Cataclasis and the Generation of Fault Gouge," Geol. Soc. Am. Bull., 85, 1515-1522.
- Griggs, D. and J. Handin, 1960, "Observations on Fracture and a Hypothesis of Earthquakes," in Rock Deformation (A Symposium), Geol. Soc. Am. Mem. 79, edited by D. Griggs and J. Handin, G.S.A., New York, 347-364.
- Hearle, J.W.S., J. T. Sparrow, and P. M. Cross, 1972, The Use of the Scanning Electron Microscope, Pergamon Press, New York, 278 pp.
- Jackson, R. E. and D. E. Dunn, 1974, "Experimental Sliding Friction and Cataclasis of Foliated Rocks," Int. J. Rock Mech. Min. Sci. & Geomech. Abstr., 11, 235-249.
- Kingery, W. D., H. K. Bowen, and D. R. Uhlmann, 1976, "Introduction to Ceramics," 2nd Edition, Wiley, New York.
- Padovani, E. R., M. L. Batzle, and G. Simmons, 1979, "Characteristics of Microcracks in Samples from the Drill Hole Nordlingen 1973 in the Ries Crater, Germany," Proc. Lunar Sci. Conf. 9th, in press.
- Rau, W. W., 1967, "Geology of the Wynoochee Valley Quadrangle" Wash. Div. Mines and Geol., 56, 51 p, 1 pl.
- Richter, D. and G. Simmons, 1977, "Microcracks in Crustal Igneous Rocks: Microscopy," in The Earth's Crust: Its Nature and Physical Properties, Geophys. Monogr. Ser., Vol. 20, edited by J. G. Heacock, AGU, Washington, DC, 149-180.
- Simmons, G., R. Siegfried, and D. Richter, 1975, "Characteristics of Microcracks in Lunar Samples," Proc. Lunar Sci. Conf. 6th, 3227-3254.
- Simmons, G. and D. Richter, 1976, "Microcracks in Rocks," in The Physics and Chemistry of Minerals and Rocks, edited by R.G.J. Strens, Wiley-Interscience, New York, 105-137.
- Stearns, D. W., 1972, "Structural Interpretation of the Fractures Associated with the Bonita Fault," in Guidebook of East-Central New Mexico, edited by V.C. Kelley and F. D. Trauger, New Mexico Geological Society, 161-164.
- Swain, M. V. and R. E. Jackson, 1976, "Wear-like Features on Natural Fault Surfaces," Wear, 37, 63-68.
- Wang, H. and G. Simmons, 1978, "Microcracks in Crystalline Rock from 5.3-km depth in the Michigan Basin," J. Geophys. Res., 83, 5849-5856.

1241 183

Weston Geophysical Research, Inc., 1978, "Feasibility of Dating the Faults in the Foundation of WNP 3 at the WNP 3 and 5 (Satsop) site of Washington Public Power Supply System, report prepared for EBASCO Services Incorporated and submitted to Washington Public Power Supply System, 26 pp.

1248 184

TABLE 1

COMPARISON OF PERRY AND SATSOP SITES WITH RESPECT TO FACTORS
AFFECTING RATE OF FRACTURE HEALING

Factor	Perry	Satsop
Host Minerals	Illite (based on EDX)	Quartz, Feldspar, Pyroxene
Elements in Host(s)	Al, Si, K, Fe	Na, Mg, Al, Si, K, Ca, Fe
Elements in Growth Minerals	Al, Si, K, Fe	Not measured
Maximum Temperature	288 ⁰ to 293 ⁰ K	288 ⁰ to 293 ⁰ K
Maximum Lithostatic Pressure	~300 bars	~300 bars
Width of Microcracks	1 to 5 microns	1 to 5 microns

A-9

1241 185

1241 186

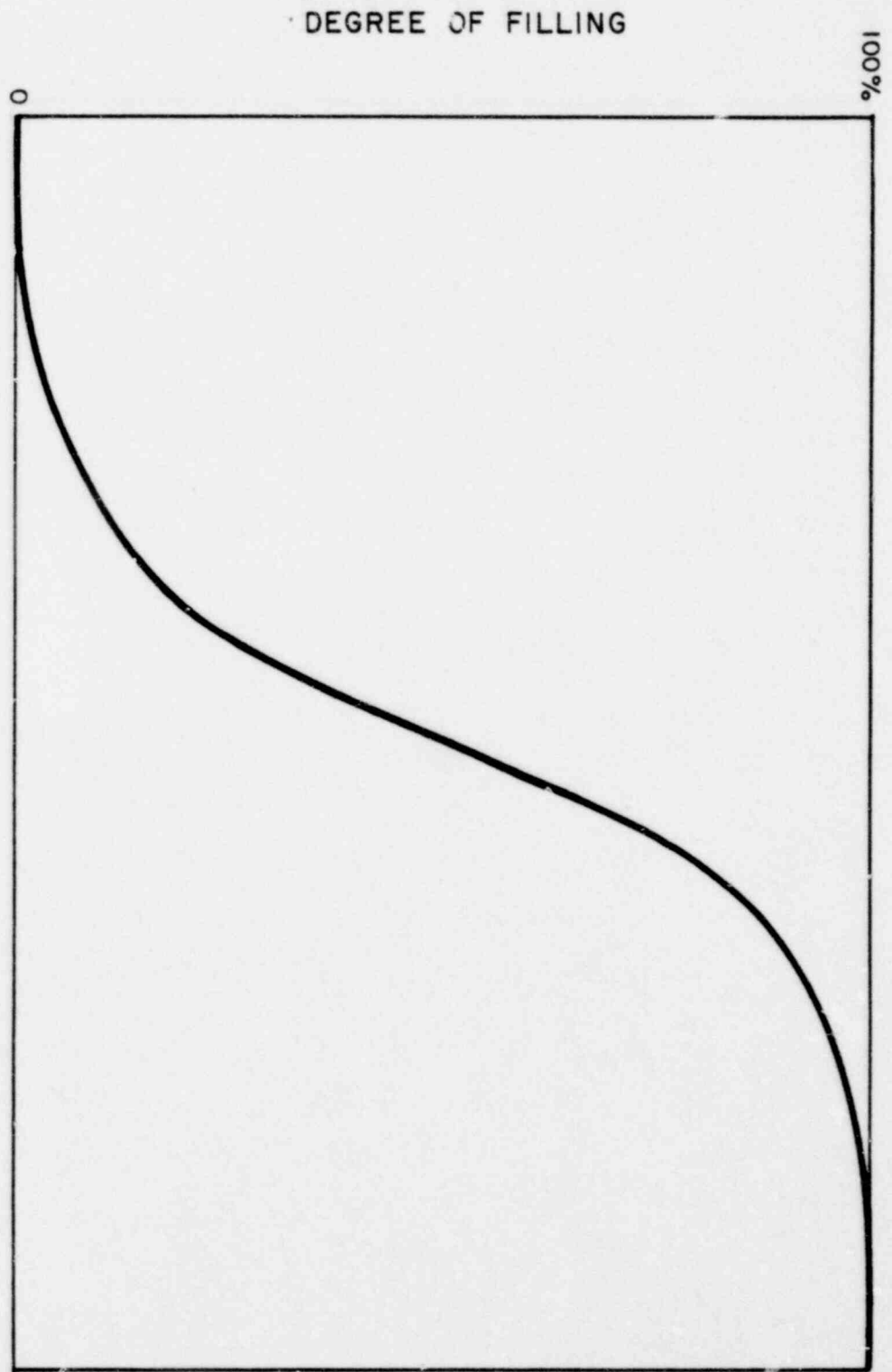


Figure 1 Healing of microcracks versus time. The curve is schematic and intended only to show general shape. The cracks are created at time t_0 and are healed completely at t_c .

1241 187

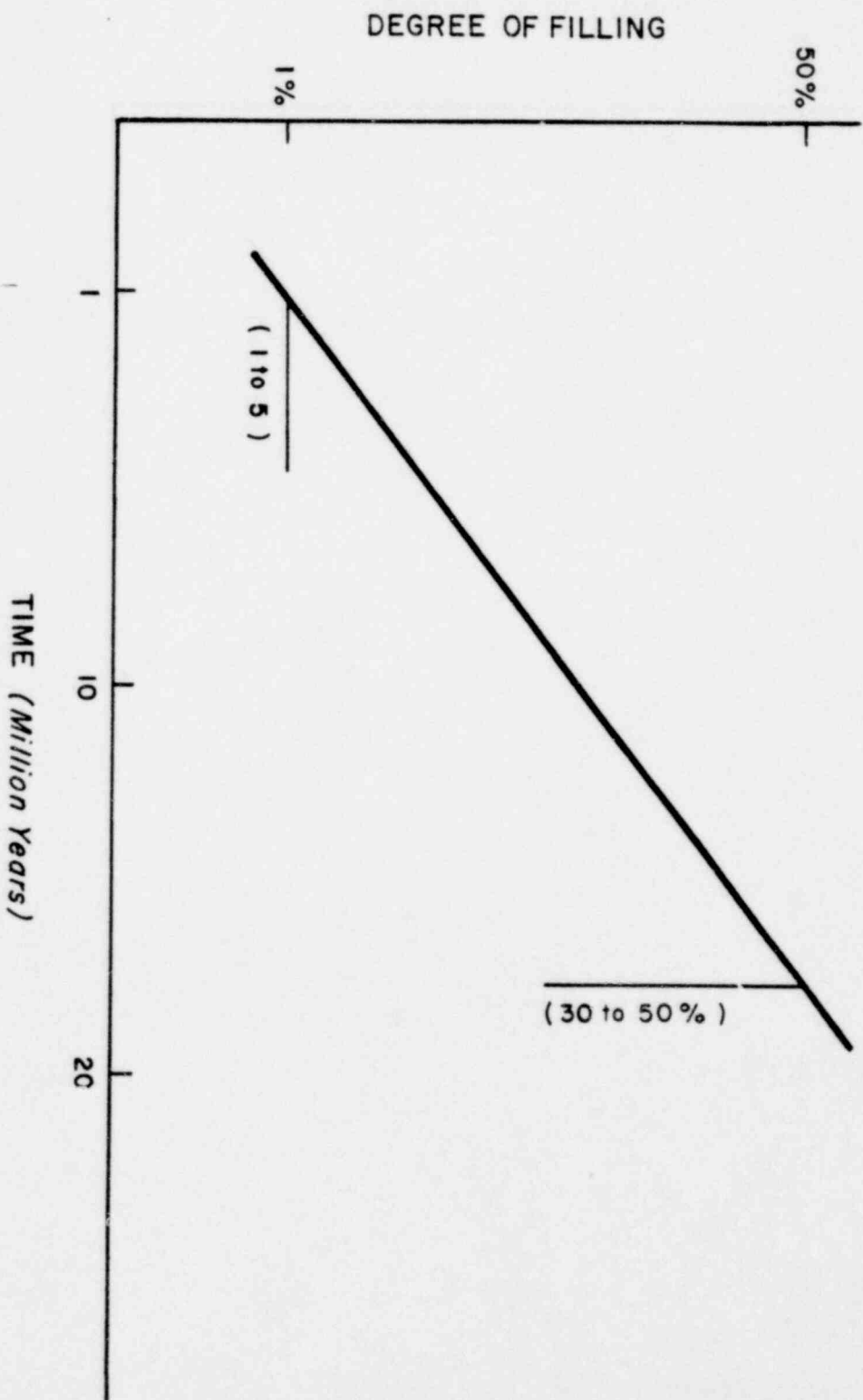


Figure 2 Current data for healing of microcracks. See text for discussion of the error bars.

POOR ORIGINAL

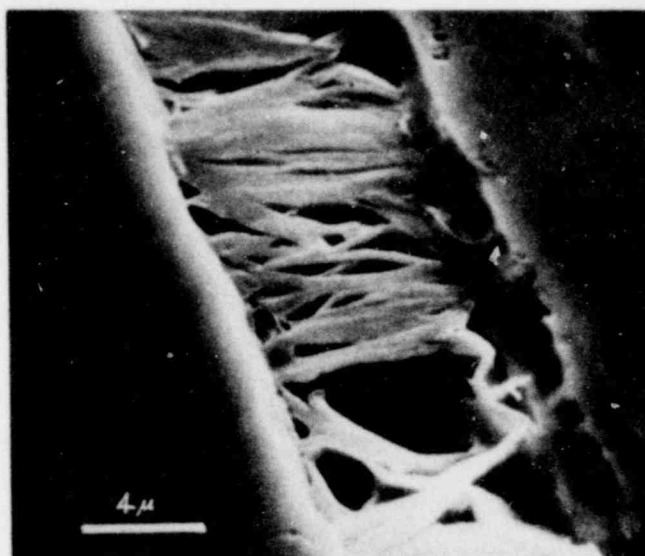


Figure 3 Partially healed microcracks from Ries Crater, Germany. SEM micrograph. Host grain is amphibole. New mineral growth is chlorite. The sample is described by Padovani *et al.* (1979).



Figure 4 Sample number 4, partially outlined with holes that have been drilled with a jackhammer, still in situ. Note the gouge zone that is contained in this sample. The webs between the individual holes were later removed. A chisel was used to split a bedding plane at the base of the sample, freeing the sample completely.

1248 188

POOR ORIGINAL



Figure 5 Sample number 25, partially sawn, still in situ. After the rear cut had been made, the sample was freed by splitting gently along a bedding plane. Note the gouge zone that extends diagonally across the sample.

THE DESIGN AND USE OF THE SCANNING ELECTRON MICROSCOPE

51

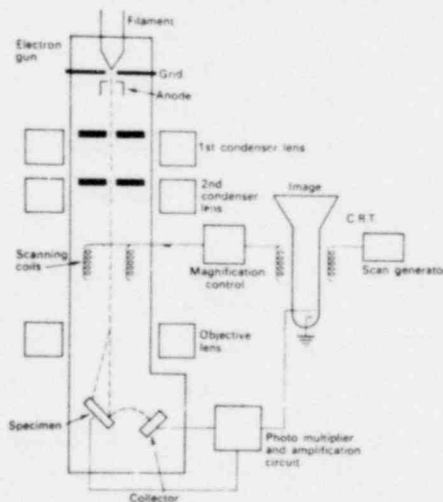


FIG. 3.2. Block diagram of a typical SEM.

1238 189

Figure 6 Block diagram of a typical scanning electron microscope. The image on the cathode ray tube is recorded photographically. An x-ray detector may be substituted for the collector.

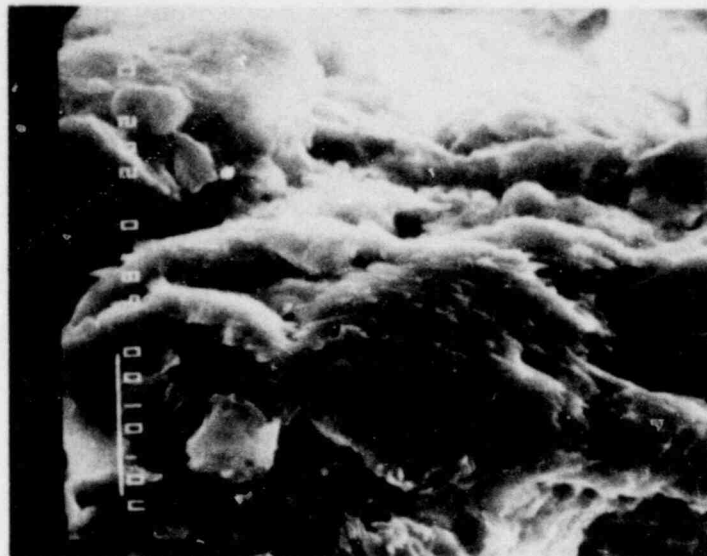


Figure 7 Typical micrograph obtained with a scanning electron microscope. PNPP sample 1. This image was made with a specimen from the gouge zone in the intake tunnel at the Perry Nuclear Site. The deformed crystals near the center of the micrograph are probably gypsum.

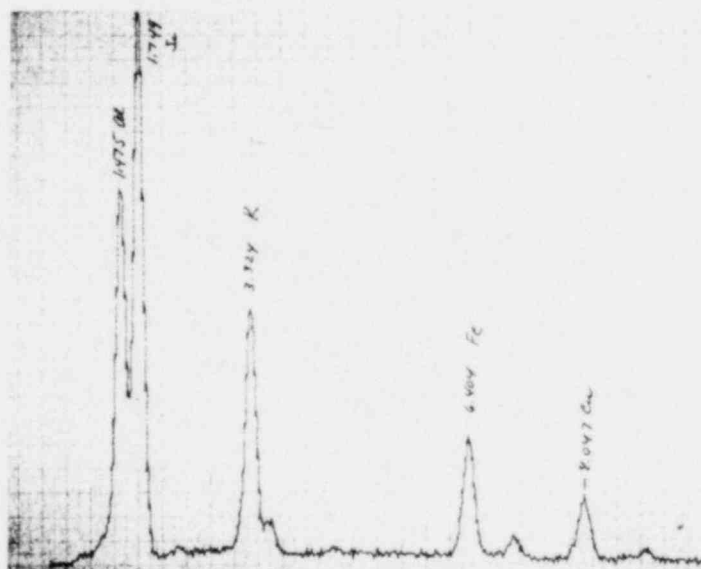
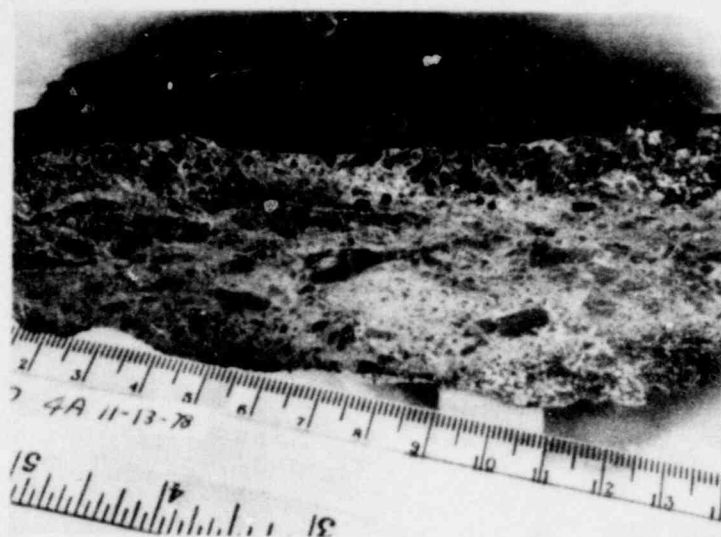


Figure 8 Typical x-ray spectrum obtained with energy dispersive systems. This spectrum was obtained from clay minerals in the gouge zone. The abscissa is energy (of x-rays) and the ordinate is counts per channel. The identification of the individual peaks is shown on the figure. The peak for copper is due to contamination within the system and not to the presence of copper in the specimen. The mineral is probably illite.

POOR ORIGINAL

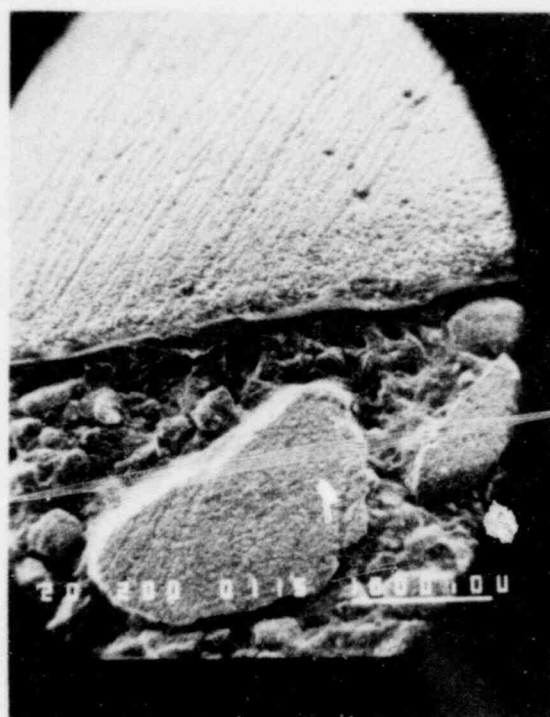
9a



COUNTRY
ROCK

GOUGE
ZONE

9b



COUNTRY
ROCK

GOUGE
ZONE

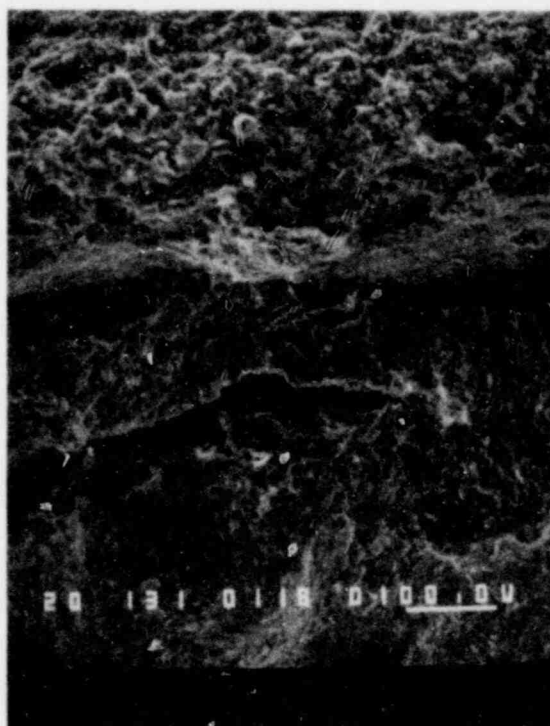
Figure 9 Figure 9a is an enlargement of an optical photograph and shows in small scale the many features that are present in the gouge and can be readily recognized on a freshly sawn surface. Note the abundant lithic fragments of shale that are set in the fine-grained matrix. Figure 9b is an SEM micrograph of the gouge (area differs from 9a).

1241 191

POOR ORIGINAL



Figure 10 Desiccation cracks observed in a sample of chlorite. These cracks were observed in the SEM during formation.



1241 192

Figure 11 Crack produced during collection or specimen preparation.

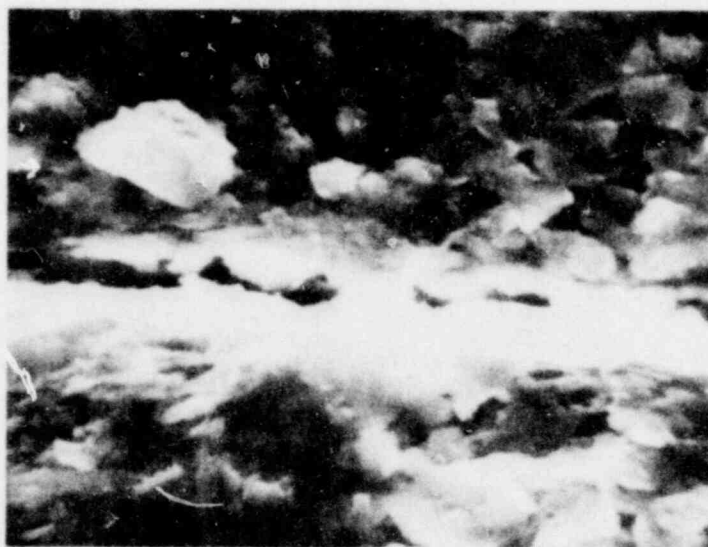
POOR ORIGINAL

12a



12b

12b



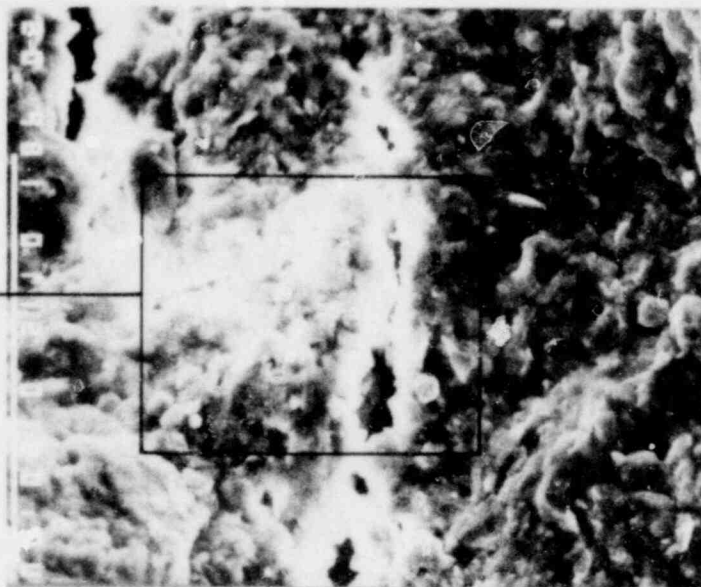
1241 193

Figure 12 A typical microcrack in the Perry samples. This crack occurs along the boundary between the gouge zone and the adjacent country rock. The enlargement (12b) shows that new mineral growth has occurred with the crack, an indication that the crack was not disturbed during the collection and specimen preparation.

POOR ORIGINAL

13a

13b



13b

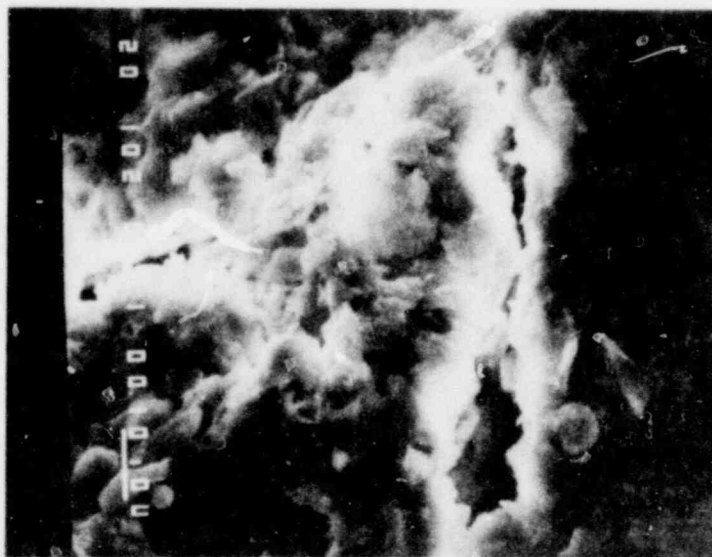
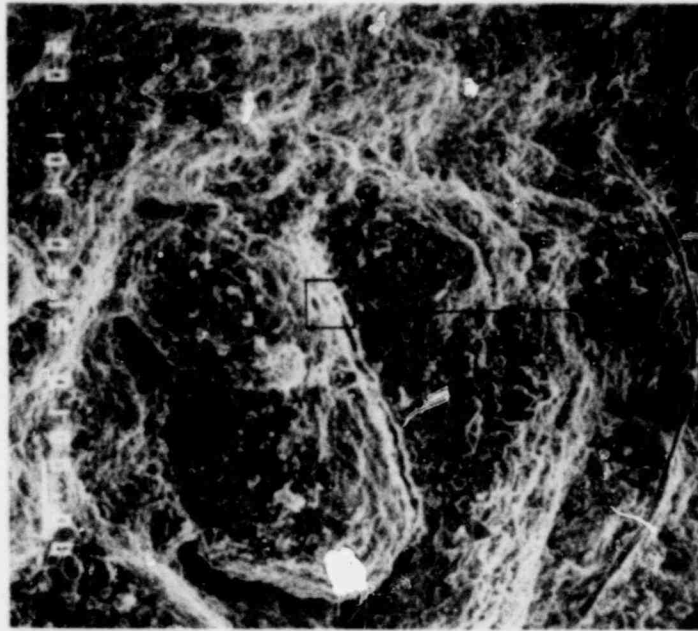


Figure 13 Microcrack in Perry sample. This variant for the microcracks in the Perry samples is relatively short and contains new mineral growths that span completely the microfracture. Note that many crystals can be seen projecting into the crack from the walls (13b).

POOR ORIGINAL

14a



14b

14b



Figure 14 A microcrack in the Perry samples (14a) at higher magnification (14b).

POOR ORIGINAL

15c

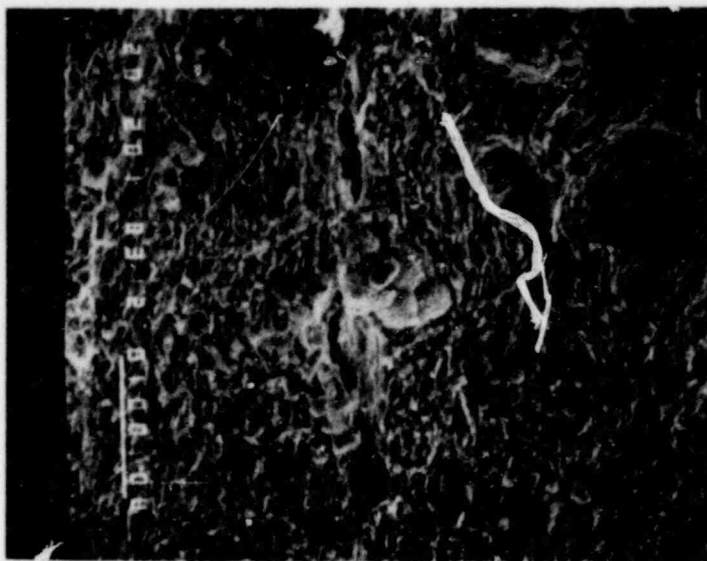


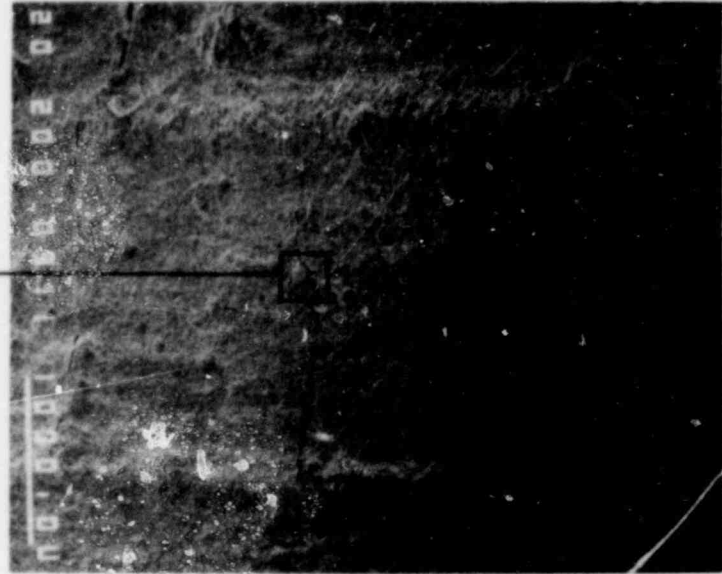
Figure 15 Slickensides in the Perry samples. The slickenslides appear to have been formed by pyrite grains that are stronger than the shale. In 15b, and 15c individual grains of pyrite can be readily observed.

1241 196

POOR ORIGINAL

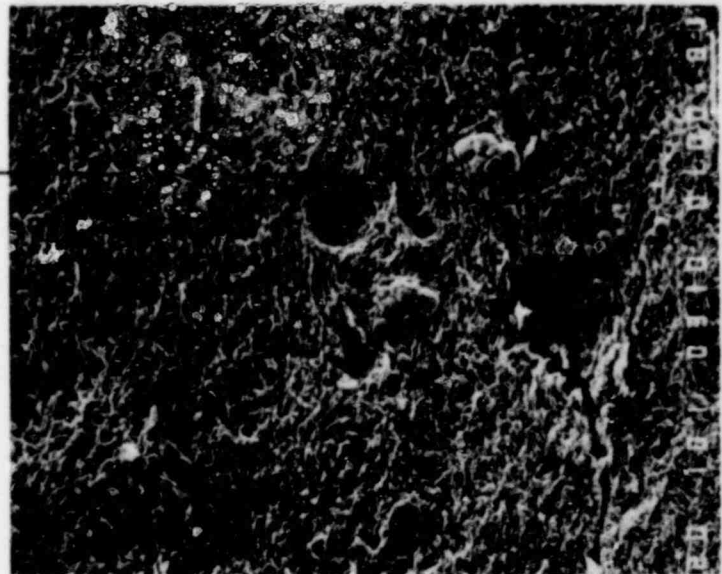
15a

15b



15b

15c



1238 197

1248 198

APPENDIX B
STUDY OF THE ISOTOPIC COMPOSITION OF WATER FROM THE FAULT
IN THE INTAKE AND DISCHARGE TUNNELS
AT THE PERRY NUCLEAR POWER PLANT

by
Dr. Gene Simmons

April 1979

1241 199

APPENDIX B

STUDY OF THE ISOTOPIC COMPOSITION OF WATER FROM THE FAULT IN THE INTAKE AND DISCHARGE TUNNELS AT THE PERRY NUCLEAR POWER PLANT

1.0 INTRODUCTION

A small fault was intersected by the intake tunnel for emergency cooling water at the Perry Nuclear Power Plant site. A small fault was also intersected by the discharge tunnel at the approximate location expected from the projection of the fault in the intake tunnel. Water enters each tunnel in the vicinity of the fault and its isotopic composition may be a useful guide to the vertical extent of the fault.

2.0 SUMMARY AND CONCLUSIONS

The isotopic ratios of D/H and $^{18}\text{O}/^{16}\text{O}$ were measured with a mass spectrograph for three samples of water from the fault in the intake tunnel, one sample from the fault in the discharge tunnel, and two samples from Lake Erie. The three samples from the intake tunnel differ insignificantly from each other and from the sample from the discharge tunnel. The two lake samples differ insignificantly from each other. However, the waters from the fault(s) differ significantly from the lake water. All three samples are meteoric.

The interpretation of the present set of data is that the 'fault water' is not Lake Erie water.

3.0 BASIS OF TECHNIQUE

The isotopic ratios of Deuterium to Hydrogen (D/H) and of Oxygen-18 to Oxygen-16 ($^{18}\text{O}/^{16}\text{O}$) in water have been shown to depend on the source of the water (e.g., Epstein and Mayeda, 1953; Craig, 1961). The ratios are measured with a mass spectrometer. Experimental details of the measuring techniques are given by Epstein (1959). The ratios are normally reported by differences relative to a standard defined by Craig (1961) and termed SMOW, an acronym derived from standard mean ocean water, where

$$\delta^{18}\text{O} = \frac{(^{18}\text{O}/^{16}\text{O})_{\text{spl}} - (^{18}\text{O}/^{16}\text{O})_{\text{SMOW}}}{(^{18}\text{O}/^{16}\text{O})_{\text{SMOW}}} \times 10^{30/100}$$

$$\delta\text{D} = \frac{(\text{D}/\text{H})_{\text{spl}} - (\text{D}/\text{H})_{\text{SMOW}}}{(\text{D}/\text{H})_{\text{SMOW}}} \times 10^{30/100}$$

and the subscript spl indicates values of the sample.

1241 200

Craig (1961) showed that the isotopic variations in meteoric waters could be represented by the equation

$$\delta D = 8\delta^{18}O + 10$$

Figure 1 is a plot of his data.

Clayton et al. (1966) examined the isotopic ratios of saline waters from several sedimentary basins. Their data are summarized on Figure 2.

4.0 DATA AND DISCUSSION

The isotopic ratios relative to standard mean ocean water, SMOW, are given in Table 1. They are also shown on Figure 3.

TABLE 1		
SAMPLE	δD_{SMOW} (0/00)	$\delta^{18}O_{SMOW}$ (0/00)
F1	-73.3 0/00	-11.5 0/00
F2	-73.5 0/00	-11.4 0/00
L1	-54.0 0/00	-7.4 0/00
L4	-52.3 0/00	-7.6 0/00
IF4	-70.6 0/00	-11.7 0/00
FD10	-79.3 0/00	-11.4 0/00

The isotopic ratios of all three water samples are near the Craig (1961, curve for meteoric water. Therefore, the water from the fault is meteoric water.

The ratios for F1, F2, and IF-4 are very close to each other. If we take the differences to be an indication of experimental precision, then the isotopic ratios for the water from the fault in the discharge tunnel differ from the values for the intake tunnel by approximately the experimental error. We therefore conclude that the waters from the fault(s) in the two tunnels have a common source, which is not Lake Erie. The data are consistent with a single fault intersecting both tunnels.

1248 201

The ratio of the water from the fault differs significantly from the ratio of the sample of Lake Erie water. Sample L1 was collected near the lake surface, L2 near the bottom. Both samples were obtained near the projection of the fault in the intake tunnel dip to the lake bottom. On the basis that the isotopic ratios of the waters from the fault in both tunnels differ greatly from the ratio for water from Lake Erie, we conclude that the fault water is not Lake Erie water.

5.0 REFERENCES

- Clayton, R. N., I. Friedman, D. L. Graf, T. K. Mayeda, W. F. Meents, and N. F. Shimp, 1966, "The Origin of Saline Formation Waters," J. Geophys. Res., 71, 3869-3882.
- Craig, H., 1961, "Isotopic Variations in Meteoric Waters," Science, 133, 1702-1703.
- Epstein, S., 1959, "The Variations of the O^{18}/O^{16} Ratio in Nature and Some Geologic Implications, in Abelson, P. H. (editor)," Researches in Geochemistry, John Wiley and Sons, New York, 217-240.
- Epstein, S. and T. Mayeda, 1953, "Variation of O^{18} Content of Waters from Natural Sources," Geochimica et Cosmochimica Acta, 4, 213-224.
- Faure, G., 1977, Principles of Isotope Geology, John Wiley and Sons, New York, 464 pp.

1241 202

POOR ORIGINAL

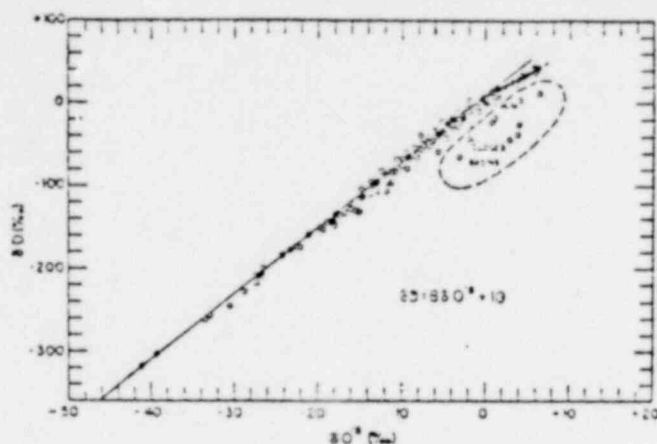


FIGURE 1 Deuterium and oxygen-18 variations in rivers, lakes, rain, and snow, relative to 'standard mean ocean water' (SMOW). Points which fit the dashed line at the upper end of the curve are rivers and lakes from East Africa. (After Craig, 1961)

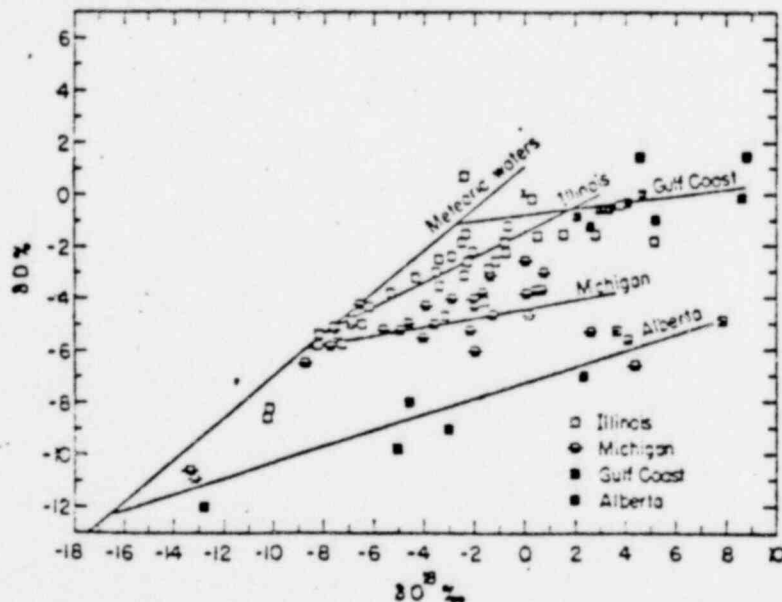


FIGURE 2 Isotopic compositions of brines. The 'meteoric waters' line is the line determined by Craig (1961) and shown on Figure 1. (After Clayton et al., 1966)

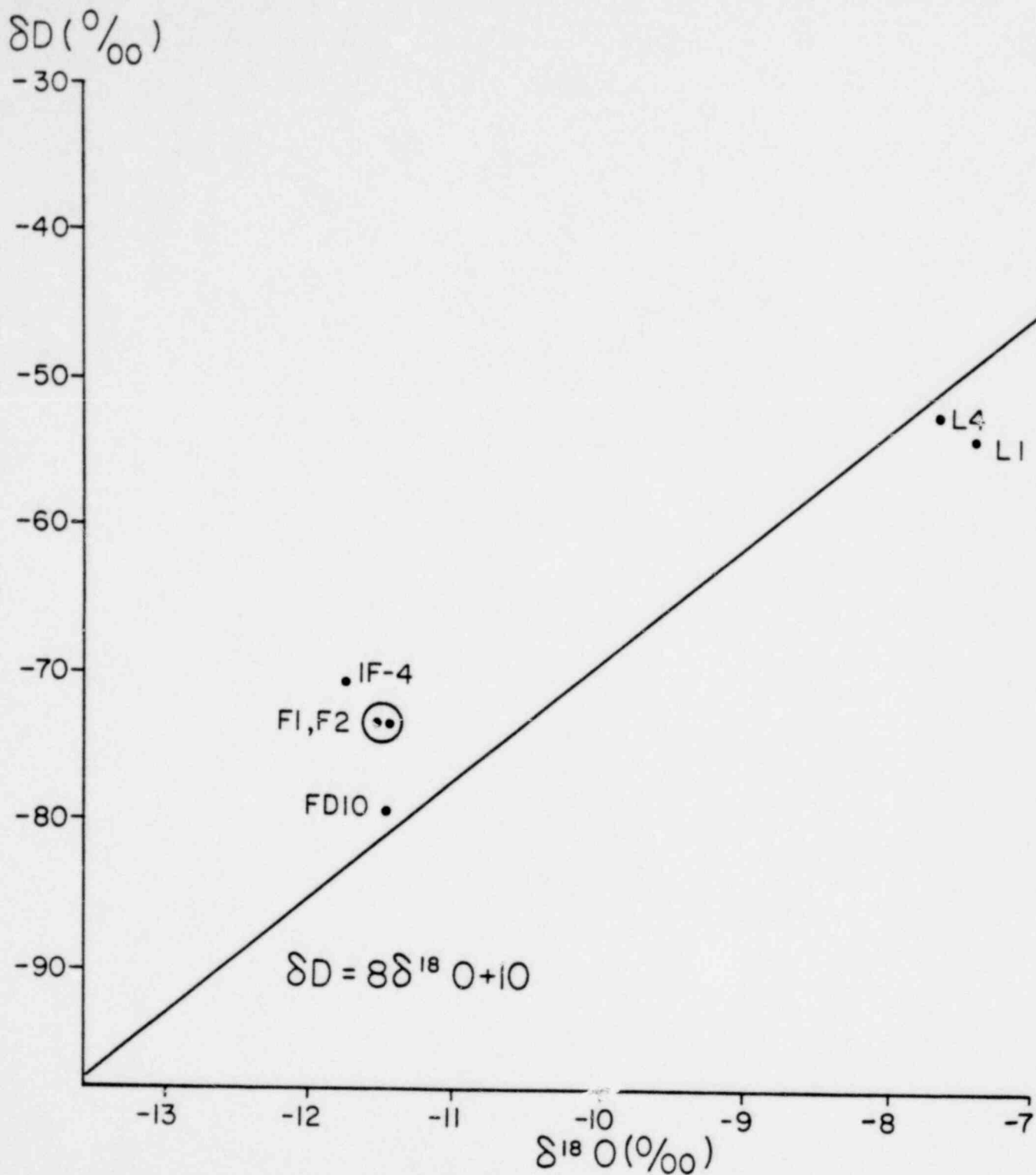


Figure 3. Isotopic compositions of the waters from PNPP. F1, F2, and IF-4 denote samples from the fault in the intake tunnel. FD10 denotes water from the fault in the discharge tunnel. L1 and L4 denote water from the top and bottom, respectively, of Lake Erie.

1246 205

APPENDIX C
GEOPHYSICAL METHODS

prepared by
WESTON GEOPHYSICAL CORPORATION

April 1979

1241 206

APPENDIX C

GEOPHYSICAL METHODS

1.0 INTRODUCTION

The following sections discuss the geophysical techniques employed during the investigation of the fault discovered in the intake and discharge tunnels at the Perry Nuclear Power Plant site. These techniques include magnetics, gamma radiation, logging, and in-situ velocity measurements.

2.0 THE MAGNETIC METHOD

The magnetic method is a versatile, relatively inexpensive, geophysical exploration technique. Magnetic data can be acquired on land, over water, or in the air. Aeromagnetic surveys and deep water marine studies are commonly used as a reconnaissance tool for tracing large-scale geologic structure, especially basement depth. Land and coastal water marine data are more useful in tracing smaller, more localized geologic structures, such as mineral and ore deposits, and for detailed geologic structural modeling. Land and coastal water marine surveys yield more detail and higher resolution, since the measurements are taken closer to the anomaly source. Land magnetic data can also be used to locate buried, man-made structures such as pipelines and tunnels, and for archaeological prospecting.

2.1 EARTH MAGNETISM

Magnetism, like gravity, is a "potential field" method. For a given magnetic field, the magnetic force in a given direction is equal to the derivative of the magnetic potential in that direction. The source of the earth's magnetic potential is its own magnetic field (F) and the inducing effect this field has on magnetic objects or bodies above and below the surface. The earth's field is a vector quantity having a unique magnitude and direction at every point on the earth's surface. This magnetic field is defined in three dimensions by angular quantities known as declination and inclination. Declination is defined as the angle between geographic north and magnetic north, and inclination is the angle between the direction of the earth's field and the horizontal. The earth's total magnetic field is measured in "gammas" (γ) (where $1 \text{ gamma} = 10^{-5} \text{ Oersted}$) and varies from about 25,000 gammas near the equator to 70,000 gammas near the poles.

The earth's magnetic field is not completely stable. It undergoes long-term (secular) variations over centuries; small, daily (diurnal) variations (less than 1% of the total field magnitude); and transient fluctuations called magnetic storms resulting from solar flare phenomena.

1246 207

The earth's ambient magnetic field can be modified locally by both naturally-occurring and man-made magnetic materials. There are two types of magnetism involved: induced and remanent.

In the case of induced magnetization, the earth's ambient field is enhanced by materials which can behave like a magnet when an external magnetic field is applied.

Crustal rocks become "magnetic" due to the presence of magnetic particles, usually magnetite or related iron oxide minerals, in their compositional structure. These particles act as small dipoles, which can be uniformly oriented by an external magnetic field, making the host rock "susceptible" to magnetic induction by the earth's field.

These "susceptible" rocks (or any magnetic object) will thus receive an "induced" magnetic field (\vec{H}), which represents a local perturbation in the main earth field. The net field (\vec{F}_t) in the vicinity of this perturbation is simply the vector sum of the induced and earth fields. Although the induced field is not necessarily parallel to the ambient field, for cases where $|\vec{H}| < .25 |\vec{F}|$, which is generally true for most geologic applications, the directional difference between the net field (\vec{F}_t), and the ambient field (\vec{F}) is negligible. Thus, the induced field really serves to enhance the ambient field. The degree to which the ambient field is enhanced is a function of the "susceptibility" of the material, or its ability to act like a magnet.

Remanent magnetization is produced in materials which have been heated above the Curie point allowing magnetic minerals in the material to become aligned with the earth's field before cooling. The remanent field direction is not always parallel to the earth's present field, and can often be completely reversed. The remanent field combines vectorially with the ambient and induced field components. The contribution of the remanent components must be considered in magnetic interpretations.

2.2 INSTRUMENTATION

At present, the most widely used magnetometer is the "proton precession" type. This device utilizes the precession of spinning protons of the hydrogen atoms in a sample of fluid (kerosene, alcohol, or water) to measure total magnetic field intensity.

Protons spinning in an atomic nucleus behave like tiny magnetic dipoles, which can be aligned (polarized) by a uniform magnetic field. The protons are initially aligned parallel to the earth's field. A second, much stronger magnetic field is produced approximately perpendicular to the earth's field by introducing current through a coil of wire. The protons become temporarily aligned with this stronger field. When this secondary field is removed, the protons tend to realign themselves parallel to the earth's field direction, causing them to precess about this direction at a frequency of about 2,000 hertz. The precessing protons will generate a small electric signal in the same coil used to

polarize them with a frequency proportional to the total magnetic field intensity and independent of the coil orientation. By measuring the signal frequency, one can obtain the absolute value of the total earth field intensity to a 1 gamma \pm 1 gamma. The total magnetic field value measured by the proton precession magnetometer is the net vector sum of the ambient earth's field and any local induced and/or remanent perturbations.

The total field proton precession magnetometer is portable and does not require orientation or leveling, as is required with vertical field instruments. There are a few limitations associated with the precession system, however; the precession signal can be severely degraded in the presence of large field gradients (greater than 200 gammas per foot) and near 60-cycle A/C power lines; also, interpretation of total field data is somewhat more complicated than for vertical field data.

2.3 FIELD TECHNIQUES

In the field, the operator must avoid any sources of high magnetic gradients and alternating currents, such as power lines, buildings, and any large iron or steel objects. The operator should also avoid carrying any metal articles. Readings are taken at a predetermined interval which depends on the nature of the survey, the accuracy required, and the gradients encountered. Base station readings, if required, are usually made several times a day to check for diurnal variations and magnetic storms.

Depending on survey requirements, one should determine the magnetic susceptibility and remanent magnetism for the rock units in the survey area. If this information is not available, several representative rock samples should be collected and analyzed. One must properly mark the in-situ orientation of these samples with respect to north direction and horizontal plane. Susceptibility and remanent field measurements are obtained using standard laboratory techniques.

2.4 INTERPRETATION

Lateral variations in susceptibility and/or remanent magnetization in crustal rocks give rise to localized anomalies in the measured total magnetic field intensity. Geologic structural features (faults, contacts, intrusions, etc.) which correlate with susceptibility and/or remanent magnetization variations will cause magnetic anomalies, which can be measured and interpreted to quantitatively define the geometry of this causative structure.

After diurnal effects and regional gradients have been removed, magnetic anomalies can be studied in detail; derivative operations and frequency filtering can be employed.

Because it is a potential field method, there is an infinite number of possible source configurations for any given magnetic anomaly. There is also an inherent complexity in magnetic dipole behavior. Remanent field

effects further add to the complexity. But if the various magnetic field parameters (inclination, declination, and susceptibility) are well defined, and some reasonable assumptions can be made regarding the nature of the source, an accurate source model can generally be derived.

Magnetic anomalies can be analyzed both qualitatively and quantitatively. The physical dimensions of an anomaly (slope, wavelength, amplitude, etc.) often reveal enough to draw some general qualitative conclusions regarding the causative source.

Precise interpretation must be done quantitatively, however, and there are two basic approaches, each ideally requiring prior knowledge of earth and remanent magnetic field parameters. Modeling can be performed by various approximation methods, whereby one reduces the source to a system of poles or dipoles, or assumes it to be one of several simple, geometric forms (vertical prism, horizontal slab, step, etc.). The magnetic properties for this simplified model can be rather easily defined mathematically. Simple formulas can be derived which relate readily measurable anomaly parameters, such as slope, width, and amplitude ratios, to the general dimensions of the anomaly source, including depth to top, thickness, dip, and width normal to strike. Since these methods involve very limiting geometric assumptions, the results can only be treated as good approximations except for very simplified sources.

The second and more accurate quantitative method utilizes computer iteration techniques to directly calculate the resultant magnetic anomaly for a two- or three-dimensional geometric model constructed to fit the expected geologic source. This method allows one to develop by trial and error a model whose calculated magnetic field anomaly matches the observed anomaly as closely as possible.

In both two- and three-dimensional computer modeling, the source body is spatially defined by one or more n-sided polygons. In the two dimensional case, a vertical polygon of infinite length in a direction normal to the magnetic profile is used to define the source. Each polygonal segment then represents the vertical edge of a rectangular prism, which is infinitely long in the profile direction. The magnetic effect of each of these prisms is computed and summed with appropriate sign convention to give the net magnetic effect of the body circumscribed by the polygon, and thus, the magnetic anomaly.

In three dimensions, a series of horizontal polygons are stacked vertically to define the source. The net magnetic effect for the total volume is then obtained by computing the effect of each polygon, integrating it over the vertical extent of the body, and summing the results for all of the polygons used. The polygonal geometry allows a great deal of flexibility in defining an anomaly source and can encompass a wide range of geologic forms.

1246 210

3.0 GAMMA RADIATION LOGGING

3.1 PURPOSE AND BACKGROUND

Gamma radiation logging can provide an efficient method for correlating geologic units in uncored boreholes. The logging probe measures gamma radiation resulting from the natural radioactivity of the uranium (U), thorium (Th), and potassium (K^{40}) in nearby bedrock or soils. Although the radiation from either the U or Th series is much greater than that of K^{40} , the background radiation from each element is approximately equal because the potassium isotope is far more common.

The intensity of gamma radiation decreases rapidly as it passes through a material. This attenuation is exponential and dependent on the energy of the radiation and the absorption coefficient of the particular material. For the average energy of natural radiation, the range of penetration in sediments is roughly 1 foot with about half the gamma rays detected in the borehole originating within 5 inches of the borehole wall.

The natural radioactivity in sedimentary rocks and metamorphosed sediments is generally higher than that in igneous and other metamorphic types, with the exception of potassium-rich granites. In sediments, the gamma ray log reflects mostly shale content because radioactive elements tend to concentrate in clays and shales; sands and carbonates usually have low radioactivity. Subtle changes in rock composition not readily apparent to the inspecting geologist may be revealed by the gamma ray log.

3.2 EQUIPMENT AND PROCEDURE

The logging system consists of a probe containing a scintillation crystal and photomultiplier tube, an electronic counting unit, a strip chart recorder with variable scale settings, and a power winch.

Gamma radiation incident on the scintillation crystal is converted to light through interaction with the crystal. This light enters a photomultiplier tube where it is converted to a pulse of electricity which is conditioned and transmitted through the cable to the counting unit. The average number of pulses per time unit (seconds or minutes) is plotted versus depth on the strip chart recorder.

In logging, the probe is lowered to the bottom of the borehole and measures the radiation as it is raised. Boreholes are generally logged twice to determine the "repeatability" of the data.

Statistical variations in radiation emission, significant at low counting rates, can generally be smoothed out by integration over a short time interval. If the hole is logged too quickly, however, the smoothing effect leads to erroneous results, and data are shifted in the direction

1246 211

of logging. The logging speed must be adjusted for the bed thicknesses and radiation levels. The length of the detector (the scintillation crystal) with respect to the bed thickness also affects the shape of the resulting log. Optimum resolution for thin beds is obtained with a short detector and a slow logging speed.

3.3 INTERPRETATION

The interpretation of gamma logs is relatively straightforward. The interface between beds of different natural radioactivity can be located with reasonable accuracy if it is assumed to occur halfway between the two count levels for thick beds (<6 ft.). For thinner zones, the location of the maximum count rate can be taken as the center of the zone.

In making correlations, all available geologic information is taken into consideration. This includes unit thickness and composition, and position in the geologic column. The gamma ray log displays this information in the form of the radiation level within a particular unit, as well as the gamma ray signature for that unit (the frequency of minor deviations from the average radiation level). If other geophysical information is available, it is also considered in the final interpretation.

4.0 IN-SITU VELOCITY MEASUREMENTS

4.1 PURPOSE

In-situ velocity measurements provide a reliable determination of material properties. The velocity measurements together with known or estimated densities are used to determine the dynamic elastic moduli of the material. It is necessary to obtain the data on material in place; velocity measurements made with laboratory samples may be strongly effected by alteration of the material in obtaining the sample, and by differences between the in-situ and test-imposed stress conditions.

4.2 EQUIPMENT AND PROCEDURE

In-situ velocity measurements are based on the determination of the time required for elastic waves, generated at a point source, to travel to a series of vibration-sensitive devices (geophones or seismometers). For in-situ velocity measurements, usually the geophones contain three orthogonal seismometers, one vertical and two horizontal. These three components allow the seismologist to estimate the mode of vibration of the material in the vicinity of each geophone.

Seismograms are obtained using a portable 12- or 24-channel seismograph system which amplifies and filters the seismic signal detected by the individual geophones and provides a photographic record for each of the 12 channels (Figure 1). Timing lines are provided across the entire recording at two-millisecond intervals allowing direct reading to one

millisecond. The seismograph is equipped so that the background noise level can be observed for all geophones simultaneously, enabling the operator to determine if the noise level is sufficiently low to minimize trace interference.

Depending on the requirements of the survey and specific site conditions, in-situ velocity measurements are acquired in a number of ways, depending upon the deployment of source and geophones (Figure 2):

1. source and receivers in different boreholes (cross hole);
2. source in borehole and receivers on the surface (uphole);
3. source on the surface and receivers in borehole (downhole);
4. high frequency source and receivers in the same hole (sonic logging);
5. source and receivers in tunnel; or,
6. source and receivers on surface.

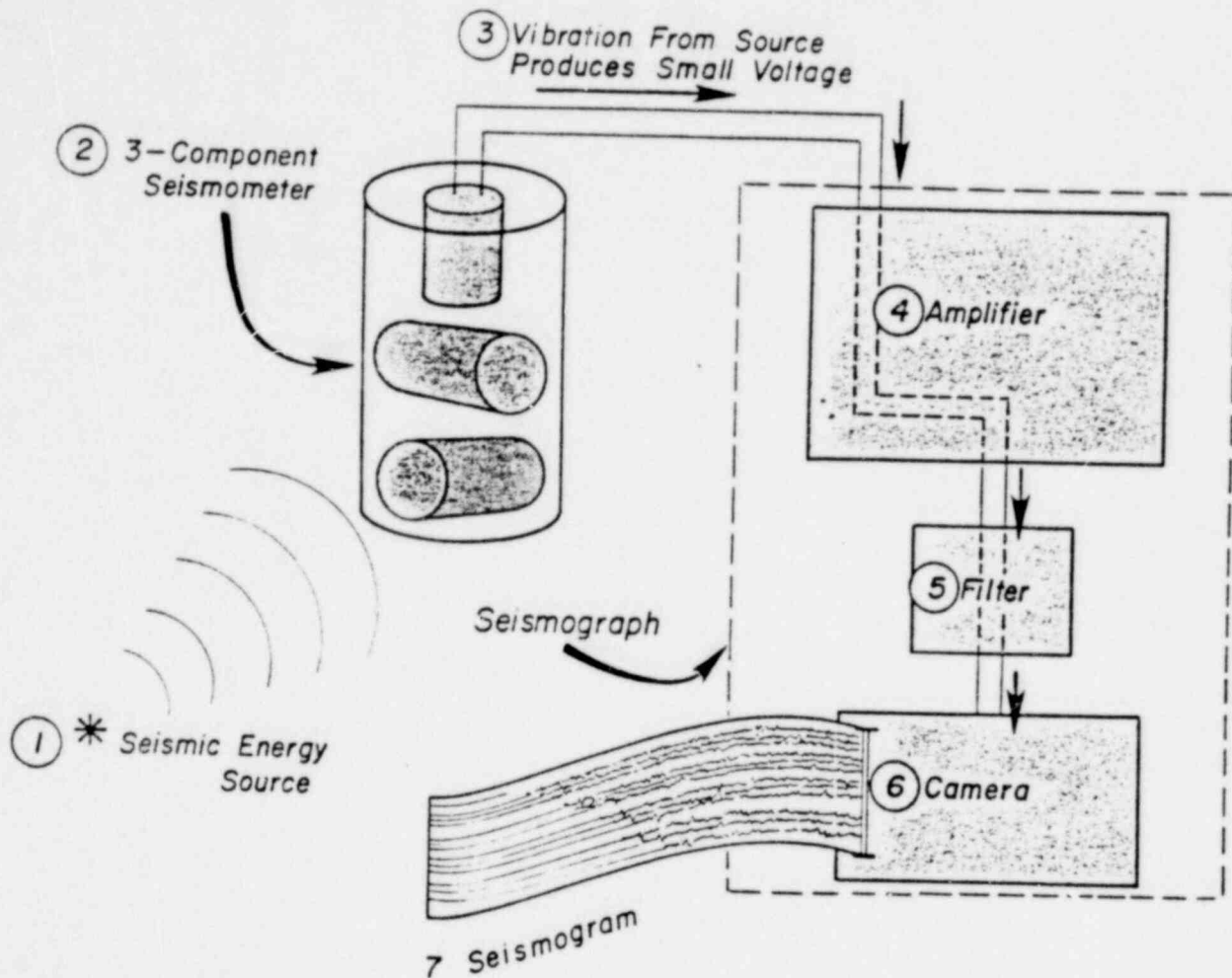
4.3 INTERPRETATION

The interpretation involves picking the arrival times of two forms of seismic waves at each geophone and determining the relationship between arrival times for each wave type. The two waves are the compressional ("P") wave and the shear ("S") wave. The "P" wave is transmitted as a series of compressions and rarefactions, and the particle motion is parallel to the direction of propagation. The "S" wave, on the other hand, exhibits a particle motion perpendicular to the direction of propagation. Therefore, the information on particle motion given by the three-component seismometers can be used as an aid in determining the wave type of arrivals.

When the arrival times are plotted against distance from the source, the velocity of the material is determined by the inverse slope of the best linear fit to the data.

1248 213

POOR ORIGINAL



SEISMIC INSTRUMENTATION

FIGURE 1

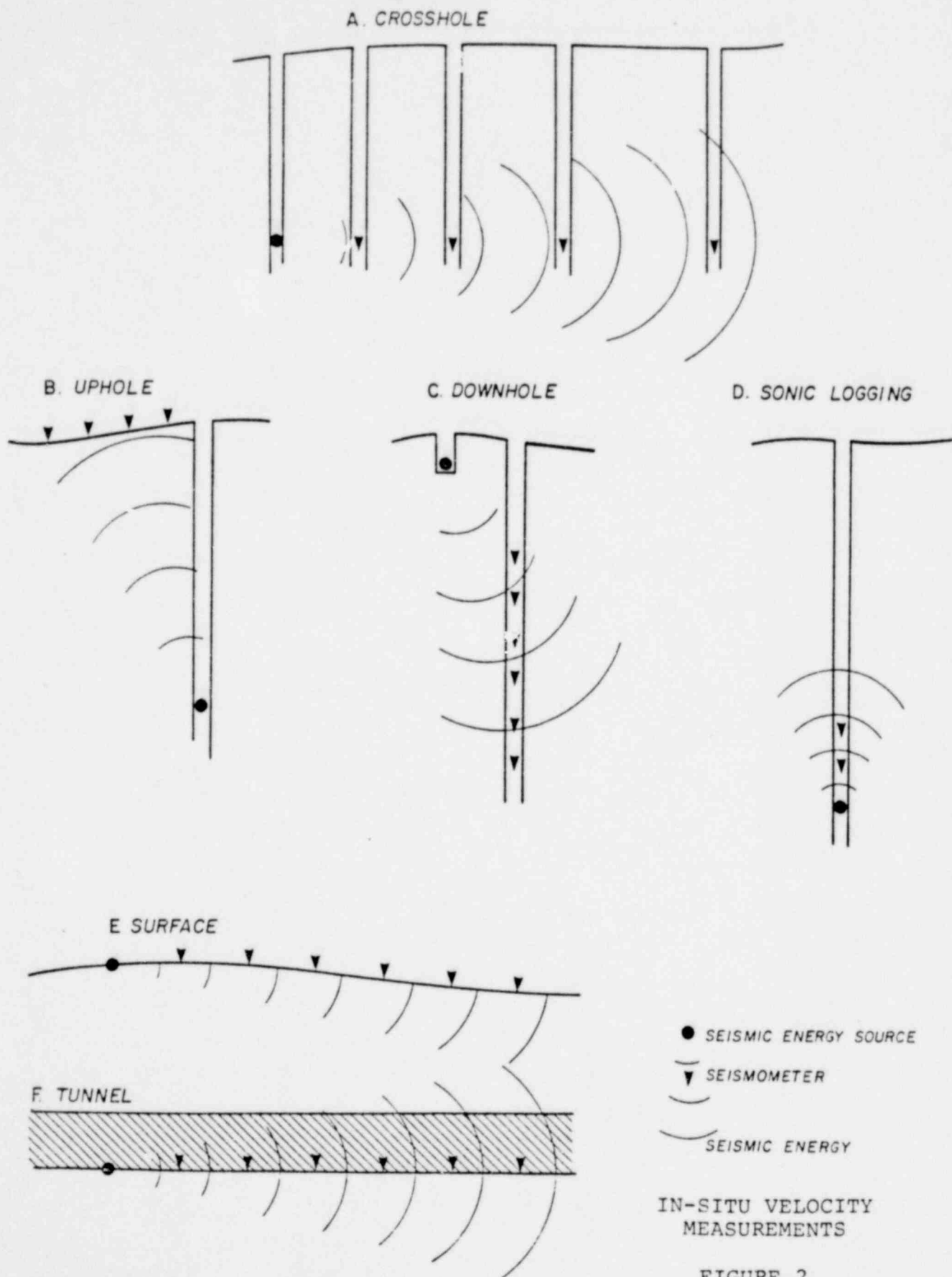


FIGURE 2

12~~91~~ 216

APPENDIX D
INDEPENDENT REVIEWS OF COOLING WATER TUNNEL FAULTING

1248 217

Mr. James Murphy
Ohio Historical Society

1241 218

Bedrock Deformation in the Water Intake Tunnel, Perry
Nuclear Power Plant, Lake County, Ohio

James L. Murphy
The Ohio Historical Society
Columbus, Ohio 43211

On January 19, 1979, I examined bedrock exposures of the Chagrin Shale exposed in a water intake tunnel at the Perry Nuclear Power Plant, Lake County, Ohio. Details of this and a similar exposure in the outlet tunnel are described in GAI Reports 1986 and 1997, which have been available for study.

Based upon my examination of the actual outcrop and supplementary evidence presented in the above-mentioned reports, I believe that the low angle thrust fault and related small anticlinal fold are essentially identical with similar features found nearer the surface during excavations for the power plant (Gilbert & Associates, 1975).

It is my belief that such bedrock deformation was caused by the horizontal component of localized stresses created during the Pleistocene by either the advance of the ice sheet(s) and concomitant depression of the crust, or in reaction to removal of the weight of the overlying ice (glacial rebound). This would mean that the deformation occurred some time during the last one million years. I am inclined to believe that it is related to the last (Wisconsinan) glaciation but conclusive proof of this is lacking. The deformation could be related to any one of the major

glaciations that covered northern Ohio, and different faults and folds may owe their origin to different glaciations. In any case, further movement along such features is not to be expected, and these are not, therefore, classifiable as capable faults.

In reviewing the original reports (GAI 1986, 1997) on the deformation exposed in the cooling system tunnels, I would make the following additional statements:

1) Based upon my knowledge of similar faults in the Chagrin Formation of northeastern Ohio, I believe that in all probability, two separate faults are represented, one in each tunnel. The chief evidence for this is the considerable difference in strike represented in the two exposures and the rather local nature of similar faults exposed elsewhere in the Chagrin.

2) I believe that the hypothetical subsurface projection of the fault(s) shown in Figure 2 (GAI 1997) is incorrect and doubt that the fault(s) extend quite so far, either laterally or vertically. (It should be noted that the vertical exaggeration used in Figure 2, though stated in the figure, gives a somewhat misleading impression of the magnitude and dip of the fault.) Presumed evidence of the extension of the fault seems somewhat equivocal and cannot be taken as conclusive proof of the existence of the fault at the distance and depth projected. Even were the fault of the size and extent presumed, I believe the proposed glacial mechanism still the most probable cause of the deformation.

3) The possibility of penecontemporaneous deformation of the unlithified Chagrin sediments is completely out of the question in these instances

and, I think, would immediately be dismissed by any geologist who examines the exposure in the intake tunnel. In this regard, I suggest that detailed close-up photographs be taken of the lower portion of the fault as exposed in the (north)east wall, a few feet above the base of the tunnel, where rather large (approximately 3 inches in diameter) fragments of detached Chagrin shale occur in the fault "gouge", conclusively demonstrating that the deformation occurred subsequent to lithification.

4) Deformation by deep-seated late Paleozoic tectonism cannot be entirely ruled out of the question as a possible cause of some Chagrin deformation, but it is considered an unlikely possibility in the present instance, particularly in view of the fact that similar faulting and folding (notably in the on-shore NPNPP excavations) rapidly diminishes and disappears with depth. Such is also believed to be the case with the water system tunnel faults. Although they are deeper than previously studied examples in the Chagrin Formation, they are nonetheless comparatively shallow "surficial" phenomena unrelated to deep-seated tectonism.

James L. Murphy
February 19, 1979

1241 221

Newspaper Account of 1818 "Kingston" Earthquake

Michael Hansen of the Ohio Division of Geological Survey has given me the following information regarding a newspaper account of a 1818 earthquake that has been believed to have had its epicenter at Kingston, Ross Co., Ohio.

The Cleveland Register of March 16, 1819, reprints a news item from the Quebec Gazette (no date) stating that "Two severe shocks of an earthquake were felt at Kingston and its vicinity on the morning of the 7th December. They were accompanied with a rumbling noise. The disturbance was not as long as those of 1812 but were equally violent."

Since the newspaper item originally appeared in a Quebec newspaper, it is evident that the earthquake occurred at Kingston, Ontario, rather than Kingston, Ohio. The only known copy of this issue of the Cleveland Register is at the Western Reserve Historical Society in Cleveland.

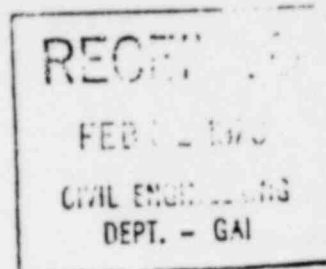
James L. Murphy

1248 222

Dr. Robert G. LaFleur
Rensselaer Polytechnical Institute

1241 223

Robert G. LaFleur
Geologist
Taborton Road
Sand Lake, New York 12153



January 30, 1979

Dr. Lane D. Schultz
Gilbert Associates Inc.
625 Lancaster Avenue
Reading, Pennsylvania 19603

Dear Lane:

On January 19, 1979, with L. D. Schultz and J. Murphy, I inspected the reverse fault which intersects the intake tunnel of the Perry Nuclear Power Plant, and subsequently reviewed GAI Reports No. 1986 and 1997 describing this feature and other near-surface bedrock deformations. The following comments summarize my impressions of the tunnel fault.

1. I see no evidence which suggests the deformation occurred while the Chagrin shale was in a poorly consolidated state. Soft-sediment deformation is usually indicated by the presence of flow structure, wispy sediment tails, mess-bedding, deformed and pulled-apart plasts, etc. Early Paleozoic slope clastics and carbonates in the Taconics commonly show such features in deep water rocks - by comparison the Chagrin deformation, with the exception of bedding irregularities attributable to compaction and minor sole marks, is devoid of such features. Brittle fracture is represented by the tunnel fault. Drag and adjacent open folds maintain good parallel banding. Gouge breccia is angular and untorn. I would conclude from this the tunnel fault deformation occurred after consolidation was completed.

2. The depth of active influence, observed elsewhere (200m.), of overriding ice may be enough to permit inclusion of the tunnel fault in the same glacitectonic category as the shallow features. However, 1) the fault sole shows no clear sign of passing into bedding plane orientation at reasonable depth; 2) the fault dip direction is considerably at variance with the usual direction of

1243 224

Erie lobe movement (from the NE or N); 3) it seems difficult to see how glacier movement alone would produce a deep structure at all (when the ice can tear up the surface rocks instead) unless there were an existing weakness plane which override could activate. There is no indication in the tunnel that the fault might have a multiple movement history. Elevated methane pressure in the Chagrin would enhance movement along a deep fault, but there is little proof abnormal pressures existed during glaciation. I think it is unreasonable to expect the Chagrin was frozen deeply enough to permit ice expansion along such a weakness plane to motivate faulting.

I agree with the proposed glacitectonic origin for both the tunnel fault and shallow deformation, but I am not completely persuaded that active ice, ground-coupled in the presence of permafrost, is necessarily responsible for these features. I cannot rule this process out on the basis of the evidence at hand, but would point out that it is certain that glacier loading and unloading, glacial quarrying of the Erie basin, and episodic glacial lake development caused vertical stresses and might also have permitted horizontal stress development sufficient to produce the structures. In this sense a more passive role of glaciers in regional crustal movements is indicated. It may be important to this notion that the strike of the Chagrin deformations agrees well with the regional trend of the Erie basin axis and south edge - more than it appears to agree with a direction normal to common ice flow. In addition, deep permafrost, to my knowledge, does not appear to have been widely developed at this latitude during the Late Wisconsin - these glaciers rather were temperate, wet-based, and often advanced through proglacial lakes.

3. Although the upper and lower limits of the tunnel fault are not determined, I would expect the fault to intersect the bottom of Lake Erie. The gouge water chemistry does not rule out

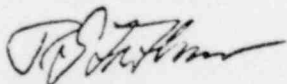
1246 225

hydraulic connection with the lake. Water movement along the fault should be directed, as recharge, toward the lake. Interpretation in the TX borings of intersections with the fault trace projected to depth appear reasonable. Absence of mineralized gouge suggests the fault is confined to the Chagrin, but one might also attribute this to a younger (than Paleozoic) age for the fault.

4. One can only conjecture what role the Salina salt played in glacier-induced crustal warpings, and particularly its influence in maintaining and cumulating abnormal horizontal stress. I point this out only to convey the idea that oscillating Pleistocene glaciers may have triggered more complicated "late" tectonic settings in which a ductile substrate influences development of faults in overlying rocks, perhaps like the one exposed in the intake tunnel.

In any event I support the conclusion that the tunnel fault is related to some manifestation of glaciation - not necessarily as young as Late Wisconsin. In view of its movement sense, it may be related to crustal loading (down-warping) of the Erie basin while near-surface rocks were in a state of horizontal stress. I see no reason to consider the tunnel fault active, capable, or of post-glacial age.

Yours truly,



Robert G. LaFleur

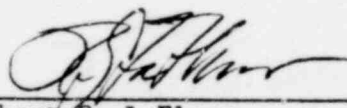
1241 226

RGLaF:vb

At the request of Dr. Lane D. Schultz, I visited the office of Gilbert Associates on April 12, 1979 and inspected documents describing the shallow deformations at PNPP and those exposed at Warners Creek and Hell Hollow.

I support the conclusions reached by several others that the shallow structural features are the result of glacial ice drag - those exposed at PNPP and also the compressional folds and related thrusts shown in the creek sections. The correctly-oriented fold asymmetry, thrust sense, shallow depth, and participation of bedrock with till are all persuasive features indicative of an active glaciotectionic origin. There is little one can add to the carefully documented and considered opinions offered by C. E. Herdendorf, J. L. Murphy and the Gilbert Associates Staff.

As a minor point one might note the occurrence of rare near vertical faulting, illustrated by Hell Hollow faults #1, 2, and 3 which appear to post-date the compressional structures. Comparable relations are not apparent at PNPP; compressional (glacially induced) movement there is the terminal event. If high-angle faulting at Hell Hollow is the result of slumping, one might conclude there is no evidence for fracturing during application or removal of glacial ice load. That is, post-glacial uplift has no structural manifestation at PNPP. If, on the other hand, the Hell Hollow faults are due to post-glacial uplift, PNPP is still free of such features. My impression that the intake tunnel structure is neither of active or passive glaciotectionic origin remains - although the notion seems plausible that a million-year-old crack along a much older fault zone might be a manifestation of a passive, early glacial event. I see no reason to relate the tunnel fault to the surface structures. It is also clear that the shallow deformations do not resemble pop-ups. Stability of the bedrock since the glacial override seems apparent.



Robert G. LaFleur

4/12/79

1248 227

Dr. Barry Voight
Penn State University

1241 228

BARRY VOIGHT
CONSULTANT
GEOLOGY AND GEOTECHNICS

324 SOUTH PATTERSON STREET
STATE COLLEGE, PENNSYLVANIA 16801
TELEPHONE (814) 238-1131 U.S.A.

INVESTIGATION OF COOLING WATER TUNNEL FAULTS,
PERRY NUCLEAR POWER PLANT, OHIO

1248 229

INVESTIGATION OF COOLING WATER TUNNEL FAULTS,
PERRY NUCLEAR POWER PLANT, OHIO

Barry Voight

	<u>PAGE</u>
1. Summary of Report -----	1
2. Introduction -----	4
3. Tunnel Fault Description -----	5
a. Intake Tunnel -----	5
b. Discharge Tunnel -----	8
c. Extent of Faults -----	10
d. Mutual Geometric Relationships -----	16
4. Age of Faulting -----	19
5. Rock Stress Investigations -----	31
a. Orientation and Magnitude of Stresses -----	31
b. Possibility of Future Slip on Existing Fault--	41
6. Regional Tectonic Framework -----	48
a. Structure under Lake Erie -----	48
b. Structure of Southwest Ontario -----	50
c. Structure South of Lake Erie -----	52
d. Relationship of Inferred Structure to Seismicity -----	56
7. Origin of Tunnel Faults -----	66
8. References -----	73

1241 230

FIGURE CAPTIONS

1. Drillhole log, TX-4; fault intercept.
2. Drillhole log, TX-7; possible fault intercept
3. Drillhole log, TX-11; possible fault intercept.
4. Fault slip vs. distance along fault plane from tunnel base.
5. Direction of σ_{\max} at the PNPP site in comparison to regional measurements.
6. Sketch of PNPP structural trends with hypothetical stress orientations (a) before and (b) after faulting, and (c) measured stress orientations in TX-11.
7. Joint orientations PNPP foundation exposures. 220 Measurements. Plot by WGC.
8. σ_1 and σ_2 vs depth, TX-11.
9. Stresses in vertical plane perpendicular to tunnel fault.
10. Mohr diagram comparing calculated stresses in vicinity of tunnel fault to minimum strength envelopes.
11. Structure in the Dover field, Canada.
12. "Graben" in salt production shaft, Fairport Harbor, Ohio
13. Regional seismicity (WGC base) and structural anomalies.
14. Regional seismicity and selected structural anomalies.

1241 231

1. SUMMARY OF REPORT

The tunnel thrust faults represent a single fault with splays or a closely-associated en-echelon set of faults that extends at least 750 ft along northeast strike and at least 600 ft along a 15° dip angle to the southeast. Slip gradient information suggests that the faults die out at elevation 450 ft within about 20 vertical feet above the tunnel crown. If so a toe buttress of "solid" rock about 70 ft thick lies between the terminated fault and the lake bottom. Insufficient information is available to conclusively establish whether or not the faults terminate to the southeast between elevations of 300 ft and 150 ft, or continue to a deeper level. There is no evidence to suggest an increase in dip angle toward the southeast, but the possibility has not been eliminated.

Consolidation tests on two samples of the fault gouge suggest a maximum vertical effective consolidation pressure of about 9 ± 4 tsf. This value is consistent with vertical compression of fault gouge by a somewhat greater thickness of overburden than exists today, or by minor late Pleistocene ice sheets associated with deposition and compression of till deposits recognized at the PNPP site. The gouge consolidation pressure is not consistent with compression by the four or more Pleistocene ice sheet maxima. The latest of these events, associated with the Kent Till, occurred about 21,000 YPB, with an end moraine 70 miles or so south of the PNPP site and an inferred overburden pressure on the order of 100 tsf. Local arching effects are not considered so severe as to preclude such an event from leaving a marked imprint on gouge consolidation characteristics. It is therefore considered likely that the last movement of the tunnel fault occurred not more than 20,000 YBP.

An ENE maximum compression stress field orientation exists at the PNPP site, as determined by the hydrofracturing method. This corresponds to a regional orientation of stress that extends throughout Ohio and across much of New York State and southern Canada. Inasmuch as a northwest orientation for causative maximum compression was associated with the tunnel thrust fault, the tunnel fault is considered to be older than the age of the existing system. A lower bound age for movement on the fault is thus suggested, viz. about 10,000 YBP, giving a rather restricted estimated age range, 10,000 - 20,000 YBP, and an estimated age of $15,000 \text{ YBP} \pm 5,000$.

Magnitudes of rock stresses were measured for the depth range of 394-718 ft, giving the following rounded-off average values:

maximum horizontal stress = 1500 psi
minimum horizontal stress = 900 psi
vertical overburden stress = 400-800 psi

Similar values have been recorded throughout the midwest, New York, and southern Canada. Measured stresses were resolved for the vertical plane perpendicular to the tunnel fault, and the question of recurrent slip was examined. The results show that below about 200 ft depth (elevation about 300 ft), the fault plane may be considered to be strongly clamped by frictional resistance, and no recurrent motion seems possible. Accordingly, it may be academic whether or not the fault terminates at 150-300 ft elevation or continues in a down-dip direction. At shallower levels, the fault plane is apparently less strongly clamped (stresses are inferred

by extrapolation), but slip is not considered likely because it would require deformation of the inferred toe buttress. On balance the data suggest that the tunnel fault should probably not be regarded as "capable" despite its relatively young age.

The last movements on the tunnel faults were apparently generated by northwest-orientated compressive stresses associated with a rebounding crust during deglaciation of the Laurentide maximum ice sheet. Nucleation of the fault at some earlier time is not precluded by the available data.

1241 234

2. INTRODUCTION

The writer was retained by Gilbert Associates, Inc., in February 1979 as a reviewing consultant with the principal task of establishing the origin of the tunnel faults, as considered in relation to the Perry Nuclear Power Plant. This report presents the results of the investigation which followed.

I am grateful to L. D. Schultz and R. Wardrop of Gilbert Associates, Inc., for their cooperation, assistance, and courtesy in many matters related to my investigation. At my recommendation Gilbert Associates, Inc. approved additional drilling, rock stress investigations, and consolidation testing of fault gouge, and the cooperation in these endeavors of the Pennsylvania Drilling Company, of J.C. Roegiers and J. D. McLennan, University of Toronto, and of A. Dvinoff, Woodward-Clyde Consultants, is hereby acknowledged. I also appreciate the cooperation of the Weston Geophysical Corporation in providing data from their tunnel mapping and regional seismicity programs.

1241 235

3. TUNNEL FAULT DESCRIPTION

a. Intake Tunnel

The deformed zone begins at about station 10 + 40 and extends to station 10 + 90. The principal structure is essentially a low-angle thrust with approximate attitude of 050/17 SE (strike N 50°E, dip 17° SE). In detail, the fault zone is comprised of a series of irregular steps, with local dips varying from zero, parallel to bedding, to 50° SE on one of the riser surfaces. Dip slip, which virtually coincides with net slip, ranges from about 1.6 ft near the Crown to about 2.5 ft near the invert. The slip difference is taken up by splay faults and minor structures of various kinds which distribute the strain within a volume of rock adjacent to the main thrust surface.

The zone of observable deformation extends locally as much as 10 ft above and 6 ft below the fault, as measured perpendicular to the fault surface, but is ordinarily much less. Splay faults are best developed in the footwall above the spring line. The splays are themselves thrust faults, with dip slip on the order of an inch. Like the main thrust they are influenced by bedding-controlled anisotropy. Their attitude varies from "horizontal" (i.e., parallel to bedding) to an inclination of about 20° (average of 14 measurements) to bedding. They appear to die out in bedding planes at horizontal distances of 13 ft or less from the fault plant. Curvature of layering occurs adjacent to the main thrust and splays. Some of the curvature may be attributed to displacement along a fault surface of upward-increasing dip. Normal drag folds are locally well developed, affecting layering within a foot or two of the thrust.

Fold hinge lines are nearly horizontal and trend approximately 050° , parallel to the strike of the fault surface. Hinges are often rounded, and most folds are approximately parallel (bed-normal thickness about constant) and locally concentric. Angular hinges occur locally, most often in close association with the fault boundary surface (e.g. East Wall, Station 10 + 63 - 65). Axial planes are not always well-defined but seem to strike about 050° , parallel to the fault surface.

Flexural slip is indicated by thin gouge zones parallel to layer boundaries on fold limbs. Most folds are fractured, intensely so adjacent to the main thrust where folding, splay faulting and fracturing are closely associated. Systematic small-scale open fractures appear locally on fold hinges at high angles to the deformed layers. No mineralization was observed in fractures. The fault zone is commonly filled with a grey breccia-gouge, about half of which is comprised of particles in the clay-silt range, with the remainder angular sand- to gravel- size fragments of shale and siltstone. Rock fragments contained within the brecciated or gouge-filled fault zone are not randomly orientated, but are preferentially orientated such that their mean strike azimuth is approximately parallel to that of the fault. This suggests rotation of the fragments about an axis normal to fault slip. Gouge is irregularly distributed along the main thrust, with the thickness range varying from about half a foot to less than an inch. The splays also contain gouge, to a maximum thickness of about half an inch. Gouge thickness appears to be a function of fault offset (slip), the relative attitudes of bedding

and the fault surface, roughness of the fault surface, and deformability of fault boundary layers. Physical properties of the gouge are discussed subsequently.

Under low-angle illumination, striations and grooves were discovered on bedding and riser fault surfaces and on gouge adjacent to it. These features were produced by frictional wear associated with faulting. Groove lengths appear to be about 0.1 ft or more, adjacent to the main fault. Striation orientations are parallel to the fault dip azimuth. The orientations of striations, minor folds, and tabular fragments in the fault zone all require the dominance of dip-slip in faulting. A small right-lateral component is indicated by striations orientated at 15° to the fault dip azimuth at Station 10 + 58, west wall.

A minor syncline with a steep axial plane appears in the hanging wall at Station 10 + 51. The hinge is rounded on the bottom and continues below the invert muck. The fold dies out toward the crown through a zone of conjugate shears and bedding plane slip, with offsets on the order of 0.1 ft. Local gouge on layer boundaries throughout the fold suggests deformation by flexural slip. The fold probably reflects the influence of a local shear force on the buckling of a multilayer under axial (horizontal) load. It could reflect a dip change in the thrust surface, located below the tunnel at about Station 10 + 50.

1248 238

b. Discharge Tunnel

Two deformed areas are present. One such area extends from about station 13 + 24 to 13 + 62. The principal structure is a low angle thrust, with approximate attitude 060/15 SW. In detail the thrust surface is comprised of connected bedding plane fault and riser segments, with local splays. In places a single fault zone is present, sometimes characterized by breccia-gouge as much as 0.3 ft thick, and sometimes by intensely fractured rock; in other places the fault zone is comprised of a "nested" sequence of a half-dozen individual faults, with thin gouge layers separated by fractured rock. The zone of significant deformation is rarely more than 3 ft thick. Conjugate splay faults are best developed between Station 13 + 50 and 13 + 60. The mean angle for riser faults (including splays) from bedding is 26° (13 measurements). Dip slip on the principal fault ranges from about 2 ft near the invert to about 1.5 ft near the crown, with splay faults and other minor structures accommodating the strain (associated with the slip difference) over a larger volume of rock adjacent to the fault surfaces.

On the whole the structure and its associated minor structural elements closely resembles the intake tunnel fault. Striations on the fault surfaces are normal to the fault strike, indicating dip slip motion.

Drag fold hinge lines have negligible plunge and have azimuths approximately parallel to the fault strike. Folds are essentially parallel, with hinges that vary from sharply angular

1246 239

to rounded. The strike of the axial planes parallelsthe fault strike, as do the strike of folded limbs.

From Station 11 + 50 to 11 + 80, a small thrust termination is exposed. Strike is about 020, with irregular dip, roughly 20SE. Vertical offset is less than half a foot near the invert. The fault terminates in a cluster of conjugate thrusts (displacement on the order of 0.1 ft) with NW and SE dips, which pass into bedding planes. The layering takes the approximate form of a monocline with axial plane attitude 015/25SE. Offset near the crown is virtually negligible.

1258 240

c. Extent of Fault

Most of what is known about the faults is based on the tunnel exposures. In map view it is known that the faults extend at least 750 ft along strike. The extent of the faults beyond tunnel exposures to the southeast, along the dip, and southwest and northeast along strike is unknown. It might be inferred from the "splay" that the main fault will terminate toward the southwest, and increase in size toward the northeast. How far it goes, and how large the slip becomes, are purely matters of conjecture.

In profile, limited additional information on extent of fault is available from boreholes TX-1 to TX-6 in the intake tunnel, with the most distant of these holes penetrating the fault TX-4 at Station 7 + 44. Based on the assumption of a linear slip gradient, approximately 14 ft of slip was predicted for the fault at the TX-4 location. This figure corresponds to 4.1 ft of predicted vertical offset. Two ironstone bands (key beds) in the TX-4 hole suggest (but do not prove) an actual vertical offset of 3.8 ft, corresponding to about 13 ft of slip (Fig. 1).

A tentative identification of the fault in TX-7 was reported by GAI (Gilbert) (Nov. 78) based on core recovery loss and clay at elevation 245 ft (Fig. 2), although no anomaly was later observed on the WGC (Weston) velocity log. This depth was consistent with a straight-line extrapolation, using the observed fault dip from tunnel exposures and previous borehole data. No fault was later distinctly recognized in the nearby TX-11 hole to elevation

POOR ORIGINAL

-11-

GILBERT ASSOCIATES, INC. SOIL AND ROCK CLASSIFICATION SHEET

PROJECT: P.N.P.P. W.O. _____ SITE AREA _____
CONTRACTOR: _____ COORDINATES _____
DRILLER: _____
CLASSIFIED BY: RTW DATE: 9/15/78

SHEET 18 OF 19
DRILL HOLE NO. TX-4
ELEVATION _____
GWL 0 HRS _____
24 HRS _____

Depth Ft.	Sample No.	SPT Blows/ 6 in.	Ft. Rec.	Profile	DESCRIPTION Density (or Consistency), Color Rock Or Soil Type - Accessories	U.S.C.S.	R.Q.D.	Soil Or Rock		REMARKS Chemical Comp, Geologic Data, Ground Water, Construction Problems, etc.
								Range	Grain	
								Size	Shape	
								Core	Rec.	
85		6 12 18						Run	Core	
					85.0-86.45 - Med. hard, med. gy. shale and siltstone, tr. lt. gy. siltstone					Lt. gy. wash
					"Fe" band @ 85.35'					9/15/78 Man cage accident @ 12:33 p.m. prevented afternoon coring Coring stopped @ 87.0' - Core barrel raised several inches and water left running in hole over night - Coring resumed - 9/18/78 Driller notes starting @ 87.0 - continuing to 88' - Milky gray wash
86					Top of Fault Zone - 86.45'					
					15.5" of recovery over 30.5" of run					
					4" lt. gy. sandy shall					
					4" med. gy. shale					
					3 1/2" Broken, lt. gy. siltstone	80%	5.0		3.65	
					4" lt. gy. sandy shale					
88					Clay remenants in partings and around broken prices					
					Bottom of Fault Zone -- 89.0'					
					89.0-90.0 - Med. hard, med. gy. shale, some lt. gy. siltstone in 1/4" bands					
					"Fe" band @ 89.15'					Lt. gy. wash
90					Long piece - 14"					

POOR ORIGINAL

-12-

GILBERT ASSOCIATES, INC. SOIL AND ROCK CLASSIFICATION SHEET

PROJECT: P.N.P.P. W.O. SITE AREA North Shoreline Bluffs SHEET 8 OF 8
 CONTRACTOR: Herron Testing COORDINATES N 50, 490.93 DRILL HOLE NO. TX-7
 DRILLER: Joe Minarchick E 9, 095.96 ELEVATION 618.1
 CLASSIFIED BY: R. T. Wardrop DATE: 10/12/78 GWL 0 HRS
 48 HRS 99.7"

Depth Ft.	Sample No.	SPT Blows/ 6 in.	Ft. Rec.	Profile	DESCRIPTION Density (or Consistency), Color Rock Or Soil Type - Accessories	U.S.C.S.	R.Q.D.	Soil Or Rock		REMARKS Chemical Comp, Geologic Data, Ground Water, Construction Problems, etc.
								Range Size	Grain Shape	
350		6 12 18						Core	Rec.	
								Run	Core	
350					338.2'-363.6' - Med. hard, med. gy. shale w/some dk. gy. brn. siltstone lam. little lt. gy. sandy shale bands, tr. thin lt. gy. siltstone lam.		29.2%	10.0'	10.0'	Long piece - 5-1/2"
					a) High concentration of siltstone lam. from 350.2'-351					
					b) Thin fissile shale seams @ 362.8' and 364.0'		41.7%	10.0'	10.0'	Long piece - 10"
					c) Clay remnants in partings @ 352.65', 362.8', and 361.6'					
					d) 1/8" seam of pyrite @ 356.5'					
					363.6'-371.3' - Med. hard, dk. gy. shale to med. gy. shale, w/ some dk. gy. brn. siltstone lam. 1/8"-1/2" thk. tr. lt. gy. sand shale, tr. thin siltstone lam.		36.9%	10.0'	9.1'	Long piece - 6 1/2"
					a) X-bedded sandy bands @ 365.95 and 366.3'					365-375' run cored smoothly, yet @ fast rate
					b) Clay rem. in partings @ 368.5'					Driller has very difficult time pulling barrel after 365'-375' run
					c) Seam of thin fissile shale @ 368.4'					
					FAULT ZONE -371.3'-372.4'		57.1%	10.0'	9.96'	Bottom 3' of barrel coated w/1/16 thk. layer of lt. gy. clayey film when retrieved
					10" of core missing (2) 1" core pieces w/clay remnants - pieces do not interlock w/each other or w/core above and below					Long piece - 28"
					372.4'-395.0' - Med. hard, dk. gy. shale w/some dk. gy. brn. siltstone lam., some lt. gy. sandy shale bands, tr. thin lt. gy. siltstone lam.					Drill water getting plugged up in bottom of hole
					a) 4" thk. sandy band @ 380.6' and 6-1/2" @ 386.4'		29.2%	10.0'	9.75'	Pieces 2 1/2"-4"
					BOTTOM OF HOLE 395' (elev. 223.1')					Long piece - 10"
					(b) clay rem. in partings @ 376.5', 379.0', 382.55', 382.65', 383.6', 391.35'					No detectable methane
					(c) Broken seams of rock frags. @ 375.4', 385.05', 392.45' (4"), associated w/clay rem. @ 392.45' and 393.3'					
					(d) Thin fissile seams @ 386.1'					
					(e) Possible "Fe" band @ 394.3'					

-100 (depth 730 ft), despite the fact that improved multiple-tube boring techniques were used so that core-recovery loss would not have been the necessary basis for fault identification. If the fault indeed passes through TX-11, it must do so along a thin bedding plane segment associated with little damage to hanging and foot walls.

A possible bedding plane fault in TX-11 (Fig. 3) may be interpreted on the basis of thin clay seams observed at 470-425 ft and 485-490 ft depths (elevation approximately 140-160 ft). Unfortunately these segments of core were disturbed, e.g. by impact of the flying gas-propelled core barrel on the drill platform, so that the interpretation of broken rock here is not unambiguous. A gas pocket at this elevation would not be inconsistent with a fault interpretation (indications of gas pressure were sporadically observed in TX-11, especially between depths of 310-510 ft). The interpretation is strengthened by the fact that the 155 ft elevation in TX-11 corresponds exactly to a straight-line extrapolation from the known location of the fault in TX-12 and its inferred possible location in TX-7. If this interpretation is correct, the fault extends at least 1150 ft in the dip direction.

Core loss in TX-7 is possibly explicable by drilling technique, and because of the uncertainties associated with TX-7 and TX-11, an alternative interpretation was considered, namely that the fault surface steepens toward the southeast. Drilling of an inclined borehole (TX-12) using a multiple-tube wireline technique was recommended in order to assess this interpretation. The TX-12 hole was drilled from approximately the TX-7 site, but angled 30° toward the northwest. A zone of broken rock and gouge (three seams, 1.5-3 inches thick) was found between depths

POOR ORIGINAL

GILBERT ASSOCIATES, INC.

SOIL AND ROCK CLASSIFICATION SHEET

SHEET 10 OF 14-
 DRILL HOLE NO. TX-11
 ELEVATION 624.04
 GWL 0 HRS
 24 HRS

ACTOR: P.N.P.P. W.O. SITE AREA NE Parking Lot
 Pa. Drilling Co. COORDINATES N 781586.77
 R. Wardrop Jim Adams E 2369,806.12
 ASSIGNED BY: R. Wardrop DATE: 4/25/79

Depth Ft.	Sample No.	SPT Blows/ 6 in.	Fl. Rec.	Profile	DESCRIPTION Density (or Consistency), Color Rock Or Soil Type - Accessories	U.S.C.S.	R.Q.D.	Soil Or Rock		REMARKS Chemical Comp, Geologic Data, Ground Water, Construction Problems, etc.
								Range Size	Grain Shape	
6		12	18					Core	Rec.	
								Run	Core	
460					Med. hard, m. grey, shale interlam. w/ little hard, lt. gy. siltstone, little dk. br. shale - fissil shale seams. 1/4" thick @ 451.5' - load cast horizons @ 451.35'; 454.2'		82%	5.0'	5.0'	Minimal gas bubbling wash in hole - lt. gy. wash w/ occasional brn. influxes - long piece - 18"
					Same, w/ some hard, lt. gy. siltstone lam., brn. shale lam. 1/8" - 1" thick Sandy shale band @ 458.0' - 458.6' (x-bedded) Siltstone band @ 458.85' - 459.15'		83%	5.0'	5.0'	Same wash & gas long piece - 17"
					Same, w/ little lt. gy. lam. & some gy. brn. oily shale lam. 0-3" thick, heavily concentrated in the 463.75' - 465.0' interval		85%	5.0'	5.0'	Same long piece - 14"
470					Same, lt. gy. siltstone band from 465.3' - 465.7' & 466.55' (2 1/2')		83%	5.0'	4.94'	Some long piece - 18"
480					Some, rock shattered from 473.7' - 474.3'. Thin clay seams and fissile shale @ 470.75', 472.85', 474.5' (3/4"). Very thin clay seam @ 471.6'	4/25/79 rx disrupted see Remarks		5.0'	5.0'	Gas blows column of water out of hole. Barrel lifted 20' out of hole when retreated only 1/2 way by wire line - barrel lands on drillers platform greatly disturbing sampled work stopped gas left to bleed off over long piece - 13" night
					Some, shale is med. to lt. gy. w/ trace gy. brn. lam. lt. gy. siltstone band @ 479.4' - 479.85' Fissil shale @ 476.2' (v. thin)		95%	5.0'	4.96'	long piece - 13"
					Same, tr. lt. gy. siltstone lam. w/ one band @ 480.55' tr. of iron staining in thin seam @ 483.4' Load cast horizon @ 481.3'		100%	5.0'	5.0'	Min. gas long piece - 30"
490					Same, some little lt. gy. siltstone lam. little dk. brn. shale lam. lt. gy. x-laminated sandy shale band @ 485.8' - 486.05'	rx disrupted see Remarks		5.0'	4.75'	Barrel pulled to half way retreat when gas raises it up into rotation block. Barrel left there while gas bleeds off over bench. - Upon returning barrel is being repeatedly hammered into rotation block under slightly less pressure
					Fractured rx. w/ clay (probably pulverized rx. from hammering effect) @ 486.05' (1/4") 487.9' (1/4") & 488.4' (1/4")		93%	5.0'	5.0'	long piece - 14"
					Same, tr. siltstone lam., tr. brn. shale siltstone band from 494.6' - 494.9'					Driller pulls barrel slowly allowing hydrostatic head on gas pressure long piece 20"
500					Same w/ some lt. gy. siltstone & sandy shale lam. bands @ 492.8' - 495.50' (x-laminated)		97%	10.0'	9.92'	

of 376.0 and 380.4 ft (elevation approximately 300 ft) which undoubtedly represents the fault zone. This depth corresponds exactly to a straight-line extrapolation from tunnel exposures through TX-4, and therefore no significant curvature of the fault surface is indicated to the 300 ft elevation. Despite excellent core recovery, local stratigraphy could not be used to determine offset. Drilling continued to 420 ft with no further structural disturbances noted. From the data of TX-12, the fault extends along dip with certainty at least 600 ft.

The drill data available at present permit three interpretations:

- (1) The fault terminates between TX-12 and TX-11.
- (2) The fault passes through TX-11 along a bedding decollement perhaps at elevation 140-160 ft.
- (3) The fault steepens between TX-12 and TX-11 (indeed, probably between TX-7 and TX-11) and passes beneath TX-11 giving a minimum average dip angle between TX-12 and TX-11 of 36° .

Hypothesis (3) is weakened (but not ruled out) by the lack of any significant concave-downward curvature between the tunnel exposures and TX-12. Hypothesis (2) is enhanced by the straight-line correspondence of fault elevations between the tunnel exposures and boreholes TX-1 to 7 and TX-12, and by the offset suggested by TX-4.

1241 246

d. Mutual Geometric Relationships

The three tunnel fault structures display similar deformational style, magnitude of slip, slip gradient, moderately brittle deformational mode, and are clearly genetically related. The main discharge tunnel fault is very nearly on strike (044°) with the intake tunnel fault. The two exposures are in many respects virtually identical, and interpretation in terms of a "single fault" model is reasonable. (In an alternative model the two structures are considered as separate elements in an en-echelon system). The Station 11 + 50 discharge tunnel structure strikes so as to intercept the main discharge tunnel fault. Because of its smaller slip magnitude, it is interpreted as a splay fault to the main discharge fault.

Similar slip gradient on all three fault exposures (Fig. 4; data were taken from the tunnel maps prepared by Weston), and the observed termination in the discharge tunnel, suggest that the structures have propagated from some lower elevation. This conclusion has a bearing on genetic interpretation. Furthermore, the slip gradient (about 4 ft of slip per 100 ft of fault) suggests that the principal intake and discharge tunnel faults will terminate within about 40 ft or so of the tunnel crowns as measured along the fault surfaces, or within roughly 20 vertical feet above the crowns. The faults therefore should not reach the elevation of the lake bottom. In this light the Lake Erie bottom video survey results seem understandable.

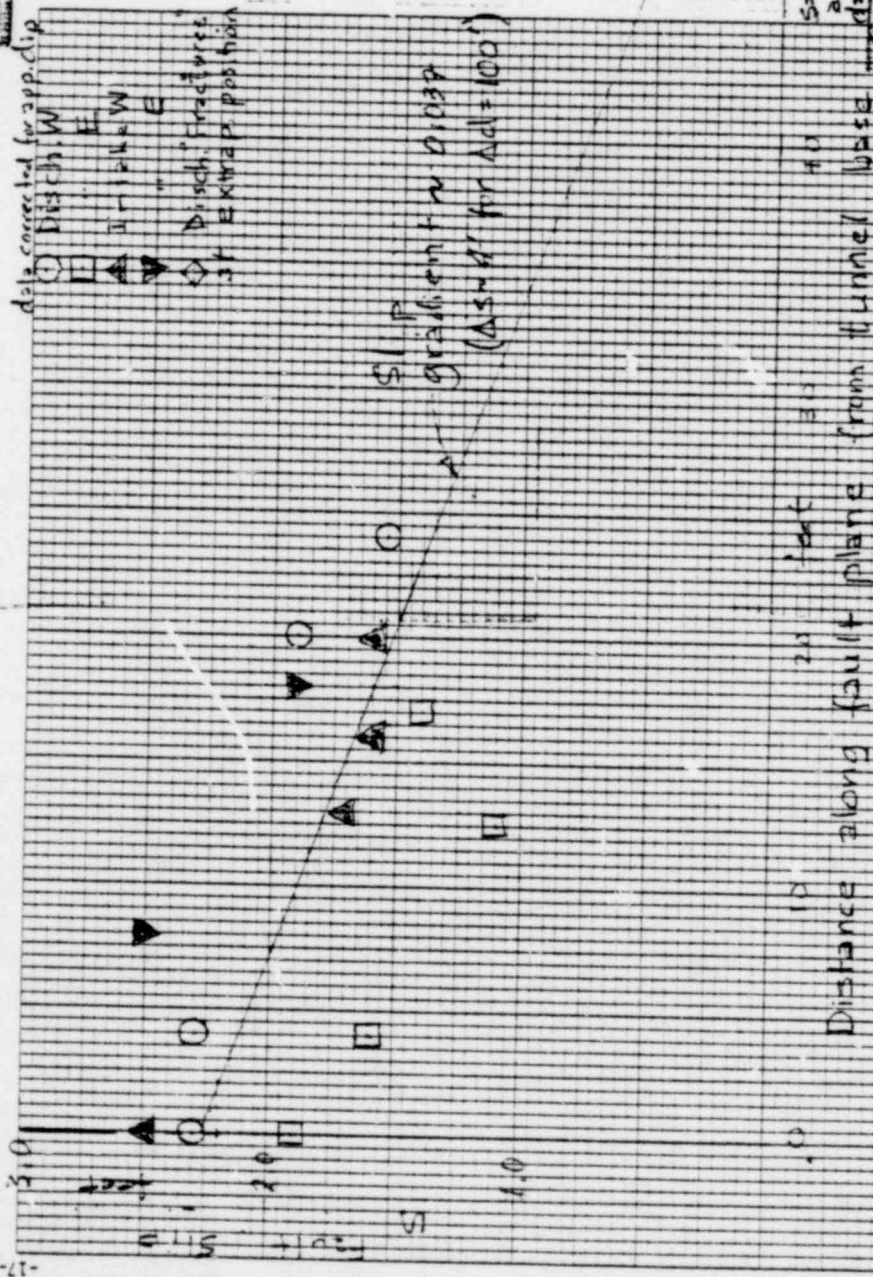
The discharge tunnel "splay", if projected eastward, intercepts the intake tunnel. No such structure was observed in

POOR ORIGINAL

EUGENE DIEZGEN CO.
MADE IN U.S.A.

EUGENE DIEZGEN CO.
MADE IN U.S.A.

NO. 340-10 DIEZGEN GRAPH PAPER
10 X 10 PER INCH



the intake tunnel, which indicates that either the entire splay dies out towards the southwest, or that it is present below the intake tunnel but has terminated on an elevation below the intake tunnel invert. Either interpretation is consistent with observed evidence.

1241 249

4. AGE OF FAULTING

Based on test results and visual observation the gouge is classified in soil mechanics terminology as a gray, stiff to very stiff silty clay with abundant sand and gravel-sized soft friable shale fragments.

Consolidation tests were conducted on two relatively undisturbed samples from the Intake Tunnel, and on one remolded slurry specimen. Plasticity limits and compression indices were similar for all three samples. Details are given in the Woodward-Clyde report of July 5, 1979, in Appendix VII.

Maximum past consolidation pressure (P_c) was estimated for two samples of the gouge by the standard methods of Casagrande (1936) and of Schmertmann (1955). The results are summarized as follows:

Sample	P_c (tsf)		Cc' (unit strain)	PL	LL
	Casagrande	Schmertmann			
I-2	8.0	12.0	0.110	18	27
I-4	4.5	6.0	0.112	19	28

The agreement of the two methods is considered satisfactory, and on the basis of these results the maximum past consolidation pressure of the gouge is taken as about 9 ± 4 tsf (say 125 ± 55 psi). For comparison, consider that the tunnel depth at the fault locality is about 110 ft. Ignoring the 15 ft of lake water above the top of rock, the corresponding total vertical pressure is about 119 psi (8.6 tsf). Average effective vertical pressure, assuming a standard

. 1241 250

fluid pressure-overburden ratio of about 0.4 is 71 psi (5.1 tsf). (The fluid pressure gradient assumed is about 0.43 psi/ft). This value falls near the lower limit of the estimated range of uncertainty for maximum past consolidation pressure. On these grounds, while one could not conclude with certainty that the fault gouge was subjected to greater vertical pressure than that existing at the present time, the results suggest such a possibility.

If it is assumed that, because of erosion, present overburden thickness at tunnel level is less than the maximum value of overburden to which the fault at tunnel level had once been subjected, a vertical pressure of perhaps 6-9 tsf can be postulated for tunnel level under lake level conditions similar to those at present. If a prehistoric decrease in pore pressure is postulated, e.g. associated with lake drainage prior to the establishment of Early Lake Erie (470-ft level) at 12,000 YBP, maximum overburden pressure can be increased to about 9-12 tsf. The entire range of values (6-12 tsf) is consistent with gouge data.

The maximum past consolidation pressure estimated by the Casagrande method for upper and lower tills at the PNPP site is 4.3 tsf (average of 3 tests; range 4.0-5.0 tsf) and 6.0 tsf (average of 10 tests; range 4.3-10.0 tsf). (Appendix 21, Foundation Investigations and Design Analyses, PNPP).

The results indicate that both tills have been consolidated in the geologic past to pressures well in excess of the pressure imposed by present overburden (about 1 tsf). The probable loading mechanism is glacial ice.

124d 251

Assume for the moment that the tunnel fault was present at the time the lower till was subjected to its maximum consolidation pressure of about 6 tsf. This corresponds to an ice sheet at least 200 ft thick. Pressure at tunnel level was about 5 tsf more, and eroded rock and till could account for about 1 tsf, for a total of 12 tsf.

This is within the range of consolidation test results for the gouge, and it could be argued that the gouge and lower till were subjected to maximum consolidation loads by the same event. The argument is strengthened by lending more weight to the Schmertmann-method calculations (which seems reasonable), or by assuming a higher fluid pressure-overburden ratio for the gouge.

A consistent argument can also apparently be given in regard to the maximum past consolidation pressure sustained by the upper till (4 tsf) to which must be added 2 tsf for assumed intervening till and 5 tsf for rock overburden. The estimated total of 11 tsf at tunnel level falls within the range of uncertainty for P_c of the gouge.

These arguments are summarized as follows:

- (1) Hypothesis: Maximum consolidation pressure for fault gouge corresponds to present overburden.

Result: Pressure estimate at tunnel level is 5 tsf,
near lower limit of range of uncertainty for P_c .

Interpretation: Hypothesis cannot be rejected but
additional pressure mechanism seems likely.

1254 252

- (2) Hypothesis: Maximum consolidation pressure for fault gouge corresponds to conditions of pre-existing overburden or pre-existing groundwater conditions.

Result: Pressure estimate at tunnel level is 6-12 tsf, consistent with estimated values for P_c .

Interpretation: Hypothesis cannot be rejected.

- (3) Hypothesis: Maximum consolidation pressure for fault gouge corresponds to maximum pressurization of lower till.

Result: Pressure estimate at tunnel level is 12 tsf, near upper limit of data range for P_c .

Interpretation: Hypothesis cannot be rejected.

- (4) Hypothesis: Maximum consolidation pressure for fault gouge corresponds to maximum pressurization of upper till.

Result: Pressure estimate at tunnel level is 11 tsf, within range of uncertainty for P_c .

Interpretation: Hypothesis cannot be rejected.

The radiocarbon date of $14,480 \text{ YBP} \pm 310$ derived from the lacustrine sediments over the upper till suggests that the upper till is at least as old as Hiram Till (14,500 YBP). (GAI Report No. 1997, Nov. 7, 1978). Compression of the Hiram Till could be accomplished by an ice sheet associated with the Hiram advance or by a younger ice sheet, corresponding to the Ashtabula Till (13,000 YBP). The lower till may represent the first part of an advance-retreat glacial deposition couplet, in which case it could correspond to the Hiram

1248 253

advance, or it may represent a separate late Wisconsinian movement. In the latter case, it could correspond to Lavery Till (16,500 YBP).

The late Wisconsin maximum is associated with Kent Till about 21,000 YBP with an end moraine 70 miles or so south of the PNPP site. Sugden (1977) suggests a thickness for this Laurentide Ice Sheet of 1 km at the PNPP site. Comparable advances also occurred during the early Wisconsinian (Titusville Till, ca. 40,000 YBP), the Illinoian, and perhaps pre-Illinoian (Lessig and Rice, 1962) times. The increase in overburden pressure associated with a 1 km thick ice sheet is on the order of 100 tsf. It is difficult to conceive of circumstances that would prevent such events from leaving a marked imprint on gouge consolidation characteristics, even granting uncertainty in the selection of appropriate fluid pressure-overburden ratios and some redistribution of stress in the vicinity of the fault. I conclude that the formation of fault gouge was to a large extent, and perhaps exclusively, associated with faulting younger than the Kent advance. For similar reasons exclusively Paleozoic or early Mesozoic faulting can be rejected; several thousand feet of overburden corresponds to an effective overburden pressure on the order of 100 tsf. The possibility of incremental fault propagation is not excluded, but this discussion is focused upon the last fault movement capable of forming new gouge or significantly disturbing pre-existing gouge.

1249 254

On the above grounds, assuming the data as representative, the tunnel fault reflects significant movement younger than about 20,000 YBP. The data are consistent with compression of fault gouge by a lesser ice sheet than that associated with the Laurentide maximum. Three candidate ice sheets are associated with Lavery, Hiram, and Ashtabula Till. The youngest of these is about 13,000 YBP suggesting that if the fault is related to a glacial mechanism, its age is probably in the range 13,000-20,000. But the mechanism of faulting is uncertain, so the 13,000 age is not a firm lower bound. The hypothesis that maximum gouge consolidation pressure corresponds to present overburden and fluid pressure cannot be wholly rejected by consolidation test data, but the data suggest the operation of additional effective vertical pressure mechanisms. Drainage of the rock mass at about 12,000 YBP yields a more consistent predicted pressure, as does the assumption of a greater prehistoric thickness of overburden. But lacking adequate data on erosion rates it is not possible to be very precise in the matter of a lower-bound age on these grounds. I would judge the minimum age to be on the order of several thousand years, but this is merely a guess. However, rock stress orientation information (to be discussed in the following section) suggests that the fault developed under different stress conditions than that in evidence today. On these grounds a lower bound of about 10,000 YBP is proposed. Finally, it would not seem surprising if, over the past ten thousand years or so the gouge developed a few cracks, and mineralization in extremely small amounts (such as reported by WCC) occurred within them.

1241 255

This estimate of the age of the last movement of the fault differs by two orders of magnitude with a "minimum age" estimate of 1,000,000 yr offered by WGC, based on rate of microfracture "healing". However, the lack of agreement is not disturbing to me because I do not believe that there is an adequately demonstrated basis for the "mineral growth vs. time function" proposed by WGC for the PNPP site. Inasmuch as this function forms the foundation for the WGC age estimate, the accuracy of the WGC inferred age is open to serious doubt. By the same token, the age of faulting as based on the consolidation tests reflects certain specific assumptions regarding boundary conditions and material behavior. Error is possible to the extent that actual behavior differed from that assumed. These aspects are discussed below:

(1) There is considerable precedent in the use of consolidation tests to establish past consolidation pressure. The adequacy of the method has been tested in civil engineering practice (e.g., Casagrande and Fadum, 1944; Zeevaert, 1953; Schmertmann, 1955). There is also precedent in the interpretation of past consolidation pressure in terms of geologic history, and in instances in which the maximum past consolidation pressure has been reliably determined by geologic evidence or other independent means, agreement between the actual maximum past consolidation pressure and that determined by consolidation tests on "undisturbed" samples has been quite satisfactory (Terzaghi and Peck, 1967, p. 77). There is also precedent for quantitative determinations of ice sheet thickness

from consolidation test data, both in Europe and in North America (e.g., Kogler and Scheidig, 1948; Dücker, 1951; Harrison, 1957, 1958).

(2) The "sealed" block samples, from which the test specimens were prepared, sustained moisture loss during storage. The effect of water loss is commonly to produce intergranular stresses within the samples, which could lead to an overestimated value of past consolidation pressure. In the present instance no interpretive problem arises from this possible effect.

(3) Lateral strain and squeezing of gouge at the time of faulting seems likely. Therefore the early strain history of the gouge may be described as complicated. However, the strains associated with subsequent vertical loading conditions, such as burial by ice, meet the standard assumptions associated with consolidation testing. The assumption of zero lateral strain associated with ice sheet compression seems valid, at least to a reasonable approximation.

(4) Because fault gouge exhibits a complicated strain history, it is possible that its past-fault consolidation characteristics are not necessarily identical to those of similarly-graded sediments of different origin. There is little information in the published literature to directly assist interpretation of the matter of fault gouge consolidation. On the other hand, silts of similar grain size gradation which have been contorted by the directional drag of overriding ice have been subjected to consolidation testing, and glacially-induced distortion of this kind seems reasonably analogous to disturbance by

1241 257

faulting. The directional stresses and associated strains in such disturbed silts were shown by Harrison (1958, p. 77) not to have affected the maximum past consolidation-pressure value induced by the thickest over-riding ice sheet.

(5) Pore water under pressure must be permitted to drain away during consolidation. The hydrostatic pore pressure distribution observed in most boreholes in shale in and near the PNPP site lend support to this assumption.

Because of the drainage factor, there may also be an effective upper limit to the distance from a glacial margin over which past consolidation pressures can be accurately determined (Harrison, 1958, p. 77). But in Indiana, this distance seems to be no smaller than about 30 miles (associated past consolidation pressures are about 50 tsf) (Harrison, 1958, p. 81, 83), suggesting that this factor does not pose a problem.

(6) Is the gouge so old that soil mechanics tests are no longer applicable, e.g., has the bulk material sustained changes due to aging such that consolidation characteristics have been altered? The answer appears to be, no. Successful preconsolidation estimates by consolidation tests have been conducted on materials of Tertiary age. Tillis and lake silts overridden by four oscillations of the Wisconsin ice margin were subjected to consolidation tests by Harrison (1958), and the past consolidation pressures thus established were used to reconstruct a paleoglacier map of the vanished East-White sublobe of central Indiana. There is no indication of diagenetic changes or

significant chemical changes in the gouge material that would significantly alter consolidation properties. Further indication is that compression indices for undisturbed and slurry samples are identical. The consolidation behavior of the surface tills (which are also comprised mainly of comminuted shales) is similar, and the past consolidation pressures established by consolidation tests of tills are consistent with the data obtained from tests on fault gouge.

(7) The bulk laboratory samples were not specifically orientated, but the prepared consolidation test samples are considered to be approximately horizontal ($\pm 15^{\circ}$) based on bulk sample shape and size and location sampled.

(8) As described in Section 3 of this report, the fault itself is not horizontal, but is comprised of a series of irregular steps with local dips varying from zero (parallel to bedding) to about 20° on riser surfaces. Gouge thickness is not uniform. One may therefore question whether or not the maximum pressure exerted by overburden and an overlying glacier is transmitted everywhere to the gouge, because of "arching" (stress concentration) effects.

My personal opinion is that severe arching effects associated with the distribution of vertical pressures in this case are extremely local. The slight average dip of the fault surface ($15-17^{\circ}$) does not favor the development of vertical stress arching over large domains. (Horizontal stresses may be a different matter entirely). The shale strata of the hanging wall have been disturbed (fractures, splays,

etc.) to distances as great as 10 feet as measured perpendicular to the fault surface. The shale is wholly thin bedded, and there is evidence that the shear strength parallel to bedding is small. Evidence for bedding plane slip is observed where minor bending has occurred. Splay faults and fractures are common; thin gouge seams are associated with the fractures. The hanging wall rock mass is therefore weak and very flexible.

Therefore the capability of the bulk material to sustain significant horizontal shear stresses as required in order for significant arching to occur seems slight. Those portions of the fault zone characterized by broad patches of gouge, several feet long and several inches thick, are thus likely to be subjected to, at least to a first approximation, full overburden pressures.

The consolidation results themselves lend some support to this view. The gouge consolidation tests are internally consistent in that two separate samples from different locations produced results that are in good accord, with respect to consolidation behavior and past consolidation pressures. They are externally consistent in comparison to calculations considering present overburden pressure, and to pressures inferred from extensive consolidation testing of near-surface glacial tills. The burden of proof would seem to reside with those who might doubt the gouge results because of the possibility of non-representative behavior associated with arching. Further sampling and testing is of course possible, although only at considerable effort and expense.

1251 260

To conclude this section, it must be acknowledged that not all possibilities for error have been absolutely eliminated. Still, on balance, in my opinion the best available estimate of the age of the last movement on the fault is that provided by interpretation of the consolidation test data for the fault gouge. Accordingly, the last movement of the fault probably occurred no more than 20,000 yr ago, and the age for this last movement is estimated at 15,000 YBP \pm 5000.

1241 261

5. ROCK STRESS INVESTIGATIONS

a. Orientation and Magnitude of Stresses

A program of stress measurements was strongly recommended, because I considered it incautious to select or render judgment on design details to ensure safety against possible fault displacement without adequate information on rock force fields.

The test program was carried out at my recommendation by J.C. Roegiers and associates using the hydrofracturing technique. I was at the PNPP site at the time the measurements were carried out at TX-11 and I am satisfied that the results obtained represent a state of the art capability.

This discussion is based on the data contained in the preliminary report by J.C. Roegiers and J.D. McLennan, dated July 1979, and subsequent telephone conversations. Details of the stress investigation are given in Appendix IV, and a summary of results is provided in Table 1.

The direction of maximum compression is east-northeast. The result on stress orientation was not wholly unexpected because stress orientations in western New York and southern Ohio were known to display similar trends (Fig. 5). Specific tests at the PNPP site were nonetheless considered necessary in the interests of safety. Figure 6 is a sketch map which illustrates the relation of the tunnel fault and other structures to various stress fields. Stresses at (a) and (b) refer to stress orientations theoretically associated with a northeast-striking thrust with (a) the condition just prior to faulting, and (b) the condition after faulting has occurred,

Table 1. Hole TX-11: Summary of Stresses for Hydrofracturing Data.

Hydraulic Fracture Identification	Fracture Horizon (ft)	P_o (psi)	σ_3 (psi)	σ_2 (psi)	σ_1 T=Lab (psi)	T=Field (psi)	T=1000 (psi)	σ_2 (selected (psi)	σ_1 average) (psi)	θ_1 (deg)	$\sigma_{H,F}$ (psi)
1	718	311	796	1061	1971	--	1931	1061	1951	--	1230
3	654	283	733	1023 823	1943 1343	1413 813*	1643 1043	923	1367	080	1030
4	514	266	686	906	--	1281	646*	906	1281	067	
5	574	249	634	849	929	1033	29*	849	981	100	930
6	511	221	586	921 721	1246 646*	-- --	1826 1226	821	1526	94	1150
7(a)	454	197	577	1137	1987	1917	1947	1137	1950	37	1170
(b)	pre-existing joint assumed: 730 min							730 min	1450 max	085	970 min
8(a)	394	171	411	971 551	1881 681	-- --	2096 836	761	1358	--	870
(b)								971	1988	--	1150

Note: $\sigma_{H,F}$ indicates calculated total horizontal stress in plane perpendicular to tunnel fault.

θ_1 is azimuth of σ_1 axis; 076° assumed for Fractures 1, 8 in calculating $\sigma_{H,F}$.

8(b) based on assumption $\sigma_2 = 971$. Asterisk indicates σ_1 values impossibly low.

POOR ORIGINAL

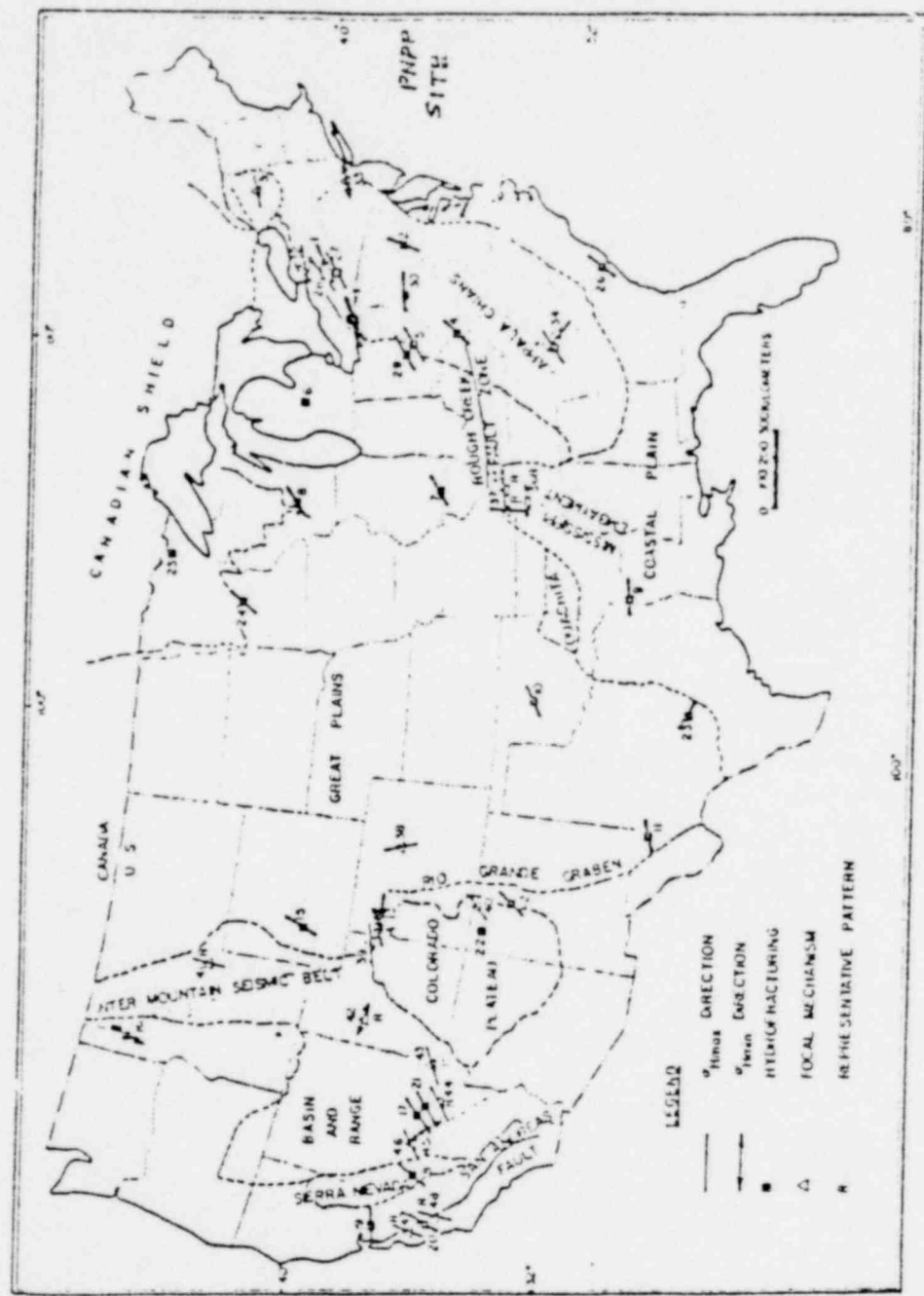


Fig. 5

1241 264

with the northwest stress system diminishing to some residual value. The northeast stresses remain relatively unchanged, but because in (b) they are greater than the relaxed northwest stresses, the assignment of principal stresses changes. As a result of faulting, the assignment of σ_1 is changed from the northwest to the northeast. Still, the two principal stresses in map view are orientated perpendicular and parallel to the fault strike, for both conditions (a) and (b).

The measured stress orientations in the hydrofracturing program suggest an average azimuth for σ_1 of 076° ; neglecting the measurement of Fracture 7, the mean value is 085° , and the range of four values is 067° to 100° .

At face value the 085° orientation of σ_1 is evidently not compatible with the formation of an 050° thrust either by the analogy in Fig. 6 of (a) or (b), by directed pressure or stress-relaxation. There is no evidence of strong anisotropy in the rock mass which would permit structures to form at high obliquity to principal stresses. The present 085° orientation of σ_1 thus suggests that the local stress system formerly associated with the development of the tunnel fault has been altered. The stress field at the PNPP site closely corresponds now to a regional field that apparently extends from the upper Mississippi Valley area to New York. The tunnel fault is therefore considered to be older than the age of this regional stress system. Without doubt Pleistocene ice loading profoundly altered the stress systems in the upper crust, and the present stress system is considered

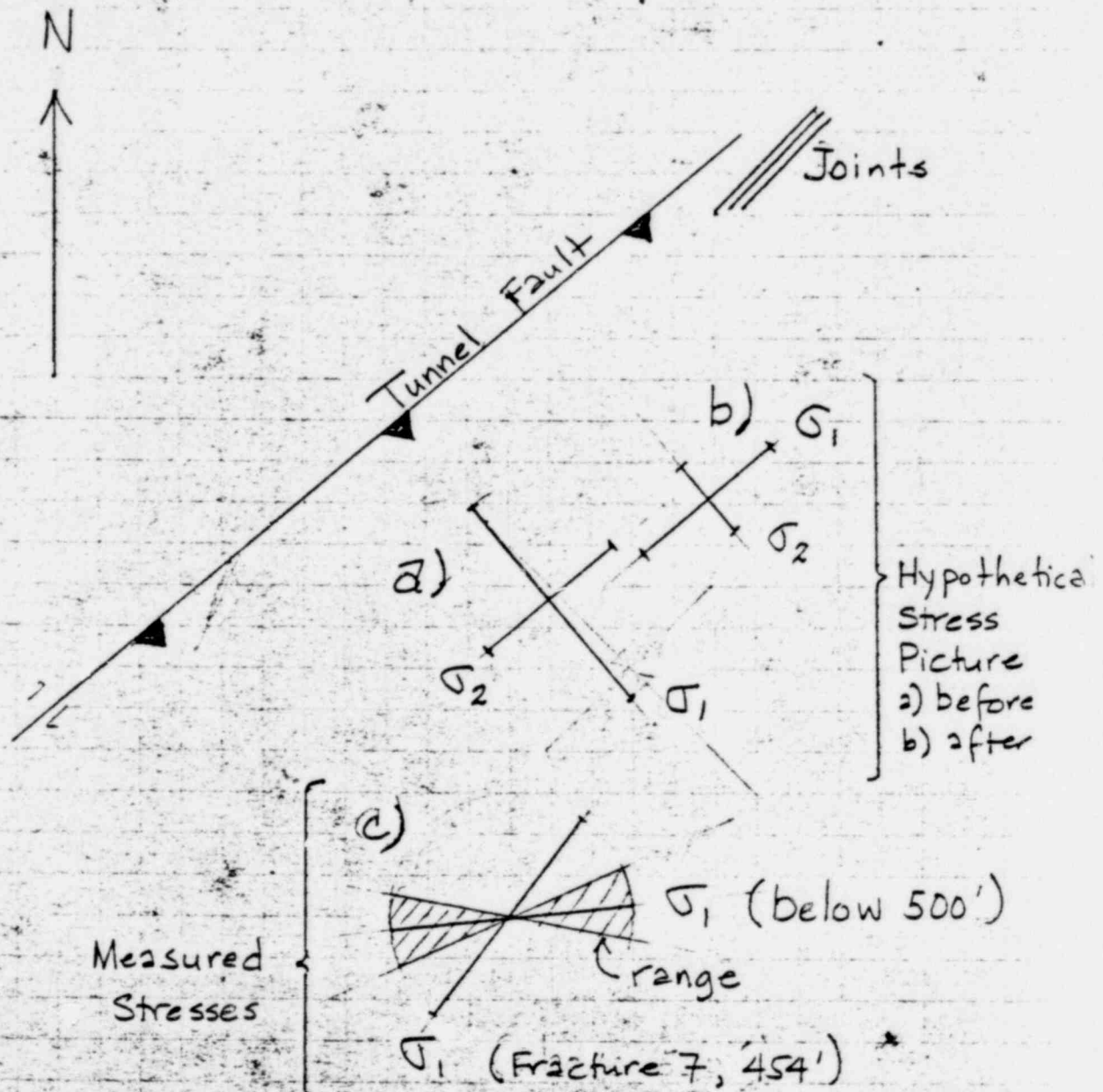


Fig. 6

1250 266

to have developed following retreat of the ice sheet. A stress system associated with ice-deformed crust seems consistent with that inferred for the tunnel fault. A minimum age for faulting is therefore suggested, viz. on the order of 10,000 YBP. This is consistent with the interpretation of fault age based on gouge consolidation tests, and leads to an estimated age of 10,000-20,000 YBP.

The poorly defined fractures at 037° indicated for Fracture 7 differs from the 085° average from Fractures 3-6. This orientation permits an interpretation in terms of Figure 6(b), with 037° not greatly different from the strike of the tunnel fault. Fracture 7 lies above the proposed intersection point of the tunnel fault with TX-11, so that it may be possible to formulate an argument in regard to behavior of the hanging wall as distinct from the foot wall. On the other hand, it may be simplest to interpret Fracture 7 as influenced by pre-existing joints. The pole maximum of 220 foundation joints as compiled and plotted by WGC is associated with 044° , with 037° lying within the range of significant pole concentrations, e.g. $026-054^{\circ}$ (Fig. 7).

Details concerning stress magnitudes must be interpreted with caution due to complex fracturing sequences associated with hydrofracturing. These sequences renders difficult the estimation of instantaneous shut-in and breakdown pressures. Some uncertainty must therefore be attached to the individual principal stresses σ_1 and σ_2 calculated from these selected critical pressures.*

* σ_1 and σ_2 are assumed to be in the horizontal plane.

JOINT ORIENTATIONS -37-
from FOUNDATION BEDROCK
Geology
Perry NPP
C.I. = 4%
n = 220
90°

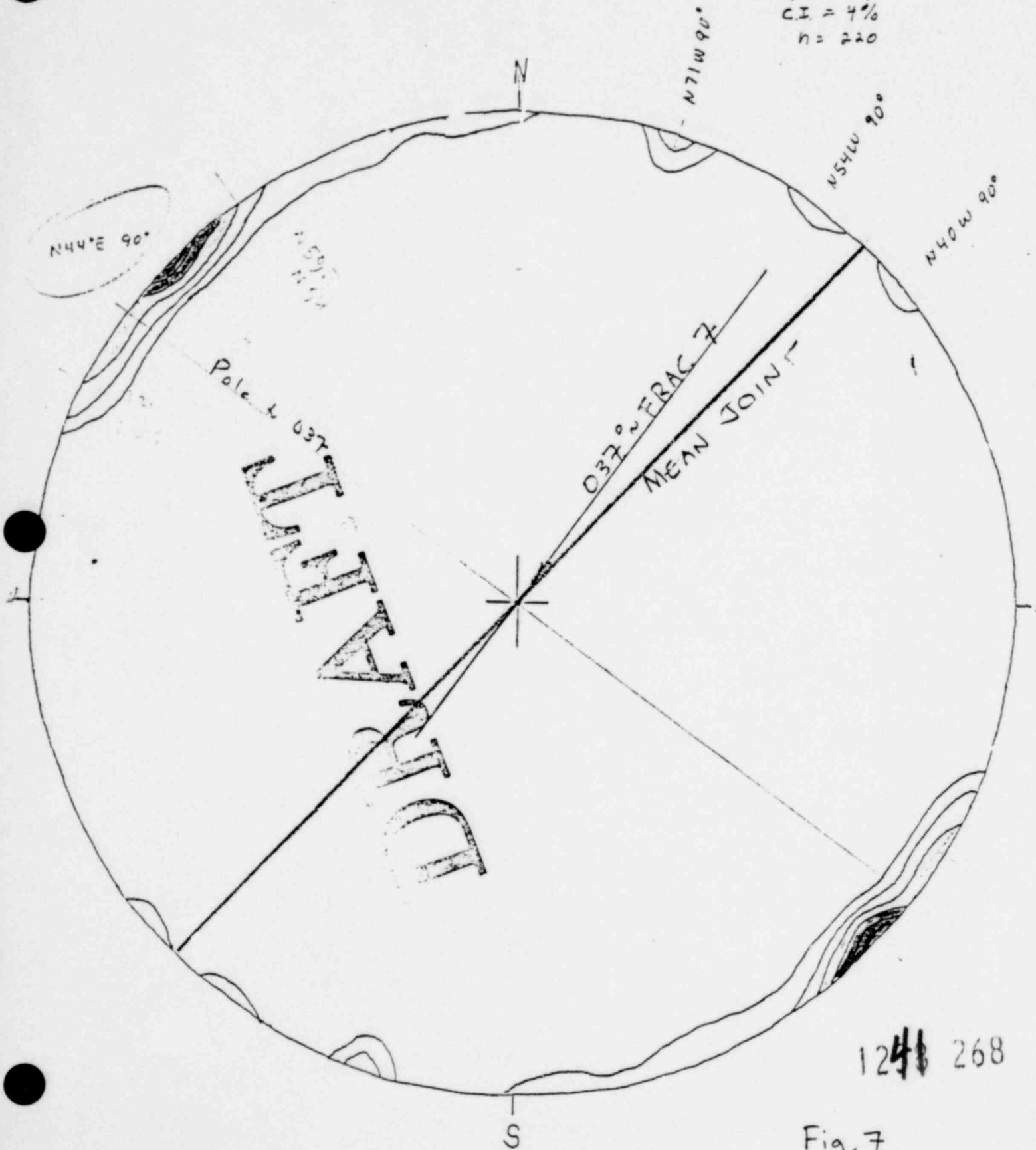


Fig. 7

The average values probably give a true indication of average stress conditions at the site. For the full depth range of 394-718 ft, and rounding off values to the nearest hundred psi:

maximum horizontal stress = 1500 psi = σ_1
 minimum horizontal stress = 900 psi = σ_2
 vertical overburden stress = 400-800 psi = σ_3

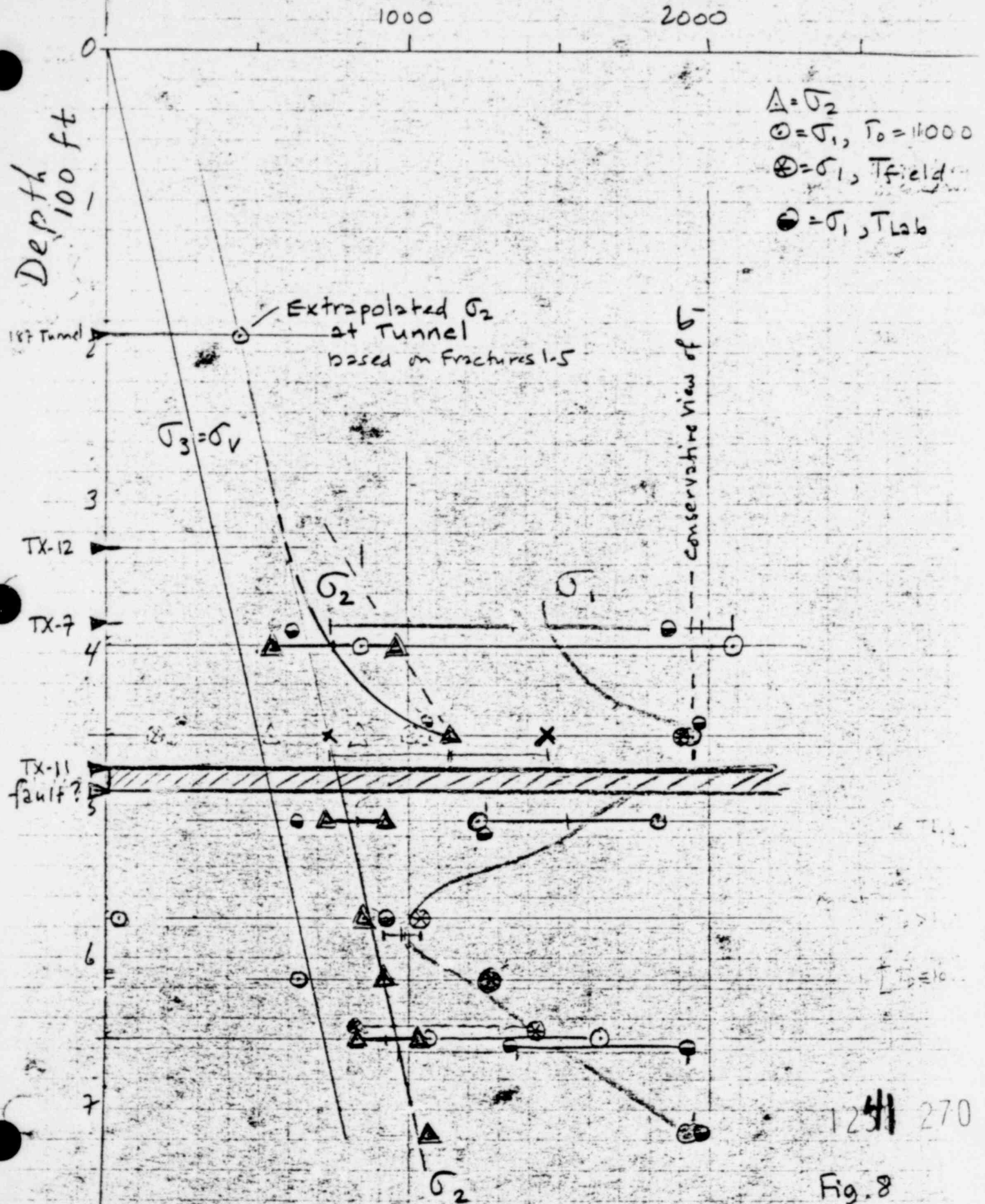
Similar values have been determined in other engineering and mining sites (including nuclear power plants) in Ohio, New York, and southern Canada.

Furthermore, despite uncertainties associated with individual measurements, certain trends seem to possess validity. The gradient of σ_2 below about 500 ft seems to parallel that for overburden pressure, such that approximately $\sigma_2 = \sigma_v + 250$ psi (Fig. 8). Some uncertainty must be attached to the Fracture 7 calculations; tabulated values based on $\sigma_2 = 1137$ are considered as upper bounds. If the orientation of Fracture 7 is considered controlled by pre-existing fractures, with actual σ_1 oriented at 085° , a range of values seems compatible with the data, viz. $\sigma_2 = 730-1137$, $\sigma_1 = 1450-1137$. Despite this uncertainty, Fractures 7 and 8 suggest possibly greater values of σ_2 than at lower levels; higher than average σ_1 values are also evident for Fractures 6-8. To a certain extent σ_1 reflects the selected values for σ_2 , so that trends exhibited by the two principal stresses are not wholly independent.

Extrapolation of stress values to higher elevations is uncertain because of the apparent increase in stress between 511 and 394 ft. Estimation of σ_2 above 394 ft based on extrapolation of

POOR ORIGINAL Stress, σ , τ , psi

-39-



the data trend from Fractures 1 to 6 is considered to be a lower-bound. Upper-bound values are not clearly defined.

The reason for the apparent increase in stresses at and above 511 ft is not clear. One possibility, however, is that the tunnel fault indeed passes through TX-11 between Fractures 6 and 7. Higher horizontal stresses could therefore be interpreted as stress concentrations associated with this fault. One alternative possibility is to consider the high values as stress concentration effects below a downward-terminated stress-relief fault.

1291 271

b. Possibility of Future Slip on Existing Fault

Consideration of this important matter is examined by comparing rock stress information to rock strength.

The value of horizontal stress in the vertical plane perpendicular to the tunnel fault ($\sigma_{H\perp F}$) was calculated from selected stress values and θ_1 orientations as given in Table 1, assuming an 050° azimuth for the tunnel fault. Subtracting out formation pressure, effective stress values for the vertical plane perpendicular to the tunnel fault (σ'_V , $\sigma'_{H\perp F}$) are given in Table 2 and plotted in Figure 9. The average value of the horizontal effective stress $\sigma'_{H\perp F}$ is about 800 psi.

Stresses for Fractures 6-8 are greater than those for Fractures 1-5; the trend appears similar to that previously discussed for principal stresses. The specifics for Fracture 7 are uncertain, depending on interpretation of the 037° fracture orientation. Accordingly, $\sigma'_{H\perp F}$ for Fracture 7 could be as low as 669 psi.

Extrapolation of stresses to shallow elevations is uncertain. Data for Fractures 1-5 permit a lower-bound estimate. A reasonable estimate would appear to be the average of stresses calculated for Fractures 7 and 8. An upper-bound is not well defined.

Vertical effective stresses are given by average overburden pressure in psi (taken as $1.1 \times \text{depth in ft}$), subtracting out formation pressure (Table 2).

Consolidated-undrained triaxial compression tests with pore fluid pressure measurements, or other test methods appropriate for measuring the effective stress strength parameters, were not

Table 2. Summary of Effective Stresses in Vertical Plane Perpendicular to Tunnel Fault

Hydraulic Fracture Identification	σ'_V (psi)	$\sigma'_{H_{\perp F}}$ (psi)	
1	479	919	
3	436	747	
4	409	664	
5	382	681	
6	341	917	
7(a)	302	973	
(b)		668	
8(a)	262	699	
(b)		979	
TX-12	226	836	Average of 7,8
Tunnel Level (a)	69	836	Average of 7,8
(b)		400	Lower-bound extrapolation

1241 273

Stresses in Vertical Plane
perpendicular to tunnel fault

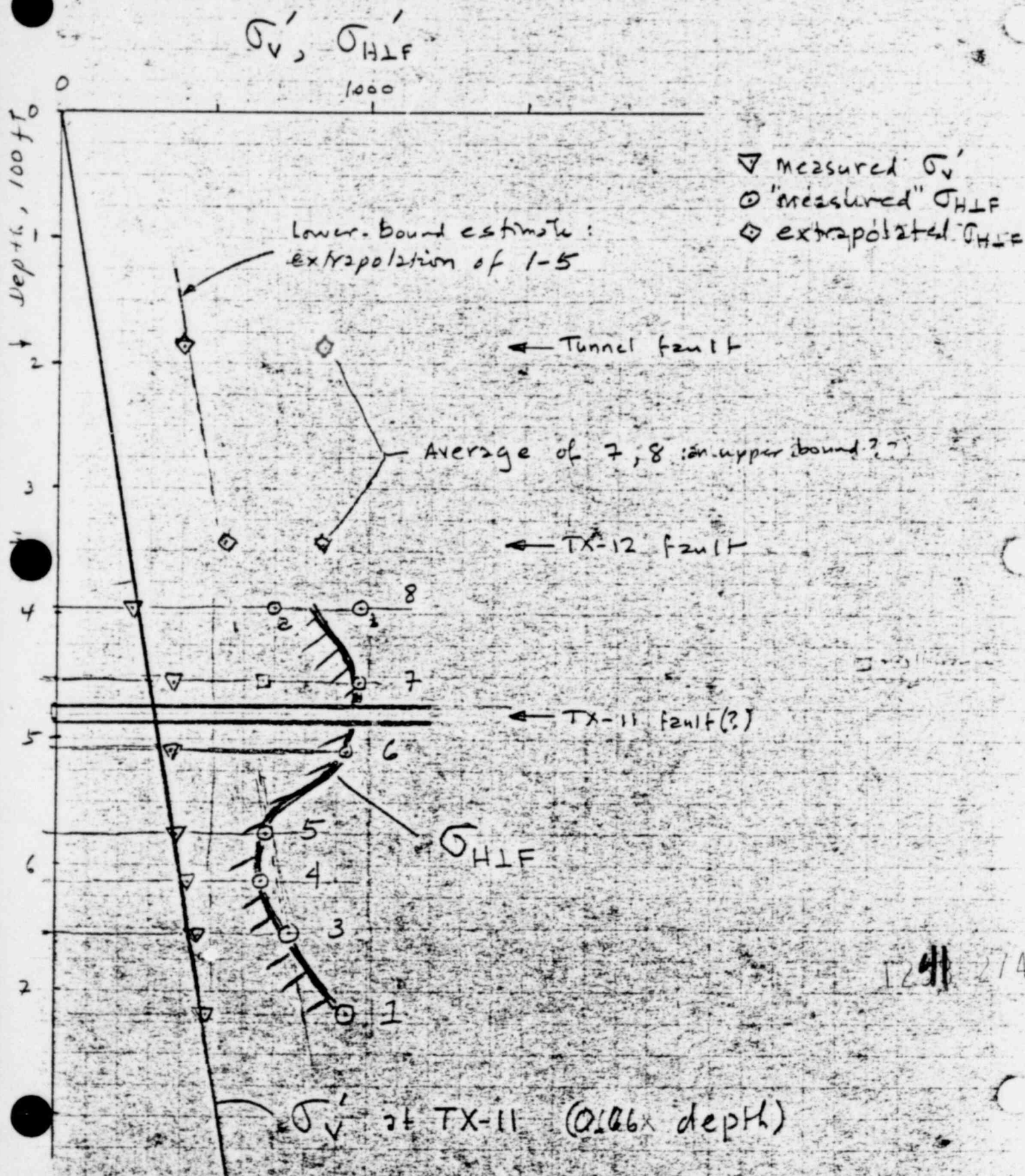


Fig. 9

conducted owing to lack of suitable samples. The effective angle of internal friction for the fault gouge has been estimated at $30-37^{\circ}$ based on published correlations (Woodward-Clyde Consultants, letter of November 20, 1978). This is also consistent with plasticity limit correlations (Voight, 1973). The increase of apparent friction angle at low confining pressures associated with roughness of the fault surfaces is estimated at 10° .

A conservative estimate of strength for a given segment of the fault zone is given by zero-cohesion envelopes inclined at $40-47^{\circ}$ in a shear stress-normal stress diagram. These envelopes are lower-bound estimates inasmuch as additional strength may be obtained, e.g. through cohesive resistance.

These strength envelopes are plotted in Figure 10 along with Mohr circles which represent assumed conditions in the vertical plane normal to fault strike. For each circle, the overburden stress and an estimate of the $\sigma'_{H\perp F}$ horizontal stress is plotted. All stresses are "effective" values corrected for fluid pressure. Numbers attached to the stress circles are hydraulic fracture identification numbers. In addition, stress circles are estimated for the 335 ft level, corresponding to the tunnel fault positively identified in the TX-12 borehole, and for tunnel level. Minimum normal stresses which correspond to observed and inferred fault depths (in various boreholes) are noted on the horizontal axis.

Results are as follows. Stresses associated with Fractures 1-5 permit construction of a stress envelope well below minimum strength. The stress circles associated with Fractures 6-8, which

1248 275

POOR ORIGINAL

Fig. 10

Hyd. pressure
40°

Tunnel Fault + Low-Confining pressure
Strength Envelopes

Min. stress
1-5

TX-12

Tunnel

Effective Normal stress, 100 psi

TX-7
TX-12

Tunnel

Shear stress, 100 psi

include conservative stress estimates, are larger in diameter but lie within the field of stability. These circles bracket conditions for the possible location of the tunnel fault in TX-11. Similar stresses are predicted for TX-12 at fault depth, using the average stress value from Fractures 7 and 8, as a conservative estimate of σ_{H1F} . The TX-12 circle therefore also lies within the field of stability. The inferred stress circles for tunnel level lie approximately tangent to the minimum strength envelope (lower-bound stress estimate) or slightly above it (more conservative stress estimates). This suggests that either the lower-bound stress estimate is correct, the actual strength envelope is positioned somewhere above the minimum strength envelope, or both. Indeed, the second argument is probably true.

The conservative interpretation is to suggest that stresses along the tunnel fault may be relatively marginal in terms of strength for a limited range of depth, viz. about 100-200 ft.

Below elevation 300 ft stresses are less than minimum strengths, so that the fault plane may be considered to be "clamped" by friction. From this viewpoint no motion seems possible below elevation 300 ft, and if so it may be academic whether or not the fault terminates between TX-12 and TX-11 or passes through TX-11.

Above the 100 ft depth the fault terminates, and a buttress of relatively less deformed bedrock perhaps 70 ft thick is inferred to be present between this termination and the lake bottom. Rupture of this buttress would require stresses measured in thousands of psi. The actual stress conditions within the buttress are not known. However, because deformation of the buttress would be required for significant fault slip to occur over the 100-200 ft depth range,

1258 277

the possibility of renewed fault slip seems small and probably could not be caused by small increases of boundary stress or of pore fluid pressure, or small local decreases in rock strength.

On balance the stress data suggests that the tunnel fault should probably not be regarded as "capable" despite its relatively youthful age.

1248 278

6. REGIONAL STRUCTURAL FRAMEWORK

In the following sections, the regional tectonics for the area surrounding the PNPP site is briefly reviewed. The purpose of the review is to provide a framework for discussion of the origin of the tunnel faults and an examination of regional seismic patterns.

a. Structure under Lake Erie

Reconnaissance aeromagnetic studies by Myers (1977) and Ahern (1975) of Lake Erie suggest a pattern of discontinuous, narrow, approximately symmetrical 200-800 gamma positive anomalies aligned in a general east-west or E-NE trend. Details of contour configuration will undoubtedly change as additional data tracks become available, but analysis in broad terms seems justifiable with present data. Axes of the largest two anomalies are respectively located 7 and 30 miles offshore, north of the PNPP site. The anomaly nearer to the site has a maximum value exceeding 300 gammas and extends 40 miles or more along a trend of about 060° . The second of these anomalies has a maximum value over 800 gammas near its eastern end, and extends westerly for a similar distance. Models show that the observed anomalies could result from structurally-controlled intrusions composed of peridotite or gabbro of average magnetic susceptibility intruded along an E-W or NE-SW fracture zone during a magnetically normal epoch (Myers, 1977, p. 96). The anomaly source rocks could be clusters of stocks, sills, and dikes, rather than a single unit. Myer's estimate of time of intrusion is Mesozoic, based on intensity of remanent magnetization. Dike

1248 279

and linearly-aligned pluton cluster trends suggest that extensional stress directions in the northeast shifted from northwest to north or northeast between Early Jurassic and Early Cretaceous time (McHone, 1978). The north-south extension direction inferred from the magnetic anomaly trends suggests an approximate age of 125-160 mBP, which supports Myers' estimate.

Gravity anomaly distributions as given by WGC complement the magnetic data, and support the concept of a possible system of faults with northeast trend located just offshore from the PNPP site and extending tens of miles southwestward, virtually parallel to the shoreline. This trend corresponds with a straight-line segment of the Lake Erie shoreline southwest of the PNPP site, which M.J. Clifford (personal communication, 1979) considered as a possible (but unproven) reflection of structural control. Other high gradient gravity anomaly areas within a 50 mile radius of the site conceivably could reflect faulting; there is a correspondence between observed surface faults and gravity contours in the Lake Erie region (e.g., Electric fault, Bowling Green fault).

1248 280

b. Structure of Southwest Ontario

In southwest Ontario, normal faults with throw of 100 ft or more occur predominantly in east-west (Electric, Dawn faults) and north-south (Clearville, Willey faults) trends. The faults penetrate basement rocks and penetrate the Paleozoic section. Accumulation in lower Paleozoic oil and gas fields is structurally controlled.

The east-west trending Dover "syncline" south of the Electric fault is also of interest. Oil accumulation occurs in a structural depression containing porous dolomitized Ordovician limestones, a feature resulting from migration of Mg-bearing solutions through faults and fractures. The syncline structure reflects some faulting, but mainly is due to solution-influenced subsidence (Fig. 11). The structure is of special interest inasmuch as it documents the relation of pre-existing structure to a solution feature. At Dover, deformation in the Upper Ordovician and above mainly reflects the geometry of zones of intense leaching which in turn reflects old structure. Analogous deformation may be present associated with the Salina, south of Lake Erie. The geometry of the zone of deformation at the Cleveland Salt Mine is not unlike Fig. 11.

1291 281

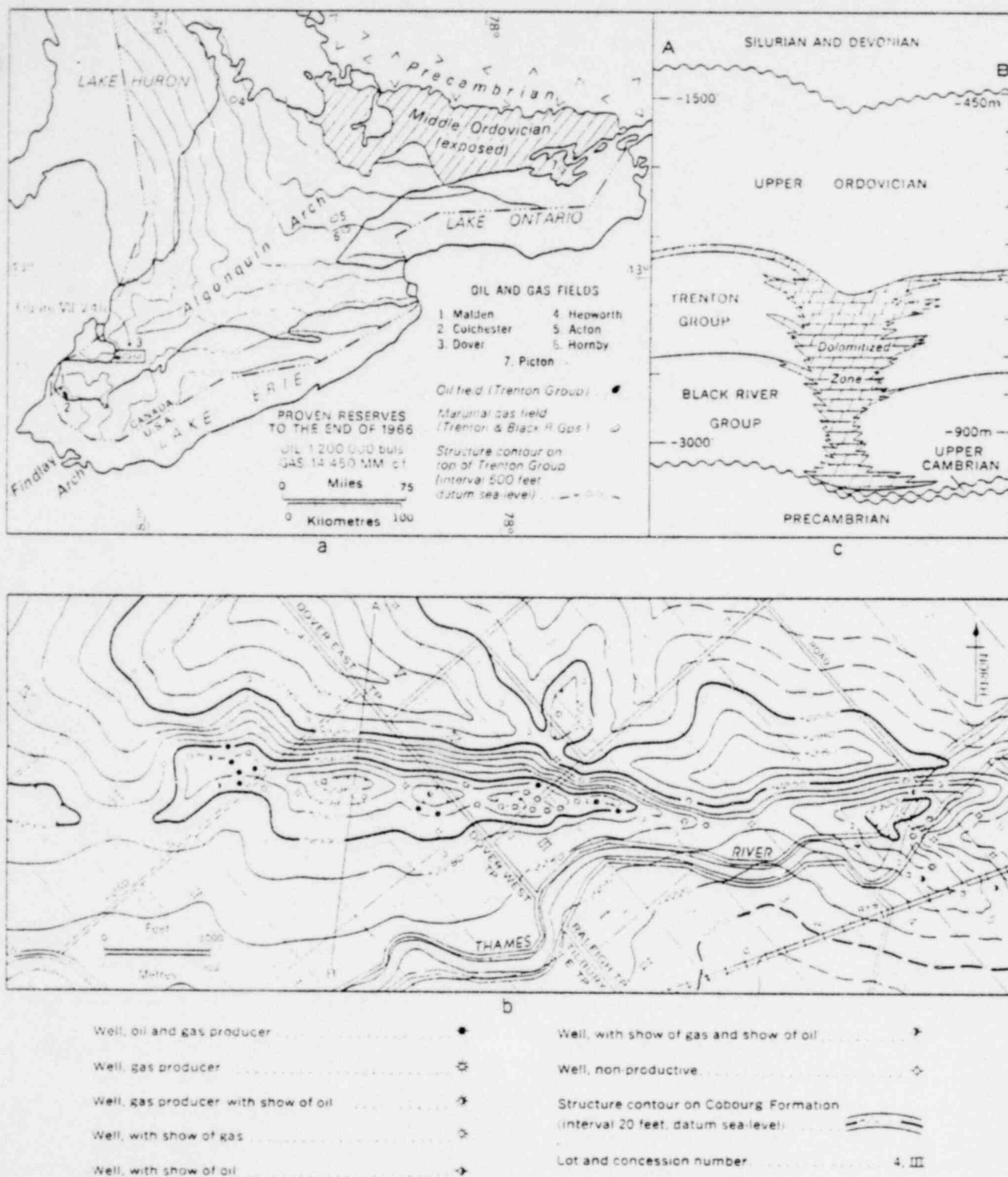


FIGURE 11 Middle Ordovician oil and gas fields of southwestern Ontario (by B. V. Sanford). (a) Distribution. (b) Structure contours on Middle Ordovician Trenton limestones in the Dover field. (c) Cross-section along line A-B through Dover field.

Fig. 11

c. Structure south of Lake Erie

Much of what is known is based on information from oil and gas wells.

Structure contours indicate in Portage, Mahoning, and Columbiana Counties (40-60 miles south of PNPP site), structures with northwest trend and length up to 10 miles. They are probably faults but none has actually been drilled through. The structures were apparently active during the Paleozoic. Subsurface structure mapping tends to focus on "larger" structures that show up despite inadequate well-head elevations; low amplitude structures (closure or displacement <20 ft) are indistinguishable from apparent structure due to inaccurate well-head elevations (A. Janssens, personal communication, 1979).

In addition, local structural closures have been mapped on the Onondaga (Devonian) Limestone. As far as is known these structures are not present below the salt, and Janssens has presumed that the features may reflect post-depositional salt movements resulting in local "domes".

No regionally-mappable feature based on well control has been recognized at the PNPP site (although well control in the vicinity of the site is not particularly dense).

A small normal fault with easterly strike has been reported in the Fairport Harbor Salt Mine. A set of normal faults has been reported at the Cleveland Salt Mine (Jacoby, 1970; Heimlich et al., 1974). I visited this site in the company of L. Schultz in April 1979. The overall structure appears to be a NW-trending asymmetric

"syncline" or "graben", in which the salt beds have deformed mainly by flowage, whereas dolomite beds have deformed by brittle fracture and faulting. Vertical offset is reported as 47 ft; this offset is distributed over a distance of 200 ft or so on the western border, and over a wider distance on the east. Formerly open fissures are now filled with salt. No evidence of recent tectonic movement was observed.

I interpret the structure as a feature which developed over a period of time in association with withdrawal of subjacent support. The cause of the loss of support is not known from available evidence, but could reflect either the local tectonic development of a graben or a structurally-influenced solution channel. Smaller scale (to 6 ft diameter) solution channel features are present in the mine (see Heimlich et al., 1974), and at the moment I prefer the latter interpretation. In this regard the Dover "syncline" in southwest Ontario seems in many respects analogous.

A small normal fault with easterly strike has been reported in the Fairport Harbor (Morton) Salt Mine. Figure 12 shows a minor graben structure from the Grand River access shaft near the top of the salt. The salt beds show no displacement by faulting, but top beds of salt have been locally removed by solution. Normal faults with about a foot of maximum slip affect overlying beds. The observed fault slip directly reflects solution. On the other hand, the salt beds are themselves bent below the fault, suggesting that the solution sites may have been influenced by pre-existing structure.

1241 284



FIGURE 12
 "GRABEN" IN PRODUCTION SHAFT
 MORTON SALT COMPANY MINE
 FAIRPORT HARBOR, OHIO

POOR ORIGINAL

In Ashtabula County, a structural "nose" has been defined by well control. Its location is indicated by the 2300-2500 contours of the lower Silurian Packer Shell carbonate unit, which has a northeast trend. Structural relief may be about 50-75 ft, with relative displacement upwards of the southern block. This structure can also be mapped on older rocks, down to basement, and on Devonian formations as well (A. Janssens, personal communication, 1979). Its movement history may be very complex.

There has been no certain identification of Alleghanian structures in northeast Ohio, but the Cambridge Arch structure in east-central Ohio has been attributed to horizontal thrusting (slip on the order of 1 mile) above the Salina E Salt (much as the Burning Springs anticline in West Virginia is associated with a Salina F-4 decollement (Clifford and Collins, 1974, AAPG Bull. 58:1891; Janssens, Deyling and Ott, 1976, AAPG Bull. 60:1621). The NNE-trending Cambridge Arch follows the "pinchout" of the E salt. In northeast Ohio, the "pinchout" boundary swings generally ENE (Clifford, 1973, Ohio Geol. Surv. Rept. Inv. 90) passing by at least 8 miles south of the PNPP site. This is about the trend and position noted for the Ashtabula County "nose" structure, and it is possible that the stratigraphic "pinchout" was structurally influenced. Local "pinchout islands" occur within the area of E salt deposition, one of which occurs 25 miles south of the PNPP site. Such "islands" should have impeded movement on an E salt decollement. Still, accentuated arching and local thrusting in the vicinity of the Ashtabula "nose", related to E salt decollement tectonics, cannot be ruled out. Decollement jump to the F-1 salt which extends under the PNPP site also seems possible.

d. Relationship of Inferred Structure to Seismicity

This discussion deals basically with the seismic data base presented by WGC (the April 19, 1979 version of Appendix VIII). The main revision involves the March 1943 earthquake, now regarded as an event of approximate magnitude 4.7, located at 41.61N, 81.33W (D. Gordon, and G. Leblanc, personal communications, 1979).

Figure 13 is a map containing inferred epicentral locations and twenty possible zones of structural weakness as inferred from aeromagnetic data, Bouguer gravity anomalies, oil and gas drill information, and geologic mapping. A word of caution: it should be emphasized at this point that not all of these features are of proven tectonic origin. Whereas features suggested by mapping or oil and gas drilling are perhaps more likely tectonic in origin, alternative explanations may indeed apply to anomalies recognized from gravity or magnetic patterns. Accordingly, to emphasize this uncertainty trends indicated by oil and gas or mapping data are indicated by dashed lines, and trends suggested by geophysical trends are dotted. Still, studies elsewhere have shown that earthquakes observed in conjunction with gravity anomalies commonly occur in high gradient areas (Hintze et al., 1977, p. 50, and cited references). This association may reflect fault reactivation (resurgent tectonics) or crustal rigidity variations effecting strain energy release patterns. Data concerning these anomalies are tabulated in Table 3.

Earthquakes possibly associated with each anomaly are also noted, with due allowance made for epicenter and structure location

1248 287

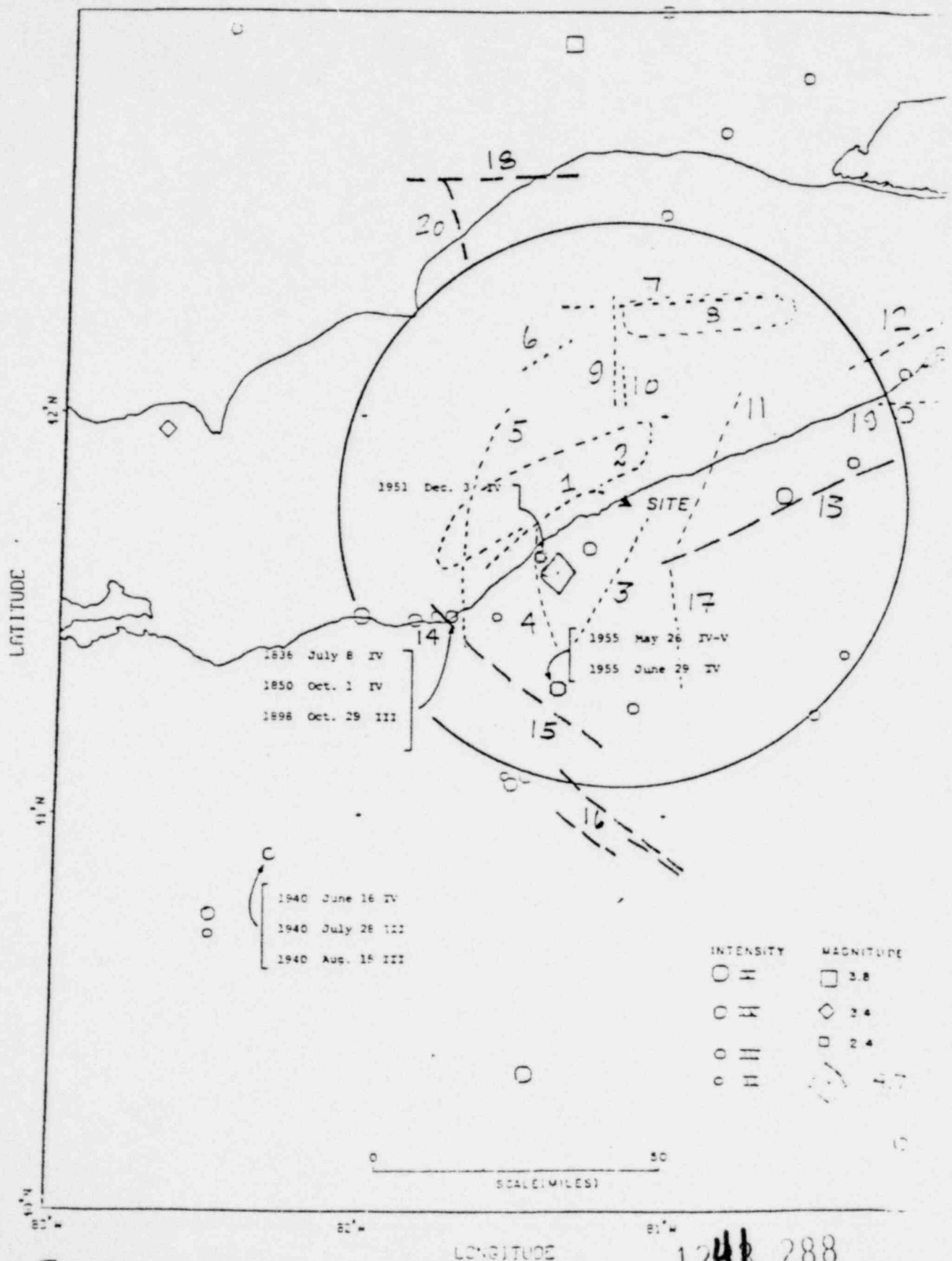


Fig.13

Table 3. Anomalies and Possibly-Associated Earthquakes within 50-mile Radius of PNPP Site.

Minimum distance to PNPP site miles	Anomaly	Trend	Basis	Possible Seismic Association	Remarks
<5	1	ENE	gravity	1858,1943,1951,1929	1,2 could reflect same structure
<5	2	ENE	magnetic	1857,1858,1928,1958, 1906a,1836,1850,1898, 1951	" " "
<5	3	NE	gravity	1857,1858,1943,1955(2)	
18	4	N-S	gravity	1943,1955(2),1929,1951	
25	5	NNE	gravity	1960a,1928,1958,1836, 1850,1898,1929	
30	6	NE	gravity		
35	7	E-W	gravity	1823	7,8 may reflect same structure
30	8	E-W	magnetic	1823	" "
10	9	N-S	gravity	1823	9,10 could reflect same structure
10	10	N-S	magnetic		" "
10	11	NNE	gravity	1857,1858	Anomaly indicated by WGC (2/5/79) Fig.2-5 G.4.
40	12	ENE	gravity	1857,1921,1934o	
12	13	ENE	oil-gas drilling; gravity	1857,1934n,1934o, 1858	
35	14	NW	Cleveland Salt Mine structure	1906a,1928,1958, 1836,1850,1898,1929	14,15 could reflect same structure weakness zone.
35	15	NW	oil-gas drilling	1885a,1955(2), 1885j	" "
50	16	NW	oil-gas drilling	1885j,1932;1940m	3 structures indicated
15	17	N-S	gravity	1857,1885(2),1858	
55	18	E-W	gravity oil-gas drilling	1823	extension of Electric fault

1241 289

45	19	E-W	gravity	1857, <u>1934</u> _o , 1934 _n	
50	20	NNW	oil-gas drilling; gravity		extension of Clearville caults.

Earthquakes are identified by year; month where needed given by lower case letter following date. Dates underlined for anomaly closest to plotted epicenter. Half-underlined dates indicate several anomalies are equally close to earthquake. Bracketed number indicates several earthquakes in same year.

12~~48~~ 290

uncertainties. As suggested in WGC reports, to most epicenters must be assigned a relatively large uncertainty, e.g. a "radius of uncertainty" of 10 miles or so, sometimes more. Nevertheless, it is considered that the historical seismicity data, interpreted with care, provide valuable insightson the spatial distribution of seismic activity and its relation to inferred geologic structure. Epicentral uncertainties were expressed as radii mainly using values given by WGS (Appendix V, Evaluation of Local Seismicity around Perry Nuclear Power Plant Site) dated April 10, 1979. A radius of 10 miles was used where uncertainty was unspecified. To the 1858 epicenter is attached an eastward uncertainty of 20 miles.

Earthquakes are listed in association with all anomalies mapped within a "circle of uncertainty" surrounding the plotted epicenter. By this tabulation procedure, it was possible to separate anomalies which have essentially no association with seismicity from those which display a possible association. Table 4 identifies six anomalies which are considered to possibly represent zones having potential for seismicity within a 40 mile site radius (see also Fig. 14).

Earthquake epicenters located nearest to a given anomaly are identified by underlined dates. Thus of eleven earthquakes registered for Anomaly 14-15, three epicenters are closer to this anomaly than to any other, six are considered rather close, but are at the same time equally close to other anomalies (the date is half-underlined), and two contain the anomaly within their radii of uncertainty, but are closer to other anomalies. A fairly strong argument can be made concerning the interpretation of this anomaly as a potentially seismic

Table 4. Anomalies with Possible Potential for Seismicity within 40-Mile Radius of PNPP Site.

Anomaly	Trend	Possible Seismic Association	Minimum distance to site(miles)
1-2	ENE	1943;1836,1850,1857,1858,1898, 1906a,1928,1929,1951,1958	5
3	NE	<u>1858</u> ;1857,1943,1955(2)	5
4	N-S	<u>1943</u> ;1951; <u>1955</u> (2);1929,1943	18
5	NNE	<u>1929</u> , <u>1836</u> , <u>1850</u> , <u>1898</u> ,1928,1943, 1958	25
13	ENE	<u>1857</u> , <u>1934n</u> ;1934o;1858	12
14-15	NW	<u>1960a</u> , <u>1928</u> , <u>1958</u> ;1885a, <u>1836</u> , <u>1850</u> , <u>1898</u> , <u>1955</u> (2); <u>1885j</u> ;1929	35

Underlined dates indicate anomaly is closest to plotted epicenter. Half-underlined dates refer to earthquake epicenters equally close to two anomalies. Bracketed number indicates several earthquakes in same year.

1298 292

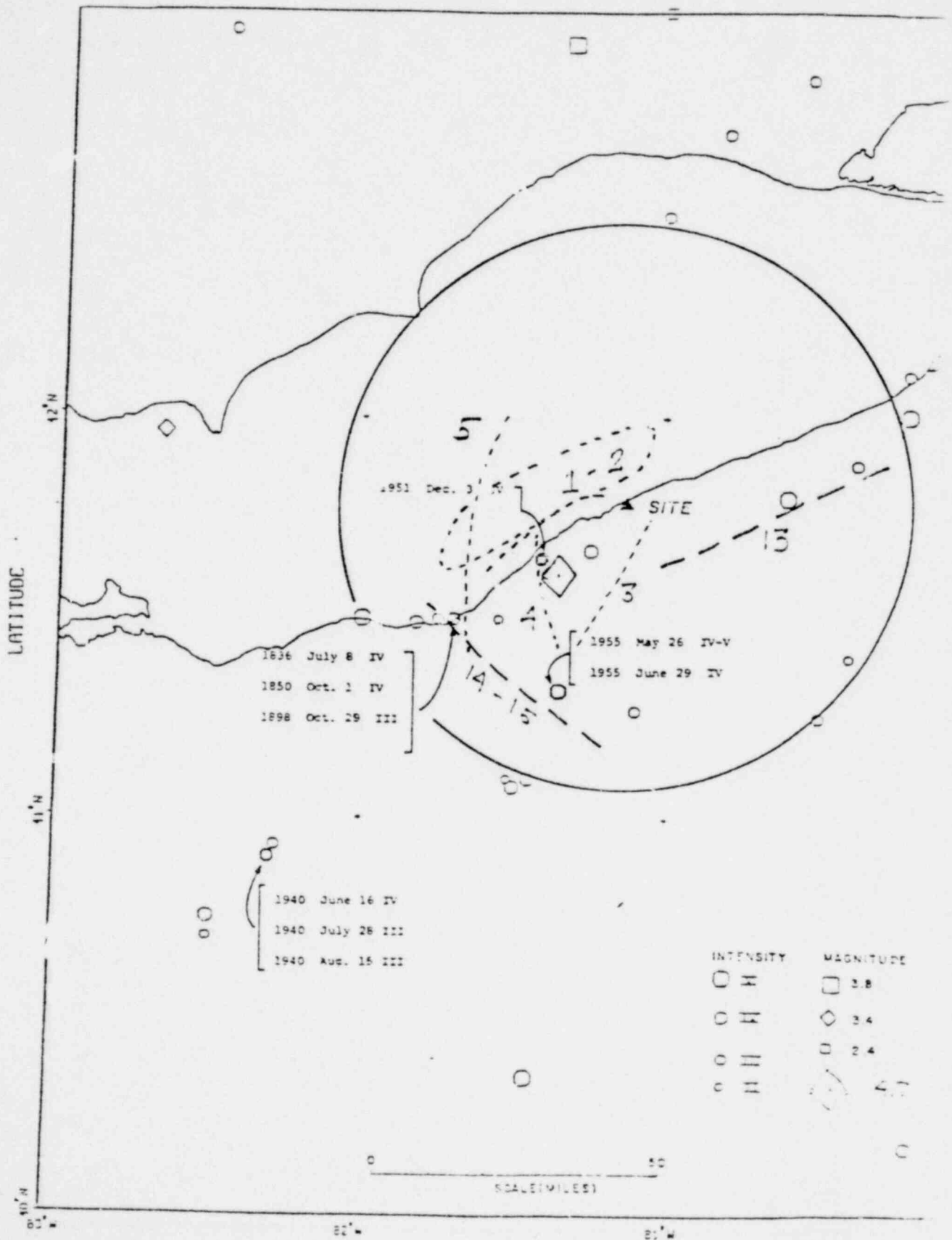


Fig. 14

structural zone. No recent deformation is however in evidence at the Cleveland Salt Mine through which the anomaly passes, although the structural trend is reinforced by oil and gas well data. Any recent deformation along this inferred zone of structural weakness near Cleveland must occur at some different spatial location.

In contrast, Anomaly 3 lists only five earthquakes, only one of which is underlined. This (1858) event is not well located. As regards the others, 1857 is not well-located, 1943 is well-located but its connection with Anomaly 4 seems strong, and a 1955 (2) connection requires extrapolation along strike. In sum, a correlation of Anomaly 3 with seismicity is not well-founded. This is significant in view of its proximity to the PNPP site and its possible connections with Anomalies 13, 1-2 and 4.

Anomaly 13, identified mainly by oil-gas well data but possessing gravity anomaly attributes as well, registers four earthquakes. Two dates are underlined. The structure may continue westward (data is sufficient to establish its termination). This is the Ashtabula County "nose".

Seven dates are assigned to Anomaly 5, five of which are considered rather closely juxtaposed. Most of this activity is from the Cleveland area, where Anomalies 5 and 14 apparently intersect; Anomaly 1-2 perhaps intersects Anomaly 5 just offshore. Assignment of individual epicenters near Cleveland to specific anomalies is therefore not straightforward.

124b 294

Both the magnitude 4.7 1943 earthquake and the 1951 Willoughby earthquake have been instrumentally located and are correlated with Anomaly 4. The 1955 Aurora earthquakes occur about on strike near the apparent southern limit of Anomaly 4.

Eleven earthquakes are listed for Anomaly 1-2, which approaches the PNPP site near its eastern boundary. However, many of the earthquakes listed are associated with the large regions of uncertainty for Cleveland area earthquakes. These epicenters are mostly plotted at near-shoreline locations, although the actual epicenters may in some cases be located under Lake Erie. The lack of "underlined dates" tabulated for Anomaly 1-2 could reflect this bias.

In sum, correlation with seismicity seem reasonably good for Anomalies 4,5,14-15,13, weak for Anomaly 3 and uncertain for Anomaly 1-2. Nearest strongly-correlated anomalies to the PNPP site are Anomaly 13 (12 miles) and Anomaly 4 (18 miles). The PNPP site itself lies within the circle of epicentral uncertainty only for the poorly located 1858 earthquake.

But it must be observed that the "good correlations" referred to have not confirmed the reality of specific structures associated with the various anomalies, although our suspicion regarding them is enhanced. Seismicity in the greater Cleveland area is poorly understood, and the above correlations were attempted in the hope of merely providing a first approximation of the relation between seismicity and tectonics. Indeed, seismicity in the eastern United States remains poorly understood even in regions where active

1241 295

instrumental research has been conducted.

Finally, the relationship of structures inferred by anomalies to measured stresses is discussed. It is assumed that earthquakes occur on preexisting unhealed faults that are preferentially orientated within a region of (approximately) uniformly oriented stresses.

There is justification for assuming that the orientation for σ_1 is a representative regional orientation.

Anomalies 4 and 5 are approximately orthogonal to this stress trend, suggesting the possibility of thrust faulting in basement of the greater Cleveland area on N-S striking faults with shallow or moderate E or W dip. Thrust faulting of a possibly analogous nature has been reported from Attica, N.Y., and from Blue Mountain Lake in the Adirondacks, based on fault plane solutions from earthquakes. No fault plane solutions are available for earthquakes in the vicinity of the PNPP site region.

Slip can be expected to occur on preexisting faults lying within about $10-50^\circ$ of σ_1 , depending on the specifics of frictional coefficients. If faulting occurred on Anomaly 14-15, a left-lateral strike slip component could be expected. Similarly, motion on structures associated with Anomalies 3,13 or 1-2 would probably involve significant right-lateral strike slip motion. These predicted motions are clearly unlike those inferred for the tunnel faults. There is no evidence that favors a connection between the seismic and existing stress patterns in the greater Cleveland area and the PNPP tunnel fault.

1248 296

7. ORIGIN OF TUNNEL FAULTS

Table 5 contains a relatively complete list of possible mechanisms considered in relation to the tunnel faults. These are grouped according to age. Apart from the evidence on age, distinctions between, on the one hand, faulting associated with differential warping mechanisms of Paleozoic or Mesozoic age, and Alleghanian compression on the other hand, would be based primarily on geometry. Geometric data on tunnel fault strike and shallow-level dip are available, but the extent of the fault remains uncertain. Sufficient data is not available to firmly establish whether the fault simple dies out to the southwest, steepens in attitude to merge with a high-angle basement fault, or merges with a bedding-plane decollement, perhaps at the level of Salina salt. Discrimination among all hypotheses is thereby rendered difficult.

As discussed previously, I believe the tunnel faults to be of Pleistocene age and the range of possibilities can therefore be reduced. A few comments seem nevertheless appropriate for other categories, inasmuch as Pleistocene deformation could be influenced by older structural features.

Regarding mid-Paleozoic deformation, the concept of sediment deformation can be conclusively ruled out by the brittle nature of the observed deformation. The tunnel fault formed following lithification of the shale sequence.

Differential compaction over buried reefs seems a potential mechanism for production of deformational structures, but to my knowledge the subject has not been previously discussed for this region. Leaching and collapse on a large scale has been discovered, particularly in relation to patch and pinnacle reefs in southwest Ontario. Elongated

Table 5. Possible Genetic Classes for Tunnel Fault Origin

1. Paleozoic Tectonics
 - a. Soft or semi-lithified sediment deformation
 - b. Basin-arch differential warping
 - c. Appalachian (Alleghanian) Orogenesis
 - d. Gravity salt tectonics
 - e. Differential compaction over Niagaran (Mid-Silurian) reef
 - f. Collapse following structural- or reef-influenced solution of salt
2. Mesozoic-Tertiary Tectonics
 - a. Regional differential uplift
 - b. Rifting (Taphrogenesis)
 - c. Gravity salt tectonics
 - d. Collapse following solution of salt
3. Pleistocene-Recent Tectonics
 - a. Ice-sheet traction (glacitectonics)
 - b. Subsurface salt tectonics activated by glacial loading
 - c. Differential down-bowing with glacial advance
 - d. Differential rebound with glacial retreat
 - e. Surficial stress-relief ("Pop-up" family of structures)

1248 298

collapse features have resulted from fault or joint influenced solution. The most extensive period of leaching occurred before the lower Devonian (Sanford, Geol. Survey Canada, Paper 65-9), although post-Devonian leaching is not rare. But reefs of significant dimensions do not appear to be present in the near-site region; reef-associated differential compaction or solution collapse mechanisms are not likely related to PNPP faulting, directly or otherwise.

Southeastward gravity movements on Appalachian Basin salt is a new concept, and cannot be addressed in much detail. No features described in the literature seem to clearly indicate such a mechanism on a large scale. But the salt beds extend from the Appalachian to Michigan Basins in a swath about 60 miles wide, so that for a limited region (which includes the PNPP site), such a mechanism would seem technically feasible. Most of the individual salt layers show however no such regional continuity, but the B salt is a possible candidate.

Local mine exposures do display evidence of dome-like fold growth in selected salt layers, and sporadic structural "domes" are in evidence within the general region of the PNPP site, so that some activity of the salt is in evidence. The Cambridge Arch- salt decollement association is further evidence for this. Activity of the salt is judged to have been most likely in late Paleozoic or early Mesozoic time, when overburden pressures and formation temperatures were about at peak values. Relatively high loading conditions were also probably associated with Pleistocene

glaciations, with high stress gradients near ice sheet boundaries. It is possible that "domes" formed under these conditions and were somewhat elongate parallel to the ice sheet border. But available time for flowage was relatively brief, and temperatures may not have been very high.

With differential warping is commonly associated local faulting, usually of a dip-slip high-angle nature, in which pre-existing zones of weakness are mobilized. Such fault movements with east or northeast trends have been documented in the general region, both in Ontario and south of Lake Erie, and some of the anomalies previously discussed may reflect such features. When movements on deep high-angle discontinuities disturb overlying sedimentary formations, faulting in the younger formations can proceed with progressively decreasing dip angle. Thus shallow low angle thrusts (as observed at the PNPP site) are compatible with high-angle dip-slip movements at depth. Variations in fault dip depend on the specifics of the initial geometry, ambient stress conditions, boundary (displacement) conditions, and material properties, including anisotropy. In this regard, the observed influence of anisotropy for the tunnel faults (alternating shifts from bedding-plane to riser segments along the faults) would be expected to occur in any shallow thrust propagating through anisotropic shale. It should not be considered as evidence favoring a deeper similarly-styled mode of decollement tectonics rather than deeper high-angle faulting. High-angle basement faulting associated with proposed Mesozoic rifting would, however, tend to produce normal faulting in overlying formations,

1248 300

not thrust faults. But younger recurrent movements on such rift faults under different ambient stress conditions could indeed promote high-level thrusts, as discussed above.

The geometric extent of the tunnel fault is not known well enough to establish whether it is a discrete, shallow level structure analogous to features commonly classified under the category of "pop-up", or a shallow-level segment of a larger feature that extends directly or by en-echelon development to some deeper level, possibly to connect with some older fault or zone of structural weakness.

"Pop-up" structures may form at any time; some have been observed in the process of formation, whereas many are Pleistocene in age, associated with surficially-high stresses related to glacial* or glacio-isostatic adjustments. Under these conditions, genetic category 3e can be regarded as a sub-class of 3c or 3d.

Rock deformation by direct glacial loading has occasionally produced thrust structures in bedrock elsewhere to the depth observed at the PNPP site, but the direction of fault slip has invariably been in the direction of glacier flow. The geometry of features associated with the PNPP tunnel fault suggest growth from a lower to an upper level (toward the north), and slip gradient suggests termination of the fault well below lake bottom. This evidence argues against an origin through direct drag of an overriding ice sheet.

Significant crustal warping occurs due to glacial advance and retreat (glacio-isostasy). A fault produced by a major glacial advance would be subjected soon afterward to loading from the overriding glacier. But an imprint of this event should then be left in the consolidation behavior of the gouge.

*Horizontal stresses of considerable magnitude can be built up by cycles of glacial loading and unloading (cf. Voight, 1966; 1967, pp. 337-340).

In particular, intense faulting, fracturing, and seismic activity have been attached to the deglaciation phase, when the glacio-isostatic uplift rate is near its maximum (Mörner, Geology, 6:41-45). This mechanism is clearly consistent with the age estimate of 20,000-10,000 YBP for the last movements on the tunnel fault, for this time represents deglaciation from the Laurentide maximum ice sheet.

In general terms I prefer the hypothesis of fault motion due to differential rebound associated with retreat from the Laurentide maximum. Surficial stress relief, considered in these terms to be a subclass of glacial rebound, remains viable inasmuch as the extent of fault is uncertain.

If simple, near-surface stress relief has occurred, nucleation of the fault may presumed to be somehow related to stress and pore fluid (water and methane) pressure gradients within the Devonian shales. The alternative is that fault growth has been influenced by (probably recurrent) movement on deeper seated fractures or faults, either by direct propagation or by en-echelon deformation. The strike of the tunnel fault would then be conditioned in large part by the strike of the pre-existing feature. The possibility of nearby subsurface structural features of northeast strike is suggested by the anomaly maps, lending weight to a hypothesis in which motion on the tunnel faults were directly produced or were influenced by recurrent movements on old faults during deglaciation rebound. The salt tectonic mechanism is not rejected, but seems less likely in view of its somewhat exotic nature.

Finally, neither the age estimate as noted above, nor the observations of the fault zone preclude a more complex, possibly hybrid mechanism of fault development. Because emphasis in the above discussion has been placed on the last significant motion, two

possibilities seem open: either the fault nucleated and propagated entirely within the 10,000-20,000 YBP range cited above, or nucleation occurred at some earlier date, with the last significant propagation event occurring with the 10,000-20,000 YBP period. Thus it is possible to conceive of incremental propagation of the tunnel fault, involving, for example, intermittent periods of growth associated with glaciations of Illinoian, or early Wisconsinan age, separated by intervening periods of relative stability. The available data do not however permit resolution of the story in such fine details.

1241 303

8. REFERENCES

- Ahrens, J.L., 1975, Aeromagnetic reconnaissance survey of Lake Erie: M.S. Thesis, Ohio State University, 153 p.
- Casagrande, A., 1936, The determination of preconsolidation load and its practical significance, Proc. 1st Int. Conf. Soil Mech. Found. Eng., p. 60.
- Dücker, A., 1951, Ein Untersuchungsverfahren zur Bestimmung der Mächtigkeit des diluvialen Inlandeis: Hamburg min.-geol. Staatsinst. Mitt., 20:3-14.
- Harrison, P.W., 1957, A clay-till fabric: its character and origin, J. Geol. 65:275-308.
- Harrison, W., 1958, Marginal zones of vanished glaciers reconstructed from the preconsolidation-pressure values of overridden silts, J. Geol. 66:72-95.
- Heimlich, R.A., Manus, R.W., and Jacoby, C.H., 1974, General Geology of the International Salt Company Cleveland and Mine, Cleveland, Ohio. Field Trip No. 1, Field Trips in North-eastern Ohio (Contrib. 96, Dept. Geology, Kent State Univ., Kent, Ohio).
- Hintze, W.J., Braile, L.W., Keller, G.R., and Lidiak, E.G., 1977, A tectonic overview of the central midcontinent, Purdue Univ. for U.S. Nuc. Reg. Comm., NUREG-0382, 106 pp.
- Jacoby, C.H., 1970, Faults in salt mines - their impact on operations, in 3rd Symp. on Salt 2:447-542.
- Kogler, F., and Scheidig, A., 1948, Baugrund und Bauwerk: Berlin, Wilh. Ernst.
- Lessig, H.D., and Rice, W.A., 1962, Kansan drift of the Elkton, Ohio, rift, Amer. Journ. Sci., 260:439-454.
- McHone, J.G., 1978, Distribution, orientations, and ages of mafic dikes in central New England, Geol. Soc. Am. Bull., 89:1645-1655.
- Morner, N.A., 1978, Faulting, fracturing, and seismicity as functions of glacio-isostasy in Fennoscandia, Geology, 6:41-45.
- Myers, C.P., 1977, Aeromagnetic reconnaissance survey of Lake Erie, M.S. Thesis, Ohio State Univ., 172 pp.
- Schmertmann, J.M., 1955, The undisturbed consolidation of clay, Trans. ASCE, 120:1201.
- Smith, W.E.T., 1966, Earthquakes of eastern Canada and adjacent areas, 1928-1959, Pub. Dominion Obs., XXXII (3), 121 pp.

1241 304

- Sugden, D.E., 1977, Reconstruction of the morphology, dynamics, and thermal characteristics of the Laurentide Ice Sheet at its maximum, Arctic and Alpine Res., 9:21-47.
- Terzaghi, K., and Peck, R.B., 1968, Soil Mechanics in Engineering Practice, 2nd ed., J. Wiley, 729 pp.
- Voight, B., 1966, Correlation of large horizontal stresses with tectonics and denudation, Proc. 1st Int. Cong., Int. Soc. Rock Mech., Paper 4.9.
- Voight, B., 1967, Interpretation of rock stress measurements, Proc. 1st Int. Cong., Int. Soc. Rock Mech, III: 332-348.
- Voight, B., 1973, Correlation between Atterberg plasticity limits and residual shear strength of natural soils, Geotechnique 23:265-267.
- York, J.E., and Oliver, J.E., 1976, Cretaceous and Cenozoic faulting in eastern North America, Geol. Soc. Am. Bull., 87:1105-1114.

1241 305